Second Messenger modulation of the Human Ether a g
Related Gene (HERG) potassium channel

Sarah Louise Cockerill

Thesis submitted for the degree of Doctor of Philosoph

Department of Cell Physiology and Pharmacology
University of Leicester
U.K.

December 2004

ProQuest LLC
789 East Eisenhower Parkway
P.O. Box 1346
Ann Arbor, MI 48106-1346

Abstract **Sarah Cockerill**

Second Messenger modulation of the Human Ether a go-go Related Gene (HERG) potassium channel

HERG (*human ether-a-go-go related gene*) encodes the major pore-forming subunit of I_{Kr}, a current which is vital for normal repolarisation of the cardiac action potential. Attenuation of I_{Kr} can lead to long QT syndrome, which can predispose individuals to arrhythmias and sudden cardiac death. Given the physiological importance of HERG potassium currents, it is important to understand how they are regulated by intracellular signalling pathways.

Whole cell voltage clamp and calcium imaging techniques were used to investigate modulation of HERG channels expressed in HEK 293 cells by second messenger pathways. Stimulating protein kinase C (PKC) by $G_{\alpha q/11}$-coupled muscarinic receptor stimulation to elevate diacylglycerol (DAG) and calcium, using OAG (an analogue of DAG), or elevating calcium using ionomycin resulted in a sustained decrease of HERG current. This HERG current response is likely to be mediated by α or β (calcium-sensitive) isoforms of PKC. ^{32}P labelled phosphate incorporation into HERG in OAG treated and non-treated cells was used to determine if PKC directly phosphorylates the channel. Two protein bands at 155 and 135 kDa, corresponding to mature and core glycosylated forms of HERG respectively, were observed in untreated cells, indicating phosphorylation under basal conditions. Stimulation of PKC significantly increased phosphorylation of both bands. HERG currents were also attenuated by activation of cAMP dependent protein kinase (PKA). However, in contrast to PKC, PKA stimulation resulted in a net dephosphorylation of HERG. Overall, the phosphorylation assays suggest HERG channel phosphorylation is dynamically regulated by PKC, PKA and protein phosphatases.

In the course of this study it was also found that HERG is directly blocked by caffeine. Caffeine block is open/inactivation state dependent. Caffeine binds within the inner cavity, to sites that include Phe656 and Tyr652.

Contents

Acknowledgements

Firstly, I would like to thank my supervisors, Dr. John Mitcheson and Professor Nick Standen, for their support, guidance and knowledge that lead to the production of this body of work.

Many thanks go to past and present members of lab 347 for the help they have given me, especially Matt for the useful discussions (although not all work-related!), and for lending me his rig on the odd occasion, and SeungHo for preparation of oocytes.

My thanks also go to members of labs 354 and 201, who put up with me as I learnt about the perils of western blotting and radioactivity!

I would like to thank the Cell Physiology and Pharmacology Department as a whole, both past and present members, for both the good times, and the times I'd most like to forget (mostly drunken!). The uniqueness, and colourfulness of the department has kept me amused throughout my time here!

My thanks also go to my parents, who have supported me throughout the past three years in whatever way they could – even when they didn't understand what I was doing or why! These thanks also extend to supporting me in every way during my undergraduate studies.

Importantly, my sincerest gratitude goes to Carl, without whom I am sure I would have completely lost any remaining sanity! Thank you for the support, love, company and wicked sense of humour when it was most needed!!

Finally, I would also like to thank the British Heart Foundation for financial support of this PhD.

Publications

Cockerill SL, Willars GB, Standen NB, Mitcheson JS, Cytosolic calcium attenuates HERG channel currents expressed in HEK 293 cells via a protein kinase C dependent pathway, J. Physiol., 552P (2003, Manchester meeting) (Blue Riband Prize winner)

Cockerill SL, Tobin AB, Willars GB. Standen NB, Mitcheson JS, Phosphorylation by protein kinase C of HERG potassium channels expressed in a mammalian cell line, J. Physiol., C7 (2004, Glasgow meeting)

Abbreviations

ADP	*adenosine diphosphate*
AKAP	*A kinase anchoring protein*
ATP	*adenosine triphosphate*
AVN	*atrioventricular node*
BAPTA	*1,2-Bis (2-aminophenoxy) ethane-N, N, N', N'- tetraacetic acid*
Bis-1	*bisindolymaleimide-1*
CaMKII	*calcium calmodulin kinase II*
cAMP	*cyclic adenosine monophosphate (Cyclic AMP)*
CHO	*chinese hamster ovary*
CICR	*calcium induced calcium release*
CNBD	*cyclic Nucleotide Binding domain*
CREB	*cyclic AMP-response element binding protein*
DAG	*diacylglycerol*
DEPC	*diethylpycarbonate*
DMSO	*dimethylsulphoxide*
EAG	*ether-a-go-go gene*
ECG	*electrocardiogram*
ERG	*ether-a-go-go related gene*
ERK	*mitogen activated protein kinase*
FFA	*free fatty acids*
GEF	*guanine nucleotide exchange factor*
GP	*guinea pig*
GPCR	*G-protein coupled receptor*
GTP	*guanine triphosphate*
HCN	*hyperpolarisation activation, cyclic nucleotide gated cation channels*
HEK 293	*human embryonic kidney 293*
HERG	*human ether-a-go-go related gene*
HRP	*horseradish peroxidase*
IBMX	*3-isobutyl-1-methylxanthine*
IP_3	*1,4,5-inositol trisphosphate*

I-V	*current-voltage*
KchIP3	*Kv Channel Interacting Protein 3*
KHB	*Krebs-Henseleit buffer*
LB	*Luria-Bertani*
LPC/LysoPC	*lysophosphatidylcholine*
LQTS	*long QT syndrome*
MCh	*methacholine*
MERG	*mouse ether-a-go-go related gene*
MESA	*MOPS EDTA sodium acetate*
MinK	*minimum conductance potassium channel*
MiRP	*MinK Related Protein*
NMS	*N-metyhyl scopolamine*
OAG	*1-oleoyl-2-acetylglycerol*
PAS	*Per-Arnt-Sim domain*
PdBu	*phorbol 12,13-dibutyrate*
PDK1	*3-phosphoinositide-dependent protein kinase-1*
PI3K	*phosphatidylinositol 3-kinase*
PIP_2	*phosphatidylinositol-4,5- bisphosphate*
PIP_3	*phosphatidylinositol-3,4,5- trisphosphate*
PKA	*protein kinase A*
PKB	*protein kinase B (Akt)*
PKC	*protein kinase C*
PLA_2	*phospholipase A2*
PLC	*phospholipase C*
PLD	*phospholipase D*
PMA	*phorbol 12-myristate 13-acetate*
RERG	*rat ether-a-go-go related gene*
ROS	*reactive oxygen species*
RPM	*revolutions per minute*
RT-PCR	*reverse transcriptase polymerase chain reaction*
SAN	*sinoatrial node*
SDS-PAGE	*sodium dodecyl sulphate polyacrylamide gel electrophoresis*
SHP-1	*src-homology 2-containing protein*
SOC	*salt optimised and carbon*

T3	*3, 5, 3'-triiodothyronine*
TBS	*tris buffered saline*
TEVC	*two electrode voltage clamp*
TRH	*thyroid releasing hormone*
WT	*wild type*
4M HERG	*HERG channel mutant lacking all putative PKA phosphorylation sites*
18M HERG	*HERG channel mutant lacking all putative PKC phosphorylation sites*
ΔPKC HERG	*HERG channel mutant lacking 17 putative PKC phosphorylation sites*

Chapter 1
Introduction

1.1 Potassium channel structure

Potassium channels are membrane-spanning proteins that selectively conduct potassium ions across the cell membrane, along the electrochemical gradient. The mammalian family of potassium channels can be sub-divided into three groups, based on structure:

1. Voltage gated channels, comprised of six transmembrane domains
2. Inward rectifier channels, comprised of two transmembrane domains
3. Two-pore channels, comprised of four transmembrane domains

(Hille, 2001; figure 1.1).

1.1.1 Structure of voltage gated potassium channels

1.1.1.1 Structure of the pore region

The Human Ether-a-go-go Related Gene (HERG) channel belongs to the family of voltage gated potassium channels. Each subunit has intracellular N and C termini, and six transmembrane domains, denoted S1-S6. S1-S4 form the voltage sensing domain (discussed later), and S5-S6 form the pore forming domain. Our understanding of the structure of the pore of voltage gated potassium channels has been advanced in recent years by x-ray crystallography. A number of high resolution structures of prokaryotic potassium channels have been published. Doyle et al. (1998) solved the first crystal structure of a potassium channel (KcsA), which was isolated from the bacterium *Streptomyces lividans.* KcsA has two transmembrane domains, which are joined by ~30 amino acids that form the pore helix and the 'turret', that extends above the membrane. Despite being a two transmembrane channel, it it more closely related to voltage gated channels than inward rectifer potassium channels (Kir), and has 32% sequence homology with the pore region of Shaker, the archetypal voltage gated potassium channel (K_V). The KcsA crystal structure shows a symmetrical assembly of four subunits around a central pore. The subunits are arranged in such a way that the shape was likened to an 'inverted teepee' structure, with the S2 inner helices (analagous to S6 in K_V

Figure 1.1

The mammalian groups of potassium ion channels. Schematic diagram shows 6 transmembrane domain voltage gated potasssium channels, two transmembrane inward rectifier potassium channels and four transmembrane, two-pore potassium channels. All have intracellular N- and C-termini.

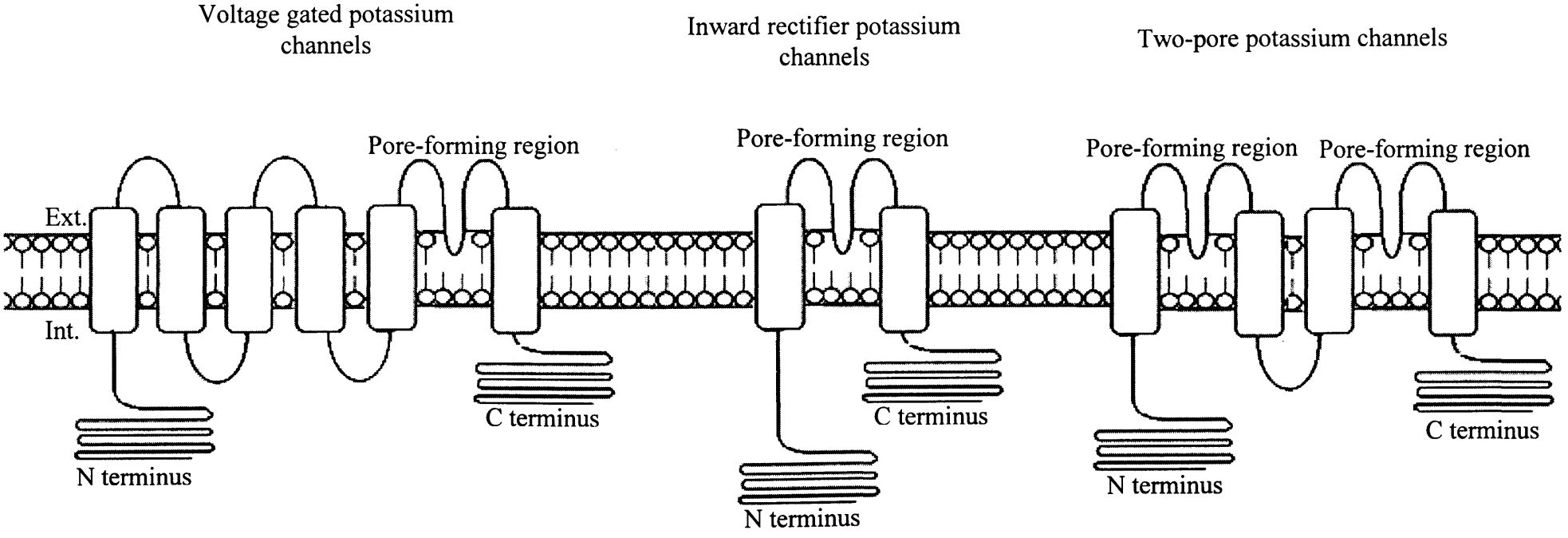

channels) being wide apart at the extracellular side of the membrane and lying closer together at the intracellular side. The central pore of the channel is a wide, aqueous cavity, which narrows toward the cytopasmic end, where the four converging inner helices are thought to form the activation gate. This gate is almost fully closed, leading the authors to propose the channel was crystallised in the closed state (figure 1.2). The pore loop contains the potassium selectivity-signature sequence (glycine, tyrosine, glycine), and forms the selectivity filter, the narrowest section of the pore on the extracellular side. The selectivity filter is lined with polar carbonyl oxygen groups pointing towards the permeation pathway that operate to stabilise potassium ions that have shed hydrating waters on entering the filter.

A further study solved the structure of a calcium-gated potassium channel, MthK, from *Methanobacterium thermoautotrophicum* (Jiang et al., 2002) and proposed a general mechanism for activation gating. The structure was crystallised in the presence of calcium, and the S2 helices are splayed open at the intracellular side relative to KcsA. This creates a large aperture on the cytoplasmic side of the pore of approximately 12Å in diameter, which provides a path wide enough for the movement of potassium ions between the cytoplasm and the selectivity filter. This led the authors to believe this channel was isolated in the open state. Comparing the crystal structures for KcsA and MthK suggests the inner helices move radially outwards upon channel activation, bending around a glycine hinge. Glycine confers flexibility to peptides because its small side groups gives it the ability to adopt many angles around the peptide bond. The glycine residue in the inner helix (S6 in voltage gated channels) is highly conserved in potassium channels, suggesting the glycine hinge may be a common mechanism of channel activation.

Once the channel is activated, ion conduction through the pore and selectivity filter is mediated by a number of different amino acids in the channel. Negatively charged amino acids at the intracellular entrance to the pore act to attract the positively charged potassium ions close to the pore, thus raising their local concentration. The walls of the cavity are lined by hydrophobic residues, allowing the hydrated potassium ions to easily pass from the intracellular solution into the central cavity. The potassium ion must then pass through the selectivity filter. The selectivity filter forms the narrowest part of the channel pore, with the main constituents of the selectivity filter being carbonyl oxygens from the glycine, tyrosine, valine and threonine resides, which are highly conserved amongst

Figure 1.2

The pore and selectivity filter of potassium channels is formed by two transmembrane domains and the peptide linker. Schematic diagram represents three α subunits of a potassium channel based on the KcsA crystal structure. The transmembrane domains are represented by alpha helical structures. M1 and M2 correspond to S5 and S6 respectively in 6 transmembrane domain channels. Red circles represent potassium ions.

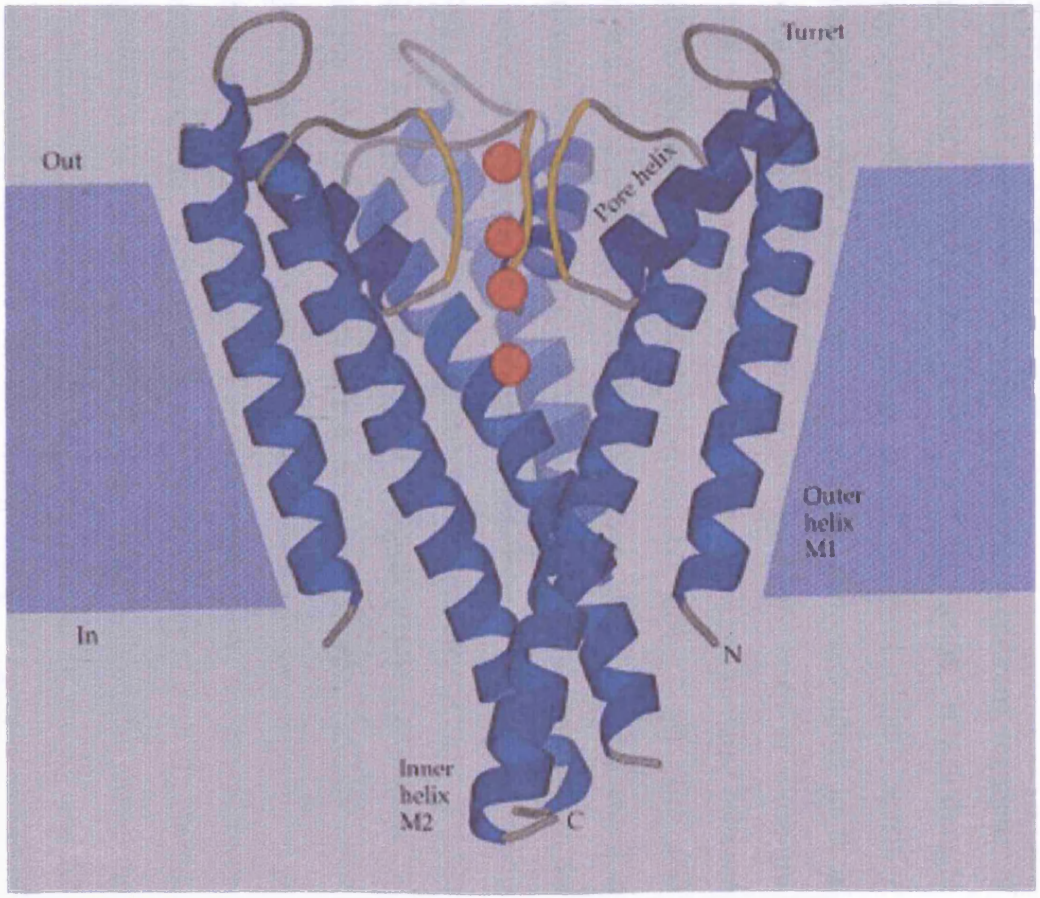

From Hille, 2001

potassium channels. This region is so narrow that a hydrated potassium ion must shed most of its water molecules to pass through. The size of the region is determined by the interaction between residues in the selectivity filter and residues in the pore helices, and it is these interactions that determine the ion selectivity of the channel.

1.1.1.2 Structure of the voltage sensing region (S1-S4)

Mammalian voltage gated potassium channels have 6 transmembrane segments, of which the fourth contains several positively charged amino acids. It was thought that this region was the main part of the voltage sensor, acting as a highly sensitive transistor, recognising transmembrane voltage changes and responding to them accordingly, to cause conformational changes and therefore open or close the channel (Hille, 2001). The S4 segment in a voltage-gated channel contains between four and eight positively charged residues at approximately every third amino acid position (Liman and Hess, 1991). Fluorimetry techniques, which detect changes in fluorescence emission caused by changes in the local environment have shown the S4 segment to move in response to depolarisation (Mannuzzu et al., 1996; Loots and Isacoff, 1998), and mutational studies have shown that neutralising specific basic residues in the S4 region alters gating of the channels (Tristani-Firouzi et al., 2002). Accessibility studies such as cysteine scanning mutagenesis, which measure the accessibility of specific amino acids to a reactive agent in the open or closed state of the channel, have shown exposure of specific residues on the intra- or extra-cellular faces of the membrane, to depend on membrane voltage (Liu et al., 2003a), again suggesting that the S4 segment is highly mobile. Studies have also shown the S4 segment to interact electrostatically with negative charges in the S2 and S3 segments (Sato et al., 2003; Papazian et al., 1995), suggesting S4 operates as part of a larger voltage sensing unit. Taken together, these studies provide evidence for models of voltage sensing in which the electrical field moves 'gating charges' across the membrane, resulting in conformational changes of the protein and opening of the activation gate. Putting this in the context of a conventional model for voltage gated potassium channels, it was hypothesised that the S4 domain moves in a helical screw motion in response to depolarisation, with the positive charges moving toward the extracellular side of the channel (figure 1.3A). A recent paper however, proposed a different structure of the voltage-gated channels.

Figure 1.3

The conventional and new model of voltage sensing. The conventional model (A) suggests a translation and/or possible rotation of the S4 domain across the membrane in response to depolarisation. The new model (B) is based upon a 'voltage paddle' on the outside edge of the channel, which moves through the plasma membrane in response to depolarisation. In both models the S4 domains are marked by +ve charges shown in red.

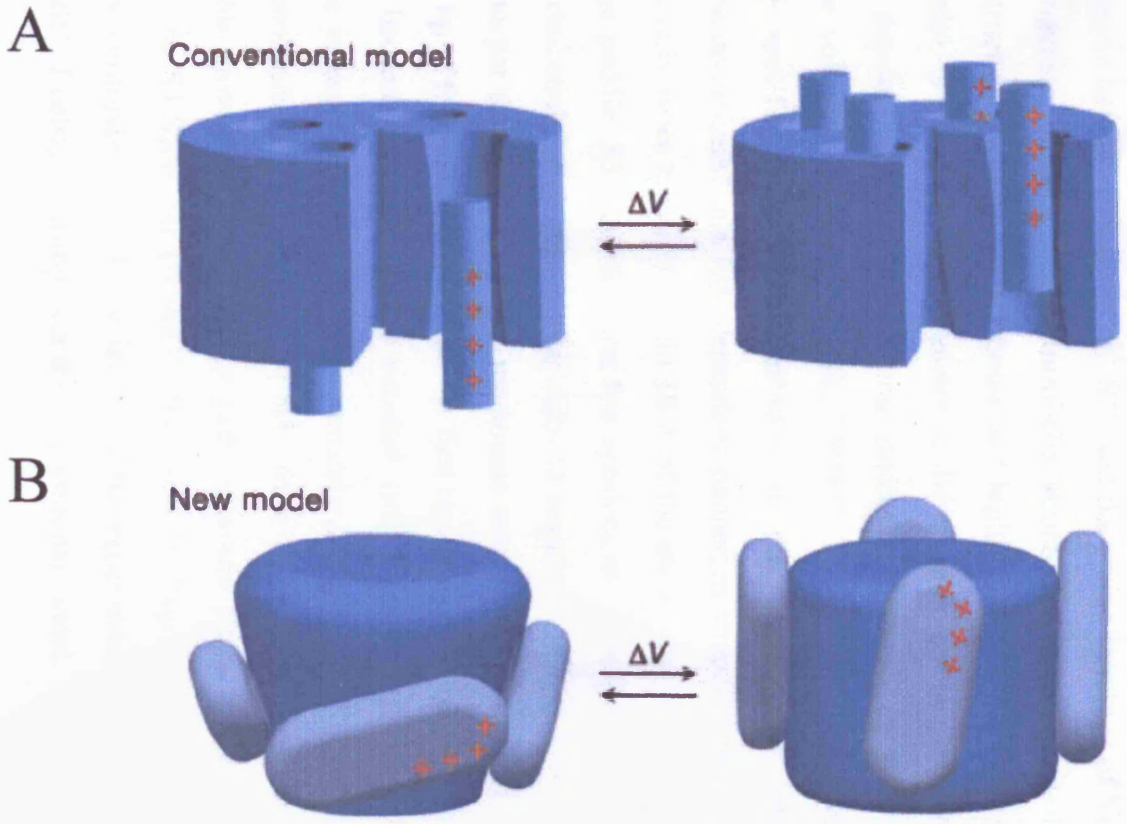

From Jiang et al., 2003a

Jiang et al. (2003a) crystallised a voltage gated potassium channel from the thermophilic archaebacteria *Aeropyrum pernix*, which they called the KvAP channel. They hypothesised that the voltage sensor (S4), which is directly attached to the S5 domain by a helical linker, might open the channel by pulling S5, and therefore S6, away from the central pore upon membrane depolarisation. The channel is hypothesised to consist of three layers, with the S5 and S6 domains forming the ion conduction pathway, S1 and S2 forming the next layer, with S3 and S4 on the outer perimeter of the structure. They found that the S3 segment was made of two separate helices, S3a and S3b. S3b and the amino terminus of S4 are tightly packed together, forming a helix-turn-helix structure, termed the 'voltage paddle'. This structure is mainly hydrophobic and highly mobile, and unlike the conventional model, is located at the perimeter of the channel and moves through the lipid upon depolarisation. Biotinylation studies were used to study the movement of the voltage paddle (Jiang et al., 2003b). This technique allows the accessibility of specific, biotinylated residues to the external or internal environment to be investigated in a state dependent manner, as streptavidin can bind to these residues only when they are within 10 Å of the membrane surface. They found the voltage paddle, S3b and the first few residues of S4 to be inaccessible from both the extracellular and intracellular sides at negative membrane voltages, therefore lying deeper than 10 Å from the membrane surface. When the channel was opened, the tip of the voltage paddle and the first two-and-a-half helical turns of S4 moved, and became accessible to the external side of the membrane. They proposed that the voltage paddles move approximately 20 Å from the internal side toward the external side of the membrane, tilting from a horizontal position to a vertical one. This movement of the voltage paddles would allow the channel to open by pulling the S4-S5 linker (figure 1.3B). This 'voltage paddle' model is novel and highly controversial. There is very little experimental evidence that supports this model of voltage sensing over the conventional model.

1.1.2 Structure of the HERG potassium channel

The HERG channel is a 1159 amino acid, 155KDa structure. As previously mentioned, it is a voltage gated channel, so consists of four pore forming (α) subunits, each having six membrane-spanning regions, with large intracellular N-

Figure 1.4

HERG channel structure. **A** Schematic diagram of one subunit of the HERG channel. The channel has 6 transmembrane domains, and large intracellular N- and C-termini. The S4 domain contains several positively charged amino acids which are thought to contribute to voltage sensing. **B** Four α subunits form a functional HERG channel. The S5, P-loop and S6 regions from all four subunits form the pore of the channel, with the S1-S4 transmembrane domains arranged around the pore.

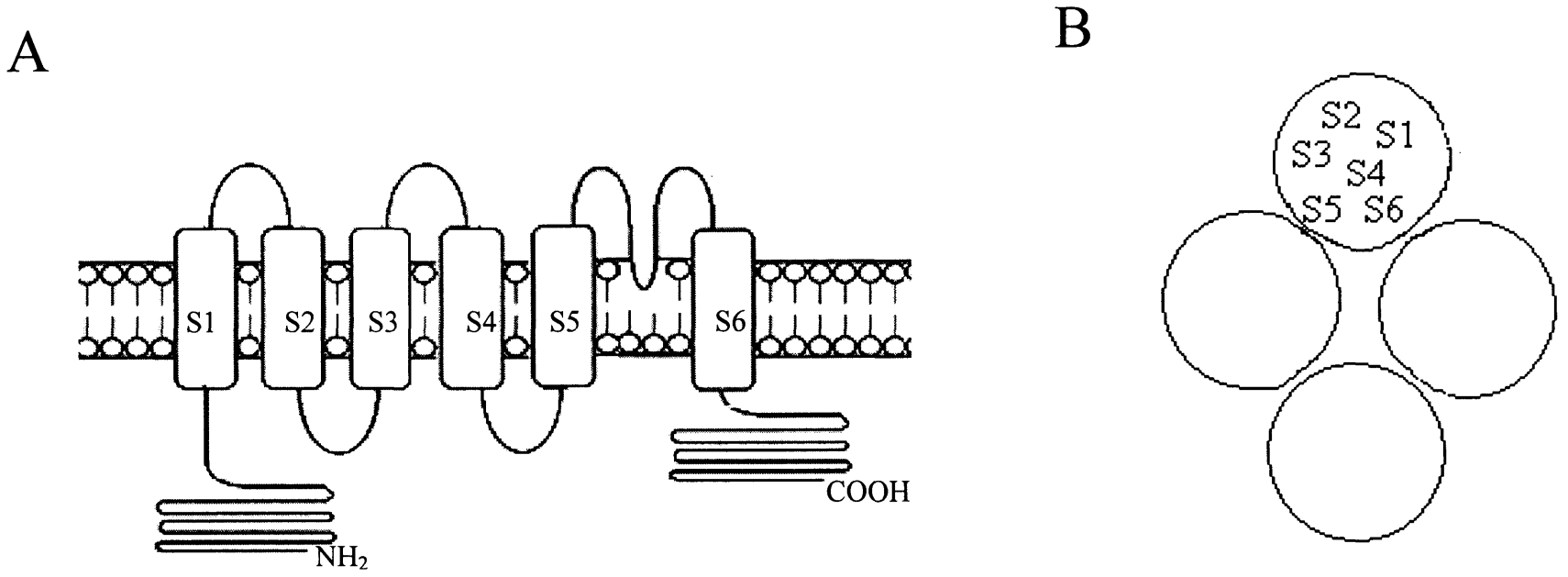

and C- termini. A schematic diagram of the HERG channel can be seen in figure 1.4. Some channels have known auxillary (β) subunits, and it is possible that all voltage dependent potassium channels have them (reviewed in Nerbonne and Guo, 2002). Thus, HERG may form a tetrameric pore-forming complex with an unknown number of β subunits. Identified β subunits have a number of roles, and increase the functional diversity of channels. Co-expression of the α, pore-forming subunits with β subunits often increases surface expression of functional channels. Co-expression can also alter the voltage dependence of activation and/or inactivation, open probability and may even confer properties that they would not otherwise have, such as inactivation (Lewis et al., 2004). β subunits can also modify regulation by signalling molecules and confer new pharmacological properties upon channels.

There is strong evidence that HERG encodes the pore forming subunit of I_{Kr}, a delayed rectifier potassium current (Sanguinetti et al., 1995; Trudeau et al., 1995). Essentially, HERG and I_{Kr} currents are very similar (figure 1.5). However, the current flowing through the HERG channel shows slightly different kinetics to those seen with I_{Kr} *in vivo*. The kinetics of HERG activation and deactivation are about 4 times slower than I_{Kr} (Sanguinetti et al., 1995), suggesting HERG may co-assemble with another subunit to form I_{Kr}. The minimal potassium channel (minK) and the minK related protein 1 (MiRP1), both single transmembrane spanning proteins, have both been implicated as β subunits that co-assemble with HERG to produce I_{Kr} current. However, the contribution of any β-subunits to I_{Kr} is controversial.

Abbott et al. (1999) used co-immunoprecipitation to show MiRP1 and HERG form a stable complex when over expressed *in vitro*. When currents were measured from cells co-expressing MiRP1 and HERG, it was found that deactivation was accelerated and voltage-dependent activation was shifted to more positive potentials. The HERG-MiRP channel also became more sensitive to block by E-4031 and clarithromycin, two well-characterised I_{Kr} blockers. A more recent paper has shown MiRP2 to suppress the expression of HERG when co-expressed in oocytes (Schroeder et al., 2000). Again, this provides evidence that members of the MiRP family of proteins may interact with HERG to form a more I_{Kr}-like current. However, other studies have observed no effect of co-expression of MiRP on

Figure 1.5

The HERG current shows similar properties to I_{Kr}. **A** Representative I_{Kr} recorded from guinea pig ventricular myocytes in response to a standard I-V protocol (described in Chapter 4). **B** Representative HERG current expressed in *Xenopus* oocytes in response to the same I-V protocol. Currents start to activate at around –40 mV, and currents during the test pulse increase until cells are depolarised more positive to around 0 mV, where currents start to decrease, due to an increasing amount of inactivation of channels. Tail currents are indicative of the proportion of activation at each test pulse, and increase up to ~ +10 mV, at which point the channels are maximally activated, and remain maximally activated at voltages positive to this.

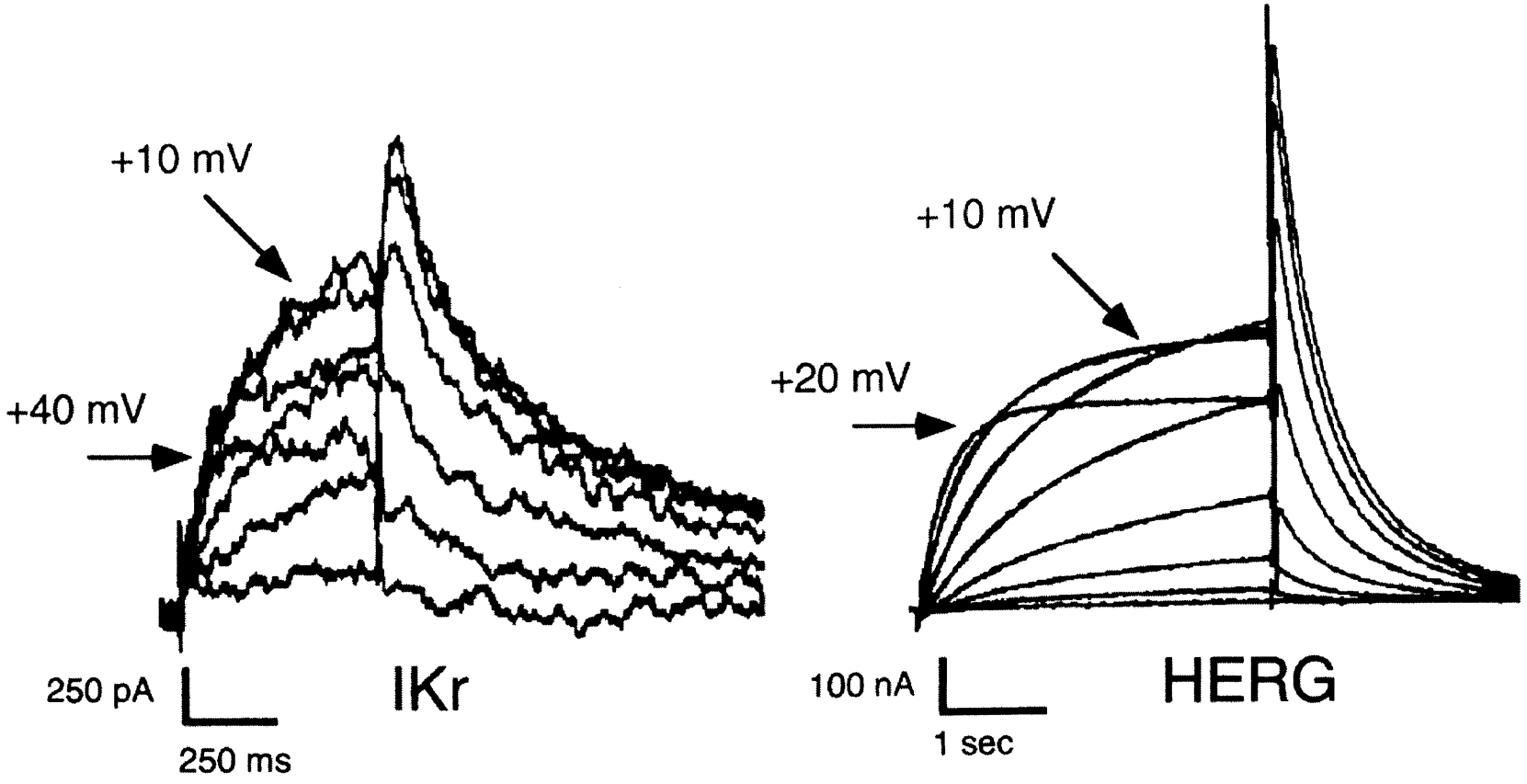

From: Bers (2001)

HERG currents. Weerapura et al. (2002) compared the pharmacological and biophysical properties of the HERG channel expressed in CHO cells with and without co-expression of MiRP1. Co-expression of HERG and MiRP1 did not significantly alter the pharmacological sensitivity of the current to quinidine, E-4031 or dofetilide. The study found co-expression of MiRP1 caused a hyperpolarising shift of voltage-dependent activation, moving it further from I_{Kr}-like properties, and therefore leading the question of how physiologically relevant this alteration would be. The group concluded that MiRP1 did not contribute to the I_{Kr} current carrying complex.

The use of anti-sense oligonucleotides to minK attenuated I_{Kr} (Yang et al., 1995) in AT-1 cells, an immortalised atrial myocyte-derived cell line, and Kubersmidt et al. (1999) showed I_{Kr} was significantly reduced, and deactivation of the current was slower in minK knockout mice. Co-expressing minK with HERG in CHO cells however amplified currents when compared to currents from expression of HERG only (McDonald et al., 1997). This study also observed that minK and HERG form stable complexes when co-expressed in CHO cells, shown by co-immunoprecipitation. Although the data indicates a role for minK in I_{Kr}, the evidence is inconclusive. There is also no direct evidence for co-assembly of HERG and minK in cardiac myocytes. Thus, the contribution of β subunits to the HERG channel remains unresolved.

1.2 Gating properties of the HERG potassium channel

The HERG channel can exist in three different states – closed, open and inactivated - and it is thought these processes are controlled by two gating processes: activation and inactivation. When both the activation and inactivation gates are open, the channel is open and can pass current. When the activation gate is closed, the channel is closed and cannot pass current, even when the inactivation gate is open. If the inactivation gate is closed, but the activation gate is open, the channel is 'inactivated', and cannot pass current. A schematic diagram of this is shown in figure 1.6. Activation and inactivation of the HERG channel are both voltage dependent, and are entirely independent of one another, yet seemingly controlled by a single voltage sensor. The mechanism of how this occurs is still largely unknown. The gating properties of the HERG channel are unusual when compared to other voltage gated potassium channels such as the Shaker channel. The HERG channel

Figure 1.6
The HERG channel has an activation and inactivation gate. Schematic diagram of two gate model of channel gating. In the closed state (**A**) both the activation and inactivation gates are closed, and so no ion flux can occur. **B** Both activation and inactivation gates are open, allowing ion flux. This is the only state in which the channel can conduct. **C** The activation gate is open, however the inactivation gate is closed, so ion flux cannot occur, thus the channel is inactivated.

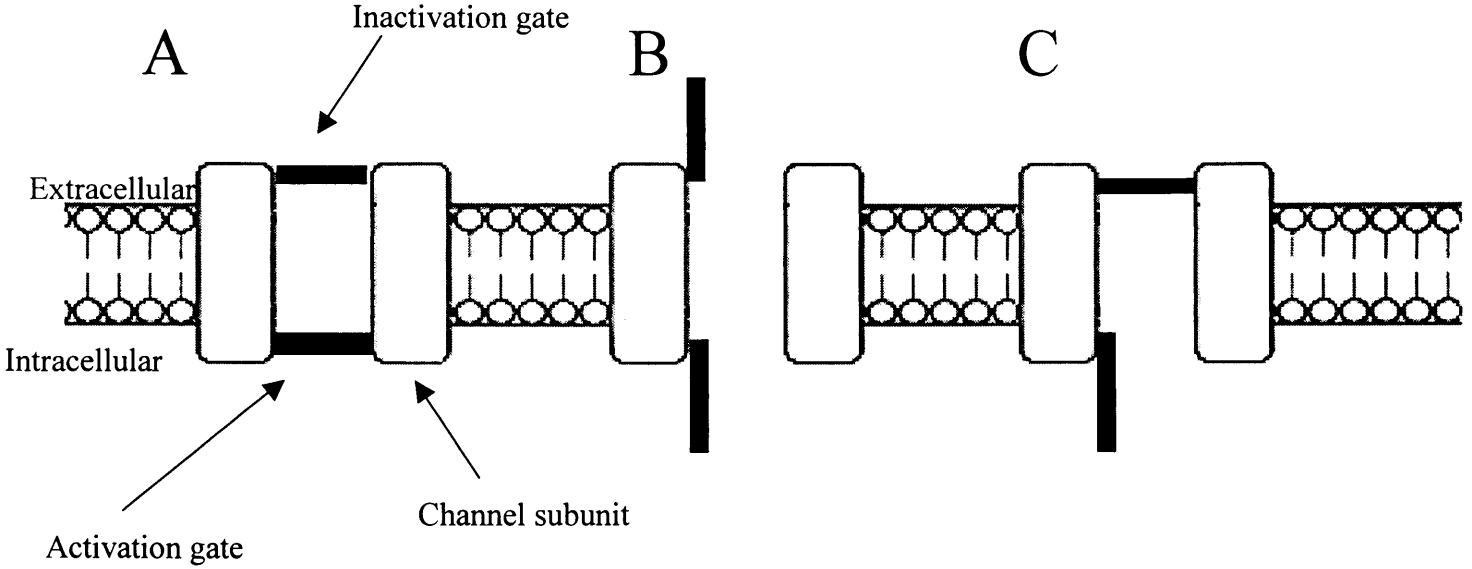

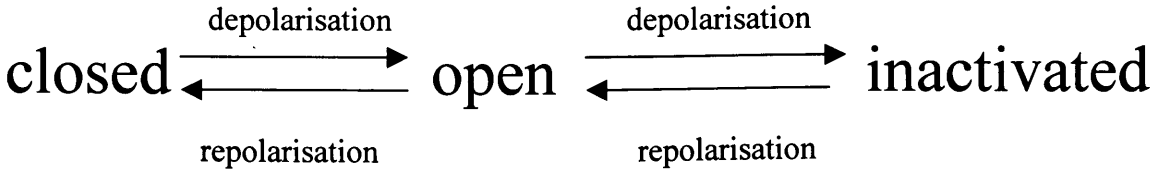

shows slow activation and deactivation, but a very significant rapid inactivation of the current during membrane depolarisation (Zhou et al., 1998; Tristani-Firouzi and Sanguinetti, 2003). The HERG current displays inward rectification. Traditionally, an inward rectifier is a channel that favours entry of ions in the inward rather than outward direction. Thus, conductance is larger upon hyperpolarisation than depolarisation. HERG current decreases at membrane potentials positive to ~0 mV. This decrease is due to an increasing amount of inactivation at positive potentials. Thus, the HERG channel exhibits a 'window current' (shown in figure 1.7). At membrane potentials below –50 mV the activation gate is not open, so no current can pass (refer to figure 1.6A). As the membrane potential becomes more positive, the activation gate of channels opens, so current can pass (figure 1.6B). However, inactivation also increases over this voltage range, so although the number of channels activated increase, the proportion of channels inactivated also increases, thus decreasing current availability. Therefore, any shifts in the voltage dependence of activation or inactivation can profoundly alter current amplitude.

1.3 Physiological roles of the HERG channel

HERG is a member of the ether-a-go-go (EAG) family of ion channels, and is most abundantly expressed in the heart (Pond and Nerbonne, 2001). It is also expressed in neuronal tissue and some cancerous tissues, namely those of epithelial, muscle and neuronal origin. The roles of HERG expression in these tissues will be discussed in this section.

1.3.1 Role of HERG in the heart

There is now strong evidence that HERG encodes the α, pore-forming subunit of I_{Kr}, a delayed rectifier potassium current (Sanguinetti et al., 1995; Trudeau et al., 1995). I_{Kr}-like channels were first described by Shibaski et al. (1987), when investigating I_K in sinoatrial node and atrialventricular nodal cell of the rabbit. This study described a current which increased in amplitude with increased extracellular potassium, that was highly selective for potassium and had a single current conductance of 11 pS. The current also showed a decrease in open probability with progressively larger depolarisations, and showed a fast onset and removal of inactivation. The study also described the channel as an inward rectifier as a result

of this inactivation. I_K was later separated pharmacologically into its two components: I_{Kr} and I_{Ks} (Sanguinetti et al, 1995).

Although not identical, HERG and I_{Kr} currents have similar kinetics (Hancox et al., 1998, figure 1.5). Both I_{Kr} and HERG are blocked by class III anti-arrhythmic drugs, the antihistamine terfenadine and the antipsychotic serindole amongst others (Brown and Rampe, 2000), and both HERG and I_{Kr} have similar single channel conductance values of around 12 pS (Sanguinetti et al., 1995). A paradoxical increase in amplitude of both HERG and I_{Kr} is seen when extracellular potassium concentration is increased, and when HERG is expressed in mammalian cell lines, the current itself is similar to that of I_{Kr} (Sanguinetti et al., 1995). I_{Kr} is one of several currents responsible for termination of the plateau phase, and repolarisation of the cardiac action potential. I_{Kr} activates slowly upon depolarisation, so does not play a role in the initial phases of the cardiac action potential. It instead plays a vital role in the latter stages of the cardiac action potential, when the outward current contributes to the repolarisation of the cardiac action potential. It is the balance of slow activation and deactivation, along with fast inactivation and recovery from inactivation of the channel that gives the current the ability to contribute to the repolarisation of the action potential so effectively. Therefore, if kinetics or amplitude of the HERG/I_{Kr} current are altered, repolarisation of the cardiac action potential is compromised. Other delayed rectifier potassium currents that contribute to the repolarisation of the cardiac action potential are I_{Ks} (slow delayed rectifer potassium current that contributes to the action potential in the ventricles) and I_{Kur} (ultra rapid delayed rectifier potassium current which contributes to atrial repolarisation) (Roden, 2002). The details of these currents, along with I_{Kr}, are shown in table 1.1.

Figure 1.7

HERG current properties. The HERG current is a window current. Activation of the channel increases as membrane potential becomes more positive from –50 mV. The $V_{0.5}$ of activation is –22.39 ± 0.84 mV. However, inactivation of the channel also increases as membrane potential becomes more positive, causing less availability of current. The $V_{0.5}$ of inactivation is –72.89 ± 1.98 mV. The steady state amplitude of current is defined by the area under both curves and is known as a window current. This data was obtained using whole cell patch clamp at 37°C from HEK cells stably expressing HERG. n=26 for activation measurements, n=13 for inactivation measurements.

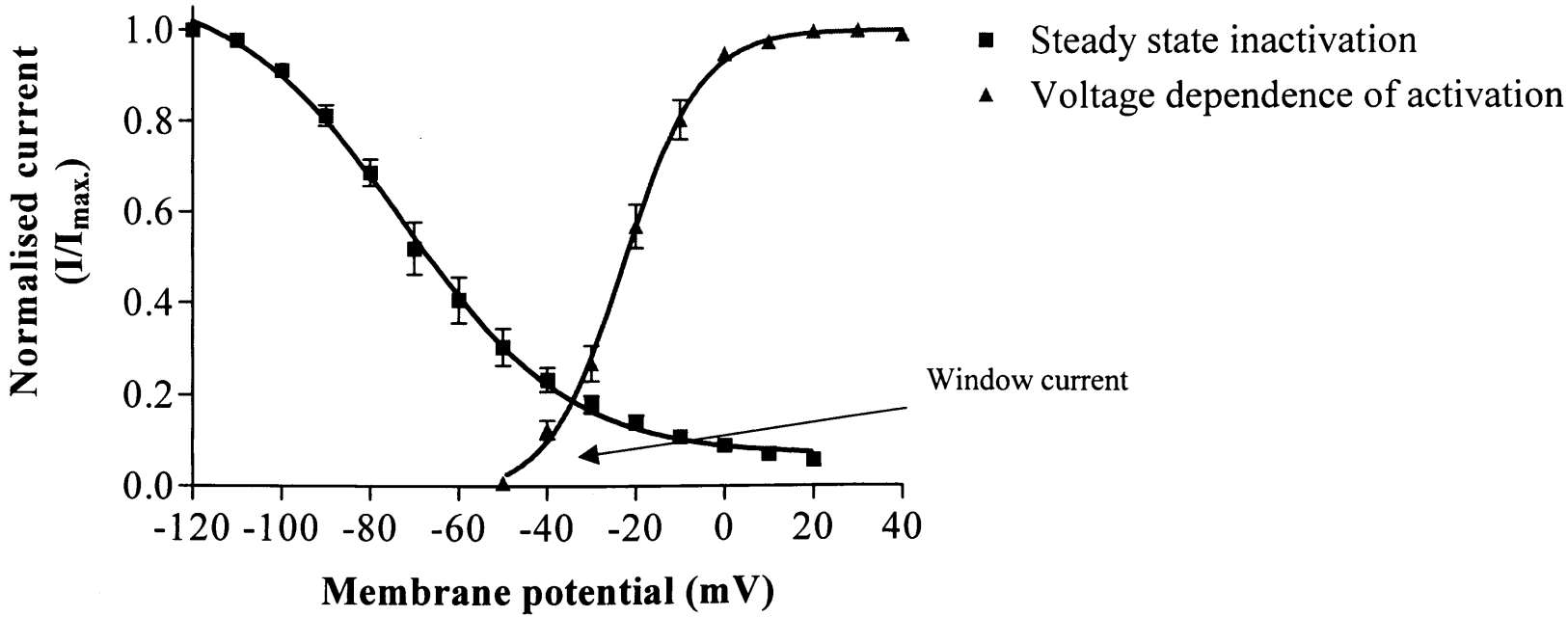

1.3.1.1 HERG current and Long QT Syndrome

Attenuation of potassium ion flow through the delayed rectifier cardiac channels can lead to long QT syndrome (reviewed in Witchel and Hancox, 2000). This causes abrupt loss of consciousness or sudden death from ventricular arrhythmia in both children and adults. It can be clinically identified on a body surface electrocardiogram (ECG), shown as a lengthening of the interval between the Q and T points (figure 1.8A and B). The interval between these two points on the ECG is representative of the time from the ventricular action potential upstroke to repolarisation. Long QT syndrome is more common in females. The QT interval is known to change with age in healthy subjects. Males and females have similar QT interval lengths during childhood, but it is shorter in adult males than females (Locati et al., 1998). This difference may induce a bias, which would favour long QT syndrome diagnosis in adult females. Long QT syndrome increases an individuals risk of cardiac arrhythmias such as Torsades de Pointes (twisting of the points, shown in figure 1.8C). In this arrhythmia, rapid cardiac contractions result in reduced ventricular filling, reduced cardiac output, and therefore a decreased blood flow to the brain, resulting in loss of consciousness. This condition can develop into ventricular fibrillation, which can be fatal. Long QT syndrome is often precipitated by stress, and it is thought that this increased sympathetic stimulation of the heart causes an increased cardiac calcium current during repolarisation. In healthy patients, sympathetic stimulation also causes a concurrent increase in the delayed rectifer potassium current I_{Ks} (discussed later), thus shortening action potential duration and protecting the heart from premature excitation caused by the large calcium current. However, in patients with long QT syndrome, this protection cannot be given, leading to early after depolarisations (EADs), caused by the increased calcium current (reviewed in Roden et al., 1996). These are observed during the repolarisation phase of the action potential, and are thought to maintain or initiate Torsades de Pointes by triggering multiple action potentials.

There are different forms of long QT syndrome. Long QT syndrome can be inherited, where the HERG gene contains mutations that reduce the function of the channel (Curran et al., 1995). There are over 100 known mutations that can occur in the HERG channel alone that can cause this. Mutations in other genes can also cause long QT syndrome. These genes encode for a variety of proteins including minK and MiRP1, ankyrin B and KCNQ1 (which

Table 1.1

Shows a summary of the kinetics of the delayed rectifier potassium currents involved in the repolarisation of the cardiac action potential

Current	Gene	Activation Kinetics	Inactivation Kinetics	Deactivation Kinetics	Associated subunits?
I_{Kr}	KCNH2 (HERG)	Rapid	Very rapid	Slow – over several seconds	MinK? Mirp1?
I_{Ks}	KCNQ1	Slow - over several seconds	No inactivation	Slow	MinK
I_{Kur}	KCNA5	Ultra-rapid 2-20mSec	No inactivation		Kvβ1 Kvβ2

Adapted from Hille (2001) and Roden et al. (2002)

Figure 1.8

Long QT syndrome is shown on a body surface ECG, and can lead to fatal arrhythmias. **A** Representation of a body surface ECG under normal conditions (i) and with long QT syndrome (ii). The interval between the Q and T points on the body surface ECG is characteristically lengthened, due to a longer period of repolarisation. **B** Long QT syndrome can lead to cardiac arrythmias such as Torsade de Pointes, for which a representative ECG is shown.

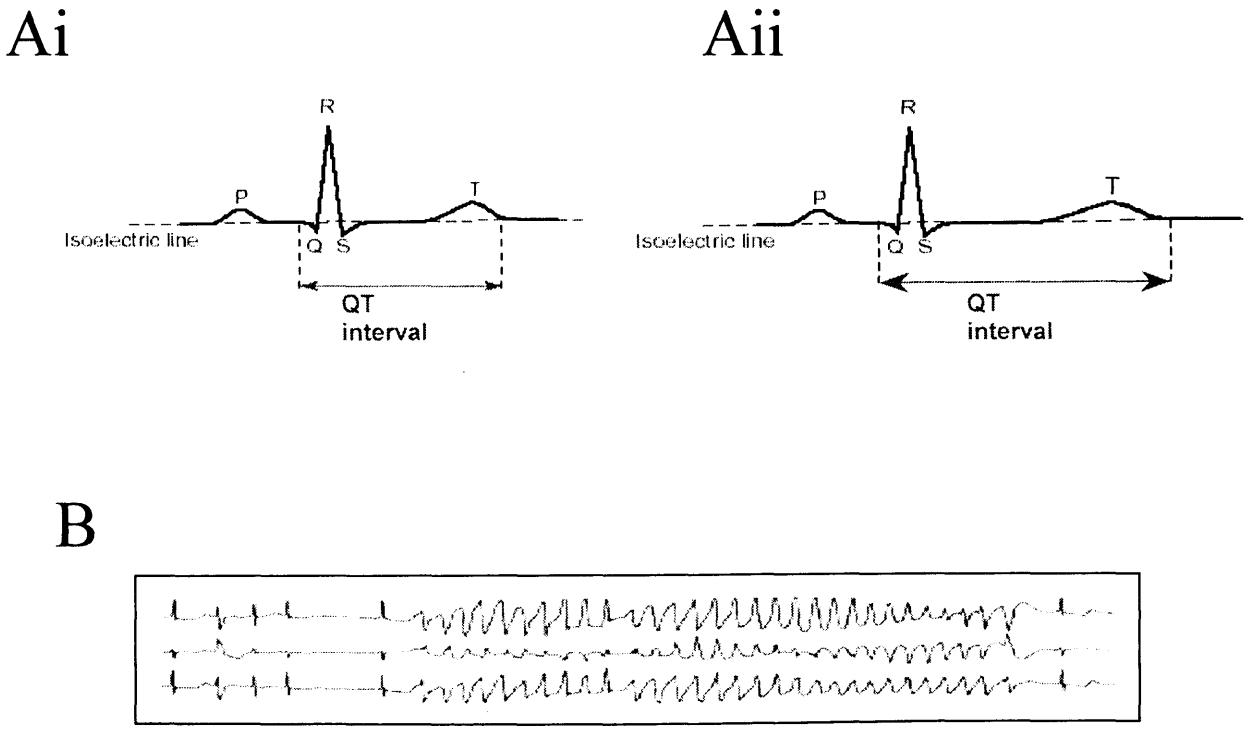

From Vandenberg, 2001

encodes the pore-forming subunit of I_{Ks}). Long QT syndrome can also be acquired (Spector et al., 1996; Busch et al., 1998; Chouabe et al., 1998). HERG/I_{Kr} current can be attenuated by many compounds and drugs. These are diverse in both structure and function, and include class III anti-arrhythmics such as ibutilide and quinidine, antibiotics such as erythromycin, anti-histamines such as terfenadine, calcium channel blockers such as bepridil, and anti-psychotics such as sertindole and pimozide (Fermini and Fossa, 2003). This promiscuous block of the channel is thought to be partly due to the HERG channel having an unusually large inner vestibule, which can trap drugs, causing an increased binding affinity (Mitcheson et al., 2000). Although the exact mechanism of block that these diverse compounds have upon the HERG channel is unknown, HERG is also unique in that it has two aromatic amino acid residues that face into this cavity, which may allow HERG to form hydrophobic, polar and cation-π interactions with drugs and make HERG more susceptible to drug block. Thus, HERG is linked to drug induced and inherited forms of long QT syndrome and the associated increased incidence of fatal arrhythmias.

1.3.2 The role of HERG in cancerous tissue

The role of HERG in non-excitable cells is yet to be fully elucidated. Studies have shown both HERG mRNA and protein to be expressed in a number of cancerous tissues of various origins. These include human melanoma cells (Meyer et al, 1998), atrial tumour cells (Bhattacharyya et al., 1997; Kabir et al., 2000), human endometrial cancer cells (Cherubini et al., 2000) and human prolactin secreting adenoma cells (Bauer et al., 2003), amongst others. The expression of HERG in primary tissues has also been shown to be specific to cancerous growth over benign tumour growth (Lastraioli et al., 2004). Smith et al. (2002) showed HERG mRNA was up-regulated in a number of different cancerous cell lines, with HERG current amplitude corresponding to this up-regulation. Exactly why HERG is expressed in these tissues has not been reported, prompting the question 'Do non-excitable cells become cancerous because they express HERG, or do they express HERG because they are cancerous?' Altered setting of the resting membrane potential (V_{REST}) may contribute to tumour cell growth. Tumour cells expressing HERG show a more depolarised V_{REST} than non-expressing cells (Bianchi et al., 1998), which may provide optimal conditions for unlimited tumour cell growth. Studies have shown HERG-expressing cells, including tumour

cells, to proliferate at a faster rate than non-HERG expressing cells (Wang et al., 2002a; Smith et al., 2002). This proliferation can be blocked using the HERG-specific blockers dofetilide and E-4031, suggesting it is HERG conductance that causes the increased proliferation rate. However, the link between these factors has not been elucidated.

HERG channels have also been implicated as pro-apoptotic proteins. Wang et al. (2002a) showed both HEK 293 cells expressing the HERG protein, and tumour cells expressing HERG endogenously, including SK-BR-3 cells (human mammary gland adenocarcinoma cells), SH-SY5Y cells (neuroblastoma cells) and HL-1 cells (rat atrial tumour cells), all to be more susceptible to apoptosis after insult, compared to cells not expressing the HERG protein, including the tumour cell lines A549 and SK-Mel-28. The same group later investigated the possible secondary messenger pathways involved in HERGs pro-apoptotic property (Han et al., 2004). In this study, expression of the HERG protein in HEK 293 cells increased apoptosis in response to H_2O_2 insult, compared to non-transfected HEK 293 cells. Expression of pro- and anti-apoptotic proteins was altered in cells expressing the HERG protein. Expression of the active forms of caspases 3 and 9, executioners of apoptosis, was raised in both basal and apoptotic cells compared to wild type cells. The active forms of the pro-apoptotic proteins p38 mitogen activated protein kinase (MAP kinase) and stress activated protein kinase (SAP kinase) were also increased in apoptotic cells expressing HERG. The pro-apoptotic effects of HERG, and expression of other pro-apoptotic proteins in these cells could be inhibited using the HERG-specific blockers dofetilide or E-4031, suggesting apoptosis was down-stream of HERG conductance. The authors suggested that an increased HERG conductance would lead to a large potassium efflux, perhaps leading to cell shrinkage. This cell shrinkage would initiate activation of death signalling proteins, such as p38 MAP kinase, or SAP kinase. This leads to an increased caspase activity, which causes cell death. Of course, these studies were carried out on the HEK 293 cell line, which is not a cancerous cell line. But if HERG is pro-apoptotic, as shown in the above studies, the question of why it is expressed in tumour cells, which are apoptosis resistant, must be asked. No studies have yet addressed this question.

In summary, although a number of observations have been made regarding cancerous cells expressing the HERG channel, the exact mechanism and reason behind an increased expression of the channel in cancerous tissues remains elusive.

1.3.3 HERG channels in neuronal tissue

In the nervous system, voltage gated potassium channels play an essential role in controlling cellular excitability by regulating action potential waveform and firing frequency, and regulating interspike membrane potential. However, as in cancerous tissue, the role of HERG expression in neuronal tissue is not yet fully understood. There is a wide distribution of ERG channels in neuronal tissue. Using the reverse transcription polymerase chain reaction (RT-PCR) and immunohistocemisty, ERG channels were shown to be expressed in a number of regions of the central nervous system, including the olfactory bulb, cerebral cortex, hippocampus, hypothalamus and cerebellum (Papa et al., 2003). ERG expression has also been shown in cerebellar Purkinje neurons (Sacco et al., 2003). Emmi et al. (2000) showed ERG channels expressed in hippocampal astrocytes and glia may contribute to the control of neuronal excitability by an indirect mechanism involving glial cells. Further evidence towards this hypothesis was provided by Meves et al. (1999) and Selyanko et al. (2000), who showed ERG channels may be involved in control of sub-threshold properties of neurons, as they underlie the slow component of the M-current expressed in neuroblastoma-glioma hybrid cells. The M-current is a low-threshold slowly activating potassium current that exerts negative control over neuronal excitability, and is inhibited by activation of the $G_{q/11}$-coupled signalling pathway.

It has been hypothesised that ERG may also contribute to neuronal survival in response to ischaemic insult. ERG1 channel currents (found primarily in the heart) are enhanced upon oxididative stress, and in response to reactive oxygen species (ROS) whereas ERG2 and ERG3 channel currents (found primarily in neuronal tissue) are not altered (Taglialatela et al., 1999). ERG1 transcripts are expressed in inhibitory interneurons in the cortex and hippocampus (Saganich et al., 2001), which are highly resistant to ischaemia, whereas ERG2 and ERG3 are expressed in CA1 pyramidal neurons, which are highly vulnerable to ischaemic insult, leading to the speculation that ERG channels may play a role in cell survival (Saganich et al., 2001). Of course, many other cellular factors are likely to differ between these cell types, and no studies have directly investigated the role of neuronal ERG in cell survival, so this role is purely speculative. ERG expression has been shown in the subventricular zone (Papa et al., 2003), which is an important layer in the differentiation and proliferation of stem cells. Although no studies have been carried out on the effect of ERG

on stem cells, it may be that ERG expression drives differentiation and proliferation in this region of the central nervous system.

In summary, although a number of observations about ERG channel expression in neuronal tissue have been made, speculating a role for ERG in neuronal excitability, cell survival and cell differentiation and proliferation, firm conclusions about the role of ERG expression in neuronal tissue are yet to be made.

1.4 Cellular signalling

The activity of cellular proteins can be altered, or modulated, by numerous signals from both the extracellular and intracellular environments. Modulation mostly occurs *in vivo* in response to extracellular stimuli, such as hormones, light and chemical stimuli (so called 'first messengers'). Cells are able to transduce these extracellular signals across the membrane via receptor proteins. G-protein-coupled receptors (GPCRs) are ubiquitously expressed, seven transmembrane domain spanning proteins, to which a specific extracellular signalling molecule can bind. GPCRs are coupled to a family of GTP binding proteins (G-proteins). G-proteins are the middle segment of a signal transduction mechanism in the cell, and couple receptor activation with effector molecules such as kinases and ion channels. G-proteins consist of three subunits, α, β and γ. Guanine nucleotides bind to the α subunit, which has catalytic activity to convert GTP to GDP. The β and γ subunits are hydrophobic and remain associated as a complex. When an agonist is bound to a GPCR, a conformational change occurs, causing the receptor to have high affinity for $\alpha\beta\gamma$. Association of this complex with the receptor causes bound GDP to dissociate and be replaced with GTP. This in turn causes dissociation of α from $\beta\gamma$. Both G-protein components are freely diffusible within the membrane, and are promiscuous in the sense they can interact with numerous different effector proteins. This interaction is terminated by hydrolysis of GTP to GDP, by the GTPase activity of the α subunit. The α subunit then reunites with the $\beta\gamma$ complex, thus completing the cycle (reviewed in Rang et al., 1998). The product of G-protein action on an effector molecule is often a 'second messenger' (see below). Second messengers can then act on further effector proteins to cause a signalling cascade, or act directly on target proteins, such as ion channels. Modulation of ion channels by second messengers can alter their activity by several mechanisms. Current amplitude can be altered by shifts in the voltage

dependence of activation and/or inactivation, and modulation can also alter the open probability of the channel to alter current amplitude. This alteration of channel properties can be due to phosphorylation of the pore-forming subunits, recruitment of accessory proteins, or phosphorylation of a β subunit. Examples of all of these mechanisms of modulation of a variety of ion channels will be discussed throughout this chapter.

1.4.1 G-protein subtypes and signal transduction

There are more than 18 different genes and splice variants encoding the α subunits of G-proteins, 5 genes encoding the β subunits and more than 12 genes encoding the γ subunit. This means there is potential for many different trimers. However, not all β subunits can combine with all γ subunits, so this limits the number of combinations. The α subunit tends to determine the function of the G-protein, and the function of the G_s, G_i and $G_{q/11}$ G-protein families will be discussed in this section. However, the βγ complex can also act on target proteins. This will be discussed in more detail later.

1.4.1.1 Cyclic 3', 5'-adenosine monophosphate (cAMP) coupled G-proteins

The G_s protein is coupled to numerous GPCRs, including the β-adrenergic receptors. When activated, G_s activates adenylyl cyclase. Adenylyl cyclase synthesises cAMP from ATP, so this activation of adenylyl cyclase causes an increased synthesis of cAMP. The effects of cAMP will be discussed later in this section. The G_i protein negatively couples to adenylyl cyclase when activated, thus decreasing its activity and therefore decreasing cytosolic cAMP levels. Thus, the cAMP levels are regulated by a number of GPCRs in one of two ways. Figure 1.9 shows these cellular pathways. Adenylyl cyclase is expressed in a number of tissues, including brain, retina, lung, testis, skeletal muscle and the heart (Simonds, 1999). There are nine mammalian adenylyl cyclase isoforms, ranging between 1164-1353 amino acids in size. Types 2, 4, 5, 6 and 7 are expressed in the heart. An overview of how these cardiac isoforms are regulated is given in table 1.2.

1.4.1.2 cAMP signalling

cAMP was the first second messenger to be identified (Sutherland et al., 1965), and it has been shown to effect numerous functions in prokaryotic and eukaryotic cells, such as the shut

down of glycogen synthesis, regulation of gene transcription and growth signalling (reviewed in Gomperts et al., 2003). cAMP can bind to effector proteins to directly alter activity. One of the most well characterised ion channel family that are modulated by cAMP are the hyperpolarisation-activated cyclic nucleotide-gated (HCN) channels. HCN channels belong to the voltage gated channel family, show ~30% homology to the *eag* family of channels, and are found in a variety of cell types, including cardiac myocytes, neurones and photoreceptors (reviewed in Robinson and Siegelbaum, 2003). The channel is open at negative potentials and closes with depolarisation, allowing the current (called I_f in cardiac cells and I_h in neurones) to support pacmaker activity in both the heart and spontaneously spiking neurones (reviewed in DiFrancesco, 1993; Pape, 1996). Elevation of cAMP augments I_f (Brown et al., 1979), and it has since been shown this is not due to phosphorylation of the channel (DiFrancesco and Tortora, 1991). The direct binding of cAMP to the cyclic nucleotide binding domain (CNBD) on HCN channels allows the channel to open more rapidly, and shifts the voltage dependence of activation (DiFrancesco and Tortora, 1991). It has been shown the CNBD domain may actually inhibit HCN channels, with cAMP relieving this inhibition when bound to the CNBD (Wainger et al., 2001). The inhibition and relief by cAMP binding depends on interactions of the CNBD with the core transmembrane domain and the C-linker, a conserved 80-amino acid region linking the S6 transmembrane segment to the CNBD (Wang et al., 2001a). In has since been shown that binding of cAMP to the CNBD by electrostatic and hydrogen bonding interactions produces a conformational change in the CNBD and C-linker, which in turn is coupled to the S6 transmembrane domain to promote channel opening (Zagotta et al., 2003).

Although this evidence shows cAMP can modulate ion channels directly, cAMP can also act as a second messenger to activate protein kinase A (PKA), which regulates a host of processes within the cell, including modulation of ion channels by direct phosphorylation. This will be discussed in the next section of this chapter.

Figure 1.9

The signalling pathways that alter cytosolic cAMP levels. Agonists acting at GPCRs coupled to either G_i or G_s alter the cytosolic cAMP levels. Activation of G_i decreases adenylyl cyclase activity, to deacrease cAMP levels. Activation of G_s increases the activity of adenylyl cyclase, thus increasing cytosolic cAMP levels. cAMP can act as a second messenger itself, directly binding to target proteins. It also causes activation of PKA, which can phosphorylate target proteins.

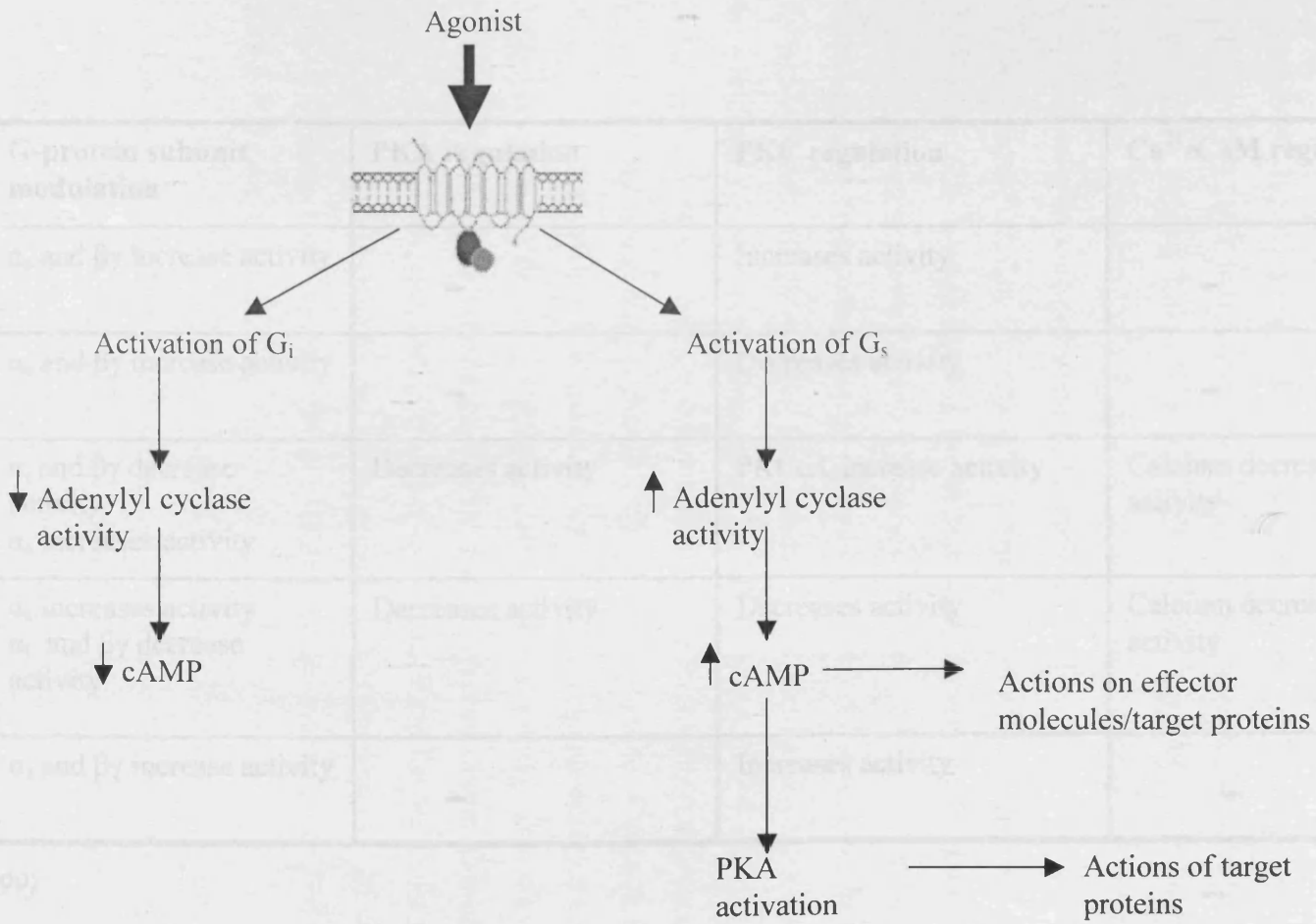

Table 1.2
Regulation of adenylyl cylase isoforms by G-protein, PKA, PKC and calcium-dependent mechanims. Table only includes adenylyl isoforms expressed in the heart.

Adenylyl Cylase subtype	G-protein subunit modulation	PKA regulation	PKC regulation	Ca^{2+}/CaM regulation
AC2	α_s and $\beta\gamma$ increase activity	-	Increases activity	-
AC4	α_s and $\beta\gamma$ increase activity	-	Decreases activity	-
AC5	α_i and $\beta\gamma$ decrease activity α_s increases activity	Decreases activity	PKCα/ζ increase activity	Calcium decreases activity
AC6	α_s increases activity α_i and $\beta\gamma$ decrease activity	Decreases activity	Decreases activity	Calcium decreases activity
AC7	α_s and $\beta\gamma$ increase activity	-	Increases activity	-

Adapted from Simonds (1999)

1.4.1.3 PKA signalling

PKA is a ubiquitous, broad-specificity serine/threonine kinase that is activated by cAMP and consists of a regulatory subunit dimer, and two catalytic subunits. Four cAMP molecules are required in order to activate PKA, with two binding to each of the regulatory subunits. Upon cAMP binding, the regulatory subunit has a decreased affinity for the catalytic subunit, therefore causing dissociation. The catalytic subunits are then able to phosphorylate target proteins. In mammals, there are four regulatory subunit genes (RIα, RIβ, RIIα and RIIβ), and three catalytic subunit genes (Cα, Cβ, Cγ; reviewed in Gomperts et al., 2003). PKA is compartmentalised within the cell through binding of the regulatory subunit to subcellular structures by A kinase anchoring proteins (AKAPs; discussed later). PKA is a known modulator of ion channel activity, modulating channels such as the Kv4.2 potassium channel, a voltage dependent, rapidly inactivating channel. This channel is expressed in ventricular myocytes, and on the soma and dendrites of dentate gyrus and hippocampal CA1 and CA3 neurons. It is thought to underlie the A-type potassium current in ventricular myocytes and dendrites. The Kv4.2 subunit has nine putative sites for PKA phosphorylation. Anderson et al. (2000) showed that the Kv4.2 subunit is a substrate for PKA. Using phosphopeptide mapping, two PKA phosphorylation sites on Kv4.2 were defined as functionally important, from the nine putative sites. These are located on the N- and C- termini of the subunit. Phosphorylation of Kv4.2 decreases current, and this is likely to be important for the increase in hippocampal neuron excitability mediated by PKA activation. The presence of an ancillary protein, the K^+ channel interacting protein (KchIP3) is required for PKA phosphorylation of Kv4.2 (Schrader et al., 2002).

The human inward rectifier current $I_{Kir2.2}$ is also modulated by PKA (Zitron et al., 2004). There is growing evidence that Kir2.2 encodes for I_{K1}, an inward rectifier potassium current that plays a significant role in the heart. I_{K1} has importance both in the terminal phase of repolariation of the action potential, and it is essential in maintaining the resting membrane potential (V_{REST}). Activation of PKA by forskolin or Ro-20-1724 significantly increased currents of cloned Kir2.2 channels in *Xenopus* oocytes, which was abolished in the presence of the PKA inhibtor KT-5720. Mutating the single putative PKA phosphorylation site, Ser430, to an alanine, removed all modulation by forskolin and Ro-20-1724, suggesting the effects of these compounds were due to a single phosphorylation of the channel by PKA. *In*

vivo, PKA-mediated attenuation of I_{K1} could induce action potential shortening, which may decrease the risk of of ventricular arrythmias (Miake et al., 2003).

The β-adrenergic receptors are coupled to the G_s-family of G-proteins. Thus, activation of these receptors causes an increase of cAMP in the cell. The β_3-adrenergic receptor and its associated cAMP/PKA second messenger pathway have been implicated in the regulation of I_{Ks}, a delayed rectifier potassium current involved in cardiac action potential repolarisation. Kathöfer et al. (2000) showed that applying isoprenaline to guinea pig cardiomyocytes caused both I_{Ks} activating and tail currents to increase by ~250%. As this may have included contamination by other currents, the study then investigated the effects of isoprenaline on *Xenopus* oocytes co-expressing the I_{Ks} complex (KvLQT1/MinK) and the β_3-adrenergic receptor. Application of isoprenaline increased current by ~99% and shifted the voltage dependence of activation by ~6 mV. Incubating oocytes in cholera toxin, to activate G_s proteins increased basal current significantly, and application of isoprenaline to these cells produced no further increase in current. Taken together, this suggests that G_s proteins are involved in the coupling of β_3-adrenergic receptors and KvLQT1/MinK channels.

1.4.1.3 Gβγ signalling

The βγ complex is able to directly modulate target proteins. The most well characterised of these is the G-protein coupled inward rectifer potassium channel (GIRK channel), that mediate acetylcholine-activated potassium currents in cardiac atrial and nodal cells. Experiments have shown the muscarinic receptors (M_2 and M_4) activate G_i to release βγ, which acts directly on the GIRK channels to activate them (Kofuji et al., 1995; Lei et al., 2000). Evidence has shown the βγ complex remains bound to the membrane during this time, so potential target proteins for βγ must be membrane-, or membrane-associated proteins, which also must carry a consensus motif for βγ binding. Other effects which βγ subunits transduce include inhibition of the L-type calcium channel (Viard et al., 2001), inhibition or activation of adenylyl cyclase (dependent on the type of adenylyl cyclase – see table 1.2; Simonds et al., 1999), and activation of MAP kinase (Guillard et al., 2003).

1.4.2 Phospholipase C (PLC) coupled G-proteins

Upon activation, both G_q and G_{11} increase activity of PLC. The phospholipase C/inositol phosphate pathway was discovered in the mid 1970's when it was noticed that many hormones the caused an increase in free calcium also increased the rate of degradation of phosphatidlyinositols. Later, it was realised that one molecule in particular, phosphatidyl inositol 4,5-bisphosphate (PIP_2) plays a key role in this pathway (Berridge and Irvine, 1984). PIP_2 is hydrolysed by the membrane bound protein phospholipase C (PLC), to form diacylglycerol (DAG) and inositol trisphosphate (IP_3). Both of these products are able to interact with other cellular proteins, and therefore act as second messengers. IP_3 binds to the IP_3 receptor found on the endoplasmic reticulum, to cause the release of calcium from intracellular stores into the cytosol, therefore increasing the cytosolic calcium concentration (Willars and Nahorski, 1995a). DAG directly binds to protein kinase C (PKC), increasing its activity.

1.4.2.1 Calcium signalling

Calcium is an abundant element, and is an important second messenger with a role in regulating many cellular processes, including muscle contraction, cell division and exocytosis. Calcium is tightly regulated both spatially and temporally by a number of signalling pathways. In the heart, intracellular calcium concentration constantly oscillates throughout the cardiac cycle, from 100 nM during diastole to over 1 μM during systole, and intracellular calcium modulates several ion channels. Intracellular calcium ions can have direct effects in gating of channels. Modulation of gating has been shown for calcium, chloride and potassium channels. Calcium-activated potassium channels are ubiquitously expressed, and can be classified into three groups – BK channels (big conductance), SK channels (small conductance), and IK channels (intermediate conductance). As well as having differing conductances, these three channel types differ in their voltage and calcium sensitivity, and pharmacology (reviewed in Hille, 2001). Calcium binds directly to BK channels, at regions called 'calcium bowls' on the C-terminus that contain many negatively charged residues (Schreiber and Salkoff, 1997). However, the SK channels do not bind calcium directly, and require the calcium sensor calmodulin to convey calcium sensitivity (Keen et al., 1999). This differing mechanism of calcium sensing may explain the different calcium sensitivities of the channels.

Another ion channel modulated by calcium is the M-type potassium channel (Gamper and Shapiro, 2003). The M-type potassium channel is present in neurons and plays a major role in determining neuronal excitability. Once class of M-type potassium current is formed from KCNQ2 and KCNQ3 subunits. Gamper and Shapiro used whole cell recording and calcium imaging, carried out simultaneously in CHO cells expressing KCNQ2/KCNQ3 channel heteromultimers. Increasing cytosolic calcium concentration from 80 nM to above 300 nM inhibited current, but this inhibtion was small and variable between cells, suggesting the calcium sensitivity of the channels in a given cell may be due to relative abundence of the channel and an endogenous calcium sensing protein. Transfecting cells with calmodulin increased the calcium sensitivity of the KCNQ2/3 currents, with currents responding quickly to changes in intracellular calcium. There was a strong dependence of the current amplitude on cytosolic calcium concentration. This dependence was lost when cells were transfected with a dominant negative form of calmodulin, which is unable to bind calcium, thus showing calcium sensitivity of KCNQ2/3 channels was mediated via calmodulin. The group also found KCNQ2/3 channel subunits were able to bind calmodulin. Using cultured rat superior cervical ganglion (SCG) sympathetic neurons, and transfecting them with a dominant negative form of calmodulin, the study found calmodulin was a requirement for bradykinin-mediated inhibition of M-current, however, it was not required for muscarinic receptor-mediated inhibition, suggesting there may be different mechanisms for inhibition.

Calmodulin has also been shown to be the calcium-sensor for L-type calcium channels (Peterson et al., 1999). Elevated intracellular calcium causes inactivation of the L-type calcium channel, thus acting as a negative feedback loop to regulate cytosolic calcium concentration. Peterson et al. (1999) suggested calmodulin is likely to be constitutively tethered to the N-terminus of the L-type calcium channel, independent of activation by calcium. However, calcium activation of calmodulin is likely to cause an IQ-like motif (calmodulin binding motif) on the C-terminus of the channel to bind to calmodulin (which remains tethered at the N-terminus), thus causing a conformational change around the intracellular side of the pore, and causing inactivation of the channel.

Thus, although calcium can modulate ion channels by binding to channel subunits, for some channels an intermediate, calcium-sensing protein is required to convey the calcium sensitivity of the channel.

1.4.2.2 Protein kinase C signalling

PKC is a protein expressed ubiquitously in cells. It is a single polypeptide, characterised by an N-terminal regulatory domain, which is between 20-40 kDa, and a C-terminal catalytic domain, which is around 45 kDa. There are also four conserved domains (C1-C4), of which there is high sequence homology within the PKC family. C1 is a cysteine-rich region, which acts as the DAG/phorbol ester binding domain. C2 contains a recognition sequence for acidic lipids and calcium. The C3 and C4 domains are the ATP- and substrate- binding lobes of the kinase core. These four conserved regions are separated by five, isozyme-specific, variable regions. PKC uses MgATP as a substrate, and typically phosphorylates serine or threonine residues. Activation of PKC requires phosphorylation at the catalytic domain and detachment of the pseudo substrate domain (autoinhibitory site) from the active site. DAG activates PKC by binding to a hydrophilic site in the C1 domain, making the domain hydrophobic and allowing C1 to interact with the plasma membrane. This interaction brings about a conformational change to separate the catalytic and pseudo substrate domain, therefore activating the protein. PKC is also activated by a number of other mechanisms. Increased cytosolic calcium activates some isozymes of PKC by causing the C2 domain to bind to phospholipids and bring about dissociation of the catalytic and pseudo substrate domains. Phorbol esters such as PdBu and PMA also activate PKC. Binding of lipids, such as lysophosphatidylcholine and arachidonic acid, activates PKC by inducing a conformational change that removes an autoinhibitory domain from the active site of the enzyme (reviewed in Gomperts et al., 2003). So far, ten different PKC isozymes have been identified, and these can be grouped into three sub-families, which are classified according to the stimuli that activate them. The conventional PKCs (cPKC); α, βI, βII, and γ, all require either phosphatidylserine, calcium, DAG or phorbol esters for activation. These are also known as the calcium-sensitive PKC isoforms. The novel PKCs (nPKC); δ, ε, η and θ, are insensitive to calcium, yet are still activated by phosphatidylserine, DAG and phorbol esters. Finally, the atypical PKCs (aPKC); ξ, ι and λ, are insensitive to activation by calcium, DAG and phorbol esters (reviewed in Mochly-Rosen and Gordon, 1998). Figure 1.10 shows the cellular signalling pathways that result in activation of PKC. PKC is involved in many diverse processes, including receptor desensitisation, regulation of transcription, ion channels, immune responses, cell growth, and learning and memory. Usually, there are several PKC

isozymes within a cell, and the various PKC isozymes clearly mediate different functions. PKC isozymes were among the first signalling proteins to be shown to change their subcellular location upon activation. They undergo translocation from one intracellular compartment to another upon activation (Wolf et al., 1985). There are several proteins that bind PKCs to specific subcellular targets. These substrates that interact with C-kinase (STICKs) link the cytoskeleton to the plasma membrane, bind phosphatidylserine and act as a substrate for PKC. Other PKC binding proteins are receptors for activated C-kinase (RACKs) and proteins interacting with C-kinase (PICKs). These are not substrates for PKC, but do show some specificity for binding PKC isoforms. The primary functions of STICKs, RACKs and PICKs is to position individual PKCs in appropriate positions to allow them to respond to a specific signal, and bring PKC into close proximity to their substrate, thus perhaps restricting any inappropriate phosphorylation events (reviewed in Gomperts et al., 2003).

Protein phosphorylation by kinases including PKC, plays a key role in the regulation of almost all eukaryotic processes. Cellular targets for phosphorylation are broad, and include ion channels, such as the AMPA receptor and the shaker K^+ channel, ion exchangers, for example the Na^+/H^+ exchange, metabolic enzymes such as ATP citrate lyase, and cyclic AMP response element binding protein, (CREB), involved in transcriptional regulation (Shabb, 2001). It is thought that PKC can act both directly and indirectly on ion channels, by directly phosphorylating the channels, or by inducing second messenger phosphorylation cascades, which ultimately lead to the modulation of the ion channel by a messenger downstream of PKC. Ion channels that are known to be regulated by PKC include the ROMK1 channel. Zeng et al. (2003) showed this channel to be inhibited by PKC in a PIP_2 dependent manner. Application of PMA and OAG to wild type and a mutant channel with a reduced PIP_2 sensitivity (containing the point mutation S219A) in *Xenopus* oocytes reduced both wild type and S219A ROMK1 currents, and this attenuation was blocked using the PKC inhibitor calphostin C. The open probability of the channel was reduced with PKC activation, but this could be reversed by direct application of PIP_2 to the cell, suggesting that PKC reduces channel activity by decreasing PIP_2 interactions with the channel. The group concluded that PIP_2 depletion by the PLC pathway was not sufficient for current attenuation, and found PKC

Figure 1.10

The cellular signalling pathways induced by activation of a $G_{q/11}$-coupled GPCR, leading to release of calcium and activation of PKC. Activation of a $G_{q/11}$coupled GCPR activates PLCβ, which hydrolyses PIP_2 to form IP_3 and DAG. IP_3 causes release of calcium from intracellular stores, and DAG activates PKC. Activation of PKC negatively feeds-back to PLCβ.

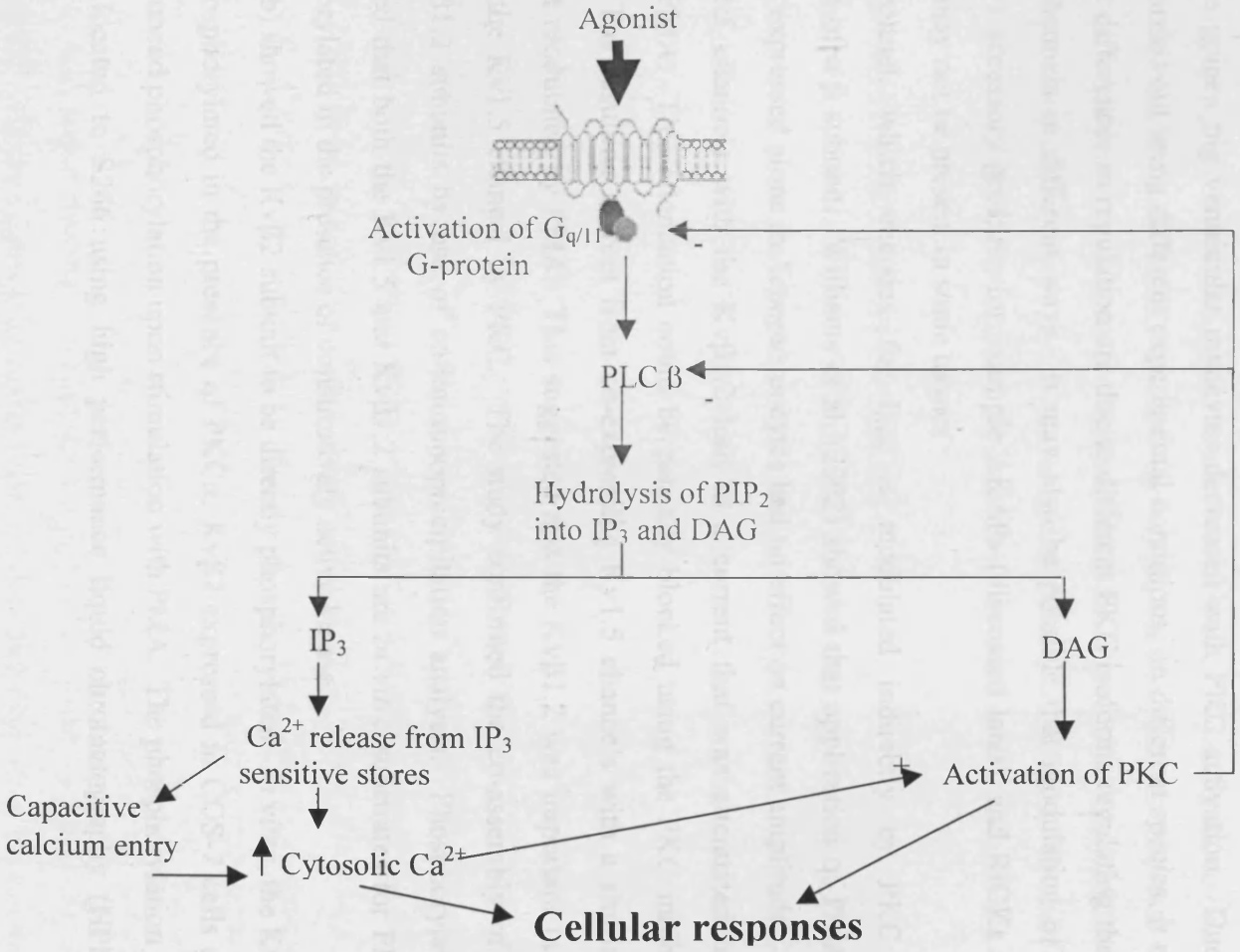

activation caused a further depletion of PIP_2 that cumulatively, caused attenuation of ROMK1 current. However, the mechanism for PKC-mediated depletion of PIP_2 was not investigated in this study.

The L-type calcium channel is another ion channel modulated by PKC. Studies activating PKC have shown a variety of $I_{Ca,\ L}$ responses. Callaghan et al. (2004) showed $I_{Ca,\ L}$ in rabbit portal vein myocytes increased in response to PKC activation, whereas Belevych et al. (2004) showed $I_{Ca,\ L}$ in guinea pig ventricular myocytes decreased with PKC activation. Due to studies being carried out using different experimental conditions, on different species, it may be possible that differences in regulation are due to different PKC isoforms regulating the L-type calcium channels in different ways. It may also be possible that modulation of the channel requires accessory proteins, for example AKAPs (discussed later), and RICKs and RACKs which may not be present in some tissues

The Kv1.5 channel, which encodes for I_{Kur}, is modulated indirectly by PKC by phosphorylation of a β subunit. Williams et al. (2002) showed that application of PMA to Kv1.5 channels expressed alone in *Xenopus* oocytes had no effect on current amplitude. Co-expressing Kv1.5 channels with the Kvβ1.2 lead to a current that was attenuated upon application of PMA. This attenuation could be partially blocked using the PKC inhibitor chelerythrine. The resulting current from co-expressing Kv1.5 channels with a similar β subunit was not modulated by PMA. This suggested that the Kvβ1.2 was important in the modulation of the Kv1.5 channel by PKC. The study confirmed the co-assembly of the Kv1.5 and Kvβ1.2 subunits by use of co-immunoprecipitation analysis. Phosphorylation assays confirmed that both the Kv1.5 and Kvβ1.2 subunits are *in vitro* substrates for PKC, and are phosphorylated in the presence of constitutively active kinase.

Liu et al. (2003b) showed the Kvβ2 subunit to be directly phosphorylated. *In vitro*, the Kvβ2 subunit was phosphorylated in the presence of PKCα. Kvβ2 expressed in COS-7 cells also showed a pronounced phosphorylation upon stimulation with PMA. The phosphorylation site on Kvβ2 was located to S266 using high performance liquid chromatography (HPLC) analysis.

1.5 Modulation of the HERG potassium channel by second messengers

The study of how HERG and I_{Kr} are modulated by native signalling pathways is still in its infancy. The HERG channel contains putative protein kinase A, B and C phosphorylation sites, as well as a cyclic nucleotide binding domain (CNBD), a tyrosine kinase phosphorylation site, 21 casein kinase II phosphorylation sites and a Per-Arnt-Sim (PAS) domain (figure 1.11), suggesting that the channel may interact with other molecules, and may be modulated by many different mechanisms. There have been several studies carried out that show the modulation of the HERG channel by protein kinases and cAMP, although responses between these studies vary greatly. These differences in results are likely to be due to the difficulties encountered when trying to isolate different branches of the second messenger pathway, along with differences between tissue types and expression systems.

1.5.1 $G_{q/11}$-activated signalling modulation of HERG

As previously described, activation of the PLC signalling pathway may cause a depletion of PIP_2 in the cell, activation of PKC and a release of calcium from IP_3 sensitive calcium stores. In this section modulation of HERG and closely related channels by these three mechanisms will be reviewed.

1.5.1.1 Modulation by phospholipids

PIP_2 has been shown to have direct effects on HERG current expressed in CHO and HEK cells (Bian et al., 2001). Directly perfusing PIP_2 into the cell increased HERG current amplitude by between 20-80%, negatively shifted voltage dependent activation of the current by 10 mV and accelerated activation. The voltage-dependence of inactivation was not significantly altered. However, the time-dependence was slowed in the presence of increased PIP_2 levels. Neither deactivation nor single channel conductance were altered with increased PIP_2 levels. Using a monoclonal antibody that disrupts interactions with PIP_2 decreased HERG current significantly, and voltage dependent activation was shifted by +7 mV. Stimulating the α_1-adrenergic receptor, therefore activating the PLC pathway, in the presence of BAPTA and PKC inhibitors attenuated current, which was abolished when an excess of PIP_2 was present. This study suggests a role of PIP_2 in the modulation of the HERG channel. When PIP_2 is depleted, HERG current is attenuated. The study suggested a direct interaction

Figure 1.11

The intracellular face of the HERG channel has numerous putative sites of phosphorylation. The HERG channel contains four putative PKA phosphorylation sites, 18 putative PKC phosphorylation sites, two PKB phosphorylation sites, one cyclic nucleotide binding domain (CNBD), one putative tyrosine kinase phosphorylation site and a Per-Arnt-Sim (PAS) domain. Not shown on the below cartoon, the HERG channel also contains 21 putative casein kinase II phosphorylation sites.

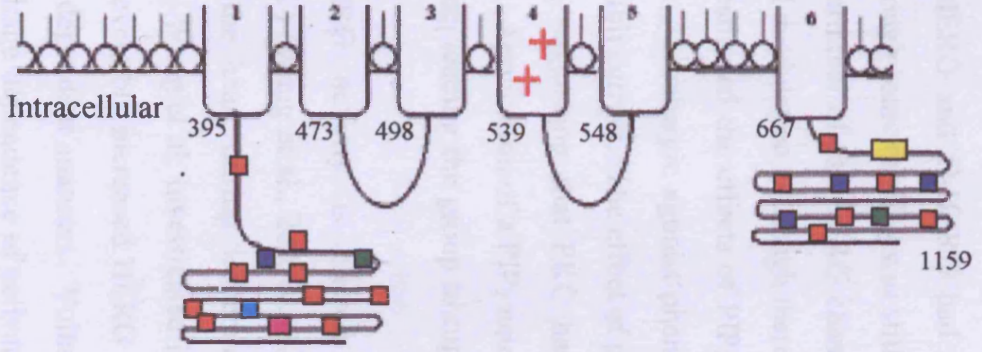

PKA phosphorylation site

PKC phosphorylation site

PKB phosphorylation site

Cyclic nucleotide binding domain

Tyrosine kinase phosphorylation site

Per Arnt Sim domain

between PIP_2 and HERG. Recently the same group studied the interaction between PIP_2 and the HERG channel further, using two HERG mutants (Bian et al., 2004). Charged segments of ion channels have been proposed as potential PIP_2 binding sites (e.g. in K_{ATP} channels, Fan and Makielski, 1997). The HERG channel contains a charged segment in the C-terminus of the channel, between residues 881-894. Bian et al. created two HERG mutants, a framedeletion of the entire charged segment (D-HERG), and a channel in which numerous mutations had been carried out to neutralise the charged segment (M-HERG). Both M-HERG and D-HERG lost the ability to be modulated by PIP_2. Using a PIP_2 binding assay, the group showed both M-HERG and D-HERG had inpaired ability to bind PIP_2 when compared to WT HERG, although some binding was still observed. The group concluded the site they mutated on the C-terminal of the HERG channel seems to be responsible for the majority of the PIP_2-mediated modulation, although there may be second PIP_2 binding site on HERG. This study also investigated the effects of PIP_2 in I_{Kr} in isolated rabbit ventricular myocytes. They found the α_{1A} adrenergic agonist phenlyephrine, which would activate the $G_{q/11}$-coupled pathway, to inhibit current. The effect of phenylephrine was accentuated in the presence of PKC inhibitors, suggesting that PKC has effects to increase current when stimulated in this cell system. Application of a PIP_2 neutralising antibody had similar effects to application of phenylephrine, leading the group to suggest that I_{Kr} is attenuated by a PIP_2-dependent mechanism.

Other studies suggest HERG activity is altered by the phospholipid metabolite lysophosphatidylcholine (LPC) (Wang et al., 2001b). LPC is present in a variety of tissues, can accumulate rapidly in the heart during ischemia and can induce action potential shortening (Liu et al., 1991). Wang et al. investigated if this was due to an interaction with HERG. They showed LPC reversibly increased HERG current when applied extracellularly to HEK cells, in a voltage dependent manner. Voltage dependence of inactivation was shifted by +20 mV, while voltage dependence of activation was unaltered. The same group (Wang et al., 2004), have shown enhancement of HERG to be specific to lysophospholipids with 16 hydrocarbons. Enhancement of current was not due to incorporation of LPCs into the membrane, nor was it due to second messenger modulation of HERG. The group hypothesised that it was due to a direct interaction between LPCs and HERG. The group also noted a difference of voltage-dependent effects between lysophospholipids of different

headgroup charge. They hypothesised that this was due to positively charged headgroups only being able to bind to negative charges on HERG, whereas headgroups containing both positive and negative charges could bind to both negative and positive charges on HERG. The study was not able to test this hypothesis directly.

1.5.1.2 Receptor dependent modulation of I_{Kr}

Early studies carried out on guinea pig ventricular myocytes showed PKC to increase I_K (Tohse et al., 1987). These studies were carried out prior to I_K being separated into its two components, I_{Kr} and I_{Ks}. Application of 12-O-tetradecanoylphorbol-13-acetate (TPA) increased I_K, but only when cytosolic calcium was at concentrations higher than 10^{-10} M. The authors postulated that calcium may modulate the current directly during calcium transients, but when calcium was at a lower concentration PKC would modulate the current, therefore allowing constant modulation of the current.

Heath and Terrar (2000) showed the involvement of PKC in the modulation of I_{Kr}, the native HERG current. This study was carried out using sharp electrode or perforated patch clamp to avoid dialysis of intracellular components out of the cell. Application of isoprenaline or forskolin to ventricular myocytes increased the tail currents of I_{Kr} by 50% and 73% respectively, and shifted voltage dependent activation more negative by 5 mV and 10 mV respectively. Isoprenaline and forskolin both activate PKA (via an elevation of cytosolic cAMP), so initially it was suggested that PKA modulated HERG current. The intracellular pathway underlying the response to isoprenaline and forskolin was investigated by the use of PKA and PKC inhibitors. Incubation of the cells in staurosporine, a non-specific protein kinase inhibitor, attenuated I_{Kr} current by ~50%, suggesting a basal modulatory role for protein kinases. Addition of forskolin to staurosporine treated cells did not initiate a response, suggesting that the forskolin response was mediated through a protein kinase pathway. To investigate the role of kinases further, specific kinase inhibitors were used. Bisindolylmalemide-1, a specific PKC inhibitor, abolished both the forskolin and isoprenaline-mediated responses. The specific PKA inhibitor KT-5720 did not inhibit the responses. These results suggested that PKC, but not PKA was involved in the modulation of I_{Kr} in guinea pig ventricular myocytes. The study also investigated the effects of isoprenaline via calcium dependent modulatory pathways. As observed previously, isoprenaline induced

an increase in L-type calcium current. It was proposed that this increase in calcium influx into the cell might activate PKC, as this increase was a requirement for PKC mediated effects. Nifedipine, a calcium channel blocker, inhibited the isoprenaline-mediated increase of current. The role of intracellular calcium was investigated further, using BAPTA-AM, a membrane permeant calcium chelator. Cells exposed to this had reduced currents compared to control cells, suggesting that calcium levels are important in the basal modulation of I_{Kr}. Application of isoprenaline to cells treated with BAPTA-AM caused a small increase in current, which was significantly less than the increase in control conditions. The study concluded that PKC enhanced the I_{Kr} in a calcium-dependent manner.

Angiotensin II acts on the angiotensin receptor, a GPCR coupled to $G_{q/11}$ that activates PKC. In cardiac myocytes, long (5 second) depolarising pulses in the presence of angiotensin II decreased both activating and tail currents, made up of both I_{Kr} and I_{Ks}, in a highly voltage dependent manner (Daleau and Turgeon, 1994). When a shorter depolarisation was applied (250 ms), only allowing activation of I_{Kr}, an increase in current was seen upon application of angiotensin II. This suggested that angiotensin-induced signals differentially modulated I_{Kr} and I_{Ks}. However, inhibitors of the different pathways were not used in this study.

A study using histamine as an agonist, also showed opposite modulatory effects on I_{Kr} and I_{Ks} (Matsumoto et al., 1999). Histamine activates the H_1 histamine receptor that is coupled to $G_{q/11}$. Dissociated guinea pig atrial myocytes were whole cell patch clamped, with cells being depolarised for 300 ms periods. The effects of histamine were highly voltage dependent. Both tail and activating I_K increased at membrane potentials between +20 mV and +40 mV, but a decrease was observed between –20 mV and –10 mV. The augmentation of I_K in response to histamine was increased when cells were depolarised for longer (3 seconds, which would measure I_{Ks}), and conversely the inhibition of I_K was more prominent when cells were depolarised for shorter time periods (200 ms, which would measure I_{Kr}). This suggests that H_1 receptor-mediated signalling oppositely modulates I_{Kr} and I_{Ks}, causing a decrease of I_{Kr}, and an increase of I_{Ks}. Using the PKC inhibitor calphostin C abolished the enhancement of I_{Ks}, suggesting that the mechanism is PKC dependent, but did not abolish the inhibition of I_{Kr}, suggesting that this is PKC independent. The study did not investigate any other possible mechanisms of modulation of I_{Kr} by histamine, although possible mechanisms include calcium release or cross talk of signalling pathways.

A variety of I_{Kr} responses to $G_{q/11}$ coupled receptors have been observed. More recently, studies have been done using recombinant HERG channels to investigate modulation by PKC. This will be discussed in the following section.

1.5.1.3 Modulation of HERG by PKC-dependent pathways

Studies on the modulation of HERG channels in various expression systems have shown conflicting results. Barros et al. (1998) investigated the modulation of the HERG channel by PKC, through a G-protein coupled receptor. This study was carried out using *Xenopus* oocytes co-expressing HERG and the thyrotropin-releasing hormone (TRH) receptor. The TRH receptor is coupled to $G_{q/11}$ G-proteins, and therefore the PLC pathway. Addition of TRH was seen to elicit significant changes in HERG channel gating mechanisms, attenuating current by ~50%, shifting the voltage dependence of activation by ~20 mV, accelerating deactivation and slowing activation. Inactivation was not affected. These effects were mimicked when the PKC activator PMA was added. Incubating the oocytes in the specific PKC inhibitor bisindolylmaleimide 1 (bis-1), abolished the TRH response. This compound also inhibited the PMA regulation of the channel. From these results, it was concluded that a PKC-dependent pathway was involved in the modulation of the HERG channel in this expression system. Although this study was not carried out in mammalian tissue, it does provide evidence for a mechanism for the physiological regulation of the HERG channel and therefore cardiac function, by a PKC-dependent mechanism. This study was not able to conclude if PKC had direct and indirect effects on the HERG channel to cause the change in kinetics seen.

However, Schledermann et al. (2001), using a neuronal cell background, investigated the modulation of over expressed rat erg1, erg2, erg3 and HERG channels by TRH in anterior pituitary cells, using the perforated patch whole cell technique. Application of TRH to these cells caused a reduction in HERG currents and a positive shift of activation. Inactivation was not altered, but deactivation was accelerated. These results correlated with those gained by Barros et al. (1998). To investigate the mechanism of TRH action on HERG, the group tried to inhibit the effects of TRH using various different modulators. PKC activity was inhibited using 1 μM bis-1, or down-regulation by 16 hour incubation in PMA, but this did not inhibit the effect of TRH, suggesting that PKC was not involved in the modulation of HERG current

in anterior pituitary cells. The group also looked at the TRH effect in the presence of other compounds to investigate the modulation of the current, including those that inhibited the cAMP-PKA pathway, inhibitors of tyrosine kinase and mitogen-activated protein kinase. Inhibition of each of these signalling pathways had no effect upon TRH modulation of HERG current. From these results, the group were unable to identify which signalling pathway(s) were involved in the TRH modulation of the HERG channel.

In a study carried out in the tsA-201 cell line (a transformed HEK 293 cell line stably expressing the SV40 T-antigen), stimulation of the M_1 and M_3 muscarinic receptors by the muscarinic agonst oxotremorine-M (oxo-M) modulated ERG current (Hirdes et al., 2004). The currents showed substantial rundown, so analysis of the effects of oxo-M was difficult. Oxo-M caused around a 30% inhibition of ERG current, which could be inhibited when the muscarinic antagonist atropine was present. Muscarinic receptor activation reduced maximal activation of the current signicantly, but had only minor effects on deactivation and inactivation of the current. Current density was significantly decreased when cells were transfected with constitutively-active forms of G_s and G_{13}, and was entirely abolished when cells expressed the constitutively-active form of G_q. It was then suggested that it was via this G-protein pathway that oxo-M mediated its effects. Expressing the dominant negative form of G_q reduced inhibtion seen with oxo-M, whereas the dominant negative form of G_{13} had liitle effect. When calcium was removed from both the internal and external solutions, and 20 mM BAPTA was added to the pipette solution, oxo-M did not have an effect on ERG current. However, when calcium levels were buffered to 129 nM, the oxo-M response was retained. These results suggested that a minimum level of calcium was required for the response to occur, but a rise in calcium was not necessary. A role for protein kinases was not established. PMA did not mimic the effects of oxo-M, and a PIP_2 neutralising antibody and inhibitors of PKC, PKB, tyrosine kinase did not attenuate the effects of oxo-M. However, some inconsistencies were observed. Although the PKC specific inhibitor calphostin C attenuated oxo-M effects by 40%, another PKC specific inhibitor bis-1 did not alter oxo-M effects. The group concluded the oxo-M modulation of ERG current was mediated through the PLC signalling pathway, but did not involve the classic messengers PKC or calcium.

Thomas et al. (2003) were able to show that the phorbol ester, and PKC activator PMA modulated HERG current in *Xenopus* oocytes. Activation of the channel was shifted by + 31

mV, current amplitude was decreased by 55%, and deactivation was accelerated by 32% after 30 minutes of PMA application. This modulation could be attenuated by various degrees by incubating the oocytes in various concentrations of the PKC inhibitors bis-1 or Ro-32-0432 prior to application of PMA. To identify potential phosphorylation sites, 17 out of 18 putative PKC phosphorylation sites were mutated. This mutant was called ΔPKC HERG. Mutation of the 18th site, Thr74, generated a non-functional channel (18M HERG). ΔPKC HERG currents showed similar kinetics to that of the wild type channel, and surprisingly, were still modulated by PMA, with this modulation again blocked with PKC-specific inhibitors. The authors suggested that although PKC does modulate the HERG current, it is not via direct phosphorylation of HERG. Thymeleatoxin, a specific activator of the conventional PKC isoforms, mimicked the effects of PMA. Co-expressing the HERG channel with minK or MiRP1 did not alter the modulation of the current, suggesting PKC modulation of the current was not through these accessory subunits. To test if cytoskeletal elements played a role in the modulation of the current, the group used cytochalasin B, which inhibits the polymerisation of actin monomers to actin filaments, and colchicine, which disrupts microtubules. Neither changed the basal current, or altered the shift in activation and decrease in current observed upon application of PMA. The PKC-dependent modulation seen by Thomas et al. could be through the putative PKC phosphorylation site at Thr74, since the effect of mutating this site could not be investigated. Thr74 appears to play an important role in the channel processing and/or basal channel activity. The modulation observed in this study may also be due to non-specific actions of PMA in *Xenopus* oocytes. Curiously, the shift in activation by PMA could be fully blocked by the PKA inhibitor KT-5720. This suggests that PMA alters the channel kinetics via PKA in addition to PKC. Another possible explanation for PKC modulation of ΔPKC HERG could involve upstream targets of PKC. PKC can activate a number of signalling molecules, including MAP kinase, which might modulate the HERG channel directly. In this instance, a PKC mediated modulation of current would be observed in the absence of PKC phosphorylation sites.

In a further study by this group, α_{1A} adrenoceptors and HERG were co-expressed in *Xenopus* oocytes, and the effects of phenylephrine, an agonist at the α_{1A} receptor, on HERG were observed (Thomas et al., 2004). Phenylephrine attenuated HERG current due to a ~ +10 mV shift in the voltage dependence of activation, and also caused a slight (9%) acceleration of

deactivation. This effect could be inhibited by either a 30 minute pre-incubation in the PKA-specific inhibitor KT-5720, or a 4 hour pre-incubation in the PKC-specific inhibitor Ro-32-0432, suggesting both kinases were required to transduce the effects of phenylephrine. However, a HERG mutant containing point mutations at all PKA phosphorylation sites and all (except Thr 74) PKC phosphorylation sites (termed ΔPKA ΔPKC HERG) continued to be modulated by phenylephrine in a manner similar to wild type currents. The authors concluded that this suggests neither PKC and/or PKA alter HERG by direct phosphorylation, but did not exclude the possibility that the remaining Thr 74 site could be responsible for phenylephrine-mediated modulation of HERG current.

Several studies have been carried out on the PKC-mediated modulation of the HERG current. These studies have provided some evidence of PKC modulation of the HERG channel, and generally have shown the trend that HERG current is attenuated with PKC activation, and activation of the channel is shifted to more positive potentials. Although this is a general trend in these studies, the detail of this modulation varies between studies, with some showing a large attenuation of current, and others a small effect. This may be due to the tissue used in individual studies, or the individual experimental conditions. Although studies have shown HERG current to be modulated when PKC is activated, no studies have provided evidence of how this modulation may occur. Modulation may occur either through direct means, (e.g. PKC phosphorylating the channel directly), or indirect means (e.g. PKC induces a further signalling cascade to modulate the channel, or directly phosphorylating an auxillary subunit).

1.5.1.4 Modulation by calcium

Several studies suggest I_{Kr}/HERG channels may be modulated by calcium dependent processes. Early studies on I_K in guinea pig ventricular myocytes showed the current to be calcium sensitive. Tohse (1990) used whole cell patch-clamp technique to show I_K increased when cytosolic calcium concentration was raised. Elevating cytosolic calcium increased the number and open probability of the I_K channels. However, since I_K had not been separated into its two components, I_{Kr} and I_{Ks}, it was not clear which channel type was affected.

Heath and Terrar (2000) investigated I_{Kr} in guinea-pig ventricular myocytes by β-adrenergic stimulation. As described earlier, they concluded that the enhancement of I_{Kr} was calcium-dependent and probably mediated by PKC. However, the data also suggested a seperate PKC independent attenuation of current when cytosolic calcium was lowered with BAPTA. It was concluded that calcium played a role in the basal regulation of I_{Kr}.

EAG, a close relative of HERG is regulated by calcium in several ways. Stansfeld et al. (1996) showed increasing intracellular calcium from 30 to 300 nM induced a rapid inhibition or rat ether-a-go-go (rEAG) channels, stably expressed in HEK cells, which was reversible. Calcium was unlikely to be an open channel blocker, and the inhibition of current by calcium was not blocked by incubation of the cells in non-specific kinase blockers, calmodulin kinase II blockers or calcineurin blockers. Subsequently, Schonherr et al. (2000) found that elevated intracellular calcium reversibly inhibited hEAG, but that cytosolic components were required. The response to calcium was lost in excised patches from *Xenopus* oocytes unless the patches were pushed back into the oocyte, a technique called cramming. The study identified calmodulin as the calcium sensor for hEAG, which bound to an amphipathic helix on the C-terminus of the channel in a calcium-dependent manner, with apparent K_d of 480 nM. More recently, calcium/calmodulin-dependent protein kinase II (CaMKII) has been shown to regulate drosophila EAG (Wang et al., 2002b). Inhibiting CaMKII with an inibitor peptide, or mutating the putative phosphorylation site on the channel, reduced current amplitude and accelerated decay of current during the depolarisations. Their results were consistent with the channel being constitutively phosphorylated by CaMKII.

At the time this project was started there was limited evidence that I_{Kr} might be regulated by calcium, and that EAG, which has high sequence homology with HERG, was highly sensitive to calcium. There have been no studies on HERG modulation by intracellular calcium.

1.5.2 Modulation of HERG by the adenylyl cyclase coupled pathway

Arrhythmias associated with familial long QT syndrome can be fatal, and are often precipitated by stress, extreme emotion and physical exertion (Priori et al., 1997). Under stressful conditions, there is release of catecholamines such as adrenaline and noradrenaline, which act on β-adrenergic receptors. This therefore suggests that β-adrenergic stimulation, and the associated cAMP/PKA pathway may be modulating channels important in cardiac

repolarisation, such as the HERG channel. HERG subunits have four putative PKA phosphorylation sites, and a cyclic nucleotide binding domain (CNBD; see figure 1.11). Thus, cAMP may be able to modulate HERG activity by dual cAMP dependent pathways. This will be discussed in this section.

1.5.2.1 cAMP modulation of HERG currents

Cui et al. (2000) observed that stimuli that caused an increase in intracellular cAMP concentration had multiple effects on HERG channels. Increasing intracellular cAMP levels by directly perfusing cAMP into the cell attenuated HERG current by 40%, and accelerated deactivation. No shift in voltage dependent activation or inactivation was observed. Further investigation into the mechanism of this modulation, using a PKA-specific peptide inhibitor, revealed that raising cAMP alone caused a negative shift in the voltage dependence of activation. Using binding assays, this study showed cAMP bound directly to HERG with an affinity of 40 μM. The group also showed HERG protein could be phosphorylated *in vitro* with the catalytic subunit of PKA. It was therefore hypothesised that the balance between the effects of PKA and cAMP produces the overall change that is seen in HERG channel kinetics during periods of elevated intracellular cAMP, which are dominated by PKA effects on the channel. Interestingly, co-expressing HERG with MiRP1 or minK, both possible β-subunits, showed the effects of cAMP binding to HERG to be predominant. Further to this study, the same group investigated the function of the cyclic nucleotide binding domain (CNBD) in the HERG channel (Cui et al., 2001). As expected, the CNBD mutants showed a decreased ability to bind cAMP. Mutating the CNBD led to a loss of functional HERG current, although surface expression was seen. It was proposed that along with the ability of cAMP to modulate the HERG channel, the ability of the channel to bind cAMP is essential for normal HERG channel function, which may be suggestive of a constitutive role for cAMP in the modulation of HERG channels.

A receptor family that is expressed in the heart, and is coupled to G-proteins is the endothelin receptors. Endothelin (specifically endothelin-1; ET-1) has previously been shown to induce a number of cardiac effects, including a shortening of the action potential and hyperpolarisation. It has been shown that the main mechanism of action of ET-1 is an inhibition of adenylyl cylcase, via the ET_A receptor. Therefore, activation of the ET_A

receptor would decrease intracellular cAMP. A study carried out by Magyar et al. (2000) elicited I_{Kr} by 1 second depolarising pulses to a variety of potentials in healthy, human ventricular myocytes. The evoked current could be fully inhibited with the inhibitor E-4031, suggesting there is no contamination with other currents. Application of ET-1 significantly decreased I_{Kr} in a voltage dependent manner. ET-1 did not affect either of the potassium channels I_{to} and I_{K1} in the same preparations. When observing action potential duration, application of ET-1 lengthened action potential when measured at both APD_{50} and APD_{90} time points. Isoprenaline, which activates adenylyl cylcase, therefore increasing cAMP levels, was shown to fully reverse the effects of ET-1, suggesting it is the inhibition of adenylyl cylcase that mediates the inhibition of I_{Kr}.

1.5.2.2 Protein kinase A modulation of HERG channel currents

Kiehn et al. (1998) investigated the effects of PMA on HERG channels in guinea pig cardiomyocytes and expressed in *Xenopus* oocytes, and found current amplitude decreased upon application of PMA. They found that although PMA is known to be a PKC activator, specific inhibitors of PKC (chelerythrine or bis-1) could not inhibit the attenuation of current that was observed. When specific PKA inhibitors were applied however (H-89 or KT-5720), the effect of PMA was attenuated greatly, suggesting a possible role for PKA in the modulation of the HERG channel. Forskolin induced similar effects to PMA, again providing evidence that that PKA shifts the voltage dependence of activation and attenuates HERG current.

The modulatory effects of PKA on the HERG channel in *Xenopus* oocytes have also been studied by Thomas et al. (1999). The HERG channel protein contains four putative PKA phosphorylation sites (figure 1.11). By mutating, and therefore effectively removing, these sites within the HERG channel (to create the 4M HERG mutant), they were able to investigate the effects of Ro-20-1724, a cAMP-specific phosphodiesterase (PDE IV) inhibitor in these mutants compared with wild type HERG. In the presence of Ro-20-1724, which increases intracellular cAMP levels and therefore increases PKA activity, the wild type (WT) activation curve was shifted by 12 mV, and current amplitude was reduced by 19%. In channels with all four phosphorylation sites mutated, this change was absent, so it was concluded that PKA produces these effects on the HERG current through direct

phosphorylation of the channel. Mutating each PKA phosphorylation site separately, then applying Ro-20-1724 to these mutants produced small decreases in current. The total decrease seen with these four mutants totalled that seen with the four PKA phosphorylation site removed. This data suggested that cAMP does not have a direct effect on the HERG channel, instead mediating its effects through PKA. This study also investigated the effects of forskolin on the 4M HERG mutant. Curiously, although effects from forskolin application were reduced in the 4M HERG mutant compared to the WT HERG channel, the study still observed a significant effect of forskolin. This is likely to be due to cAMP effects on the channel, but why these effects were not observed when using Ro-20-1724 was not discussed.

Zhang et al. (2002) also showed PKA modulation of HERG current, in HEK-293 cells and *Xenopus* oocytes. Application of 10 μM forskolin and the phosphodiesterase inhibitor 3-isobutyl-1-methylxanthine (IBMX; 100 μM) reduced HERG current expressed in HEK cells by 83%, and caused a slight, but non-significant positive shift in the voltage dependence of activation. Adding the catalytic subunit of PKA into cells through the pipette solution attenuated current by ~57%, and shifted activation by ~ +15 mV. A membrane permeable analogue of cAMP attenuated current by ~30%, but did not alter the voltage dependence of activation, however, the direct effects of cAMP were not considered in this study. Using ^{32}P incorporation techniques, the group also investigated the phosphorylation state of the channel. They found that when expressed in *Xenopus* oocytes, the channel is phosphorylated under basal conditions, and application of either PMA or forskolin in the presence of phosphatase inhibitors could not alter this amount of phosphorylation. A mutant HERG channel (4M HERG), which lacks the four PKA phosphorylation sites, showed no difference in basal phosphorylation state, suggesting that PKA plays no role in basal phosphorylation of the channel. This study suggests that although PKA seems to play a role in the modulation of the HERG channel, no direct effect of PKA phosphorylation of the channel can be observed. The group suggested that this may be due to a large number of other potential phosphorylation sites on the channel, potentially totalling around 40, and therefore any change with PKA may not be recognised using this assay method.

In summary, the effects of raising cAMP on HERG currents seen are two fold, due to separate effects of cAMP binding and PKA activation. However, it seems that the effects of PKA are predominant. The effects of forskolin or isoprenaline on HERG currents vary

between studies, but generally show a significant attenuation of current and a positive shift in voltage dependent activation. However, some anomalies remain, such as the complete loss of effect by the phosphodiesterase inhibitor Ro-20-1724 in the 4M HERG channel, as it would be expected that the effects of cAMP would remain. Since Cui et al. (2000) found the predominance of effects to change with co-expression of either MiRP1 or minK, it may be the differences in effects are due to different endogenous expression of these proteins between tissues that determine the modulation of HERG by the cAMP signalling pathway. However, without further experiments this issue remains unresolved.

1.6 Additional modulators of the HERG channel

1.6.1 Modulation of HERG by external calcium

Studies by Johnson Jr. et al. (1999) have shown the HERG channel to be modulated by external calcium. HERG currents expressed in CHO cells were decreased, and the voltage dependence of activation shifted to positive potentials by raising calcium from 1.8 mM to 10 mM. The decrease of HERG current was not due to a time-, or voltage- dependent calcium ion block, and replacing calcium with other divalent ions, such as Mg^{2+} did not have the same effect. It was hypothesised that calcium specifically interacts with, or influences the voltage sensor of the channel, but not by charge screening, since activation but not inactivation was affected. Charge screening by divalent ions would be expected to influence both voltage dependent processes. Clamping the cells using a protocol similar to that of a cardiac action potential showed that increasing calcium levels close to physiological range (1 mM-3 mM) decreased HERG current by 50%. The mechanism of this attenuation of current is not clear, but a direct interaction with specific residues Glu518 and Glu519 close to S4 has been suggested (Johnson Jr. et al., 2001).

1.6.2 Protein kinase B modulation of HERG channel currents

Protein kinase B (PKB) is a serine/threonine kinase. In mammals there are three subtypes, which share high homology. These are PKBα, PKBβ and PKBγ. The activation mechanism of PKB is not clear. Activation of receptor tyrosine kinases, can lead to the recruitment of PI-3 kinase (PI-3K) to the membrane of the cell. PI-3K phosphorylates the second messenger PIP_2 to form PIP_3. This molecule is able to then recruit PKB to the membrane, and alter its

conformation to allow phosphorylation and therefore activation of PKB. Activation of PKB requires two sites of phosphorylation. One of these sites is phosphorylated by the phosphoinositide-dependent kinase-1 (PDK-1), the other by either autophosphorylation or an unidentified kinase. Once PKB is activated, it is released from the membrane, and is able to translocate to other regions of the cell to phosphorylate target proteins. PKB is known to regulate cellular processes such as cell cycle progression, and pro-survival signals, such as increasing transcription of CREB-regulated survival genes (reviewed in Neri et al., 2002; Nicholson and Anderson, 2002).

The HERG channel protein contains two putative PKB phosphorylation sites, one on the N-terminus and one on the C-terminus (figure 1.11). Only one study has been carried out on the role of PKB in the modulation of the HERG channel (Zhang et al., 2003). HEK-293 cells stably expressing HERG were transiently transfected with either constitutively active mutants of PKB or PI-3K, thereby increasing basal PKB activity. Under these circumstances, HERG current increased by up to 50% compared to mean current amplitudes in cells only transfected with HERG. Transient transfection with dominant negative mutants of PKB or PI-3K, which caused effective 'knockout' of PKB activity, attenuated current by around 50% when compared to control HERG current amplitudes. The group concluded that the HERG channel is more likely to be modulated directly in a basal manner, since knockout of PKB led to an effect on HERG current.

1.6.3 Modulation by src tyrosine kinase and phosphatase

14 src-related kinases have been identified. They are 60 kDa proteins, which are associated with many cellular processes, via the phosphorylation of different signalling molecules, such as the focal adhesion protein p130cas, involved in integrin mediated cell adhesion, and extracellular signal related kinases (ERKs), which can mediate many physiological processes. The HERG channel contains sequence motifs that underlie interactions with cytosolic protein-tyrosine kinases (PTKs), so Cayabyab and Schlichter (2002) investigated possible modulation of endogenously expressed rERG1 (the rat homologue of HERG) and rERG2 in a highly proliferating rat microglial cell line (MLS-9 cells). Immunoprecipitating proteins from cell lysates using an anti-phosphotyrosine antibody and then probing with an anti-HERG antibody revealed the r-ERG1 and r-ERG2 channels were constitutively tyrosine

phosphorylated, which could be reduced by 25% and 40% by the protein tyrosine kinase inhibitors herbimycin A and genistein respectively. ERG current amplitude was attenuated using the same inhibitors or a src-selective inhibitory peptide. The scrambled peptide did not have any effect on the current amplitude. The src-selective activating protein increased ERG current. Co-immunoprecipitation studies carried out showed the ERG channel may exist as a macromolecular structure with src.

The same group later showed a specific tyrosine phosphatase, SHP-1, to be able to modulate ERG-1 current in MLS-9 cells. (Cayabyab et al., 2002) SHP-1 showed opposing effects to src tyrosine kinase seen in the previous study, attenuating current. Wild type SHP-1, and catalytically active SHP-1 both attenuated current when applied acutely to cells, by around 50%. This could be reversed in the presence of phosphatase inhibitors. Transfecting the wild type and catalytically active SHP-1 forms decreased basal ERG current, but western blot analysis showed there was no change in channel protein level.

This suggested that in MLS-9 cells, tyrosine phosphatases are important in the basal regulation of ERG-1 current, and it may, at least partially, be a balance of tyrosine kinase and phosphatase activity that dictates current amplitude.

1.6.4 Modulation by the Rho family of GTPases

Application of thyrotropin releasing hormone (TRH) to preparations expressing HERG and the TRH receptor produces a reduction of ERG current (Barros et al., 1998; Schledermann et al., 2001). This is thought to be due to activation of PKC through the PLC pathway, but the electrophysiological evidence for this is not conclusive. Although Barros et al. were able to fully inhibit this response using PKC inhibitors, Schledermann et al. were unable to work out a mechanism for this inhibition, provoking the theory that another signalling pathway may be involved in this regulation. The Rho protein is stimulated by guanine nucleotide exchange factors (GEFs) within the cell that are activated by $G_{\alpha 13}$-coupled receptors. Storey et al. (2002) investigated the possible mechanism of TRH-mediated modulation of ERG current expressed in GH_4C_1 cells (a pituitary cell line). Application of TRH attenuated ERG current, but this attenuation could not be inhibited by the use of either a PKA inhibtor peptide, or calphostin C to inhibit PKC, thus prompting the question of how TRH mediated its effects on ERG current. To investigate the possible role of Rho GTPases, cells were transfected with

constitutively-active $G_{\alpha 13}$, which would upregulate activity of Rho. In these cells, basal ERG current was reduced by 50%. When constitutively-active Rho was transfected into cells, similar results were observed. Currents were also reduced upon direct application of active Rho protein through the pipette solution. Cells transfected with the dominant-negative form of Rho showed no differences in basal current, however these cells showed no response to application of TRH. Taken together, this provides evidence for a potential role for the Rho GTPase in the modulation of ERG channels. The thyroid hormone 3, 5, 3'-triiodothyronine (T3) counteracts the stimulatory effects of TRH in the pituitary, and is also known to reduce spike frequency in GH_4C_1 cells. Application of T3 to cells rapidly increased ERG current by greater than 100%. Since Rac and Rho are known to have opposing effects in other processes, it was thought that Rac may modulate ERG current to cause this augmentation in response to T3. There is no widely accepted mechanism of Rac-activation by T3, however the authors postulated that T3 may activate PI3-kinase, which has been shown to increase Rac activity through activation of Rac GEFs. The constitutively-active form of Rac increased ERG current by 63%, with the dominant negative form having no effect on basal current. However, the dominant negatve form completely blocked the effects of T3 on ERG current. This study showed the opposing effects of the GTPases on ERG current, but was unable to distinguish if this modulation was through direct interactions of the GTPases with the channel, or through a further messenger cascade.

Figure 1.12 summarises the signalling pathways that may modulate the HERG channel.

Figure 1.12

Possible second messenger modulation pathways for the HERG channel that have described in the literature. Abbreviations: **cAMP**: *cyclic adenosine monophosphate*; **DAG**: *diacylglycerol*; **FFA**: *free fatty acids*; **GEF**: *guanine nucleotide exchange factor*; **IP_3**: *insositol 1,4,5-trisphosphate;* **LysoPC**: *lysophosphatidylcholine*; **PDK-1**: *3-Phosphoinositide-dependent protein kinase-1*; **PIP_2**: *phosphatidylinositol-4,5-bisphosphate;* **PIP_3**: *phosphatidylinositol-3,4,5-trisphosphate;* **PKA**: *protein kinase A*; **PKB**: *protein kinase B*; **PKC**: *protein kinase C*; **PLA_2**: *phospholipase A2*; **PLCβ**: *phospholipase C β*; **PLD**: *phospholipase D*; **SHP-1**: *src-homology 2-containing protein.*

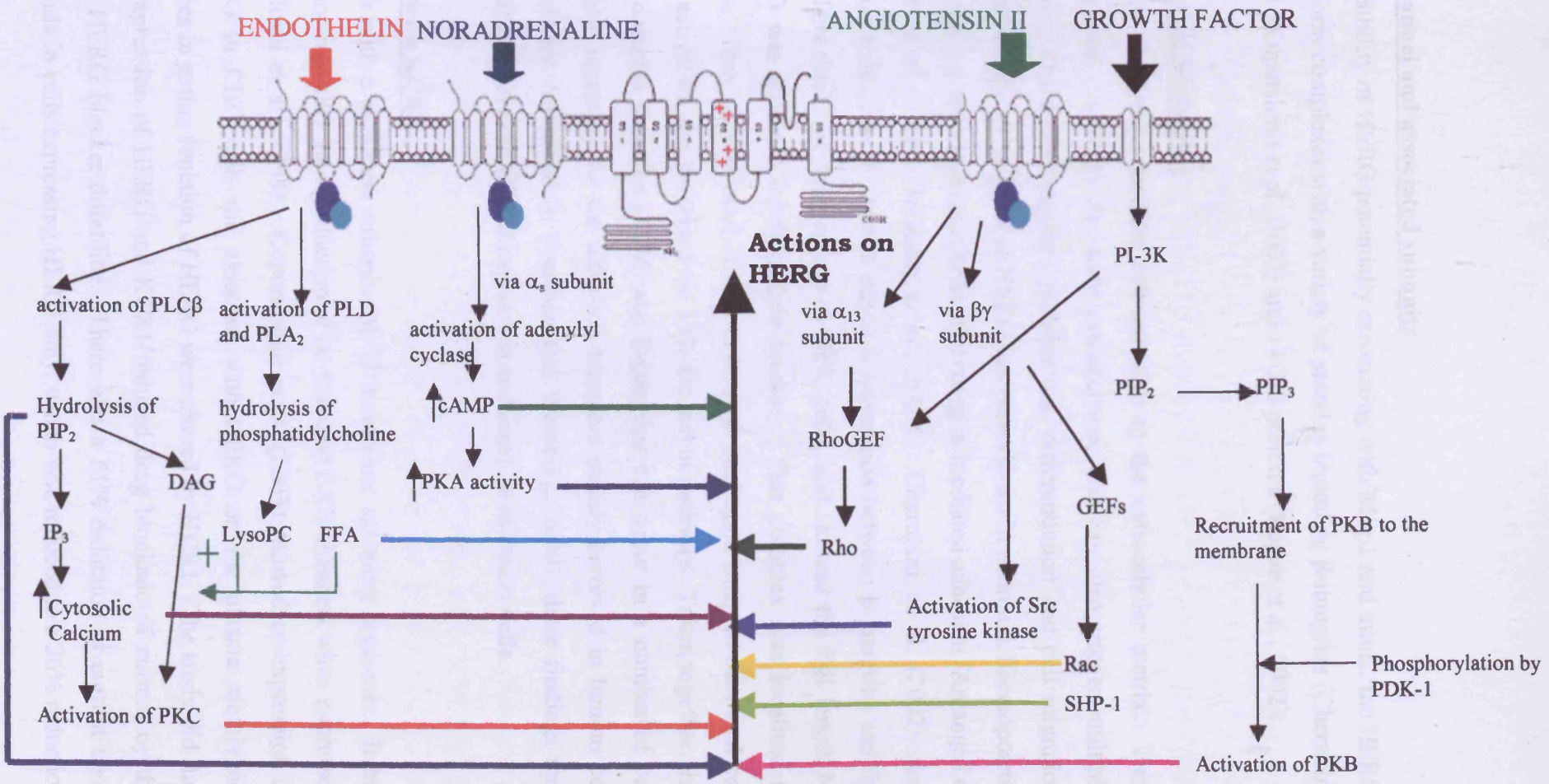

1.7 The HERG channel and associated subunits

In addition the possibility of HERG potentially associating with Mirp1 and minK, the HERG channel may also form complexes with a variety of proteins including β-integrins (Cherubini et al., 2002), KCR1 (Kupershmit et al., 2003) and 14-3-3 proteins (Kagan et al., 2002).

1.7.1 Association with β-integrins

The integrin family of proteins mediate cell adhesion to the extracellular matrix. They anchor the extracellular matrix to the actin cytoskeleton, and can also trigger multiple signalling pathways. These may regulate proliferation, differentiation and cell migration (reviewed in Juliano, 2002). Activation of HERG has been shown in neuronal, haemopoietic tumour cells and leukemic preosteoclastic cells after integrin-mediated adhesion (Arcangeli et al., 1996; Bianchi et al., 1998; Hofmann et al., 2001). Cherubini et al. (2002) used immunoprecipitation techniques to show a physical interaction between β-integrins and the HERG channel. This work was carried out in HEK cells, and showed the full length N-terminal of HERG was required for β-integrin binding. This complex was localised to caveloea/lipid rafts. They also showed HERG to be activated upon integrin mediated cell adhesion, and this activation was sustained via a G_i-dependent pathway. Taken together, this data suggests the complex between HERG and β-integrins can occur in a number of cell types. Since integrin receptors are the adhesion receptors mainly involved in tumour cell growth and proliferation (reviewed in Hanahan and Weinberg, 2000), these findings may provide a functional link between HERG expression and function in cancer cells.

1.7.2 Association with KCR1

KCR1 is a protein with a predicted structure of 12 membrane spanning segments. It has previously been shown to alter gating function of rat neuronal EAG channels when expressed in COS-7 cells (Hoshi et al., 1998). Kupershmidt et al. (2003) showed co-expression of KCR1 with HERG in CHO cells did associate with HERG on the plasma membrane, however, no changes in gating function of HERG were altered by KCR1. The study did find however that co-expression of HERG and KCR1 reduced drug blockade of current by the well characterised HERG blocker dofetilide. There was a 51% reduction of current upon exposure to dofetilide in cells expressing HERG only, which was reduced to a 26% reduction

in cells expressing HERG and KCR1. Co-expression of HERG with MiRP1 did not alter the pharmacological properties of the current, however the authors concluded that KCR1 and MiRP1 may both interact with HERG in a manner that is functionally competitive.

1.7.3 Association with 14-3-3 proteins

14-3-3 proteins are homo- or hetero- dimeric adaptor proteins that modulate interactions between components of the signalling pathway. They interact physically with the client proteins when the client is specifically phosphorylated, so the binding of 14-3-3 proteins is phosphorylation dependent. Using a yeast two-hybrid screen, Kagan et al. (2002) found there were eight potential binding sites for 14-3-3 proteins on each subunit of the HERG channel, and showed the 14-3-3 proteins to interact with both the N- and C- termini of the HERG channel. Binding of 14-3-3 caused a –11 mV shift in the voltage dependence of activation, and accelerated activation. The binding of 14-3-3 proteins to HERG after PKA phosphorylation maintained the phosphorylated state of the channel. It was also suggested that 14-3-3 binding would counteract the attenuation of HERG caused by PKA phosphorylation.

1.7.4 Association with A kinase anchoring proteins (AKAPs)

It is likely that the unique cellular functions of the protein kinases are determined by the binding of the kinases to specific anchoring proteins. A-kinase anchoring proteins (AKAPs) co-ordinate signal transduction, and do this by binding to multiple signalling enzymes near to the target substrates, for example ion channels on the plasma membrane. AKAPs are targeted to specific intracellular structures and locations, and are able to bind protein kinases, and contribute to compartmentalisation of the kinase. This allows the kinase to work highly specifically.

All AKAPs contain at least two protein-protein interaction domains, one which tethers the AKAP to various subcellular structures (e.g. ion channels) and the other to PKA. The PKA binding is through the interaction of the hydrophobic surface of an AKAP amphipathic helix and the hydrophobic surface of the X-type, four-helix bundle formed by the N-terminal domains of the RII homodimer of PKA (Colledge and Scott, 1999). The binding of PKA to tethered AKAPs has been shown to contribute to the specificity of PKA.

It is estimated that around 10-20 different AKAPs may be expressed in an individual cell. Each is located differently, and therefore each making different contributions to the kinase signalling. AKAPs introduce several levels of further complexity to the modulation of cellular proteins, since they are able to bind to PKA, PKC and also phosphatases. Cellular structures that have been associated with AKAPs include microtubles, centrosomes, the smooth sarcoplasmic reticulum, the golgi and the nucleus (Kapiloff, 2002). It is thought that AKAPs are targeted to their specific target proteins through a leucine/isoleucine zipper motif (Kass et al., 2003; Tian et al., 2003). A number of channels that interact with AKAPs have been shown to have this motif, an α-helical structure that forms coiled coils. Coiled coils are comprised of heptad repeats $(abcdefg)_n$ where hydrophobic residues occur at positions *a* and *d*, and *b, c, e, f, g* are hydrophilic residues. The leucine/isoleucine zipper motif was originally found as the motif that mediates binding of transcription factors to DNA (Kara et al., 1990), but has been shown to co-ordinate signalling pathways in a number of tissues. The HERG channel has a modified leucine zipper motif at the C-terminal of the channel (personal communication, Dr. Caroline Dart, Department of Cell Physiology and Pharmacology, University of Leicester), suggesting that it may be capable of forming macromolecular signalling complexes.

1.7.4.1 AKAPs mediate ion channel modulation

The ROMK1 channel, found in the kidney, is modulated by a PKA dependent pathway. This modulation has been shown to be dependent on AKAPs (Ali et al., 1998). Forskolin only increased current expressed in oocytes when the channels were co-expressed with AKAP 79. cAMP analogues were also applied to the channels, and again, effects were only seen when the ROMK1 channel was co-expressed with AKAP 79.

AKAPs have been shown to play a role in long QT syndrome. The slow component of the I_K cardiac current, I_{Ks}, associates with the AKAP yotiao. Yotiao is a 210 kDa protein, which is also capable of binding the NMDA receptor and protein phosphatase I in the brain (Westphal et al., 1999). The binding of yotiao to I_{Ks} has been shown to be important in PKA modulation of the channel, and can be blocked by a point mutation of the channel, G589D (Marx et al., 2002), found in some patients with long QT syndrome. The mutation lies within the leucine zipper motif of I_{Ks}, on the C-terminus and prevents binding of yotiao and modulation by

PKA. This leads to an attenuation of activity of the channel with sympathetic stimulation, and therefore prolongs action potential duration.

A series of experiments by Hoshi et al. (2003) suggest AKAP150 interaction with KCNQ2, are critical for regulation of the muscarinic receptor modulated potassium current (M-current). Co-immunoprecipitation mapped this interaction between residues 321-499 of KCNQ2 and 1-143 of AKAP150. Displacing AKAP150 using a soluble antagonist of KCNQ2/AKAP150 interaction inhibited the muscarinic M_1 receptor-mediated attenuation of current. This modulation was restored in the presence of AKAP150. Further co-immunoprecipitation studies showed the PKC isoform PKCβII to precipitate with KCNQ2, but only in the presence of AKAP150. Phosphorylation of KCNQ2 increased in the presence of an M_1-receptor agonist, but this was only seen in the presence of AKAP150. Mutational analysis showed mutation of three putative PKC sites on KCNQ2 (S534A, S541A, R543A) to decrease M_1-agonist mediated attenuation of current. Together, these data suggest that PKC directly modulates the M-current through the $G_{q/11}$ pathway, and that this modulation is dependent on interactions between the channel and AKAP150.

1.8 Conclusions and summary

HERG channel currents have important physiological roles in the heart and other cell types. It is therefore important to understand how the current responds to signalling stimuli. Studies reviewed in this chapter suggest modulation of the HERG channel is potentially very complex, and it has been reported that a number of signalling molecules within the cell regulate HERG channel activity. The modulation of the HERG channel has been reported to be both constitutive (under constant regulation), and acute (regulated in short bursts, for example upon stimulation of a signalling pathway by a GPCR). Normal functioning of the HERG channel is likely to be dependent on a number of factors. Failure of any part of the signalling pathway could lead to an altered modulation of HERG. Mutations at phosphorylation sites or other modulatory sites could lead to loss of physiologically important regulation of channel activity.

Studies investigating modulation of HERG often have conflicting results. This could be due to a number of different circumstances, such as cell-specific differences in expression of signalling molecules and/or β subunits to HERG. In addition, a number of studies carried out

to investigate the modulation of the HERG channel have used non-mammalian tissue, for which the signalling pathways may differ to mammalian tissue. Other reasons for conflicting results include the use of different agonists and inhibitors, which sometimes may not posses the required selectivity, therefore inhibiting or activating more than one signalling pathway, and potentially leading to a misinterpretation of results. Finally, different experimental conditions between laboratories may also contribute to differences. Clearly, further research is required to elucidate mechanisms that modulated HERG/I_{Kr} channel activity.

Chapter 2

Aims

The overall aim of work to be undertaken during this PhD was to understand how the potassium channel encoded by the human ether-a-go-go related gene is regulated by neurotransmitters and hormones through second messenger pathways. The variability seen in previous studies when investigating modulation of the HERG channel may result from the difficulty of precisely dissecting out mechanisms in whole cells, since there is likely to be overlap and cross talk between the second messenger transduction pathways. The aim of this project was to investigate individual signalling pathways in turn, under carefully controlled conditions.

The hypothesis of this project is that multiple intracellular regulators modulate HERG and I_{Kr}, including protein kinases A and C, calcium, and cAMP. This regulation may be through direct or indirect interactions with the channel.

The first aim was to determine if calcium is involved in the modulation of the channel. This was carried out using substances that are known to increase intracellular calcium levels, including ionomycin, caffeine, and methacholine (a muscarinic receptor agonist). The results from these experiments lead us to then investigate the role PKC plays in the modulation of the HERG channel, identify the PKC isoforms involved and the sites of phosphorylation. A further aim was to investigate modulation of HERG currents and changes in subunit phosphorylation in response to PKA activation.

Chapter 3

Materials and Methods

3.1Cell lines

HERG currents were recorded from, and biochemical assays were carried out on three different mammalian cell lines:

A) Stably transfected Human Embryonic Kidney 293 cells (HEK 293), expressing HERG (HERG-HEK cells), kindly provided by Professor Craig January, University of Wisconsin.

B) Stably transfected Human Embryonic Kidney 293 cells, expressing the muscarinic M_3 receptor (HEK-m3 cells), kindly provided by Dr Gary Willars, University of Leicester.

C) Wild type (WT) HEK 293 cells.

In addition, guinea pig ventricular myocytes and *Xenopus* oocytes were used both in biochemical assays and for electrophysiological work.

3.1.1 HERG-HEK cells

HERG-HEK cells were maintained in Dulbecco's MEM with glutamax-1, sodium pyruvate, glucose and pyridoxine (Gibco), supplemented with 10% foetal bovine serum, (Gibco) 400 μg/ml geneticin (Sigma) and 50 μg/ml gentamycin (Sigma) at 37°C in 5% CO_2 incubator. Cells were grown in 25 cm^2 flasks, and passaged every 3-4 days. To passage cells, they were washed with 6ml phosphate buffered saline (PBS; Gibco) twice, before the PBS was carefully removed, and 1ml trypsin-EDTA x1 (Trypsin; Gibco) was added, and cells were returned to the incubator for ~2 minutes. Once cells had lifted off the flasks they were suspended in 3 ml media (to make a total of 4 ml solution), before a 1:4 split was carried out. Media was changed the following day to remove any trypsin from the media.

3.1.2 HEK-m3 and WT HEK cells

HEK-m3 and WT HEK cells were maintained in MEM alpha media without nucleosides (Gibco), supplemented with 10% foetal bovine serum and 50,000 U penicillin and streptomycin (Gibco) per 500 ml, at 37°C under 5% CO_2. Cells were grown in 80 cm^2 flasks,

and passaged every 3-4 days. To passage cells, they were washed twice with 10 ml PBS, before the PBS was carefully removed, and 5 ml trypsin was added to lift cells from the flask as described above. Cells were suspended in 10 ml PBS to make a total of 15 ml, and centrifuged at 1000 rpm for 2 minutes 30 seconds. Once cells were pelleted, all solution was carefully removed, and cells were resuspended in 5 ml media, before a 1:5 split was carried out. Media changes were made every 2 days.

3.1.3 Transfection of HEK Cells

Transient transfection is a method to temporarily induce protein expression in cells. DNA of the protein of interest is inserted into the cells using a cationic lipid reagent. Positively charged lipids are formulated in aqueous solution with a neutral co-lipid, such as cholesterol, to form unilamellar and multilamellar liposomes. These interact spontaneously with the negatively charged backbone of DNA to form complexes. These complexes interact with the negatively charged cell membrane, resulting in delivery of the macromolecule into the cell. Once inside the cell, the DNA is transported to the nucleus, where it is transcribed, then expressed in the cytoplasm.

Cells were plated out on 6-well plates 24 hours before transient transfection so that they were approximately 60% confluent for transfection. Between 1-5 μg HERG DNA (WT, ΔPKC or 4M HERG, see section 3.3 for details on vectors) was used per transfection, with between 0.5-1 μg eGFP, used as a marker for transfection. For the 18M HERG mutant, up to 10 μg DNA was added per transfection, as functional expression of this mutant was not observed in studies by Thomas et al. (2003). For transfection of PKC isoforms (a kind gift from Stephen Ferguson, Robarts Research Institue, Ontario, Canada), functional studies carried out by Babwah et al. (2003), 1 μg DNA was used per transfection. Since these isoforms were GFP tagged, co-transfection with eGFP was not required. 3 μl Lipofectamine^{TM} 2000 (Invitrogen) was used per μg DNA to be transfected, and the volume was adjusted using serum-free MEM alpha media (Invitrogen) so that each transfection totalled 100 μl. The transfection mixture was left to equilibrate for 20 minutes at room temperature before being added slowly to cells. Media was replaced 6 hours post transfection, and cells were harvested for biochemical assays or electrophysiological recording 48 hours post transfection.

Mock transfections were also carried out for use as control cells. These contained Lipofectamine and serum-free media only, and were prepared and added to cells as described above.

3.2 Electrophysiological Recordings

The method of voltage clamp allows ion flow across the membrane to be measured as an electric current whilst the voltage of the cell is clamped to controlled potentials. This method allows ion channel currents to be studied at constant, known voltages. In voltage clamp experiments, the voltage is changed rapidly from one potential to another, allowing capacitive current to be isolated from ionic current. There are many configurations of the voltage clamp technique, including patch clamp, which is suitable for recording relatively small currents, and two electrode voltage clamp that can be used for recording large currents. Both of these configurations have been used in this body of work and will be described below. In brief, both methods use a feedback amplifier that receives a signal from a voltage-sensing electrode, and compares this with a command potential. The difference between the signals is amplified and applied to the membrane as a current via the current electrode, thus clamping the membrane at a specified voltage. In patch clamp conditions, one electrode is used to both sense voltage and inject current. However, in two-electrode voltage clamp, the voltage measuring and current injection are done by separate electrodes.

3.2.1 Whole cell patch clamp of HEK cells

Membrane currents in mammalian cell lines in this thesis were measured using the whole-cell patch-clamp technique (Hamil et.al., 1981). Whole cell recordings are achieved forming a high resistance seal between the pipette tip and cell membrane (Gigaohm seal) and rupturing the patch of membrane within the patch pipette using suction, to get low resistance access to the intracellular side of the membrane. This method, in addition to allowing electrical access to the entire cell, allows molecules to be introduced to the cell, such as peptides, therefore allowing manipulation of the intracellular environment. Of course, the disadvantage to this technique is cytosolic components, including ions and small proteins, come into diffusional equilibrium with the solution in the patch pipette. Potential

repurcusions of this will be discussed in chapter 4. In spite of this disadvantage, the whole-cell patching technique is the most widely used method for recording membrane currents.

3.2.1.1 Electrophysiological recordings apparatus

The recording chamber was mounted on an inverted microscope (Eclipse TE300, Nikon) (see figure 3.1). Cells could be visualised by phase contrast microscopy to allow precise positioning of the patch pipette relative to the chosen cell. The microscope was also fitted with epi-fluoresence to enable identification of cells expressing GFP, which was used in some experiments as a marker for cells transiently co-tranfected with HERG or PKC. The recording chamber was connected to the ground socket on the headstage, via an agar bridge and silver/silver chloride pellet and wire assembly. The purpose of an agar bridge is to provide an electrical connection between the bath solution and headstage without transfer of ions or solute.

A three-way manipulator (PCS-5000 series, Burleigh) was in place on this electrophysiology rig. Both coarse and fine manipulation allowed the electrode to be moved on three planes.

The microscope, headstage and manipulator were shielded against external electrical noise using a Faraday cage, and were mounted on an anti-vibration table to reduce vibrations that would otherwise damage formation and maintenance of the seal. The perfusion of physiological solution on this rig was designed to optimise relatively fast solution changing and linear flow through the recording chamber. Using a peristaltic pump (Gilson), a constant flow rate of 1 ml min^{-1} was in place. The bath volume was 0.5 ml, allowing complete bath exchange within ~30 seconds, although exchange of solutions around cells at the bottom of the chamber is likely to be slower than this. Three way solenoid valves (Lee Products) were used to switch between solution lines. Four separate perfusion lines were available. An electronic switching device controlled which line of solution was directed towards the recording chamber, with other lines returning back to solution reservoirs (figure 3.2 for a schematic diagram). All lines were primed before experiments were started to prevent air bubbles moving into the recording chamber. An in-house built Peltier device was used to heat solutions to 35-37°C before entering the chamber. This device was calibrated weekly using a second thermometer to measure the temperature of the solution in the recording chamber. Solution was removed from the bath via a suction tube. The rate of suction was

Figure 3.1
Electrophysiological rig set-up. A The recording chamber, and coarse manipulator (and headstage) were mounted on the microscope. B. The recording chamber in detail.

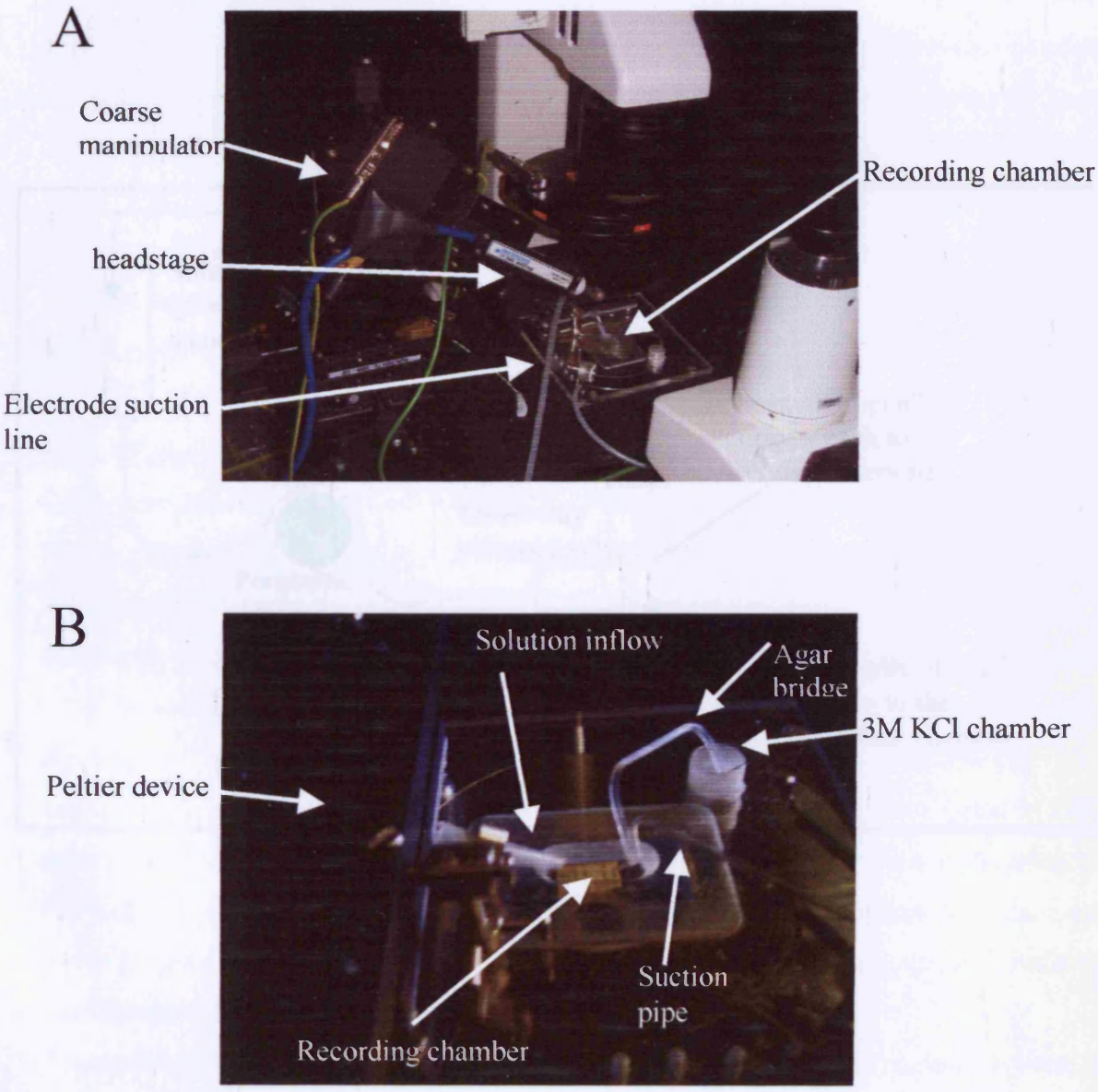

Figure 3.2
Schematic diagram of the perfusion system used on this electrophysiological rig.

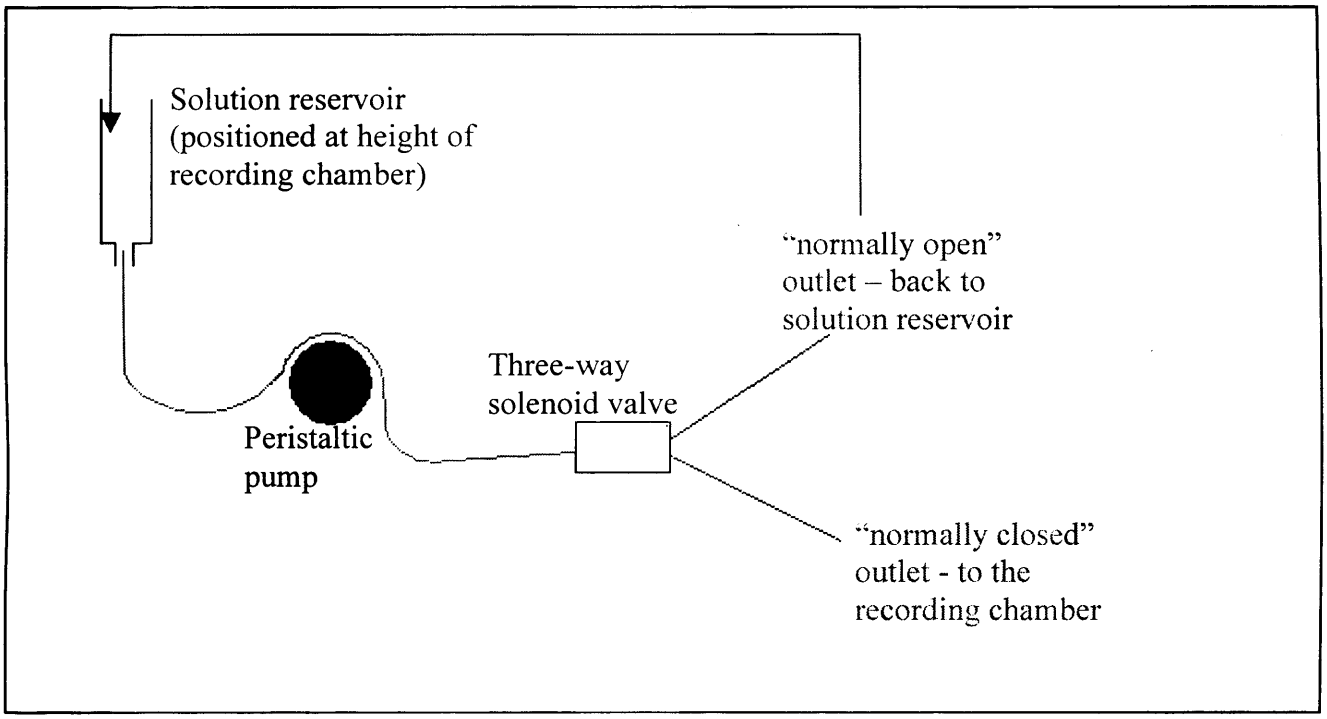

constant, and was regulated by the same peristaltic pump as the perfusion into the bath. The suction tube out of the bath was designed so that solution as well as air was sucked together. This allowed for a constant solution level in the recording chamber. The suction system included a bubble trap, which also functioned as an electrical circuit breaker, and was grounded to reduce electrical noise.

3.2.1.2 Preparation of cells

HERG-HEK cells were loosened from the flasks using either 4 ml Splittex (Autogen Bioclear), or 1 ml trypsin. 10 ml of PBS (Gibco) was added to this to dilute the enzymes and stop their actions. Cells were kept in this solution at 37°C for up to a maximum of 7 hours.
500 µl trypsin-EDTA was used to loosen HEK-m3 and WT HEK cells from the 6-well plate wells. 5 ml of PBS was added per well, and cells were pelletted by centrifugation (as for cell passage). Cells were then resuspended in 10 ml PBS. Cells were kept in this solution at 37°C for up to a maximum of 7 hours. All cells types were left to adhere to the surface of the recording chamber for 15 minutes before recording.

3.2.1.3 Recording solutions

Cells were superfused with extracellular Tyrode, containing (in mM) NaCl 140, $MgCl_2$ 1, KCl 4, glucose 10, HEPES 5, $CaCl_2$ 2, pH 7.4, at 37°C. Borosilicate glass pipettes (Harvard Apparatus) were pulled and fire polished to get final resistances of 2 to 4 MΩ. They were filled with an intracellular solution containing (in mM) KCl 130, MgATP 5, HEPES 10, pH 7.2. In some experiments BAPTA free acid was added to internal solution. pH was corrected to 7.2 with KOH.
Junction potentials arise at the tip of the recording electrode. These are a result of different anionic and cationic mobililties, and different solute concentrations between the intracellular and extracellular solutions. However, in recording conditions described here the junction potential was calculated to be 2 mV, therefore small in amplitude and unlikely to contaminate recordings.
Compounds applied to cells in electrophysiological experiments were made as at least 1000-fold stock concentrations in a suitable vehicle (typically dimethylsulphoxide (DMSO) or ethanol), and stored at –20°C. On the day of use, compounds were made up to the required

concentration in the appropriate physiological solution. Total DMSO concentration did not exceed 0.1% in solutions. Fresh compound solutions were used each day.

3.2.1.4 Acquisition of data

The patch clamp amplifier is a current to voltage (I/V) amplifier with a basic configuration as shown in figure 3.3A. To get rapid changes of membrane potential it is necessary to supply large currents due to membrane capacitance. Capacitance compensation currents are applied to the pipette input of the I/V amplifier via capacitors, so as to supply capacity current that would be otherwise supplied by the output. For this purpose, the voltage command to V_{ref} is modified by a separate parallel circuit, so that its amplitude and rise time can be varied, inverted and injected via the capacitor into the input (for modified circuit see figure 3.3B). It is adjusted to give a square, initial step on the 'pipette' current output. Calibration of the compensation circuit allows C_m (cell capacitance) and R_S (series resistance) to be read from the front panel of the amplifier. In my experiments, whole cell capacitance measurements ranged between 10 pF and 29 pF, and series resistances were between 3 MΩ and 8 MΩ. The presence of the series resistance R_S (arising from pipette and access resistance through the ruptured membrane) gives rise to an error voltage between the clamped pipette value and the true value of the membrane potential. The effect of R_S is to underestimate V_c by an amount proportional to the recorded current. Compensation for this effect (called series resistance compensation) is made by feeding back a proportion of the current signal to V_{ref}. In commercial amplifiers the value of series resistance is taken and a proportion is added to V_{ref}. In our recordings, series resistance was compensated by 60-80%.

A computer generates the voltage protocols, and records membrane current and voltage signals. It is interfaced with the voltage clamp amplifier (Axopatch 200B, Axon Instruments) via a digital/analogue converter (Digidata 1322A, Axon Instruments) (figure 3.4). In our recording conditions membrane current and voltage data were filtered at 1 kHz and recorded to the hard disk of the computer at a sampling frequency of 2.5 kHz. For experiments in which the inactivation of the channel was measured, the data were filtered at 2 kHz and recorded at a sampling frequency of 10 kHz.

Figure 3.3
Patch clamp amplifier circuits. A The basic configuration of the patch clamp amplifier, where the amplifier (FBA) maintains the (-) input at the same potential as (+) (V_R), by negative feedback through resistor R_f. B The patch clamp amplifier with an additional parallel circuit to modify the voltage command to V_{ref} to compensate for the transient initial capacity current.

A

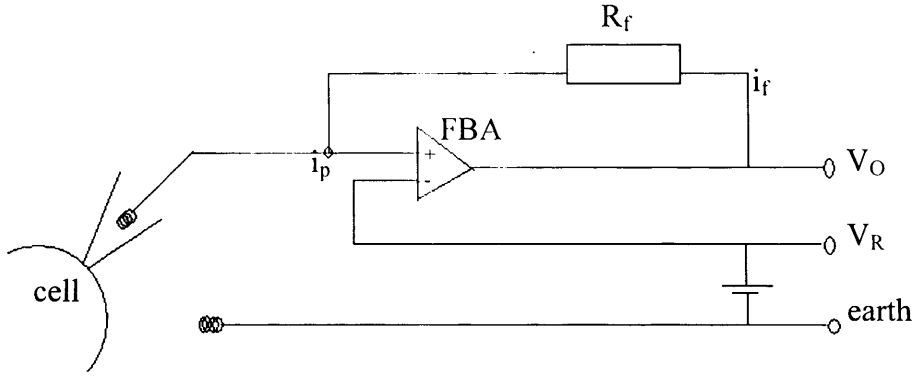

B

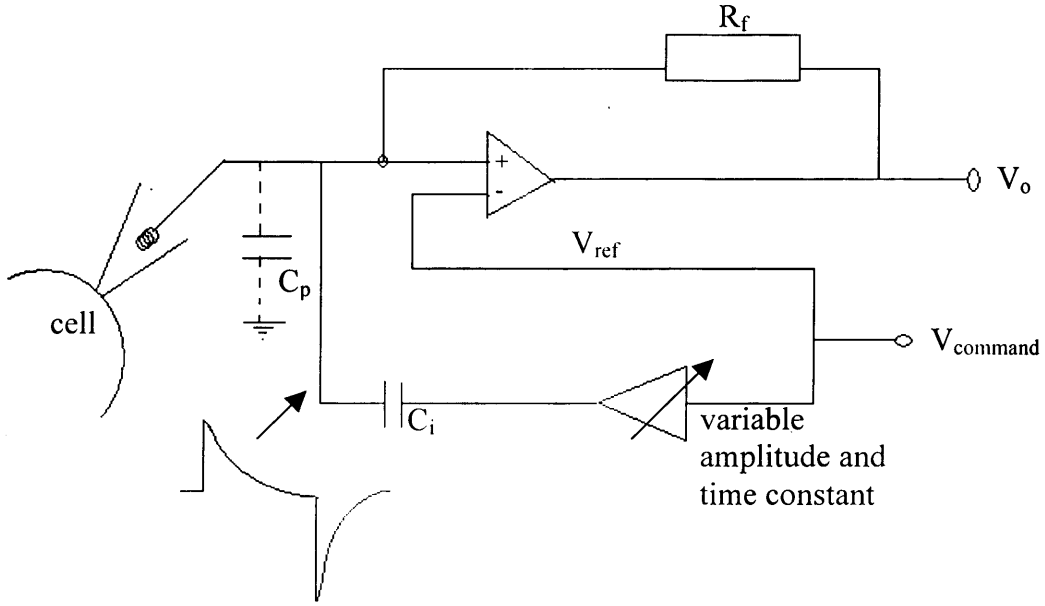

Figure 3.4
The flow of electronic data. The schematic diagram shows the flow of electronic data between the voltage clamp amplifier, oscilloscope, digidata and computer in order to generate voltage protocols, stimulate cells and record currents

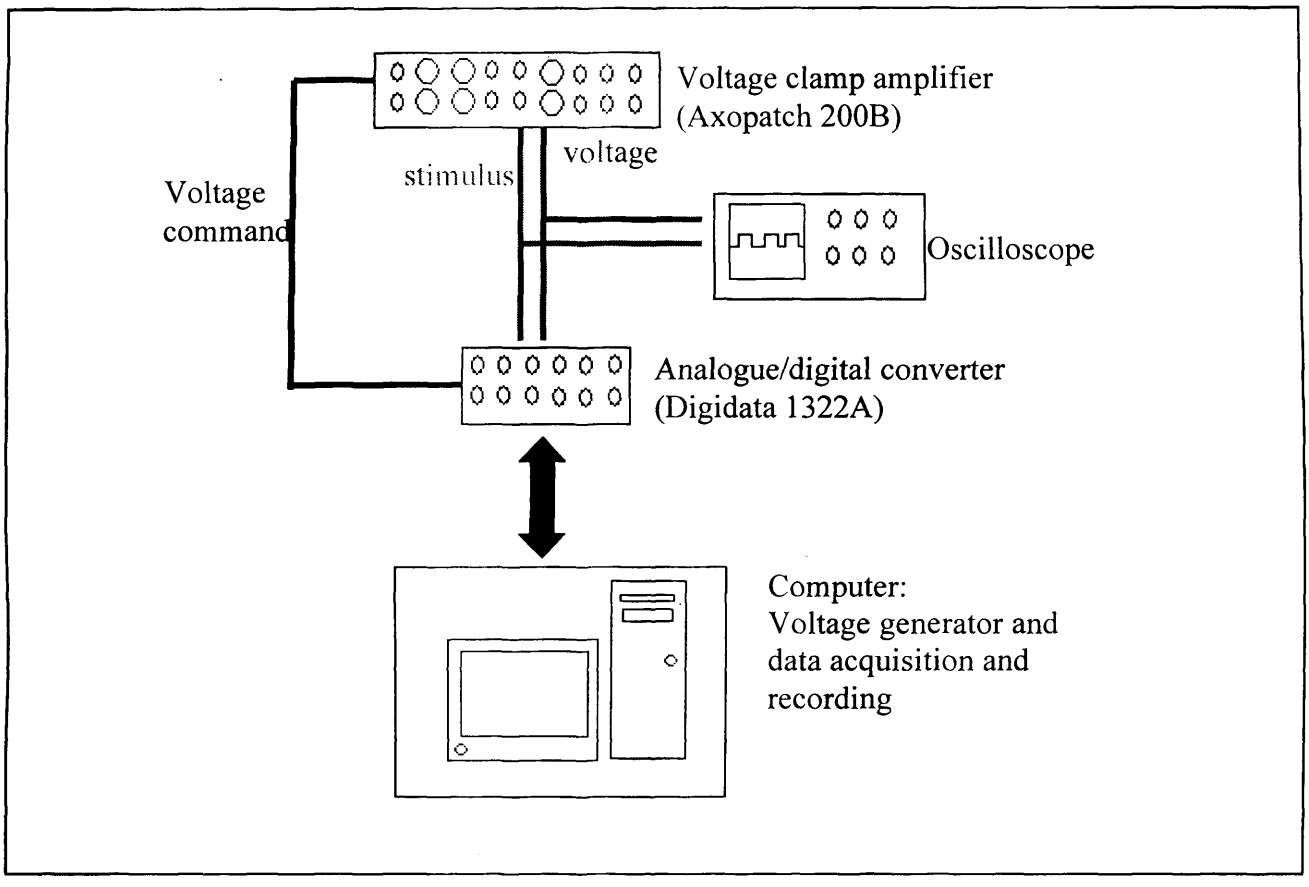

3.2.2 Voltage clamp recordings from *Xenopus* oocytes

Recordings were made in *Xenopus* oocytes using the two-electrode voltage clamp (TEVC) method. The cell is penetrated with two electrodes, a membrane potential recording electrode and a current-delivering electrode. *Xenopus* oocytes were not used in experiments investigating the modulation of the HERG channel, as we wanted to avoid potential differences in signalling pathways and protein expression in these cells when compared to mammalian cells. Oocytes were used to investigate the mechanism of caffeine block of the HERG channel. Measuring drug block of the HERG channel is often carried out on channels expressed in *Xenopus* oocytes, as channels expressed in this system do not exhibit rundown of current (described in section 4.2.5), and often recording viability is longer than in patch clamped cells.

3.2.2.1 Isolation of *Xenopus* oocytes

Isolations were carried out at room temperature. Female *Xenopus* laevis frogs were humanely killed by anaesthetic, followed by cervical dislocation and pithing to destroy the spinal cord and brain. An incision was made in the abdomen to enable ovarian lobes to be removed. Oocytes are surrounded by a follicular cell layer, blood vessels and connective tissue that needs to be removed to make electrophysiological recordings. Oocytes were separated into clumps of around 10-20 oocytes, and placed into OR2 solution, containing (in mM) NaCl 82.5, KCl 2.5, Na_2HPO_4 1, MgCl 1, HEPES 5 (pH 7.5). Between 10-15 ml oocytes could typically be collected per frog. Oocytes were washed with OR2 solution 6-7 times, or until solution was clear, pouring off excess solution and single oocytes each time. 25 ml sterile-filtered collagenase at a concentration of 1mg/ml was added to oocytes, and oocytes were placed on a rocker at 15 rpm for 1 hour. After enzymatic digest, oocytes were washed with OR2 solution until solution was clear (approximately four times), repeated with Barths solution, containing (in mM) NaCl 88, KCl 1, $CaCl_2$ 0.41, $Ca(NO_3)$ 0.33, $MgSO_4$ 1, $NaHCO_3$ 2.4, HEPES 10, pH 7.4. Oocytes were then placed in a large petri dish, containing fresh Barths solution, and the follicular layer manually removed with fine forceps. Once defolliculated, oocytes were sorted into groups of 30, and stored in Superbarths solution (Barths solution supplemented with 1 mM sodium pyruvate and and 50 $\mu g\ ml^{-1}$ gentamycin). Oocytes were stored overnight at 18°C, until they were injected with cRNA.

3.2.2.2 cRNA Injection into *Xenopus* Oocytes

Glass pipettes were pulled and tips broken to ~30 μm to ensure tips were of the correct size for injection and had sharp edges to insert cleanly through the vitelline and plasma membranes and minimise damage to oocytes. Glass pipettes were filled with mineral oil (Sigma), ensuring no air bubbles were present, mounted onto the injector (Nanoliter 2000, World Precision Instruments) and RNA pulled into the tip of the pipette. The injection pipette was then positioned over each oocyte, and pushed into the cell before the RNA was injected. Slight swelling of the oocyte was indicative of injection of RNA. Volumes of between 20 to 60 nl were injected. Depending on how well channels expressed, between 5 to 30 ng RNA were injected into each oocyte. Each pipette was used to inject up to 30 oocytes with the same aliquot of RNA. Superbarths solution was replaced every 24 hours, and dead oocytes removed.

3.2.2.3 Two-Electrode Recording from *Xenopus* Oocytes

Membrane currents in xenopus oocytes were recorded using the two-electrode voltage clamp technique. Oocytes were perfused with a low-chloride solution, containing (in mM) NaMES 96, KMES 2, $Ca(MES)_2$ 2, HEPES 5, $MgCl_2$ 1 (pH 7.6). Two-way solenoid valves (Lee Products) were used to switch between solution lines. Four separate perfusion lines were available. An electronic switching device controlled which line of solution was directed towards the recording chamber. All lines were primed before experiments were started to prevent air bubbles moving into the recording chamber. Recordings were obtained at room temperature.

Glass pipettes (World Precision Instruments) were pulled from thin walled glass and filled with 3 M KCl at least 48 hours before use. Pipettes were placed into recording solution and tips were 'brushed' or carefully broken to obtain resistances of 1-2 MΩ. Oocytes were then placed in the recording chamber, and constantly perfused with recording solution. Pipette tips were positioned close to the oocyte membrane, and electrode potential zeroed relative to the bath ground. Pipettes were then sequentially pushed into the oocyte, ensuring both pipettes were fully inserted into the oocyte, yet were far enough from each other so no interference was caused.

Individual recording protocols will be explained in section 3.2.3.

3.2.3 Voltage protocols and data analysis of electrophysiological recordings

3.2.3.1 Current-Voltage relationship of HERG

To analyse the voltage dependence of activation of the HERG current expressed in HEK cells,

current-voltage (I-V) protocols were used. Currents were elicited by applying 5 second depolarising test potentials from a holding potential of –80 mV. Test potentials were in the range of –50 mV to +40 mV in 10 mV increments. This activates channels, but inactivation also occurs during this time. Repolarisation to –50 mV allows recovery from inactivation, to give a characteristically large tail current. The tail potential was applied for 2 or 3 seconds, during which current decay due to deactivation is observed. In order for the channel to fully close between voltage sweeps, there was a 15 second delay between the start of each sweep. This voltage protocol is referred to as the 'I-V protocol' in the results text, and is shown in figure 3.5A. HERG currents expressed in *Xenopus* oocytes were recorded using two-electrode voltage clamp. Currents were elicited by a 5 second depolarising test pulses from a holding potential of –90 mV. Test potentials ranged between –60 mV to +50 mV, in 10 mV increments. Tails currents were recorded by repolarising to –70 mV for 2 seconds.

Plotting current amplitude at the end of the test potential against membrane potential shows the isochronal I-V relationship of the HERG current. Current at the end of each test potential was normalised to the maximum amplitude for each cell. Normalised current was then plotted as a function of voltage. By plotting the peak tail current against test potential, the voltage dependence of activation of the HERG current is produced. This represents the proportion of channels open at each test potential. Peak tail currents were normalised against the maximum peak tail current in each cell and mean, normalised currents plotted as a function of test potential using Prism 3.0 (Graph Pad, San Diago, USA). These data were fitted with a Boltzmann function (shown below) to obtain values for half maximal activation ($V_{0.5}$) and slope (a measure of the relative voltage sensitivity of the channels).

$$Y = I_{min} + \frac{(I_{max}-I_{min})}{(1+ \exp(V_{0.5} - x/\text{slope}))}$$

where: I_{min}: minimum value on the curve

I_{max}: maximum value on the curve

$V_{0.5}$: mid-point of the curve

Slope: gradient of the curve

Y: conductance

x: membrane potential

3.2.3.2 Time dependence of activation of HERG current

In addition to being voltage dependent, activation of the HERG current is also time dependent. In order to measure the rate of activation, an 'envelope of tails' protocol was used. Here, the channels are fully opened with test potentials to 0 mV of progressively increasing duration and channel activation is assessed from tail current amplitude following each test pulse. To measure HERG currents in HEK cells, cells were held at –80 mV and depolarisations to +40 mV were initially applied for 20 ms. This interval was increased in 20 ms increments to a maximum of 400 ms. Each depolarisation was followed by a repolarising pulse to –50 mV for 60 ms to elicit a tail current. There was a 15 seconds delay between the start of each sweep to ensure the HERG channel was fully closed. This voltage protocol is shown in figure 3.5B. The same protocol was used in *Xenopus* oocytes, but the holding potential was set to –90 mV.

To analyse these data, peak tail currents for each time interval were measured and normalised to the maximum tail current for each voltage protocol. This allows measurement of the proportion of channels open after each time period. These data were then plotted as a function of the test pulse duration and fitted with a single exponential in order to extract the time constant of activation.

3.2.3.3 Steady state inactivation of HERG current

Inactivation of HERG channel current is also voltage dependent and occurs alongside channel activation. To study the voltage dependence of steady state inactivation, a triple pulse protocol was used. In HEK cells, HERG currents were fully activated with a 1 second depolarising pulse to +40 mV from a holding potential of –80 mV. A 5 ms voltage pulse to potentials between –140 mV and +20 mV is applied, and current through non-inactivated

channels measured at the beginning of a third pulse to +40 mV. There was a 15 second delay between the start of each sweep to ensure the HERG channel was fully closed. This will be referred to as the 'steady state inactivation' protocol in the results text, and is shown in figure 3.5C.

To analyse steady state current inactivation, peak currents at the beginning of the third pulse were normalised to the maximum peak current, plotted as a function of membrane potential during the second pulse using Prism 3.0, and fitted with a Boltzmann function as described above. From this the midpoint of inactivation ($V_{0.5}$), and the slope could be measured.

3.2.3.4 Deactivation of HERG current

The voltage dependence of deactivation of the HERG channel, and the reversal potential of HERG currents expressed in HEK cells can be determined using a 'fully activated I-V' protocol. Depolarising pulses to +20 mV were applied for 1 second from a holding potential of –80 mV to allow full current activation. Deactivation was observed with 5 second test pulses to potentials within the range of –120 mV to +40 mV. A 15 second delay was in place between the start of each voltage sweep to allow the HERG channel to close fully. This voltage protocol will be referred to as 'fully activated I-V' protocol in the results text, and is shown in figure 3.5D. A similar protocol was used to measure these parameters of HERG current in *Xenopus* oocytes. The only differences were that cells were held at –90 mV, the first depolarisation was to +40 mV, and a wider range of test potentials (–140 mV to +30 mV) were applied.

To measure the time course of HERG current deactivation, current traces were fitted with the following standard exponential function using Clampfit (PClamp 8):

$$f(t) = \sum_{i=1}^{n} A_i e^{-t/\tau_i} + C$$

where: A: amplitude

τ: time constant

C: constant y-offset

i: each component

From this, time constants for the fast and slow components of deactivation could be measured and statistical significance was assessed as paired data. However, the relative proportion of current fitted by each τ value was not examined in these experiments.
This protocol also allowed the voltage at which current changes direction (reversal potential) to be determined. This was measured by plotting peak current as a function of membrane potential. The reversal potential is the potential at which the current values cross the x-axis (zero current line), when there is no net movement of ions.

3.2.3.5 Repetitive pulsing protocol

A depolarisation to 0 mV protocol was used to characterise the effects of compounds on HERG currents. Once whole cell configuration was achieved, cells were held at –80 mV and 5 second depolarising pulses to 0 mV applied to elicit maximum amplitude currents. A repolarising pulse to –50 mV was applied to cells for 2 or 3 seconds to elicit tail currents. This voltage protocol will be referred to as the 'depolarisation to 0 mV' protocol in the results text, and is shown as figure 3.5E. The voltage protocol was repeated every 15 seconds, to allow complete deactivation between test pulses. Peak tail currents from each voltage sweep were measured, and normalised to peak tail currents under control conditions. HERG currents showed rundown (a time-dependent decrease of current amplitude) when recorded in mammalian cells. Therefore, current amplitudes in test conditions were compared to data gained for rundown of current only (see section 4.2.5 for data). For these experiments deactivation time constants could be fit to currents to get absolute deactivation values. However, the proportion of deactivation fitted with each τ value was not examined.

Figure 3.5 Voltage protocols used to measure HERG channel current parameters. All protocols shown are those used to measure HERG current in HEK cells. **A** Current-voltage (I-V) protocol. **B** Envelope of tails protocol. **C** Steady state inactivation protocol. **D** Fully activated I-V protocol. **E** Depolarisation to 0 mV protocol.

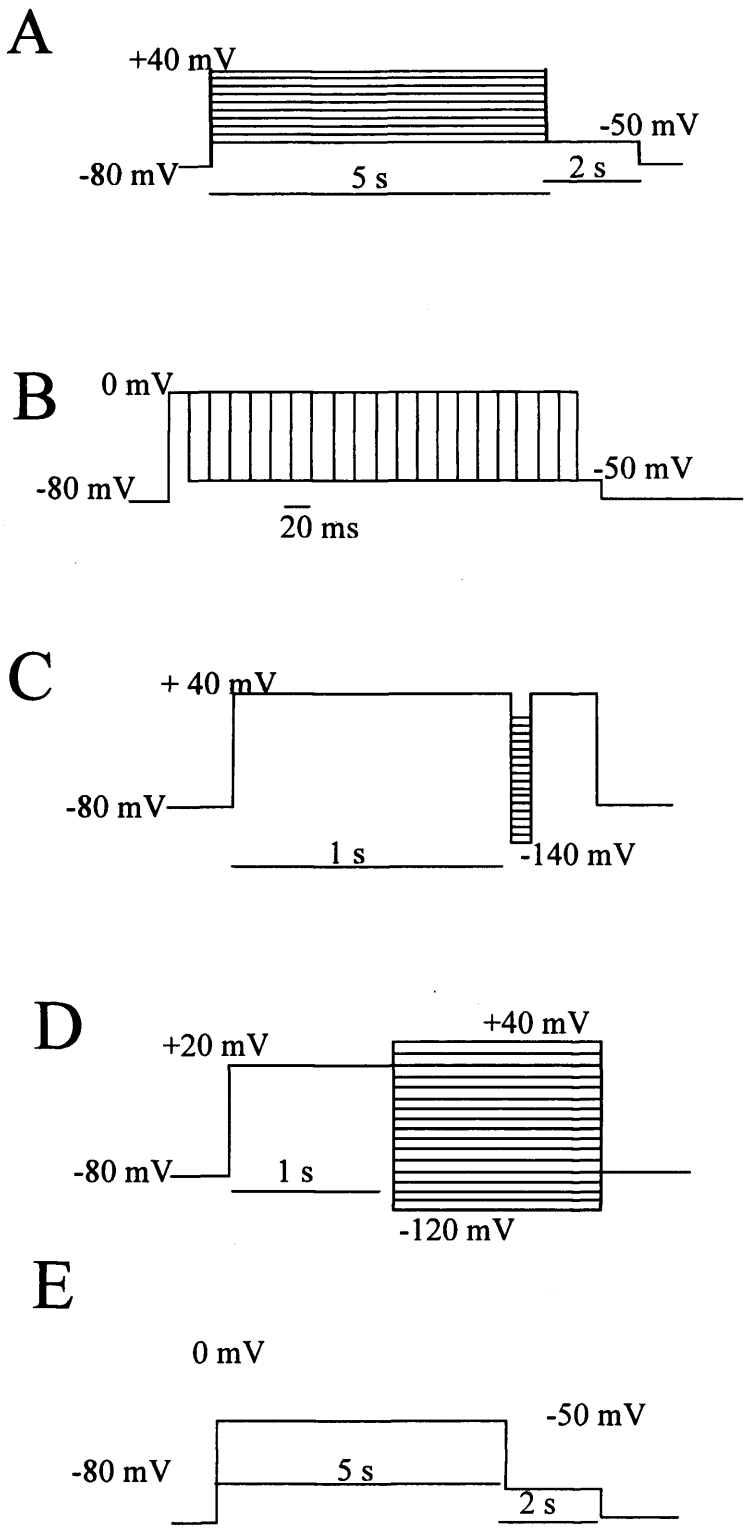

3.2.3.6 Data Analysis

Prism 3.0 (GraphPad, San Diego, USA) was used to analyse and plot results. All recordings were paired (unless stated) and the Student's t-test was used to test for significance. Significance was accepted when $p<0.05$. All data shown are mean ± standard error of the mean (S.E.M.) unless otherwise stated.

3.3 Molecular Biology

3.3.1 Restriction digests of constructs

4M HERG, ΔPKC HERG and 18M HERG cDNA constructs, in which putative phosphorylation sites have been mutated were a kind gift from Dr. Dierk Thomas (University of Heidelberg, Germany). They were supplied in the non-mammalian vector (pSP64, Promega), and needed to be subcloned into a mammalian vector (pcDNA 3.0, Invitrogen) for transfection into HEK cells (for vector maps see figure 3.6). The HERG encoding region was between HindIII and EcoRI restriction enzyme sites. pSP64 and pcDNA 3.0 constructs were subjected to a simultaneous double restriction digest with HindIII and EcoRI for 1 hour at 37°C. Hind III was used at 10 units μg^{-1} DNA, and EcoRI at 2 units μg^{-1} DNA in EcoRI buffer. Digested DNA was run on a 1% agarose gel with 0.003% ethidium bromide to enable DNA visualisation. Typically, gels were run for 50 minutes at 120 V to ensure clear separation of 3.5 and 3 kb DNA bands corresponding to the HERG encoding region and vector respectively. DNA was visualised using a UV lightbox, and the band corresponding to the HERG DNA was quickly cut from the gel, ensuring minimal exposure to UV light. Extraction of DNA from this segment of agarose was carried out using a Qiaquick gel extraction kit (Qiagen), following the manufacturers protocol. Briefly, gel was dissolved in solubilisation buffer for 10 minutes at 50°C, which solubilised the agarose gel and provided optimal conditions for DNA binding. The solution was passed through a column to bind the DNA from the gel solution. The column was then washed and the eluant discarded. The DNA was then eluted from the column with 10mM Tris.Cl (pH 8.5) and quantified by gel electrophoresis, by comparing with markers of known size and quantity (Hyperladder I, Biorad). The pcDNA3.0 vector was subjected to the same procedures to produce vector DNA with complementary sticky ends for ligating the HERG DNA into.

Figure 3.6
Vectors used in this body of work. A Vector map for the non-mammalian vector pSP64. HERG mutants were cloned between the HindIII and EcoRI restriction sites (high-lighted in blue) in the multicloning region. Taken from the Promega website. B Vector map for the mammalian vector pcDNA3. HindIII and EcoRI restriction sites are highlighted in blue. Taken from the Invitrogen website.

A

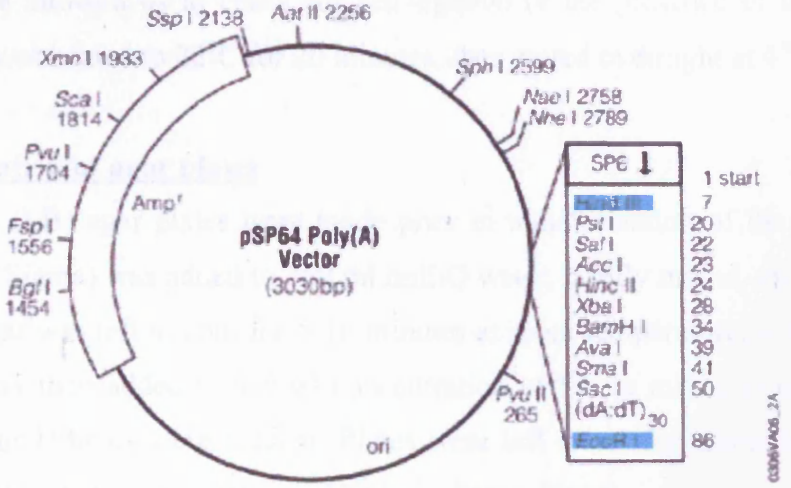

B

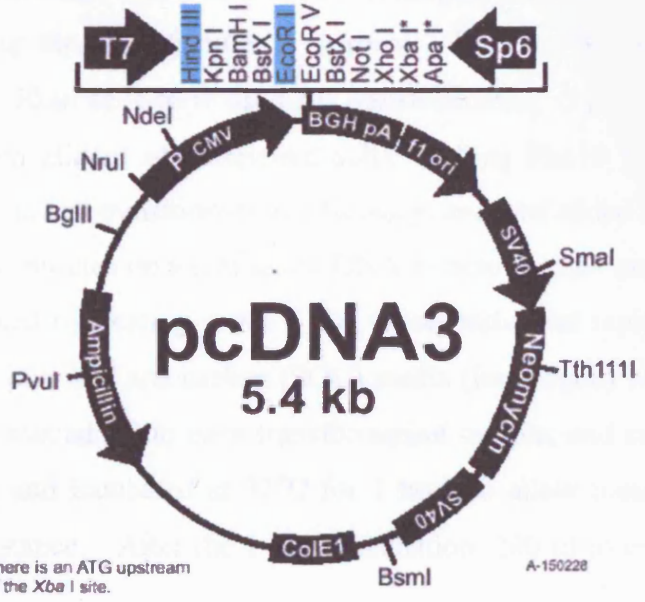

3.3.2 Ligation of constructs

The pcDNA 3.0 vector and HERG inserts were ligated together using the Roche ligation kit, following the manufacturer's protocol Briefly, the vector and insert DNA were mixed in a 3:1 molar ratio of insert:vector to give a total of 88 ng DNA, and made up to a total volume of 17 µl using PCR-grade water. 2 µl 10x ligation buffer and 1 µl T4 ligase was added. Several controls were carried out alongside the experimental reaction. These were reactions that included vector DNA only, insert DNA only, and a reaction that did not include T4 ligase. These allowed us to check for self-ligation or the presence of uncut DNA. The ligation mix was heated to 22°C for 20 minutes, then stored overnight at 4 °C.

3.3.3 Preparation of agar plates

Luria-Bertani (LB) agar plates were made prior to transformation of the DNA. 8.75 g LB agar powder (Sigma) was added to 250 ml milliQ water, briefly mixed, then autoclaved. The melted LB agar was left to cool for 5-10 minutes at room temperature, until it reached 55°C. Ampicillin was then added to a final concentration of 50 µg ml^{-1}, and plates were poured, ensuring no air bubbles were present. Plates were left to set for approximately 30 minutes and excess water evaporated off in a 37°C incubator. Plates were wrapped in clingfilm and stored upside down at 4°C for a maximum of one week.

3.3.4 Transformation of competent cells

DH5α library efficiency competent cells (Invitrogen) were transformed by taking up plasmid DNA, following the manufactuter's protocol. Briefly, the competent cells were slowly thawed on ice. 50 µl cells were used per transformation. 5 µl of ligation product was mixed gently with each aliquot of competent cells. 0.1 ng Puc18 plasmid DNA was used as a positive control to test transformation efficiency, and was added to one aliquot of cells. Cells were left for 30 minutes on ice to allow DNA to bind to sites on the cell wall and cells were then heat-shocked by heating to 42°C for 45 seconds, and rapidly transferring to ice for 2 minutes. Salt optimised and carbon (SOC) media (Invitrogen) was warmed to 42°C. 900 µl of SOC media was added to each transformation sample, and cells were placed in a shaker set at 225 rpm and incubated at 37°C for 1 hour to allow transformed bacteria to express amplicillin resistance. After the 1 hour incubation, 200 µl of each sample was spread onto

the agar/ampicillin plates. Plates were left at room temperature for 15 minutes to allow the transformation sample to absorb onto the plates, before being placed upside down in a 37°C incubator overnight. The following morning plates were checked for colonies. Each colony is a bacterial clone that has antibiotic resistance because it has taken up plasmid DNA. If colonies were detected, the next stage was to grow up single clones and extract the DNA. Plates were stored wrapped in clingfilm and upside down at 4°C until required

3.3.5 Preparation of DNA

Plasmid DNA can be extracted from bacterial cultures using commercially available kits. To prepare DNA on a small scale (mini-prep), 5 individual colonies from each plate were picked and each placed in 5 ml LB broth (20 g/l), containing 100 μg ml^{-1} amplicillin. These were placed in a shaker set at 225 rpm and 37°C, and cultured overnight. The following day, 500 μl of each preparation was taken and added to 500 μl of a 60% glycerol solution (containing 300 μl glycerol and 200 μl PCR-grade water), mixed and stored at –80°C to create a glycerol stock of individual bacterial clones containing plasmid DNA. The remaining culture was prepared using a nucleobond plasmid purification kit (BD Biosciences), following the manufacturer's protocol, and using all provided solutions. Briefly, cells were pelletted down by centrifugation (3000 rpm for 5 minutes). Supernatant was carefully removed, and cells were resuspended in buffer, before lysis buffer was added to cells in order to break up bacterial cell walls and release DNA. Neutralisation buffer was added to precipitate chromosomal DNA and proteins, which were pelletted by centrifugation to leave the plasmid DNA in solution. The supernatant was passed through a column to bind and collect DNA. The columns were washed and DNA was eluted from the column with elution buffer. Samples were run on a 1% agarose gel with 0.003% ethidium bromide to the check size and quantity of DNA. This also allowed us to check if samples were contaminated by chromosomal DNA. Typically, a miniprep would yield 6μg of DNA. DNA samples were then sent to the Protein and Nucleic Acid Chemistry Laboratory (PNACL; University of Leicester) for sequencing. Sequences were compared to the wild type (WT) HERG sequence using the vector NTI computer programme. Once sequences were confirmed, DNA was prepared on a large-scale (maxi-prepped) using similar methods. Typically, a maxi-prep of

DNA would produce 120 μg of DNA. DNA was stored in appropriate aliquot sizes (typically 10 μg/aliquot) at –20°C until required for cell transfection.

3.3.6 Preparation of template DNA

To make DNA template to use for preparation of cRNA, DNA must first be linearised. This was done using the EcoRI restriction enzymes. 10 μg of DNA was incubated in 2 units EcoRI μg^{-1} DNA, in EcoRI buffer, for 1 hour at 37°C. A sample of digested DNA was checked on a gel to ensure linearisation was complete. 100 μg/ml of proteinase K and 0.5% SDS was added to linearised DNA and incubated for 30 minutes at 50°C to denature and digest contaminating proteins, particularly RNases. The linearised DNA was then purifed using the Qiaquick gel extraction kit (Qiagen). Three volumes of solubilisation buffer and 1 volume of isopropanol were added to provide optimal conditions for DNA binding. The total solution was passed through a column, the column washed, and DNA eluted using 10 mM Tris.Cl (pH 8.5). The DNA samples were then quantified by gel electrophoesis, by comparision to Hyperladder I markers. DNA was diluted in diethylpycarbonate (DEPC)-treated water to final concentrations of 0.2 μg/ml.

3.3.7 Preparation of cRNA

The *in vitro* transcription reaction was prepared at room temperature, using filter pipette tips, and wearing lab coat and gloves to protect from contamination with RNases. *In vitro* transcription was carried out using a mMessage mMachine kit (Ambion), following the manufacturer's protocol. Briefly, 1 μg of DNA template was added to RNA polymerase enzyme mix and NTP/CAP mix, to synthesise capped RNA. The additional of a cap structure at the 5' termini greatly improves the stability of RNA when injected into oocytes. The solution was mixed thoroughly and incubated at 37°C for 2 hours. After this incubation, 1 μl of DNase 1 was added to remove DNA from the reaction, and the reaction was incubated at 37°C for 15 minutes. The quality of RNA was checked by running a sample on a 1% denaturing agarose MOPS EDTA sodium acetate (MESA) gel. If the quality and amount of RNA was of a high enough standard the protein and nucleotides were removed using NucAway spin columns (Ambion), following the manufacturer's protocol. Columns were hydrated at room temperature for 15 minutes using RNase-free water. After this time excess

water was removed from columns by centrifugation at 750 g for 2 minutes. Water was discarded, and RNA samples were added to the column without disturbing the gel bed. The column was placed in a sample collection tube and centrifuged at 750 g for 2 minutes. The spin column was then discarded. RNA was quantified using a spectrometer (Genequant II), diluted to appropriate concentrations and stored at –70°C until required for injection into *Xenopus* oocytes.

3.4 Measurement of cytosolic calcium levels

Many molecules absorb light, but the energy is usually degraded as heat. A molecule can be used as an indicator if its absorbance changes as a consequence of interacting with its environment. When some molecules absorb light, they re-emit it at other specific wavelengths. Relatively few molecules fluoresce with significant efficiency, and those that do are termed 'fluorophores'. A fluorescent indicator consists of a fluorophore linked to another component that interacts with the specific substance to be measured. In this section of work we use the calcium binding fluorescent dye fura-2. The acetoxymethyl ester of fura-2, fura-2-AM is very polar, thus making it membrane permeant. Once in the cell, the ester groups are cleaved from the molecule, trapping it inside the cell. Upon calcium binding, the fluorescent excitation maximum of the indicator shifts from 363 nm (Ca^{2+}-free) to 335 nm (Ca^{2+}-bound), whilst the emission maximum remains unchanged at ~510 nm. Fura-2 is excited at 340 and 380 nm, and the ratio of the fluorescence intensities corresponding to the two excitations is used to calcuate intracellular calcium changes (Bright et al., 1989). Thus, fura-2 is a ratiometric dye. This corrects for changes in dye concentration and distribution, amount of light, photodegredation and changes to cell size or shape.

3.4.1 Preparation of cells

To measure intracellular calcium, HERG-HEK and HEK-m3 cells were firstly loosened from the flask/well as described for electrophyiological recordings. Whilst in extracellular Tyrode they were loaded for 15 minutes at room temperature with 2 μM fura-2-AM, (Molecular Probes). Cells were then washed and left to adhere to the surface of the chamber for 10 minutes before perfusion was started. For experiments using BAPTA-AM, cells were incubated with 5 mM BAPTA-AM at the same time as the fura-2-AM incubation.

3.4.2 Imaging of cells

Cells were constantly perfused at 35°C using a peristaltic pump-based perfusion system. Flow rate was 1 ml min^{-1}. Cells were imaged using a Nikon 200 inverted microscope with a 40x objective. The fluorophore was excited with light from a delta-RAM monochromator (PTI) at 340 and 380 nm and emitted light at 520 nm was imaged with a CCD camera. Data acquisition was performed using PTI Imagemaster software. Measurements of emission at 340 and 380 nm were taken every 2 seconds from each selected region of interest, and a ratio produced. These data were then imported into Prism 3.0, where a timecourse of fura-2 ratios could be plotted.

3.5 Phosphorylation assays

Phosphorylation of proteins by kinases is central to many cellular processes, including signal trasnduction. Phosphorylation modifies proteins by the addition of negatively charged phosphate groups to serine, threonine and tyrosine residues. The phosphorylation assay used in this thesis directly allows the phosphorylation state of a chosen protein to be examined. In these experiments, cells are loaded with ^{32}P- labelled ATP. Phosphorylation of a protein causes the addition of the radio-labelled phosphate group into the protein. Upon dephosphorylation of the protein, the phosphate group is removed from the target protein by phosphatases, and the radiolabel is also removed. The technique employed here, measures the emission from the radiolabel to measure ^{32}P incorporation into the protein. The more emission (measured as a signal on a radiolabel-sensitive film), the more incorporation into the protein.

3.5.1 HEK cell phosphorylation assay

HEK cells were grown to ~90% confluency in 6-well plates. Cells were initially washed once with phosphate free Krebs buffer (warmed to 37°C), containing (in mM) NaCl 118, KCL 4.3, $MgSO_4.7H_2O$ 1.17, $CaCl_2.2H_2O$ 1.3, $NaHCO_3$ 0.34, glucose 11.7, HEPES 10 (pH 7.4). A concentration of 5 μCi/ml of [^{32}P]-orthophosphate was made up in phosphate-free Krebs buffer, and 1 ml of this solution was added to each well of cells. Cells were incubated for 1 hour at 37°C. After the incubation, 100x stock solutions of test reagents were added to the medium on the cells, gently mixed, and left to incubate at 37°C. DMSO concentrations

did not exceed 0.1%. The experiments were stopped by removal of buffer and addition of 1 ml ice-cold solubilisation buffer/well, containing (in mM) Tris 10, EDTA 10, NaCl 500, 1% Nonidet P-40, 0.1% SDS, 0.5% deoxycholate (pH 7.4). Cells were solubilised for 5 minutes on ice, collected, then cleared by centrifugation at 13000 rpm for 5 minutes at 4°C. Non-solubilised material was pelletted-out during this stage. Typically, 850 µl of cleared lysate was removed and placed into fresh tubes. Solubilised HERG proteins were immunoprecipitated by incubation with 5 µg of anti-HERG antibody (in-house, raised in rabbit against sequence CIGNMEQPHMDSRIGW, characterised by Pepceuticals, Ltd. (Leicester, UK) by ELISA) for 90 minutes at 4°C. In some experiments muscarinic M_3 receptors were immunoprecipitated, using 3 µg anti-M_3 antibody (a kind gift from Andrew Tobin, University of Leicester). Isolation of immune complexes was carried out using 180 µl protein A-sepharose beads (Amersham; 1.5 g suspended in 50 ml TE buffer (containing, in mM: 10 mM Tris, 5 mM EDTA)). Protein A binds to antibodies with high affinity, and binding to sepharose beads allows for easy isolation of the target protein. Samples were rotated and constantly mixed for 15 minutes at 4°C. The bead-immune complex was then washed using TE-β-glycerolphosphate solution, containing (in mM) Tris-HCl 10, EDTA 10, β-glycerolphosphate 20 (pH 7.4). The bead-immune complex was incubated in 15 µl Laemmli buffer, containing Tris-HCl 62.5mM, 2% SDS, 10% glycerol, 0.01% bromophenol blue, 5% mercaptoethanol (pH6.8), at 60°C for 2 minutes. This separated the antibody, protein A-sepharose beads and target protein. Proteins were resolved by 8% SDS-PAGE, and gels were run at 200 V for 60 minutes. Gels were stained with Coomassie blue stain (containing per litre: 1.5 g brilliant blue stain (Sigma), 50% H_20, 40% methanol, 10% ethanoic acid) and incubated for 10 minutes and shaken at 20 rpm. Coomassie blue stain allows visualisation of protein, and allows us to check for equal antibody loading between lanes. Excess stain was washed off for 10 minutes using destain (containing: 50% H_20, 40% methanol, 10% ethanoic acid). Gels were then dried onto filter paper for 45 minutes at 80°C, and subjected to autoradiography at -70°C for 16-24 hours, using Hyperfilm MP (Amersham). Densitometry was used to quantify intensity of bands (for detail see section 3.8.3).

3.5.2 Isolation of Guinea pig ventricular myocytes

We wanted to measure phosphorylation of the ERG subunit expressed in cardiac tissue. To do this ventricular myocytes were isolated from adult male albino guinea pigs within the weight range 250-500g using methods described previously (Lawrence and Rodrigo, 1999). The animals were killed by cervical dislocation in accordance with Home Office schedule 1 regulations. The heart was excised and immediately placed into cold, nominally calcium free Tyrode, containing (in mM) 135 NaCl, 6 KCl, 0.33 NaH_2PO_4, 5 sodium pyruvate, 10 glucose, 10 HEPES, 1 $MgCl_2$, pH 7.4 (adjusted using NaOH). The aorta was canulated and perfused for 6 minutes with nominally calcium free solution. All perfused solutions were at 37^0C. The atria were cut off and discarded. The heart was then perfused for between 6 to 10 minutes with nominally calcium free solution containing the following: BSA (prepared from factor V albumin) 1.6 mg ml^{-1}, protease (type XIV) 0.6 mg ml^{-1} and collagenase type I 1 mg ml^{-1}. Perfused enzyme solution was discarded for the first 2 minutes, then subsequently collected and recycled within the perfusion system. The time of enzyme perfusion was determined by the appearance of rod shaped ventricular myocytes from solution exiting the heart. Once these were seen, and the heart was soft to the touch, the heart was perfused for 3 minutes with normal Tyrode solution, containing (in mM) 135 NaCl, 6 KCl, 0.33 NaH_2PO_4, 5 sodium pyruvate, 10 glucose, 10 HEPES, 1 $MgCl_2$, 2 $CaCl_2$, pH 7.4 (adjusted using NaOH). The heart was then cut into three pieces, and shaken in a flask in a 37^0C water bath for 5 minutes in 10 ml normal Tyrode. Following this, heart tissue was placed into a new flask containing fresh normal Tyrode, and shaken at 37^0C. The process was repeated until the heart was completely digested. The fractions of solution were sieved to remove the remnants of the tissue and placed in a test tube. Cells were left to settle for 10 minutes, supernatant removed and then resuspended in normal Tyrode.

3.5.3 Guinea Pig ventricular myocyte Phosphorylation Assay

The full yield of cells from the ventricular myocyte isolation from a single guinea pig was used for each phosphorylation assay. The cells were split into between 3-6 test tubes and left to settle. They were then washed with phosphate free Krebs buffer, and resuspended in fresh phosphate free Krebs buffer and left to settle. A concentration of 5 μCi ml^{-1} of [^{32}P]-orthophosphate was made up in phosphate free Krebs buffer, and 1 ml of this solution was

added to each tube of cells. Cells were incubated for 90 minutes at 37°C, and were gently resuspended every 10 minutes. Test reagents were added directly to the tubes, as 100x stock solutions. Cells were left to settle during this period, and the experiment was stopped by removal of buffer and addition of ice-cold solubilisation buffer (as for HEK cell solubilisation). Cells were solubilised for 10 minutes on ice, collected, then cleared by centrifugation at 13000 rpm for 5 minutes at 4 °C. Typically, 850 µl of cleared lysate was removed and placed into fresh tubes, and solubilised ERG proteins were immunoprecipitated by incubation with anti-HERG antibody for 2 hours at 4°C. The rest of the procedure was carried out as described above for HEK cells. Gels were dried and subjected to autoradiography (-70°C) for up to 9 days.

3.5.4 Analysis of phosphorylation assays

Autoradiographs from phosphorylation assays were analysed by densitometry using the Alpha Imager 3400 system and computer programme (Alpha Innotech Corporation). Background signal of each lane was taken into consideration when measuring density of bands to control for any changes in background signal. Measuring each band gave an arbitary unit of signal strength. Using these values a percentage change in phosphorylation signal from base-line values could be calculated.

3.6 Western Blot Analysis

The technique of western blotting allows the expression pattern of cellular proteins to be investigated. Cell lysates are run on a SDS-PAGE gel to separate proteins by size, then transferred onto a nitrocellulose film. The procedure uses an antibody to detect specific proteins. This primary antibody binds to the protein of interest. A secondary antibody that has a high affinity for the primary antibody is then hybridised. The secondary antibody is conjugated to horseradish peroxidase (HRP), a molecule that allows visualisation of the antibody by the ECL+ kit (Amersham). Combined HRP and peroxide catalysed oxidation of acridan substrate generates thousands of acridinium ester molecules each minute. These react with peroxide under slightly alkaline conditions to produce a high intensity chemiluminescence with maximum emission at a wavelength of 430 nm. The resulting light

can be detected on autoradiography film. Resulting signals represent expression of the protein. This section describes the procedure for western blotting.

To identify PKC isoforms expressed in HERG-HEK cells, and to identify which are down-regulated upon chronic agonist stimulation, HERG-HEK cells were grown to ~90% confluency in 6 well plates. Phorbol 12-myristate 13-acetate (PMA), or its inactive analogue, 4αPMA, were added to cells to make a final concentration of 1 μM in the media. DMSO concentrations did not exceed 0.1%, and 0.1% DMSO controls were also carried out. After incubation with PMA or 4αPMA for 24 hours, media was removed, each well of cells was washed with 1 ml PBS, and lysed with 200 μl ice-cold solubilisation buffer (as for phosphorylation assay). Cells were solubilised for 10 minutes on ice, collected, then cleared by centrifugation. Protein concentrations were determined using the Lowry protein assay (see section 3.10). For single-well gels, samples were loaded at 360 μg total protein/gel. Proteins were resolved by 10% SDS-PAGE (for detection of PKC and β-actin proteins) or 8% SDS-PAGE (for detection of HERG protein). The Colorburst^{TM} electrophoresis marker (Sigma) was used to determine molecular weights. This produced bands at the following sizes (in kDa): 220, 100, 60, 45, 30, 20, 12, 8. Typically, gels were run at 200 V for 50-60 minutes. Once run, gels were transferred to nitrocellulose using the semi-dry blotting method. Blotting was carried out using a Trans-blot SD Semi dry transfer cell (Biorad). Typically, blotting was carried out for 25 minutes at 15 V. Samples were then blocked at 4°C overnight in 5% milk, made in 0.137 M tris buffered saline (TBS), containing (in mM) NaCl 85, KCl 2.7, Trizma base 25 (pH 8.0), with 0.1% TWEEN-20.

Primary antibodies were made up in 0.137 M TBS containing 0.1% TWEEN-20 (pH 7.4), and were applied at the following dilutions (as recommended by the supplier): PKC Isoforms: α 1:1000; β 1:250; δ 1:500; ε 1:1000; γ 1:1000; η 1:250; ι 1:250; λ 1:250; θ 1:250 (BD Biosciences), HERG: 1:1000 (in house), β-actin: 1:1000 (Sigma). All antibodies were applied for 1 hour at room temperature. During this incubation, blots were rocked at approximately 20 rpm. After incubation in primary antibody, blots were briefly rinsed with 0.137M TSB containing 0.1% TWEEN-20 and then more completely washed 3 times for 10 minutes using the same solution. Secondary antibodies were made up in 0.137M TBS containing 0.1% TWEEN-20, and were applied at the following dilutions: anti-rabbit: 1:1000

(Sigma). anti-mouse: 1:1000 (Sigma). All antibodies were applied for 1 hour at room temperature and the blots constantly rocked at approximately 20 rpm.

Protein detection was carried out using ECL+ (Amersham), following the manufacturer's protocol. Briefly, for each piece of nitrocellulose to be exposed, 500 µl Solution A was mixed with 12.5 µl Solution B. Excess wash solution was removed from nitrocellulose, and the ECL+ mix was added to the protein face of the nitrocellulose, and left for 5 minutes. After this time period, excess ECL+ solution was removed from the nitrocellulose, which was wrapped in clingfilm, ensuring no air bubbles were between the clingfilm and the protein face of the nitrocellulose. This was then placed protein-face up into a hypercassette, where it was exposed to Hyperfilm ECL (Amersham) for appropriate lengths of time (typically 5 minutes for PKC detection, 30 seconds for β-actin detection, 2 minutes for HERG detection), then developed using a hyperprocessor.

3.7 Lowry Protein Assay

The Lowry protein assay was used to quantify total protein levels in cell lysates. This allowed us to correct for protein levels when loading lysates in western blots. This assay is based on the biuret reaction. Copper sulphate is added to the protein solution in strong alkaline conditions. A purple-blue colour is produced, which results from complex formation between the cupric ions and the peptide bond. However, the biuret reaction is somewhat insensitive. The Lowry method amplifies the biuret reaction by subsequent reaction with the Folin phenol reagent. Although more sensitive protein assays are available, the Lowry assay is still widely used, and is capable of detecting protein levels from less than 25 to over 1200 µg ml^{-1} protein (Williams and Halsey, 1997).

Quantification of total protein was carried out as previously described (Lowry et al, 1951). All measurements were made in duplicate. A standard curve was created using bovine serum albumin (BSA) at concentrations of 25, 50, 100, 200, 250 and 400 µg/ml. Samples to be quantified were diluted by a factor of 20 to enable accurate measurement. The light absorbance of standards and samples were read at 750 nm. Estimation of total protein in the samples was carried out using a linear regression curve (Prism 3.0).

3.8 Muscarinic Acetylcholine receptor Binding Assay

In order to accurately estimate the muscarinic acetylcholine receptor population in the HEK cell lines used in this thesis, we used a binding assay. The radiolabelled ligand used in these experiments, [^{3}H]-N-methyl-scopolamine ([^{3}H]-NMS), is a highly specific, high affinity antagonist of muscarinic acetylcholine receptors. Use of an antagonist in these binding assays means the receptor it binds to will not be internalised and down-regulated. [^{3}H]-NMS is also relatively impermeable to the cell membrane, thus allowing only binding to receptors expressed at the cell surface. Incubating cells in [^{3}H]-NMS allows it to bind to any available receptors. After washing to remove unbound [^{3}H]-NMS, we are able to measure the muscarinic population by measuring radioactivity in each sample, and correcting for protein. Cells were plated out on poly-L-lysine coated 24-well plates two days prior to the experiment, to enable cells to be 50-70% confluent for the experiment. Each experiment was carried out in triplicate, with corresponding wells to measure total binding (TB), non-specific binding (NSB) and total protein (TP). Media was aspirated off, and all cells were washed twice with 1 ml Krebs-Henseleit buffer (KHB) containing (in mM) NaCl 118, KCl 4.7, $CaCl_2$ 1.3, KH_2PO_4 1.2, $MgSO_4$ 1.2, Na HCO_3 25, HEPES 5, glucose 10, pH 7.4. KHB was heated to 37°C and gassed with 95% O_2 / 5% CO_2 . After washing, buffer was fully aspirated and 400 µl KHB was added to each well. To define non-specific binding, 10 µM atropine was added to NSB-allocated wells to occupy high affinity receptor sites for NMS. After a 10 minute incubation at 37°C with atropine (to allow equilibration), approximately 3 nM [^{3}H]-NMS was added to all wells allocated to measure NSB and TB. Cells were incubated with [^{3}H]-NMS for 1 hour at 37°C. After this time period, plates were transferred to ice. All wells were aspirated, and cells were washed twice with 1 ml ice-cold KHB, in order to minimise dissociation of [^{3}H]-NMS from receptors. Once washed, cells were incubated with 0.1M NaOH for 30 minutes at 37°C, in order to solubilise cells. After this incubation, the full 500 µl volume was removed into scintillation vials and 4.2 ml scintillation fluid was added. Vials were then vortexed, and counted on a 3 minute [^{3}H] protocol. A Lowry protein assay was used to determine protein levels in the TP allocated wells (as described in section

3.10). Data were analysed using the following equation to work out total binding of [^{3}H]-NMS (pmol):

$$\frac{\text{Counts (d.p.m.)}}{2.22 \times 10^6 \text{ (d.p.m./}\mu\text{Ci)}} \times \frac{1000}{[^3\text{H}]\text{-specific activity (}\mu\text{Ci /pmol)}}$$

The [^{3}H] –NMS specific activity was 84 μCi /nmol

Data were then normalised to total protein and values expressed in fmol mg^{-1} total protein.

Chapter 4

Characterisation of HERG currents in HEK 293 cells and *Xenopus* oocytes

4.1 Introduction

In order to investigate modulation of the HERG channel current by second messenger systems, recombinant HERG channels expressed in the HEK mammalian cell line were used. This allowed investigation of the current in a mammalian background, without potential contamination from other currents. Although the ideal option, physiologically, would be to record I_{Kr} from ventricular myocytes, this was not done for this study. This was mainly due to the difficulty of measuring I_{Kr}, the current for which HERG is the pore-forming subunit. I_{Kr} amplitude in ventricular myocytes is small, and I_{Kr} is easily contaminated with other membrane currents, including those of ion channels, ion exchangers and transporters. A stably transfected HEK cells line was available that has been well-characterised by many laboratories (Zhou et al., 1998). For some experiments HERG was transiently transfected into HEK cells. The HEK cell background was used throughout most studies in this thesis. The *Xenopus* oocytes expression system was also used in these studies. These cells however, were not used in studies characterising the modulation of current, as there may be differences in expression of modulatory proteins in these cells compared to mammalian cells.

HERG channels have unusual kinetics compared to other voltage-gated potassium channels. Activation and deactivation are slow, occurring over several seconds, whereas inactivation of the channel is rapid (Zhou et al, 1998; Tristani-Firouzi and Samguinetti, 2003). Activation and inactivation are seemingly controlled by a single voltage sensor, which translates the change of membrane voltage into a change in protein conformation that alters channel conduction (Liman and Hess, 1991; Loots and Isacoff, 1998, Liu et al., 2003a, Jiang et al., 2003a). Activation and inactivation appear to occur independently in the HERG channel, again leading to speculation of how this can occur when seemingly controlled by the same mechanism. Therefore, the kinetics of the HERG channel are complex. The studies in this chapter aimed to characterise the WT HERG channel in both *Xenopus* oocytes and HEK cells. Although characterisation of the HERG channel has been carried out by many others previously, these experiments allowed me to ensure the currents I was observing had similar

kinetics to previous reports, and validated our experimental recording conditions. These studies also allowed me to investigate kinetic differences between HERG currents expressed in mammalian and non-mammalian tissues.

4.2 Results

4.2.1 Current-voltage relationships for HERG current expressed in HEK 293 cells

HEK 293 cells stable expressing HERG currents were voltage clamped, and currents were measured using the whole cell configuration of the patch clamp technique. Currents were elicited using the I-V protocol (for detail see section 3.2.3.1). Figure 4.1A shows a representative family of HERG currents. For clarity, currents evoked by different voltage pulses are shown as different colours. Currents during the test potential were first observed at around –40 mV, and increased until cells were depolarised to potentials greater than 0 mV. After this point the current amplitude decreased. This has been referred to as inward rectification and is due to an increasing amount of channel inactivation at more positive potentials (shown later in this chapter). Under conditions used in this study, HERG isochronal end pulse current peaks at 0 mV, before decreasing with further voltage pulses (figure 4.1B). Figure 4.1C shows the mean activation curve produced from a total of 26 cells. This data was fitted with a Boltzmann function to obtain values for half maximal activation ($V_{0.5}$) and slope factor. The $V_{0.5}$ for activation of HERG currents expressed in HEK cells was –20.51 ± 1.87 mV, with a slope factor of 7.35 ± 0.51 (n=26)

HERG currents expressed in *Xenopus* oocytes were recorded using two-electrode voltage clamp. Currents were elicited using the oocyte I-V protocol (for detail see section 3.2.3.1). A representative family of HERG currents recorded in response to this voltage protocol can be seen in figure 4.2A. For clarity currents produced at different voltages are shown in different colours. Currents were analysed as described for HERG currents in HEK cells. Figure 4.2B shows the mean isochronal I-V relationship of the HERG channel when expressed in *Xenopus* oocytes. In these recording conditions, isochronal end-pulse current peaked at –20 mV, after which currents reduced due to an increased inactivation of the channel. Figure 4.2C shows the activation curve of the current under these recording conditions, fitted with a Boltzmann function. The $V_{0.5}$ for activation of HERG currents expressed in *Xenopus* oocytes was –25.73 ± 3.12 mV, with a slope factor of 7.94 ± 0.37 (n=5).

Figure 4.1
The current-voltage relationship of the HERG channel. **A** Representative family of currents current elicited using the I-V protocol. For clarity the current from each voltage is shown as a different colour. **B** Normalised mean isochronal end pulse currents plotted as a function of voltage (n=26). **C** Normalised mean peak tail currents plotted against voltage and fitted with a Boltzmann function (n=26).

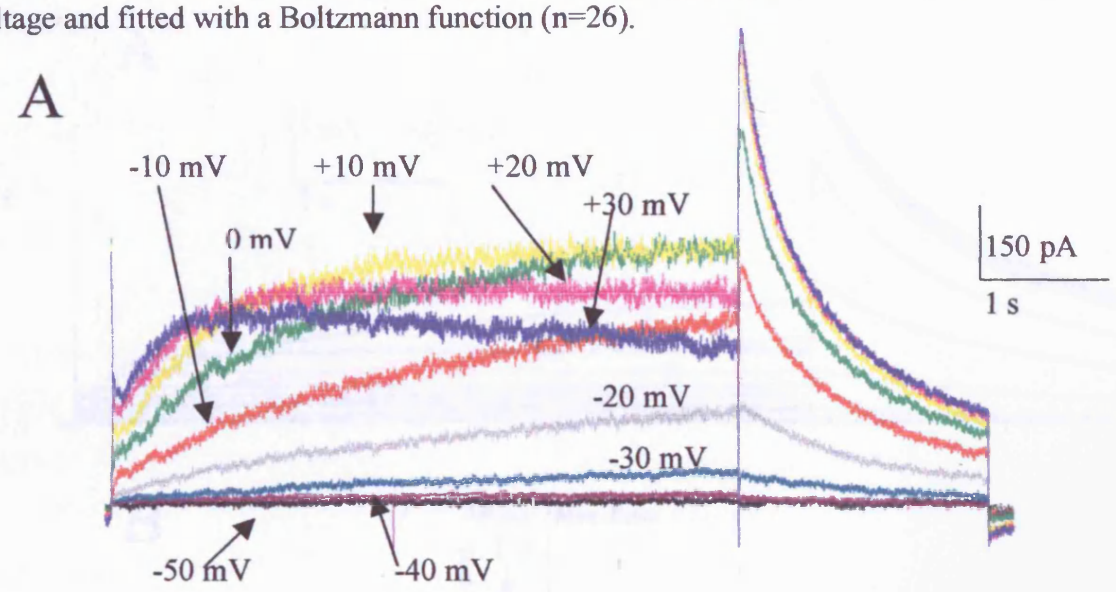

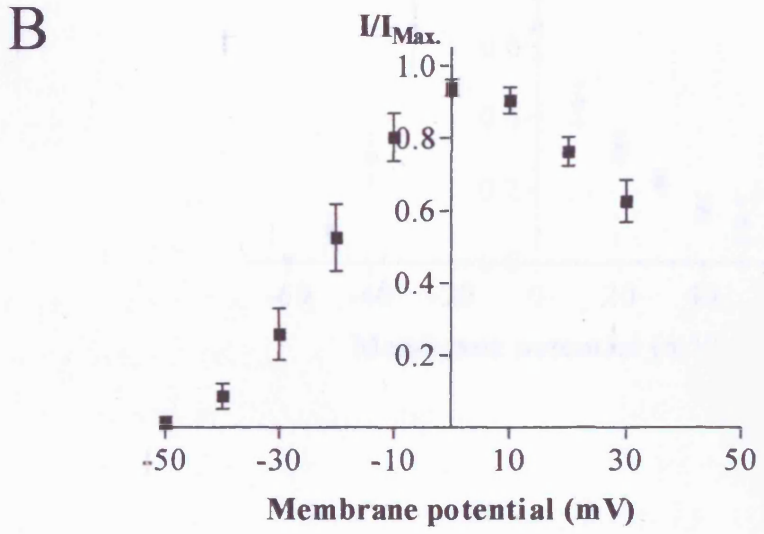

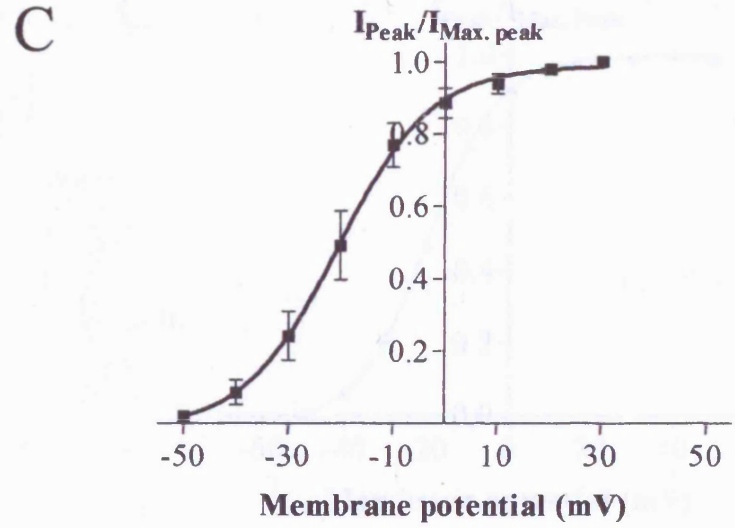

Figure 4.2
Current-voltage relationship of HERG currents expressed in *Xenopus* oocytes. A Representative family of currents elicited using the protocol shown in panel A. **B** Normalised mean isochronal end pulse currents plotted as a function of voltage (n=5). **C** Normalised mean peak tail currents plotted as a function of voltage and fitted with a Boltzmann function (n=5). Error bars are smaller than point size.

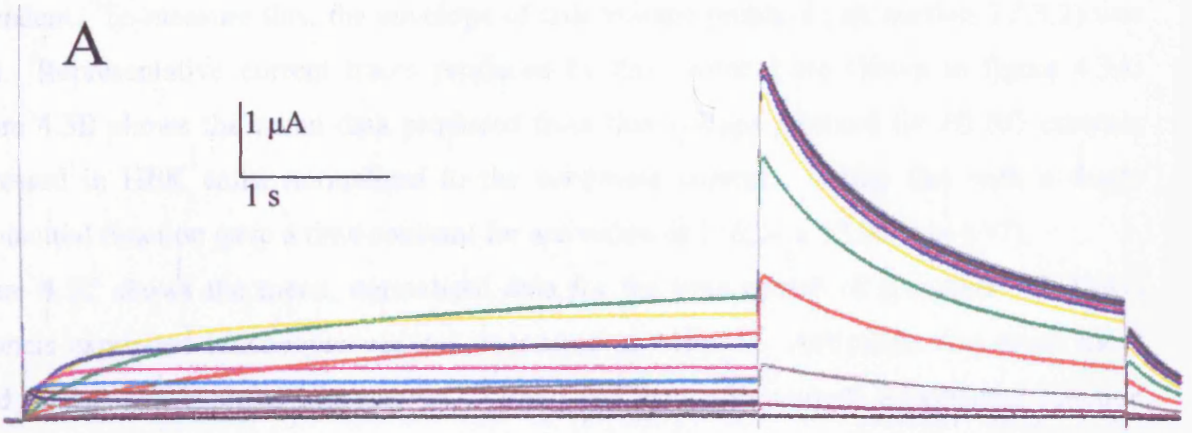

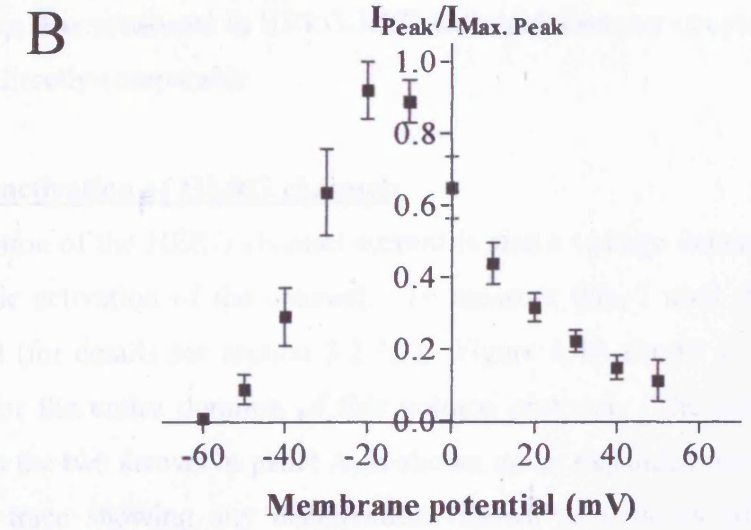

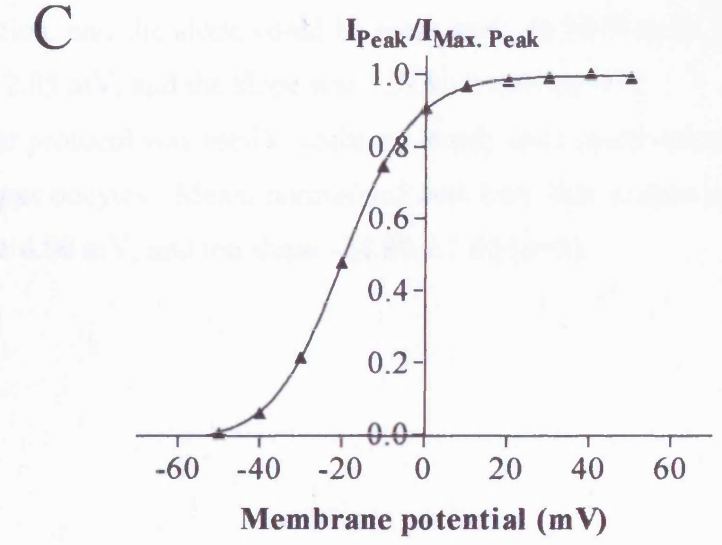

In addition to being voltage dependent, activation of the HERG current is also time dependent. To measure this, the envelope of tails voltage protocol (see section 3.2.3.2) was used. Representative current traces produced by this protocol are shown in figure 4.3A. Figure 4.3B shows the mean data produced from this voltage protocol for HERG currents expressed in HEK cells, normalised to the maximum current. Fitting this with a single exponential function gave a time constant for activation of 116.24 ± 13.06 ms (n=7).

Figure 4.3C shows the mean, normalised data for the time course of activation of HERG channels expressed in *Xenopus* oocytes, measured at +40 mV. Activation was much more rapid in channels expressed in oocytes. Fitting this data with a single exponential function gave a time constant of activation of 29.64 ± 2.44 ms (n=5). Because the time constant of activation was measured in HERG-HEK cells and *Xenopus* oocytes at different voltages they are not directly comparable.

4.2.2 Inactivation of HERG channels

Inactivation of the HERG channel current is also a voltage dependent process, which occurs alongside activation of the channel. To measure this, I used the steady state inactivation protocol (for details see section 3.2.3.3). Figure 4.4A shows a set of representative current traces for the entire duration of this voltage protocol. The section of the trace indicated between the two arrows in panel A, is shown on an expanded time scale in figure 4.4B. Any current trace showing any deactivation (shown as a decay of current at more negative potentials, seen at –140 mV in panel A) was discarded. Peak current at the beginning of the third pulse was normalised to the maximum peak current, plotted as a function of voltage (seen in figure 4.4C), and fitted with a Boltzmann function. From this the midpoint of inactivation, and the slope could be measured. In HEK cells, the $V_{0.5}$ of inactivation was –75.87 ± 2.05 mV, and the slope was –20.80 ± 0.69 (n=13).

A similar protocol was used to measure steady state inactivation of HERG currents expressed in *Xenopus* oocytes. Mean, normalised data from this is shown in figure 4.4D. The $V_{0.5}$ was –87.12 ± 4.00 mV, and the slope –24.86 ± 2.05 (n=5).

Figure 4.3
The envelope of tails protocol measures time dependent activation of HERG. A Representative currents measured from HEK cells using the envelope of tails protocol. **B** Mean, normalised time-course of activation for HERG current in HEK cells measured at 0 mV (n=7). **C** Mean, normalised time-course of activation for HERG current in *Xenopus* oocytes measured at +40 mV (n=5).

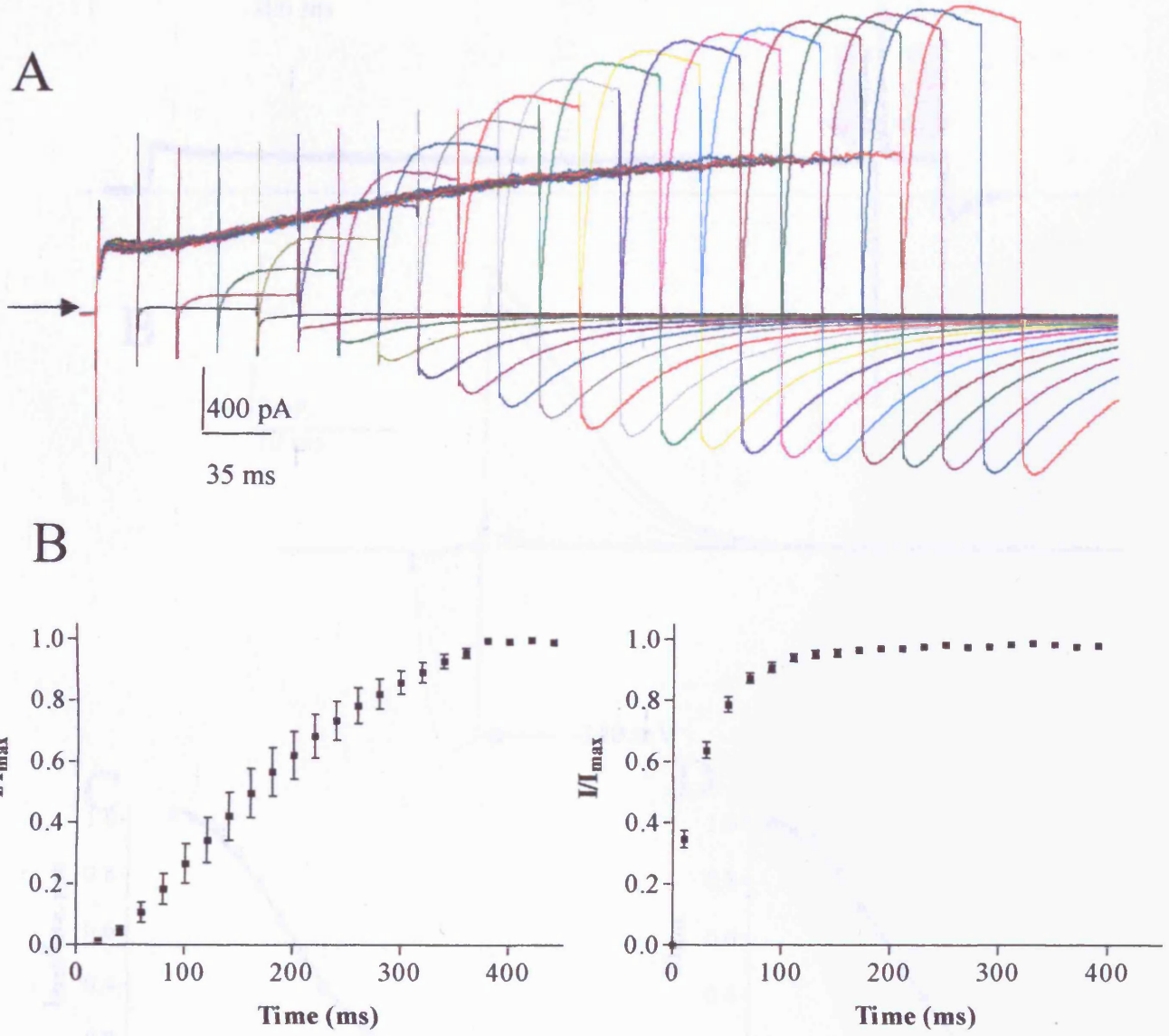

Figure 4.4

Steady state inactivation of the HERG channel in HEK cells. **A** Current traces elicited during complete steady state inactivation protocol. The dotted line indicates the zero current line. **B** Current on an expanded time scale. Current shown in B was recorded between the two points indicated by arrows in panel A. **C** Normalised mean data measuring steady state inactivation as a function of voltage in HEK cells (n=13). **D** Normalised mean data measuring steady state inactivation in oocytes (n=5). Data are fitted with a Boltzmann function (solid lines).

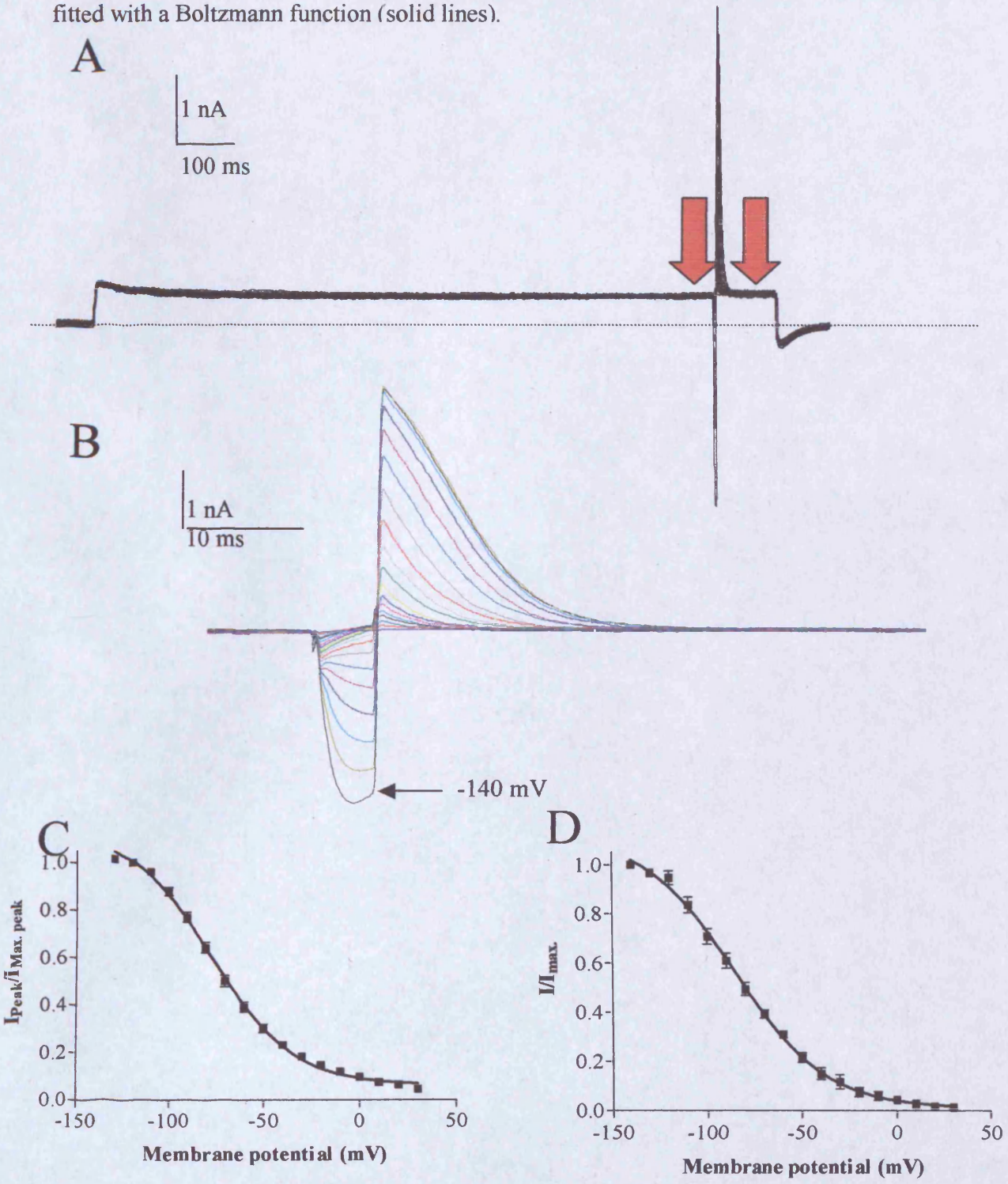

Figure 4.5

The 'fully activated I-V' protocol with HERG currents expressed in HEK cells. **A** representative current trace elicited. For clarity, current evoked at each voltage potential is shown as a different colour. Red arrow represents the zero current line. **B** Mean time constants of deactivation as a function of voltage. **C** Mean peak tail currents (measured at the point of the black arrow in panel A), plotted as a function of voltage (n=5).

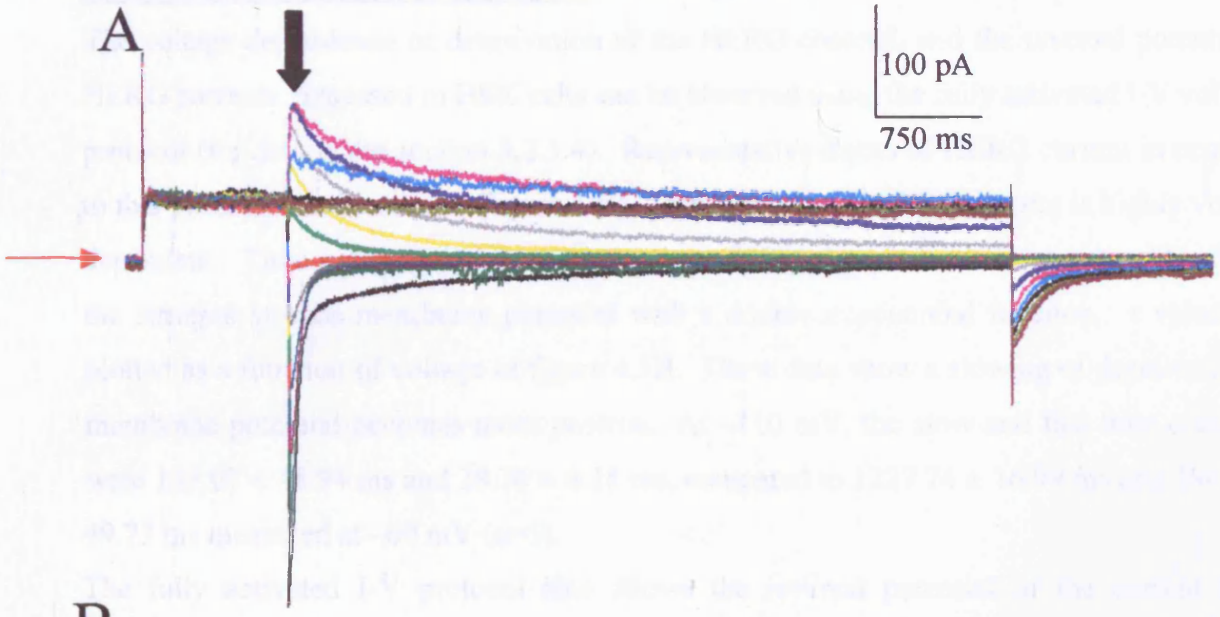

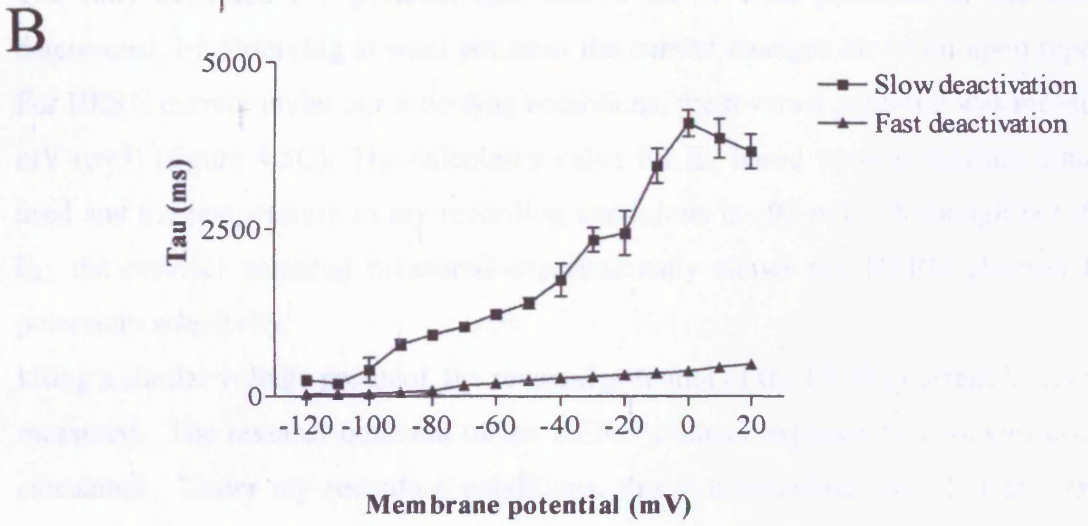

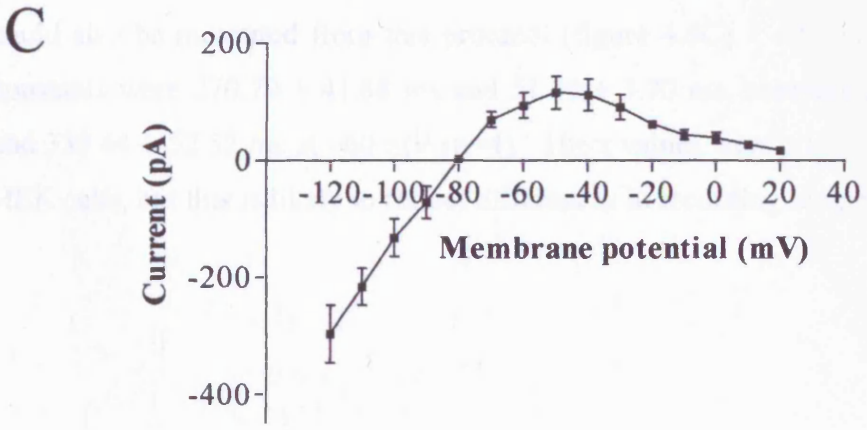

4.2.3 Deactivation of HERG channels

The voltage dependence of deactivation of the HERG channel, and the reversal potential of HERG currents expressed in HEK cells can be observed using the fully activated I-V voltage protocol (for details see section 3.2.3.4). Representative traces of HERG current in response to this protocol can be seen in Figure 4.5A. Deactivation of HERG current is highly voltage dependent. Time constants (τ) for deactivation of HERG currents were measured by fitting the currents at each membrane potential with a double exponential function. τ values are plotted as a function of voltage in figure 4.5B. These data show a slowing of deactivation as membrane potential becomes more positve. At –110 mV, the slow and fast time constants were 189.07 ± 48.94 ms and 28.76 ± 8.18 ms, compared to 1227.74 ± 16.99 ms and 194.36 ± 49.73 ms measured at –60 mV (n=5).

The fully activated I-V protocol also allows the reversal potential of the current to be determined, by observing at what potential the current changes direction upon repolarisation. For HERG current under our recording conditions, the reversal potential was measured at –79 mV (n=5) (figure 4.5C). The calculated value for E_K based upon potassium concentrations used and the temperature in my recording conditions is –92 mV. Although not the same as E_K, the reversal potential measured experimentally shows the HERG channel has a high potassium selectivity.

Using a similar voltage protocol, the reversal potential of the HERG current in oocytes can be measured. The reversal potential of the HERG channel expressed in oocytes could then be calculated. Under my recording conditions, this was calculated as –114 mV (n=4, figure 4.6B). Since I am not controlling the internal environment of the cell when I record HERG currents in oocytes, I am unable to calculate E_K. The voltage dependence of deactivation could also be measured from this protocol (figure 4.6C). At –110 mV slow and fast time constants were 270.79 ± 41.88 ms and 51.35 ± 3.70 ms, compared to 1589.83 ± 176.43 ms and 339.44 ± 52.52 ms at –60 mV (n=4). The τ values were a little slower in oocytes than in HEK cells, but this is likely to reflect differences in recording temperatures.

Figure 4.6

The 'fully activated I-V' protocol on HERG currents expressed in oocytes. **A** Representative family of currents elicited. For clarity, each separate trace is shown as a different colour. The black arrow indicates the zero current line. **B** Mean peak tail current measured where the thick black arrow is shown in panel A, plotted as a function of voltage (n=4). **C** Mean time constants of deactivation (n=4).

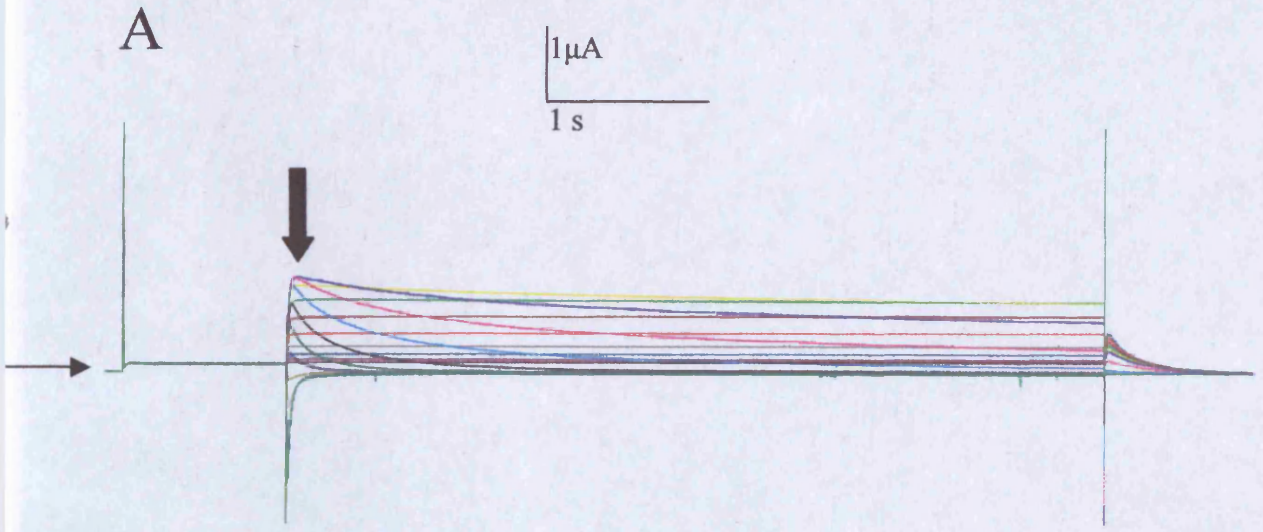

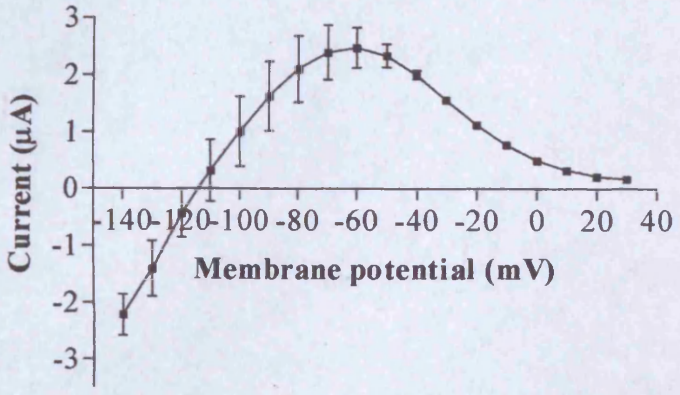

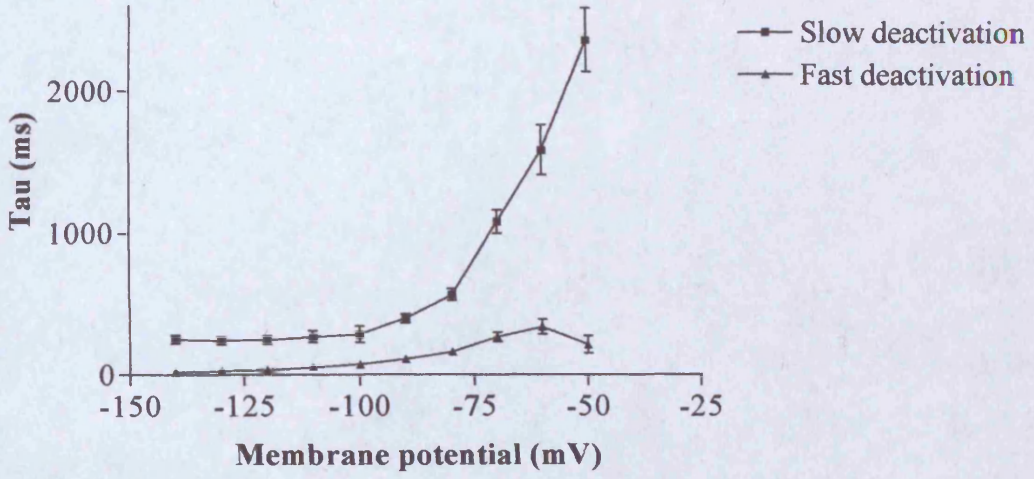

4.2.4 Dofetilide block of HERG current

The HERG channel current is blocked by a large number of pharmacological agents. This allows the HERG current to be easily identified and separated from endogenous currents. To determine if current during voltage pulses was predominantly HERG, 1 μM dofetilide, a well characterised HERG channel blocker was applied. The 'depolarisation to 0 mV' voltage protocol (for details see section 3.2.3.5) was repeated to determine when current amplitude stabilised. Dofetilide was then applied extracellularly, and repepitive pulsing continued. Current during the test pulse and peak tail current amplitude started to decrease the first pulse after dofetilide application. The onset of block by dofetilide was relatively slow. Maximal effects of dofetilde were observed after ~ 250 seconds. Representative current traces in control conditions and in the presence of dofetilide are shown in figure 4.7A. The peak tail currents from each voltage were normalised to peak tail currents before dofetilide application. The mean time course of the effects of dofetilide is shown in figure 4.7B. Decay of current in the presence of dofetilide was fitted with a single exponential function, giving a time constant of 36.63 ± 6.70 seconds (n=5). Peak tail currents with maximum effects of dofetilide were 0.41 ± 0.22% of control currents (n=5). All current elicited by the tail potential was inhibited. This suggests there are minimal contaminating currents in HEK cells that are observed at this voltage. Some current during the depolarising pulse was observed to remain after dofetilide block of HERG current. This remaining current showed a rapid activation, and a slow decay with time. It is likely that this current is a transient outward potassium current endogenously expressed in HEK cells. Although some current remained at the end of the depolarising pulse, this was small (9.13 ± 1.34% of control current). However, this contaminating current may be modulated by the various compounds applied to the HEK cells in experiments in this thesis. As a result of this of this, all effects seen from compound application in this thesis will be measured as the effects they show on peak tail current only. This allows us to be confident that we are measuring the effects of compound on HERG currents only.

I-V and steady-state inactivation protocols (see sections 3.2.3.1 and 3.2.3.3 respectively) were also carried out before and during dofetilde application. This allowed us to measure any current remaining at other voltages. Figure 4.8A shows mean isochronal current-voltage relationship in control conditions and after dofetilide application (n=5). Data has been

Figure 4.7

The current measured in HERG HEK cells is blocked by the HERG channel inhibitor dofetilide. **A** Representative current trace in control conditions and after attainting steady state block with 1μM dofetilide. Dotted line represents the zero current line. **B** The mean time-course of the effects of 1μM dofetilide application on peak tail currents (n=5).

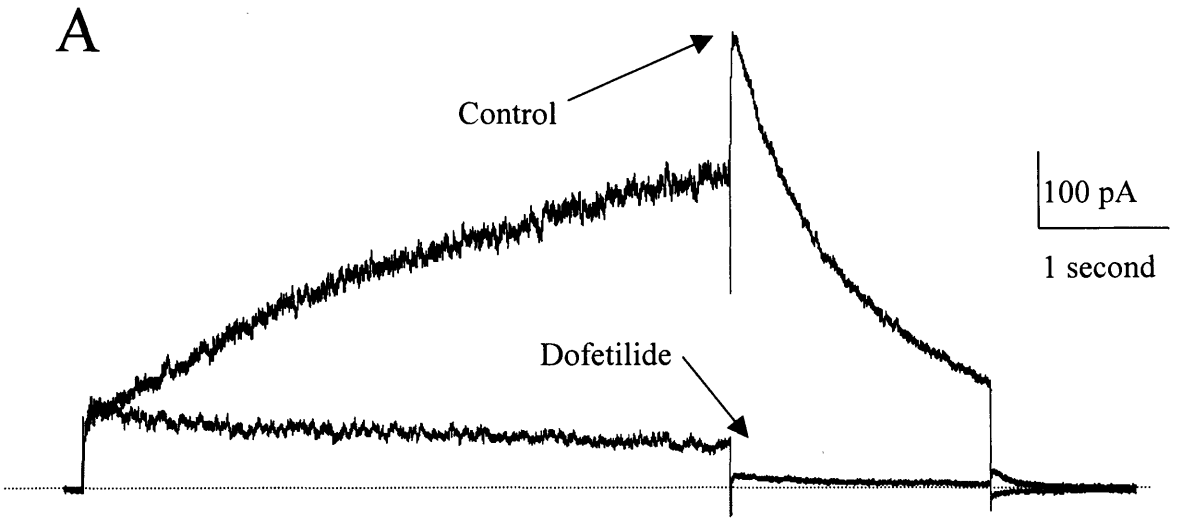

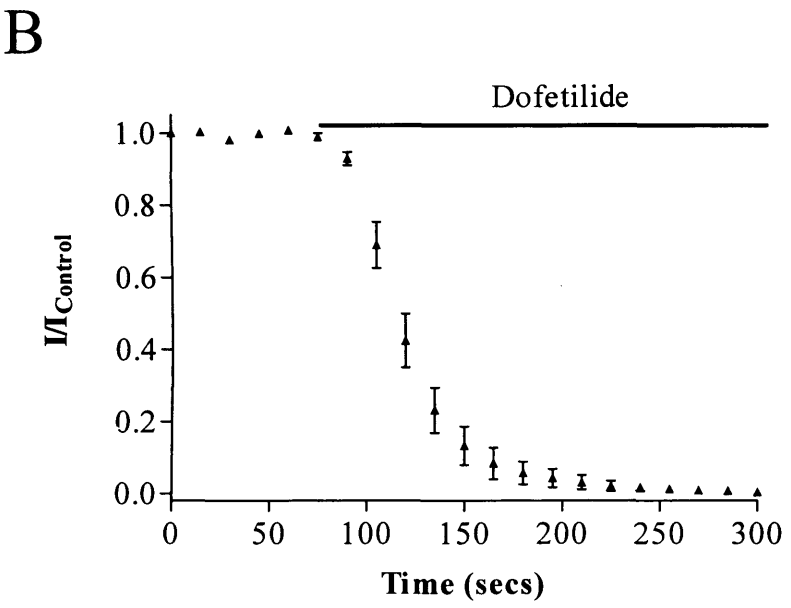

Figure 4.8
Block of HERG current by dofetilide **A** Normalised mean isochronal end pulse current from an I-V protocol in control conditions and with 1μM dofetilide. **B** Normalised mean peak tail current in control conditions and with dofetilide, fitted with Boltzmann functions (n=5, error bars are smaller than point size). C Normalised current amplitude at the beginning of the third pulse of the steady state inactivation protocol in control conditions and with dofetilide, fitted with Boltzmann functions (n=5, error bars are smaller than point size).

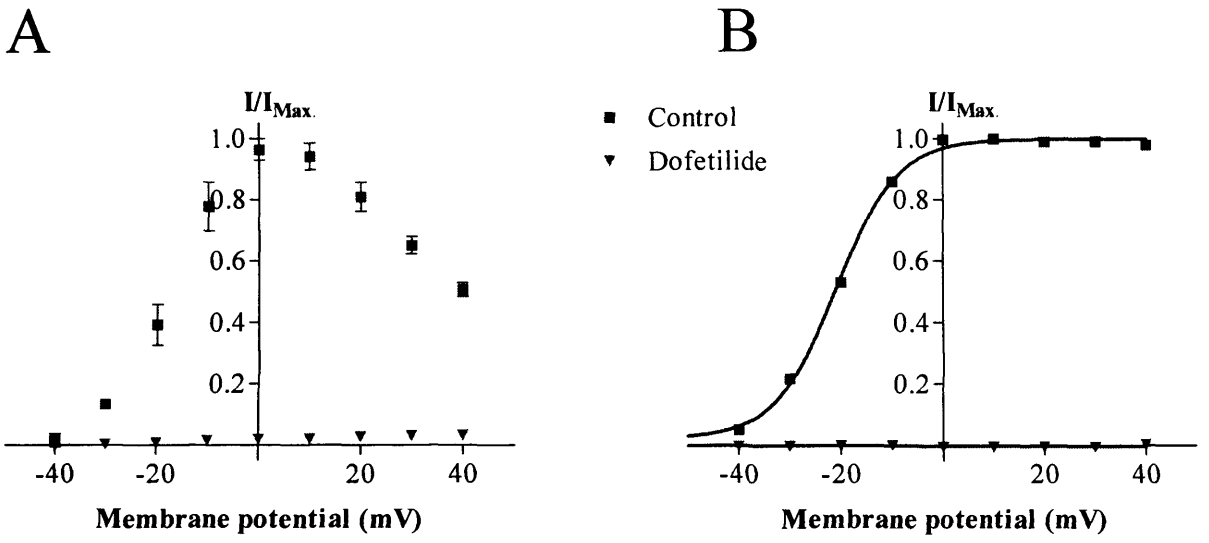

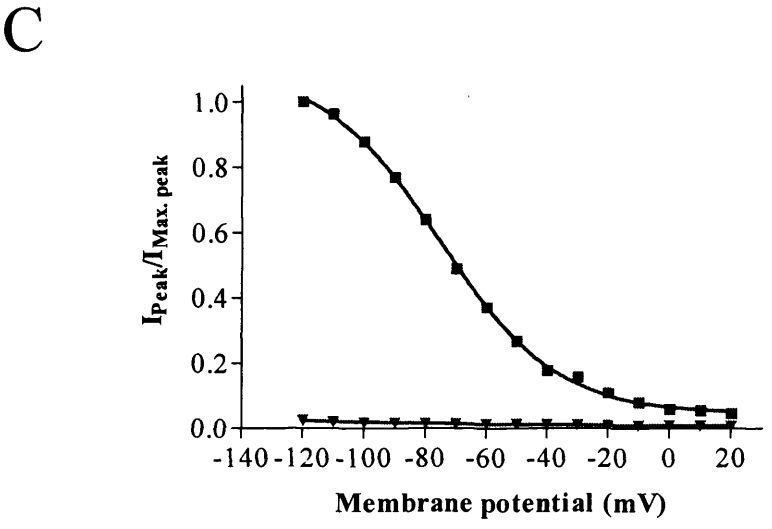

normalised to the maximal isochronal current in control conditions. It is clear that dofetilide blocks the majority of current measured using the I-V voltage protocol. However, there is a small outward current that increases with increased voltage. The amplitude of this current at +40 mV however is negligible, being 3.24 ± 1.42% of maximum current in control conditions (n=5). Figure 4.8B shows the mean activation curve of the HERG current in control conditions and in the presence of dofetilide (n=5). Data in this graph has been normalised to the maximum peak tail current in control conditions. It is clear that dofetilide blocks all current at all voltages as current remaining at the test potentials was negligible in the presence of dofetilide. Maximum current in the presence of dofetilide was observed at +40 mV, where it was 0.24 ± 0.05% of maximal control current. Figure 4.8C shows a representative steady state inactivation plot in control conditions and in the presence of dofetilide (n=5). Currents were normalised to the maximum tail current in control conditions. Using this voltage protocol, currents were negligible at all voltages in the presence of dofetilide. Maximal currents were measured at –120 mV, where currents were 2.34 ± 0.16% of control current (n=5). This suggests that only HERG currents are activated at the voltages used in this protocol.

4.2.5 Rundown of HERG current in HEK cells

Rundown of current can be defined as a decrease in amplitude of current with time in control conditions. Rundown of current is evident during whole cell patch clamp recordings, and is likely to be due to dialysis of an intracellular factor out of the cell. Rundown of ERG current expressed in mammalian tissue during whole cell recording is a well-known phenomenon (Hirdes et al., 2004). The extent of rundown of the current varies between studies. This is likely to be due to a number of factors, including intracellular solution composition and electrode size, which may alter the rate of dialysis of intracellular factors. Therefore, we needed to characterise the rundown of the HERG current in HEK cells under our recording conditions.

I found rundown to vary between cells. Some cells showed profound rundown within 30 seconds after recording started, and others seemed to show little rundown after 10 minutes. No pattern between rundown and cell parameters (current size, cell size) were observed.

Cells showing a profound rundown were discarded, as any effects of compound applied to these cells would be difficult to monitor.

In order to evaluate the rundown of current, I measured peak tail currents from HEK cells stably expressing HERG current in control Tyrode using the 'depolarisation to 0 mV' voltage protocol over a 15 minute time period. This allowed me to compare the amplitude of current in control conditions to the amplitude in test conditions. For experiments that were carried out over a shorter time period, the current amplitude at the end of the experiment was compared to the corresponding time in rundown experiments. This allowed me to test if there was any statistical significance between data sets.

The mean rundown from 35 cells is plotted in figure 4.9A. The peak tail current from the first four voltage sweeps was averaged to produce a starting value. All subsequent tail currents recorded after this were normalised to this value. After a 15 minute recording period, peak tail current was 78.56 ± 1.94% of starting current. Current rundown had a linear time course, showing on average, a decay of 1.5% per minute.

I also tested if the voltage-dependence of the HERG current changed when recordings are carried out over a long period of time. There was no significant shift in the $V_{0.5}$ for activation over time (see figure 4.9B). The midpoint of activation at the start of recording was –23.51 ± 0.58 mV, compared to –22.81 ± 1.09 mV after 15 minutes recording (n=15, $p>0.05$). The slope factor was also not significantly altered. In control conditions this was 6.83 ± 0.50, compared to 7.46 ± 0.96 after 15 minutes ($p>0.05$).

I measured steady state inactivation of the current at the start of the recording and after 15 minutes of recording (see figure 4.9C). The $V_{0.5}$ of inactivation was measured at –76.48 ± 1.45 mV at the start of recording, compared with –77.20 ± 1.48 mV after 15 minutes (n=8). This difference was not statistically different ($p>0.05$). The slope factor of the curve was also unaltered. At the start of recording this was –17.61 ± 1.20, compared to –20.09 ± 1.93 after 15 minutes ($p>0.05$).

Deactivation of the current after a test-pulse to 0 mV was measured over a 15 minute time period, and fitted with a double exponential function. Mean time constants for the start and end of the 15 minute recording period can be seen in figure 4.9D. The mean time constants at the start of recording were 1272.56 ± 55.89 ms, and 243.36 ± 14.38 ms, compared to 1275.92

± 56.27 ms and 242.93 ± 13.78 ms after 15 minutes (n=35). There was no statistically significant change in either the fast or slow time constants of deactivation over time ($p>0.05$). To summarise, results from this rundown study allow us to be confident that any effects on activation, inactivation or deactivation of the current we observe during test conditions are not due to rundown of the current.

Figure 4.9

Rundown of the HERG current expressed in HEK cells. A The mean time-course of rundown of tail current, measured over 15 minutes (n=35). B I-V protocols were run at the start and end of the 15 minute recording period to investigate changes to voltage dependence of activation. Normalised peak tail currents were plotted against test potential and fitted with Boltzmann functions (n=15). C Voltage dependence of steady state inactivation. Data was collected at the start of recording, and after 15 minutes of recording and fitted with Boltzmann functions (n=8). D Fast and slow deactivation times constants (n=35) at the start of recording (denoted by "start") and after 15 minutes of recording (denoted by "end").

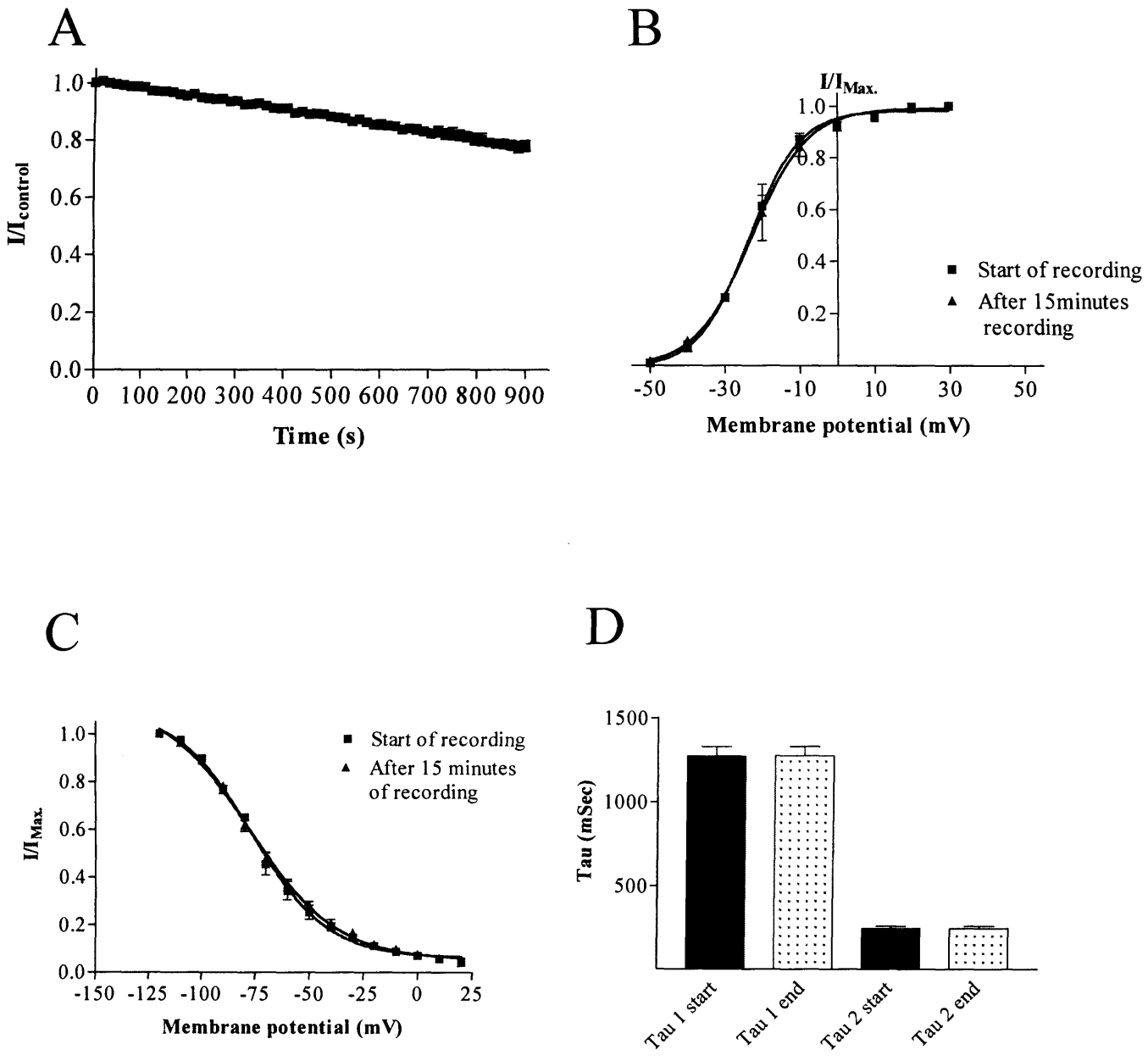

4.3 Discussion

4.3.1 Characterisation of WT HERG channel currents

In this chapter I have characterised WT HERG currents expressed in HEK cells and *Xenopus* oocytes. Zhou et al. (1998) first characterised the HERG-HEK cell line used in this thesis, and found the $V_{0.5}$ of activation was –25.9 mV, with a slope factor of 6.0, not dissimilar to values measured in my work of –20.51 ± 1.87 mV and 7.35. Other studies that have studied HERG in cultured mammalian cells have yielded a variety of results. In HEK cells, Thomas et al. (1999) showed the $V_{0.5}$ for activation was –4.3 mV and Kagan et al. (2002) measured it as approximately 0 mV. Other studies have found the $V_{0.5}$ of activation of HERG channel currents in HEK cells to be –23 mV (Han et al., 2004), -16.9 mV (Sun et al., 2004) and approximately 0 mV (Wei et al., 2002). Studies investigating HERG channels expressed in CHO cells, another mammalian cultured cell line, have also yielded varying results. Weeapura et al. (2002) showed the $V_{0.5}$ of activation was –22 mV, again not dissimilar to results from our study and that of Zhou et al. However, in a study carried out by McDonald et al. (1997), the $V_{0.5}$ of activation was measured as +12 mV. Bian et al. (2004) measured the $V_{0.5}$ of activation as +0.99 mV, Cui et al. (2000) measured it as –5 mV and Bérubé et al. (1999) as –8.5 mV. These recordings were all carried out using similar intra- and extra-cellular solutions, so the question of how these differences arise must be posed. The differences in $V_{0.5}$ values between studies may be due to a number of factors. The HERG channel is sensitive to temperature (Zhou et al., 1998), so this must be taken into account when comparing data from different studies. Test pulse duration must also be taken into account, as HERG current activation is also time-dependent (Zhou et al., 1998; Hancox et al., 1998). Short test pulses, during which HERG current may not fully activate, may cause apparent shifts in the voltage dependence of activation.

In the same cell line as that used in this study, Zhou et al. (1998) showed the presence of a small-amplitude background current, similar to that seen in my studies. Similarly to my data, the group found this background current had a linear relationship with voltage, increasing as voltage was increased during the test pulse. Again, like data shown in this chapter, no current was evoked during repolarisation to –50 mV to measure HERG tail currents.

In these HERG-HEK cells, Zhou et al. found the reversal potential of HERG current to be around –85 mV when recording currents in 4 mM extracellular potassium, again a similar

value to that measured in my data, showing the HERG channel has a high potassium selectivity. This similarity between my data and that of Zhou et al., who made and characterised the HERG-HEK cell line we used, allows me to be confident the current I am recording in HEK cells under our conditions is HERG current, and is not contaminated by endogenous currents.

When comparing deactivation kinetics measured in this body of work to other studies measuring HERG current in HEK cells, similarities are seen. Weeapura et al. (2002) fitted time constants of deactivation (measured at –50 mV) with a double exponential function, leading to time constants of ~1100 ms and ~230 ms, which are very similar to those observed in this study. Other studies measuring deactivation at –50 mV with a double exponential have shown values of ~1027 ms and ~137 ms (Zhou et al., 1998), ~1000 ms and ~100 ms (Wu et al., 2003) and ~100 ms and ~1200 ms (Sun et al., 2004). Again, similarities between this data and that in this body of work allows me to be confident the current I am measuring is HERG.

A study carried out by Wang et al. (1997) characterised the activation kinetics of HERG channels expressed in *Xenopus* oocytes. This study found the midpoint of activation of HERG currents was –21 mV, with a slope factor of activation of 7.0. This data is very similar to my own findings of the midpoint of activation being –25 mV, with a slope factor of 7.9. Other studies carried out in *Xenopus* oocytes yielded $V_{0.5}$ values for activation of –19.5 mV (Weeapura et al., 2002), -33.9 mV (Aydar and Palmer, 2001) and -19.2 mV (Schonnherr et al., 1996). Again, like in mammalian cells, a range of values have been measured. This is also likely to be due to differences in recording conditions, such as pH, extracellular concentration of divalent cations or test pulse duration.

4.3.2 Molecular basis of HERG channel gating

The kinetics of the HERG channels are unusual. HERG currents show slow activation and deactivation, occurring over a few seconds, but very rapid inactivation of the channel, which occurs over tens of milliseconds. The structural basis for these kinetics is not yet fully understood. The HERG channel is made up of four subunits, each of which have six membrane-spanning regions. The S4 domain contains six positively charged residues. It is thought these residues contribute to the voltage sensitivity of the channel. The mechanism of

voltage sensing in potassium channels is thought to involve a rotation and possible translation of the S4 domain relative to the electric field, that it is coupled to opening of the activation gate of the channel (reviewed in Swartz, 2004). So the slow activation of HERG could be due to either a slow coupling between the movement of S4 and opening of the activation gate, or a slow movement of the S4 domain in response to a change in membrane voltage. Gating currents are the currents passed by a channel in the absence of ionic current, and correspond to movement of charged residues across the membrane. Studying these currents allows the movement of the S4 domain to be observed. In a study carried out investigating gating currents of HERG, Piper and colleagues (2003) showed the time constant for the gating current upon channel opening was slow. This suggests that the movement of the voltage sensor itself is slow, although the underlying mechanism remains unknown. The amino acid sequence of the HERG channel differs from that of other voltage gated potassium channels (such as Shaker channels) in a number of ways. These include additional charges in the HERG channel. These are negative charges, and may interact with the positive charges on the S4 domain. One residue in particular, D540, when mutated, causes the HERG channel to open upon both depolarisation (like WT channels), and also with hyperpolarisation (Sanguinetti and Xu, 1999). This suggests this residue is important in stabilising the closed state of the HERG channel.

The slow closing, or deactivation of the HERG channel is thought to be due, in part, to the N-terminal domain. Studies have shown that if the first portion of the HERG channel is deleted (up to amino acid 370), deactivation of the channel is significantly faster (Schronherr and Heinemann, 1996). In more recent studies, it has been shown that just deleting amino acids 2-9 has a similar effect to deleting the whole N terminus (Morais-Calbral et al., 1998). Fast deactivation of N-truncated channels could be rescued by intracellular application of a peptide encoding the first 135 amino acids of the channel. Wang et al. (2000) later showed this effect could be attributed to the first 16 amino acids only. Wang et al. (1998) showed deactivation was accelerated in the presence of elevated extracellular potassium, consistent with the hypothesis that the inward potassium flux would decrease the ability of the N-terminus to bind to the channel and slow deactivation. Channels containing a mutation at Gly546 (which is found in the S4-S5 linker) produced a mutant identical to N-truncated

mutants, suggesting the N-terminal binds to a site close to the S4-S5 linker. The same research group were able to show it was likely that three or more amino termini were required to bind to the channel to slow deactivation (Wang et al., 2000), consistent with findings from the mERG1 channel (London et al., 1997).

Inactivation of the HERG channel, as previously mentioned, is extremely rapid when compared to the activation and deactivation of the channel. This implies that the activation and inactivation processes are not governed by the same voltage dependent process. Mutants of HERG lacking the N-terminus still show inactivation (Schonnherr and Heinemann, 1996), suggesting the HERG channel does not exhibit N-type inactivation. Inactivation of HERG can also be disrupted by point mutations without any effects on activation (mutation of S631; Schonnherr and Heinemann, 1996), again providing evidence that activation and inactivation of the channel are not governed by the same process. The EAG channel family, which is closely related to the ERG channel family, does not inactivate. The importance of the S5/P-loop region of HERG was shown in studies carried out on EAG/HERG chimeras and HERG mutants by Ficker et al. (1998). This study localised the inactivation domain to HERG to the S5-S6 domain. A number of point mutations of the HERG channel reduced or abolished inactivation. These included a mutation at residue Ser620, to threonine, and mutations at Ser631 to alanine and valine. These residues are located in the S5-S6 linker, which forms the outer mouth of the channel. Further studies have shown amino acids between points 585-594, located in the S5 domain, to also be important for inactivation of the HERG channel (Liu et al., 2002). All of these mutants have shown an altered selectivity for potassium, which is not surprising, as the S5, P-loop and S6 regions form the pore region of the HERG channel. Accumulating evidence suggests inactivation of the HERG channel is due to a collapse of the pore, or C-type inactivation. A hallmark of C-type inactivation is sensitivity to extracellular tetraethylammonium (TEA) and Smith et al. (1996) showed HERG channel inactivation was slowed by extracellular, but not intracellular, TEA. However, inactivation of the HERG channel is still much more rapid than inactivation of other voltage gated potassium channels, such as the shaker channel, which also shows C-type inactivation, albeit not voltage dependent (Roux et al., 1998). This therefore may indicate that another element is involved in inactivation of the HERG channel. One of these elements may be the

difference in residues forming the selectivity filter of the HERG channel. In the HERG channel, the selectivity filter is formed by the amino acid residues glycine, phenylalanine and glycine. However, in the majority of other voltage gated potassium channels this motif is glycine, tyrosine, glycine. It has been suggested that the tyrosine in KcSA and Shaker channels hydrogen bonds to tryptophan residues in the pore helix, thus stabilising the selectivity filter and slowing inactivation (Doyle et al., 1998). In contrast, the HERG channel lacks both the tyrosine and trytophan residues, meaning the selectivity filter may not be stabilised, leading to a more rapid inactivation (reviewed in Vandenberg et al., 2003).
Like activation, inactivation of the HERG channel is voltage dependent, implying that a region of the HERG channel must act as a voltage sensor for inactivation. Experimental data using voltage clamp fluorimetry showed the extracellular side of the S4 region to move on a similar timescale to inactivation (Smith and Yellen, 2002). This suggests that the S4 region is involved in both activation and inactivation of the HERG channel. However, how S4 movements couple to both activation and inactivation gates remains unclear.

The unusual kinetics of the HERG channel currents mean it contributes to the latter part of the cardiac action potential. I_{Kr} is one of several currents that regulates the length of the cardiac action potential. At the start of the action potential, the membrane potential becomes positive, to around +20 to +40 mV . At these voltages the HERG channel is inactivated, so little current passes through the channels. As the action potential starts to repolarise, recovery from inactivation occurs, and current starts to flow to repolarise membrane potential (Hancox et al., 1998). If I_{Kr} is reduced in any way, final repolarisation of the action potential will be slowed, therefore causing a lengthened action potential and long QT syndrome. As already discussed, long QT syndrome can be caused by both drug block, and inherited mutations of HERG, the latter of which can attenuate current by causing altered gating, trafficking or conduction of the channel.

4.3.4 Comparing HERG channel kinetics to I_{Kr} kinetics

Although HERG current and I_{Kr} are similar, there are some differences in the kinetics of the HERG current expressed in mammalian tissue, and the kinetics of I_{Kr} expressed in cardiac myocytes. This is likely to be due to a number of factors.

I_{Kr} was first identified in guinea pig ventricular myocytes (Sanguinetti and Jurkiewicz, 1990). Since then, currents with similar characteristics have been described in a number of cardiac cell types, including atrioventricular nodal cells, atria and SAN (Mitcheson and Hancox, 1999), from a number of species, including mouse (Davies et el., 1996), cat (Follmer et al., 1990) and rabbit (Cordeiro et al., 1998). The voltage dependent activation processes of I_{Kr} are similar across species and tissue type. Examples of measured $V_{0.5}$ include –13.7 mV from rabbit ventricular myocytes (Carmeliet, 1992), -10.8 mV from rabbit AV nodal cells (Mitcheson and Hancox, 1999), and –14.9 mV from guinea pig ventricular myocytes (Heath and Terrar, 1996). Generally, channel activation occurs at voltages above –40 mV, and is maximal at around +20 mV. Outward current peaks at around 0 mV, before showing inward rectification at more positive voltages. However, the time-dependence of activation varies greatly across species. When comparing gating kinetics of I_{Kr} from different species measured using similar recording conditions, it has been shown that the activation and deactivation rates of I_{Kr} in guinea-pig are relatively fast when compared to other species. Activation at 0 mV had a time constant of 40 ms. Deactivation measured at –40 mV had a time constant of 119 ms (Sanguinetti and Jurkiewicz, 1990). Kinetics of I_{Kr} measured in rabbit and canine were relatively slow in comparison. Activation at 0 mV had time constants of 400 ms and 600 ms respectively, with deactivation measured at –40 mV having time constants of 600 ms and 500 ms respectively (Clay et al., 1995; Lui and Antzlevitch, 1995). I_{Kr} measured in human atrium showed kinetics intermediate to those measured in guinea pig, rabbit and canine. Activation at 0 mV had a time constant of 200 ms, with the time constant of deactivation at –40 mV measured as 234 ms (Wang et al., 1994).

Comparing the kinetic properties of I_{Kr} to that of the HERG channel expressed in mammalian tissue, for example HEK cells, as used in our study, shows some differences between currents, including the voltage dependence of activation. Obviously, differences in recording conditions must be taken into account when comparisons are made, as temperature and pH are two conditions which have been shown to alter channel kinetics (Zhou et al., 1998, Bérubé et al., 1999). However, when recording conditions are taken into account, some similarities are seen. The deactivation rate at –40 mV of the HERG channel expressed in HEK cells (Zhou et al., 1998) was similar to I_{Kr} recorded in human atrial myocytes (Wang et al., 1994). Of course, being a human-derived cell line, HEK cells may endogenously express

subunits that may alter channel kinetics. Evidence of this has not been shown, but possible contributions of β subunits should be considered.

The I_{Kr} channel may be made up of HERG subunits and β subunits. The contribution of any β-subunits to I_{Kr} is controversial. Suggested β sunubits are minK and MiRP1. Knocking down minK expression by transfection of anti-sense oligonucleotides attenuated I_{Kr} (Yang et al., 1995) in AT-1 cells, an immortalised atrial myocyte-derived cell line. Kupershmidt et al. (1999) showed in minK knockout mice, I_{Kr} was significantly reduced, and deactivation of the current was slower. Co-expressing minK with HERG in CHO cells however amplified currents, when compared to currents from expression of HERG only McDonald et al., (1997). This study also showed by co-immunoprecipitation that minK and HERG form stable complexes when co-expressed in CHO cells. Although the data indicates a role for minK in I_{Kr}, the evidence is inconclusive. There is also no direct evidence for co-assembly of HERG and minK in cardiac myocytes.

A family of three minK related peptides (MiRPs) have been identified. (reviewed in Abbott and Goldstein, 2001). Studies have shown mutations in minK can cause long QT syndrome (Sesti and Goldstein, 1998; Schulze-Bahr et al., 1997), and data has also been produced suggesting mutations in MiRP may also cause arrhythmias (Abbott et al., 1999). Using co-immunoprecipitation, Abbott et al. (1999) showed MiRP1 and HERG formed a stable complex. When currents were measured from cells co-expressing MiRP1 and HERG, it was found kinetics of the HERG channel were altered. Deactivation was accelerated and voltage-dependent activation was shifted to more positive potentials. The HERG-MiRP channel also became more sensitive to block by E-4031 and clarithromycin, two well-characterised I_{Kr} blockers. A more recent paper has shown MiRP2 to suppress the expression of HERG when co-expressed in oocytes (Schroeder et al., 2000). Again, this provides evidence that members of the MiRP family of proteins may interact with HERG to form a more I_{Kr}-like current. Others studies however have observed no effect of co-expression of MiRP1 on HERG currents. Weerapura et al. (2002) compared the pharmacological and biophysical properties of the HERG channel expressed in CHO cells with and without co-expression of MiRP1. Co-expression of HERG and MiRP1 did not significantly alter the pharmacological sensitivity of the current to quinidine, E-4031 or dofetilide. The study found co-expression of MiRP1 to cause a hyperpolarising shift of activation of the channel, thus moving it further from I_{Kr}-like

properties. Deactivation was accelerated at potentials below the reversal potential, therefore leading the question of how physiologically relevant this alteration would be. However, at more physiologically relevant membrane potentials, deactivation was unaltered. The group concluded that MiRP1 did not contribute to the I_{Kr} current carrying complex.

A recent study has shown *Xenopus* oocytes to endogenously express a family of MiRP proteins (xMiRPs; Anantharam et al., 2003). Injecting HERG-expressing oocytes with RNAi to xMiRP2 decreased xMiRP2 expression, and increased HERG current, suggesting xMiRP2 causes a suppression of HERG current. This data also suggests the HERG current measured in *Xenopus* oocytes may due to a complex of several subunits. Therefore, this data must be taken into consideration when expressing HERG currents in *Xenopus* oocytes.

Evidence for the role of β subunits is inconclusive. Although studies have shown co-expression and co-immunoprecipitation *in vitro* and using cell lines, no direct evidence describing direct interactions between HERG and MiRPs in cardiac tissue has been shown.

Another factor that may cause differences between HERG currents and I_{Kr} is alternative splicing. A N-terminal splice variant of the HERG channel has been identified in both mouse and human cardiac tissue (London et al., 1997; Lees-Miller et al., 1997). This lacks part of the N-terminus, having only a 36 amino acid terminal, compared to 396 amino acids in the full length isoform. This splice variant, as expected from data already discussed above, shows a much faster rate of deactivation. It has been proposed that the full length HERG channel and the splice variant can form both homo-and hetero- tetramers. London et al. (1997) cloned three different ERG isoforms from a mouse heart cDNA library, named mERG1a (homologous to HERG), mERG1a' (which lacks the first 59 amino acids) and mERG1b (which has an N-terminal domain dissimilar to ERG1). They found mERG1a and mERG1b to be expressed in the heart. Expressing the mERG1a and mERG1b isoforms in *Xenopus* oocytes showed the isoforms may co-express, as mERG1b expression increased in the presence of mERG1a. Co-expression of mERG1a and mERG1b produced currents with deactivation kinetics much faster than expression of mERG1a or HERG alone. Deactivation time constants were more similar to I_{Kr} expressed in mouse cardiac myocytes. This suggests that it may be the co-expression of two isoforms of ERG that form I_{Kr}. Recently, its has been suggested that the canine cardiac I_{Kr} channel is made up of the cERG 1a (full length) and

cERG 1b (N-terminal splice variant), (Jones et al., 2004). Both variants of ERG were identified in canine ventricular tissue using western blot procedures. To test if the two isoforms were associated, co-immunoprecipitations were carried out. The study showed that ERG1a and ERG1b isoforms associate in canine ventricular myocytes *in vivo*. Using immunocytochemistry, the study was also able to show the ERG1a and ERG1b isoforms localised to the same subcellular compartment, which was characteristic of T-tubular localisation. However, this study did not measure currents made up of homo- and hetero-tetramers, so although able to conclude the two isoforms can co-localise in canine ventricular tissue, the possible physiological effects on ionic currents was not determined.

The two studies described above suggest the pore forming subunit of the I_{Kr} channel may be composed of more than one ERG isoform. Thus, the resulting kinetics of I_{Kr} in different tissues could depend on the expression levels of the different isoforms.

Another isoform of HERG has been identified in human heart (Kupershmidt et al., 1998). This isoform, $HERG_{USO}$ lacks part of the C-terminal of the channel. This isoform did not produce a functional current when expressed alone, however when co-expressed with 'full length' HERG, the kinetics of HERG were altered, attenuating current, accelerating activation and shifting activation to more negative potentials by ~9 mV. This again suggests that the full length HERG isoform is able to interact with other variants of the channel. However, in this study there was no evidence shown of protein expression of $HERG_{USO}$ in the heart, so the relevance of this data is still unknown.

In summary, it is unknown why HERG current recorded in heterologous expression systems is different to I_{Kr} recorded from cardiac myocytes. It may be due to differences in recording conditions, or expression of different α and β subunits. Although several candidates for these 'extra' subunits have been proposed, there is little convincing evidence of these subunits interacting with the HERG subunit in cardiac myocytes.

4.3.5 Rundown of the HERG current

In this body of work I have characterised HERG current rundown with time when currents are measured using whole cell recording techniques. The phenomenon of rundown has been shown in previous studies, for a number of ion channels. These include the K_{ATP} channel (Ribalet et al., 2000), calcium currents recorded in bovine chromaffin cells (Elhamdani et al.,

1995), Type IA nicotinic currents recorded from hippocampal neurons (Alkondon et al., 1994), and rERG current expressed in tsA-201 cells (Hirdes et al., 2004). In this latter study, it was shown rERG current ran 'down by approximately 1.3% per minute, which is not dissimilar to results from my study. I have shown under my recording conditions, HERG currents run down by approximately 1.5% per minute.

The exact cause of rundown of current is unknown, although it has been shown in a number of studies that using the perforated patch technique, which eliminates dialysis of intracellular contents, eliminates rundown. Warth and Hume (1997) demonstrated this for cAMP-dependent chloride channels in guinea pig myocytes, and Wanke et al. (1994), for high-voltage activated calcium currents. This suggests intracellular components, which are dialysed out of the cell during whole cell recording, may be key for maintenance of current amplitude. Indeed, for HERG currents, application of PIP_2 to the cytoplasmic face of excised patches slowed rundown (Bian et al., 2001). Similar effects of PIP_2 have been shown for the KCNQ1/KNCE1 channel complex, which encodes for I_{Ks} (Loussouarn et al., 2003). Complete rundown of current occurred within 5 minutes when patches were excised into control solution. Inclusion of 5 $\mu g\ ml^{-1}$ PIP_2 in the cytosolic solution markedly slowed rundown, although it did not abolish it entirely. Application of 1.4 mM MgATP to these cells also slowed rundown, and the group were able to show application of both PIP_2 and MgATP completely abolished rundown. The group hypothesised that PIP_2 and MgATP were both essential for the maintenance of basal I_{Ks} amplitude, using independent mechanisms.

The rundown we observed in this study, although large enough to be taken into consideration, had a linear time course and was not drastic enough to interfere with recording HERG currents using the whole cell technique. Therefore, all electrophysiological recordings from HEK cells shown in this thesis were carried out using the whole cell technique.

In conclusion, measuring HERG in a cell line may not be a perfect representation of I_{Kr} expressed in cardiac myocytes. However, the expression system I am using allows manipulation of the environment, without contaminating endogenous currents. The differences between HERG current and I_{Kr} will be taken into consideration throughout the course of this thesis when possible.

Chapter 5

Modulation of the HERG channel by second messengers

5.1 Introduction

There have been several studies that have investigated the modulation of the HERG channel by protein kinases (Barros et al., 1998; Kiehn et al., 1998; Thomas et al., 1999; Thomas et al., 2003). However, few studies have been carried out to investigate the potential for modulation of the HERG channel by intracellular calcium. Calcium is an important second messenger in the heart. In a study recording I_{Kr} in guinea-pig ventricular myocytes it was shown that the calcium chelator BAPTA significantly attenuated basal I_{Kr} (Heath and Terrar, 2000). Studies have also shown the EAG channel to be modulated by calcium. The EAG channel is closely related to HERG, with regions of high sequence homology. Stansfeld et al. (1996) and Schönherr et al. (2000) both showed elevated calcium to cause a rapid, reversible attenuation of EAG current. Stansfeld et al. hypothesised this was due to a direct effects of calcium on the channel, however the study carried out by Schönherr et al. concluded that modulation was due to binding of calcium calmodulin to an amphipathic helix on the C-terminus of EAG.

The initial aim of this body of work was to investigate if the HERG channel is modulated by changes in intracellular calcium concentrations. Two approaches were used. I raised intracellular calcium directly using the calcium ionophore ionomycin. I also used an agonist of the muscarinic M_3 receptor, which is coupled to the $G_{q/11}$ G-proteins, and causes release of calcium from intracellular IP_3-sensitive calcium stores. My results suggested calcium itself did not have a direct effect on HERG channels expressed in HEK 293 cells, but the HERG channel could be modulated by a protein kinase C (PKC) dependent pathway.

Several previous studies investigating PKC modulation of the HERG channel have been carried out in *Xenopus* oocytes (Thomas et al., 1999; Thomas et al., 2003). Modulatory pathways in these cells may differ from those in a mammalian cell system. Studies on modulation of HERG channels by PKC have yielded a variety of results. A general trend in *Xenopus* oocytes has been HERG current attenuation, due to a positive shift in the voltage dependence of activation (Kiehn et al., 1998; Barros et al., 1998). However, some studies show a large decrease in current, accompanied by a small shift in activation, whereas others

have shown a larger shift in activation with a more modest attenuation of current. These differences are important because they suggest different mechanisms of HERG channel modulation. Kiehn et al. (1998) showed the effects of PKC activation on the HERG channel to only be inhibited by PKA inhibitors, suggesting some cross-talk of signalling pathways. However, Barros et al. (1998) showed the effect to be PKC-specific, since it was inhibited by GF109203X (bis-1), a specific inhibitor of PKC.

In my studies, I sought to investigate the modulation of the HERG channel by calcium and PKC in mammalian cells, under carefully controlled experimental conditions. Contamination of HERG currents by other membrane currents with overlapping voltage- and time-dependent kinetics was minimised by over-expressing HERG in HEK 293 cells that contain small endogenous currents. A number of approaches were used to investigate modulation of the HERG channel current by PKC. As the HERG channel is highly susceptible to direct block by a variety of compounds, using several approaches gave me confidence that results using a single approach were not simply due to pharmacological blockade of the HERG channel.

5.2 Results

5.2.1 Response of the HERG channel currents to rises in cytosolic calcium

5.2.1.1 Application of ionomycin

Application of the calcium ionophore, ionomycin, causes an increase in cytosolic calcium by allowing calcium entry into the cytosol from both the external environment (Bolger et al., 1983) and intracellular stores (Poggioli et al., 1982). Ionomycin and calcium form a lipid-soluble complex, giving the ability to convey calcium across the cell membrane (Bennett et al., 1979). In my studies, 5 μM ionomycin was used as a tool to elevate cytosolic calcium, and investigate how this altered HERG channel currents. I carried out calcium imaging on HERG-HEK cells, to determine the time course and amplitude of calcium changes in response to ionomycin. I found 5 μM ionomycin to cause a large increase in cytosolic calcium levels in these cells. Figure 5.1A shows typical changes in cytosolic calcium in response to ionomycin application. In 18 cells, the mean cytosolic calcium rise was from a baseline value of 0.92 ± 0.10 (fura 2 340/380 ratio) to a value of 3.66 ± 0.29 in the presence of ionomycin ($p<0.05$). This elevation of calcium was maintained upon superfusion of cells with control Tyrode.

To measure the effects of ionomycin on HERG channel current stably expressed in HEK cells, the 'depolarisation to 0 mV' voltage protocol was used. Cells were pulsed repeatedly using this protocol until current amplitudes stabilised, before switching to a solution containing 5 μM ionomycin. Ionomycin had rapid effects on the HERG current. Figure 5.1B shows representative current traces in control conditions and once the maximal effect of ionomycin application had been attained. Attenuation of current occurred on the first voltage pulse, with the maximal effects of ionomycin occurring within 120 seconds (figure 5.1C). The time course of ionomycin effects in individual cells were fit with single exponential functions, and the mean time constant was 48.38 ± 18.11 seconds (n=6). Current remaining after ionomycin application was 59.64 ± 4.32% of control. The effect of ionomycin was sustained, and was not significantly reversible after a five minute washout period. To investigate whether the attenuation of HERG current at 0 mV was due to a shift in voltage-dependent properties, HERG currents were measured at a range of potentials with the I-V protocol. A representative family of currents in response to the I-V protocol, and the

Figure 5.1

Application of ionomycin attenuates HERG current. **A** Representative fura-2 ratio showing changes in cytosolic calcium in a single cell in response to ionomycin. **B** Representative HERG current traces in control conditions and during 5μM ionomycin application. **C** Time course of HERG current response to ionomycin (n=6). Peak tail currents were normalised to control amplitudes and the mean normalised current amplitudes plotted against time.

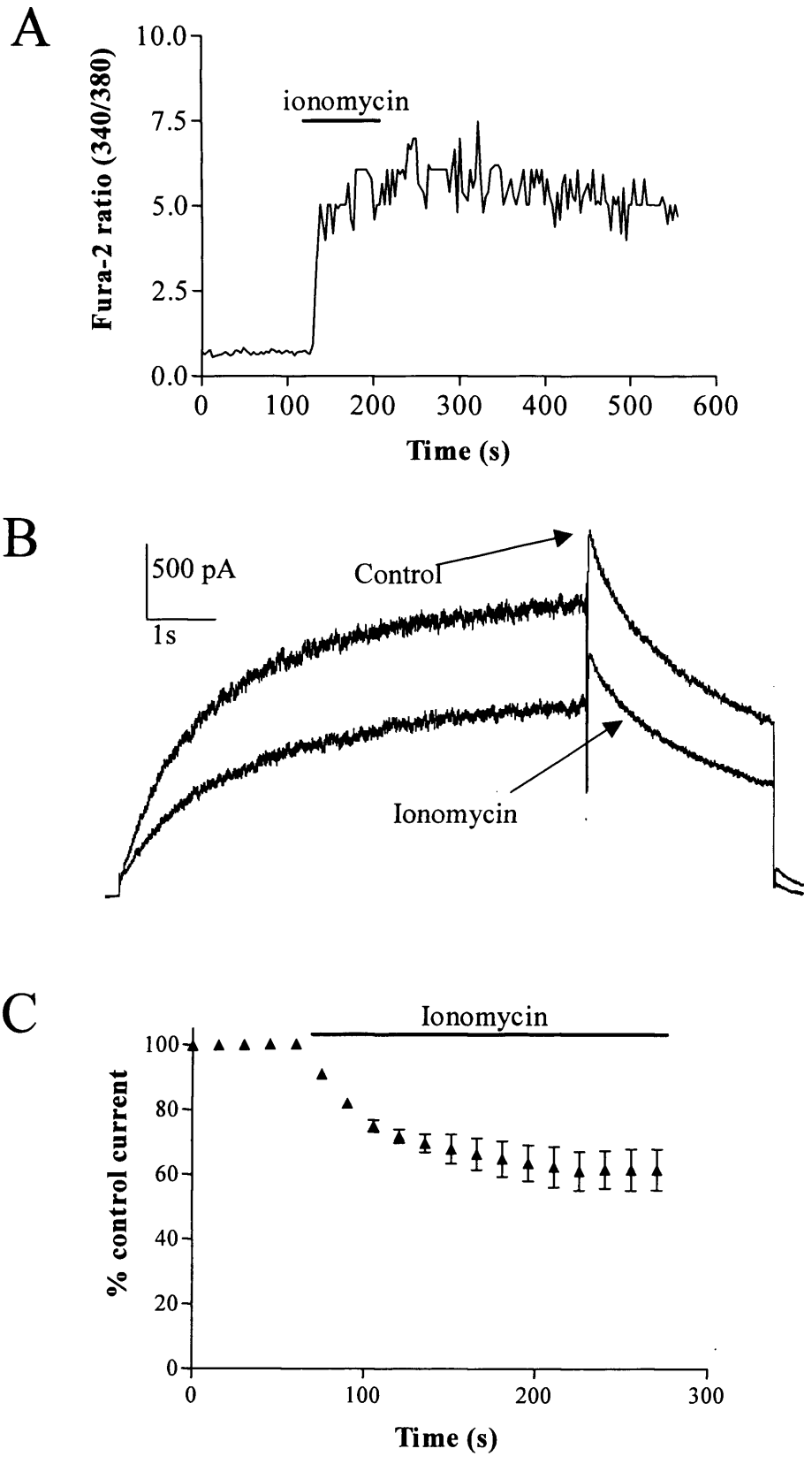

Figure 5.2
Ionomycin does not significantly change activation or inactivation of the HERG channel. **A**. A family of currents evoked by the I-V protocol before (left) and during (right) 5 μM ionomycin. For clarity, only current evoked at –40, -20, 0 and +20 mV are shown **B**. Voltage dependence of activation of HERG current in control conditions and with 5 μM ionomycin. Peak tail currents are normalised to maximum amplitudes and plotted against test potential (n=5). **C** Voltage dependence of inactivation measured with the triple pulse protocol in control and with 5 μM ionomycin (n=5).

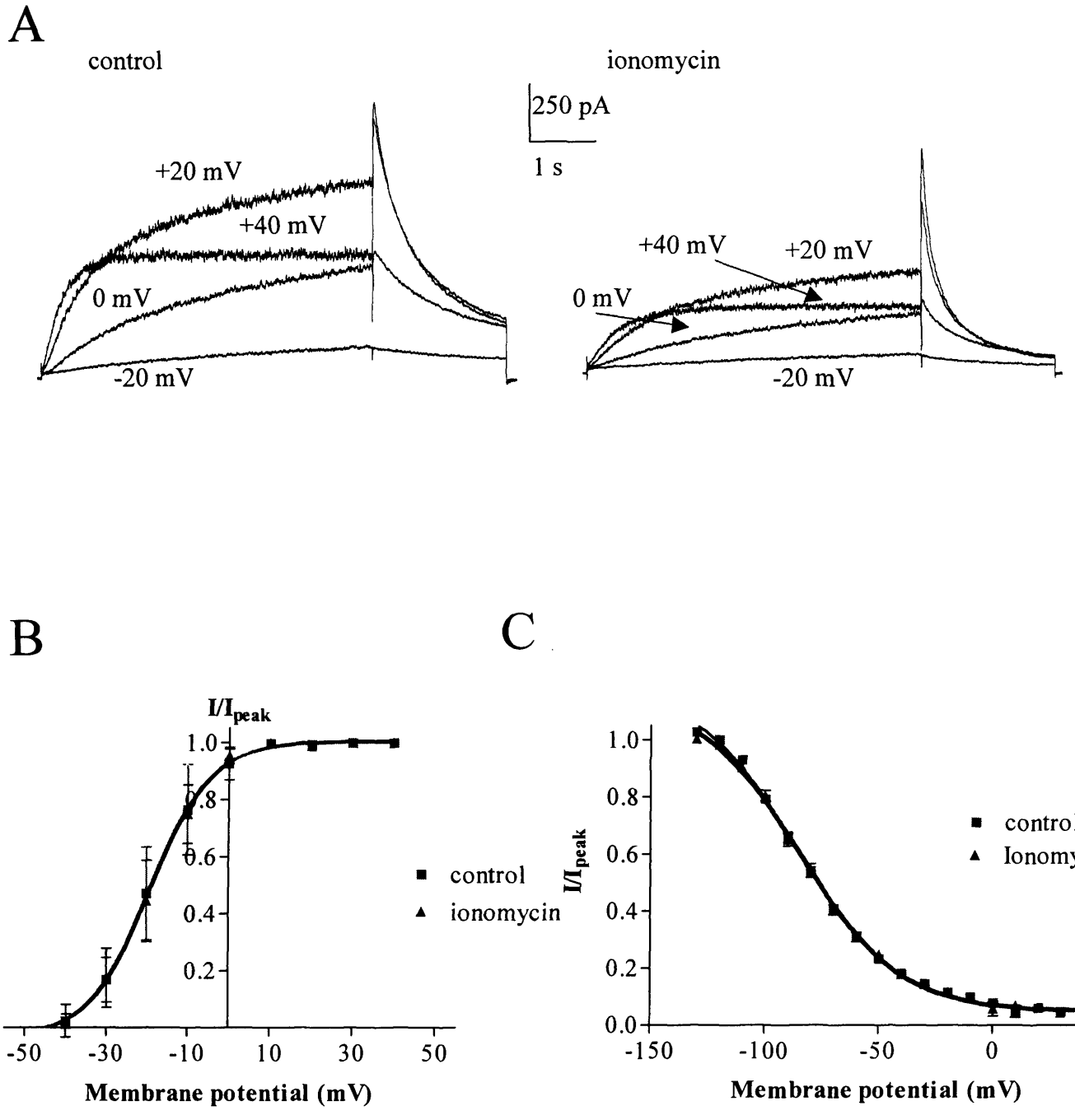

mean activation curves are shown in figures 5.2A and B. Ionomycin decreased current amplitudes at all potentials. There was a small positive shift in the $V_{0.5}$ for activation of 1.71 ± 0.68 mV (n=5), which was not significant (p>0.05). The slope of the activation curve was unaltered (7.25 ± 0.25 in control compared to 7.24 ± 0.22). We also tested if the attenuation of current was due to a change in the inactivation properties of the current. Figure 5.2C shows the mean results on the voltage-dependence of inactivation before and during ionomycin application. I found the $V_{0.5}$ of inactivation to shift by 1.46 ± 1.55 mV in the presence of ionomycin, but this was not a significant change (n=5, p>0.05). The slope factor was also unaltered by ionomycin (–21.09 ± 0.31 in control compared to –22.01 ± 0.16 during ionomycin application). We also investigated if ionomycin alters the deactivation properties of the HERG channel. Current deactivation of the channel measured at –50 mV showed a small but insignificant acceleration (p>0.05). The slow and fast time constants were 1303.00 ± 31.83 ms and 240.52 ± 17.74 ms in control conditions, compared to 1293.04 ± 125.22 ms and 204.81 ± 13.67 ms with ionomycin (n=6, data not shown). The positive shift of activation and inactivation, and the acceleration of deactivation kinetics of the channel in the presence of ionomycin were not significant. It is unlikely that the combination of these two effects leads to the attenuation of current in the presence of ionomycin. Ionomycin may decrease current by decreasing open probability and/or decreasing surface expression of HERG channels.

5.2.1.2 Activation of the $G_{q/11}$-coupled pathway

Ionomycin raises calcium to very high, sustained levels. To determine if calcium release from intracellular stores via a receptor mediated and physiologically relevant mechanism could also alter HERG currents we used methacholine, an agonist to the muscarinic M_3 receptor. The muscarinic M_3 receptor is a G-protein coupled receptor coupled to PLC via $G_{q/11}$ proteins that increases cytosolic calcium by opening IP_3 receptors on the ER. I first tested if application of a supra-maximal concentration (1 mM) of methacholine to HERG-HEK cells could raise calcium by stimulating the endogenous population of receptors. However, cytosolic calcium in these cells did not change upon application of methacholine. A representative trace showing cytosolic calcium levels in HERG-HEK cells in response to methacholine is shown in figure 5.3A. The baseline fura-2 340/380 ratio was 0.92 ± 0.14.

Figure 5.3
HERG-HEK cells do not respond to the muscarinic receptor agonist methacholine. A Representative fura-2 ratios showing cytosolic calcium in a single cell in response to 1 mM methacholine. **B** Response to 1 mM methacholine of HERG currents. Peak tail currents were normalised to control amplitudes and the mean normalised current plotted against time (n=5).

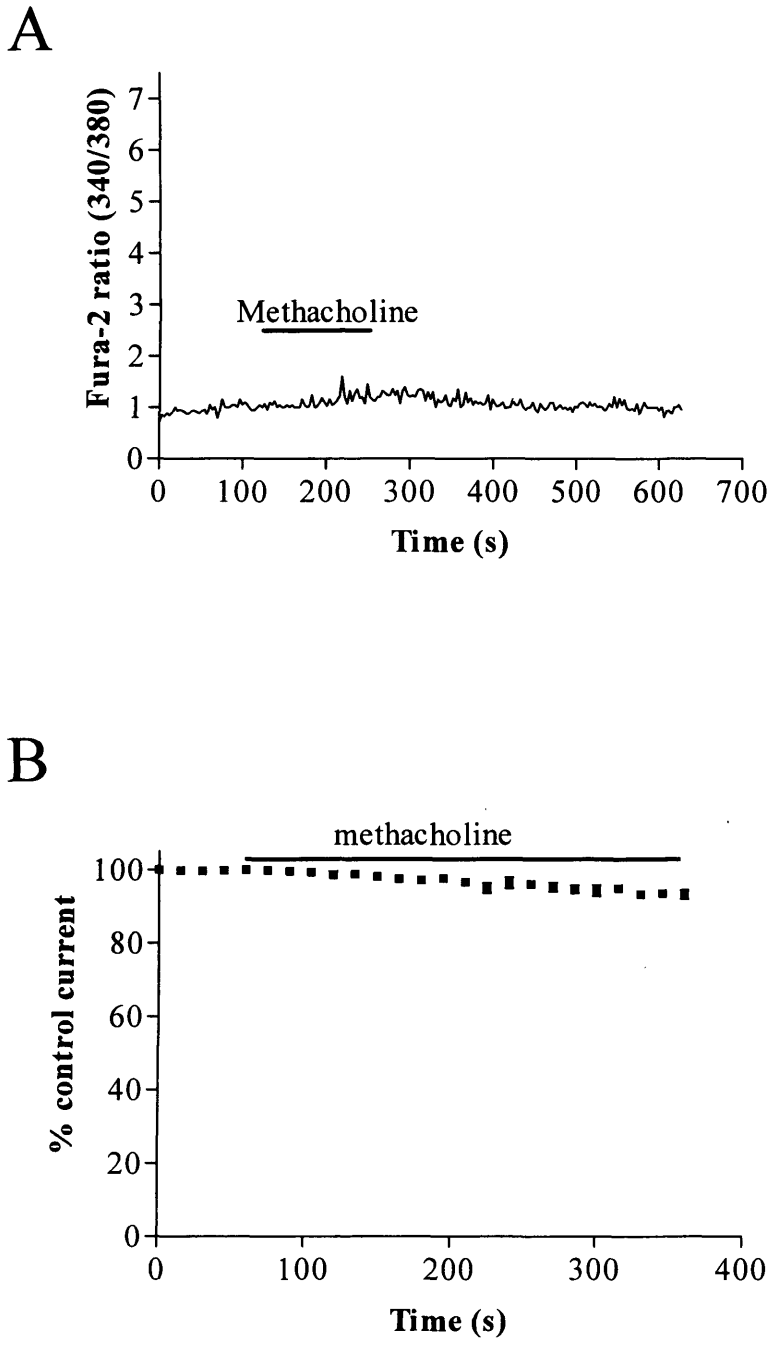

Maximal fura-2 340/380 ratio was 1.04 ± 0.13 (n=7, p>0.05). Application of methacholine to HERG-HEK cells did not alter HERG current amplitude. After 300 seconds of methacholine application, peak tail current was 93.43 ± 3.12% of control current (n=5). The mean time-course of methacholine effects on peak tail current is shown in figure 5.3B. The effect of methacholine was not significantly different to the mean rundown of the current (p>0.05). These studies indicate that stimulating endogenous muscarinic receptors with methacholine did not cause significant calcium release or effect HERG currents, also indicating methacholine does not block HERG channels. Robust increases in calcium have been previously described in a HEK cell line over-expressing the M_3 muscarinic receptors (HEK-m3 cells; Tovey and Willars, 2004). Using radioligand binding I measured the muscarinic receptor population in HERG-HEK and HEK-m3 cells. The muscarinic population in the HERG-HEK cell line is low. HERG-HEK cells only expressed 8.32 ± 0.78 fmol/mg total protein. I found the HEK-m3 cell line to have an unsurprisingly high population of muscarinic receptors. The mean expression from three independent experiments was 1573.31 ± 65.66 fmol/mg total protein, thus showing a 189-fold difference in expression between these cell lines. Subsequent experiments on receptor mediated elevation of cytosolic calcium were done on HEK-m3 cells transiently transfected with HERG. Calcium imaging was used to investigate the effects of the muscarinic agonist methacholine on cytosolic calcium levels. Figure 5.4A shows representative fura-2 ratios showing the rapid and large rise in cytosolic calcium levels in response to application of 1 mM methacholine. In response to methacholine, the fura-2 340/380 ratio rapidly rose from a baseline of 0.66 ± 0.12 to a peak value of 10.86 ± 1.65, then rapidly decayed in the continued presence of agonist to a value of 0.59 ± 0.15 with a mean time constant of 13.23 ± 2.46 seconds (n=8). The peak in cytosolic calcium is likely to be due to release from intracellular stores, and the rapid decay is likely to be due to removal from calcium from the cytosol back into the internal stores or external environment, thus maintaining a low cytosolic calcium concentration. To measure the effects of methacholine on HERG channel currents, the 'depolarisation to 0 mV' voltage protocol was used. This protocol was continued until currents reached a steady amplitude, then methacholine was applied. Figure 5.4B shows representative currents in control conditions and after the maximal response of methacholine had occurred. Upon extracellular application of methacholine, HERG currents were slowly attenuated. The mean

Figure 5.4

Methacholine attenuates HERG current in cells co-expressing the muscarinic M_3 muscarinic receptor. **A** Cytosolic calcium levels in a single HEK-m3 cell in response to 1 mM methacholine application. **B** Representative HERG current traces in control conditions and in the presence of 1 mM methacholine from HEK-m3 cells transfected with HERG. **C** Time course of HERG current response to methacholine. Peak tail currents were normalised to control amplitudes and the mean normalised currents plotted against time (n=8).

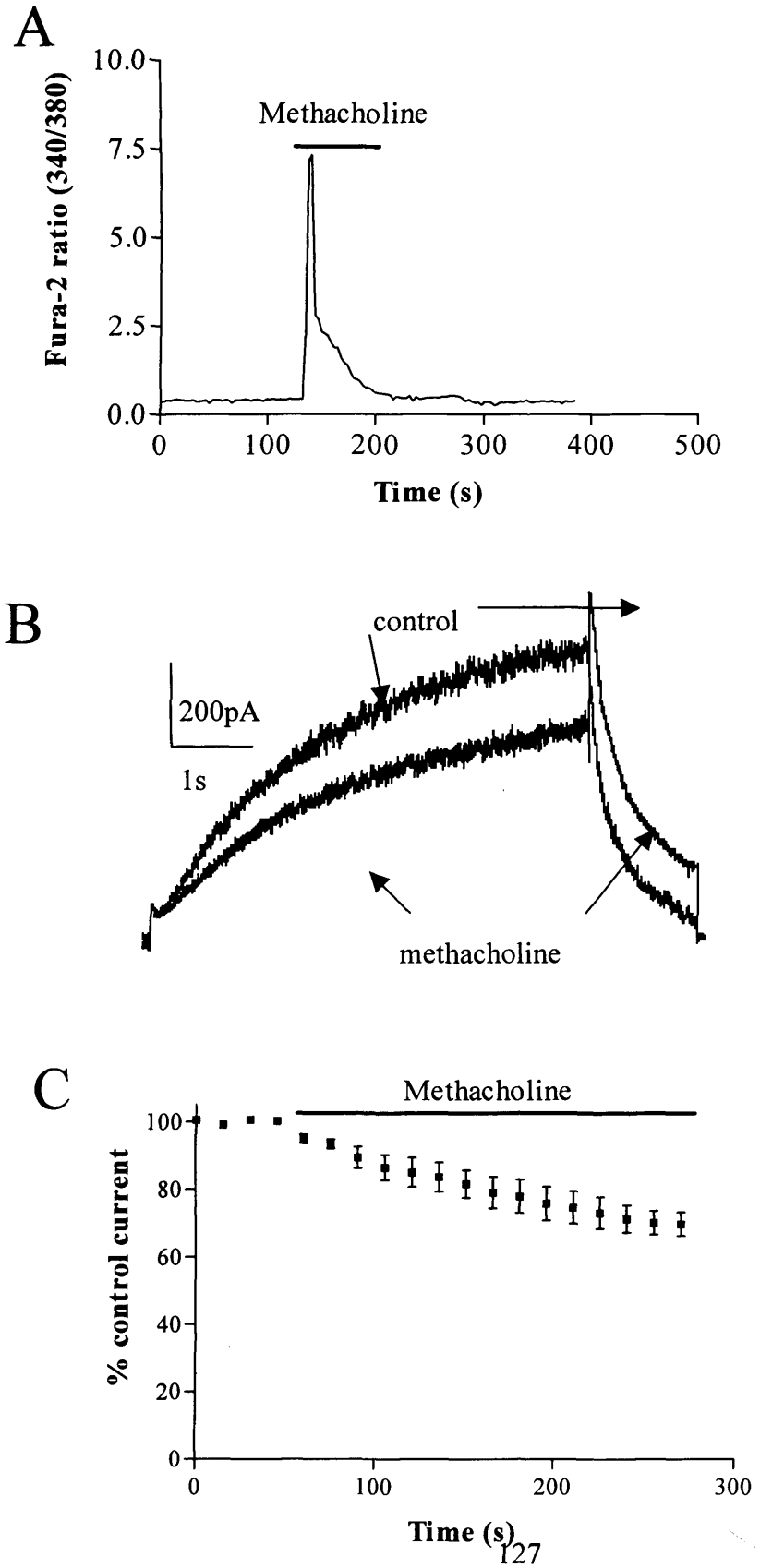

time constant of methacholine effects was 301.04 ± 59.79 seconds (n=8). This was much slower than the time constant for ionomycin effects and much slower than the calcium elevation in response to methacholine. Currents in methacholine were 73.16 ± 2.17% of control currents (n=8, $p<0.05$, figure 5.4C). To investigate if the attenuation of current was due to a change in voltage dependence, the activation, inactivation and deactivation properties before and during methacholine application were compared. The $V_{0.5}$ for activation was positively shifted significantly by 5.11 ± 1.31 mV, which was a small, but significant shift (n=5, $p<0.05$, see figure 5.5A). The slope factor was unaltered. The voltage dependence of inactivation was not significantly altered by methacholine (figure 5.5B). However, the time constants of deactivation at –50 mV were significantly faster ($p<0.05$). In control conditions, the fast and slow time constants were 1241.03 ± 44.71 ms and 233.21 ± 5.59 ms, whereas in methacholine they were 1021.43 ± 33.84 ms and 170.63 ± 23.31 ms respectively (n=8, figure 5.5C).

These data suggest methacholine attenuates HERG current in several ways; a positive shift in voltage dependence of activation (meaning there are less channel open at a particular voltage), and an acceleration of deactivation, meaning channels close faster. However, these factors are not sufficient to account for the 27% decrease in current. It is likely that the open probability and/or number of channels available is also reduced.

5.2.1.3 Cytosolic calcium buffering

Ionomycin and methacholine caused an attenuation of current at all potentials with small or insignificant effects on voltage dependent kinetics of activation and inactivation. However, the time courses for decreased HERG current amplitude did not correlate with changes to cytosolic calcium, suggesting HERG modulation may not be due to the rise in calcium alone. To investigate this further, we used the calcium chelator 1,2-bis (2-aminophenoxy) ethane-N, N, N', N'- tetraacetic acid (BAPTA) to buffer cytosolic calcium to low levels, therefore allowing us to investigate if the response of the HERG channel currents is calcium dependent.

Calcium imaging with fura-2 was used to check BAPTA would buffer the increase in calcium in response to ionomycin and methacholine application. Cells were incubated in 5 mM of the

Figure 5.5

Methacholine application shifts activation and accelerates deactivation, but does not alter inactivation of the current. A Mean HERG activation curves in control conditions and in the presence of 1 mM methacholine. Peak tail currents were normalised to control amplitude and plotted as a function of membrane potential (n=5). **B** Voltage dependent inactivation of HERG measured using the triple pulse protocol (n=5). **C** The slow (i) and fast (ii) time constants of current deactivation in control conditions and with 1 mM methacholine. * shows significance of $p<0.05$ vs control.

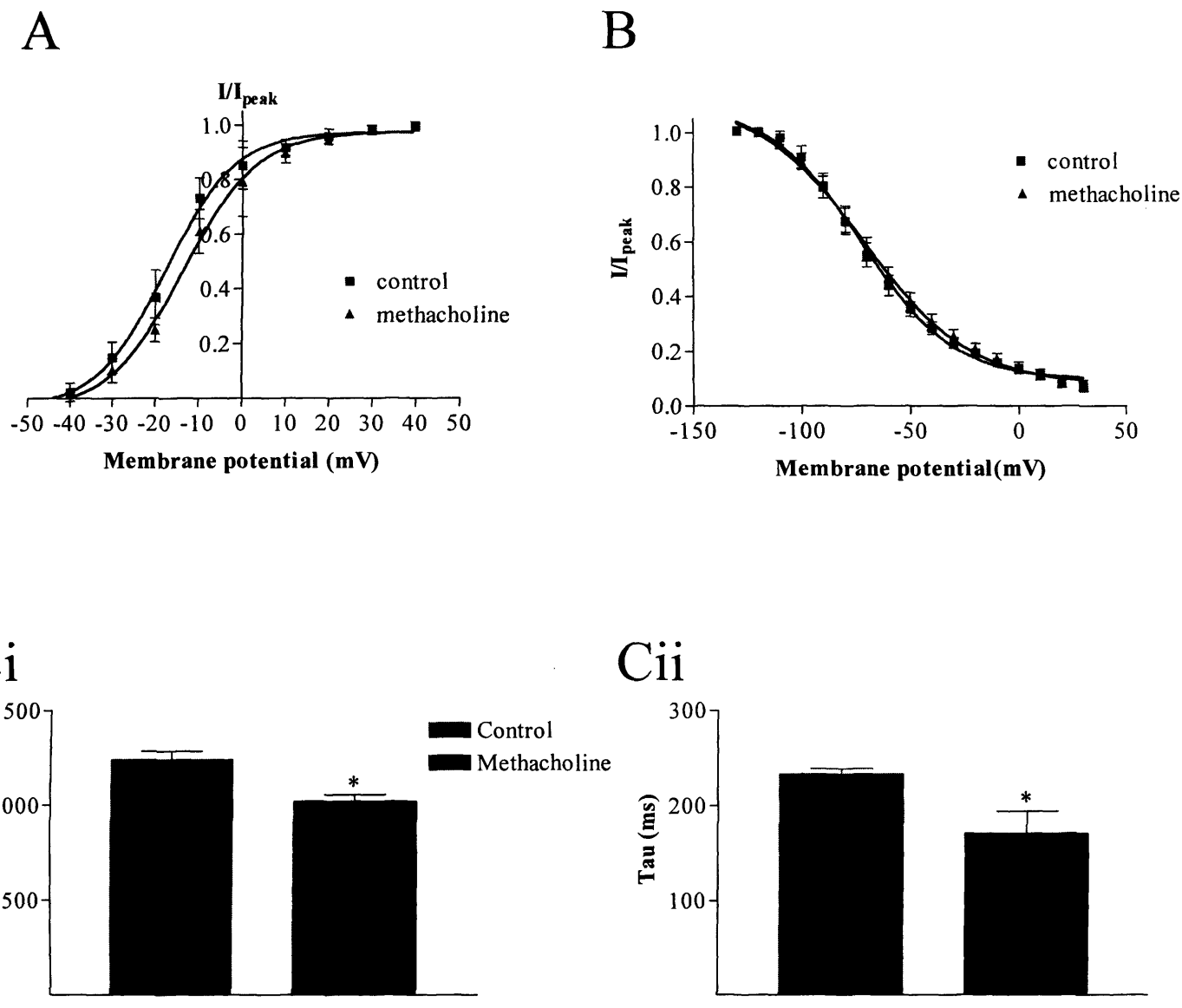

membrane permeable (acetoxymethyl ester) form of BAPTA (BAPTA-AM) for 15 minutes prior to recording. Cells were then transferred to the recording chamber, allowed to settle and the perfusion started. Following incubation with BAPTA-AM, ionomycin and methacholine did not cause a significant change in the cytosolic calcium levels in the cells. Representative traces are shown in figure 5.6. The baseline fura-2 340/380 ratios were also lower when compared to cells in the absence of BAPTA - 0.52 ± 0.16 in HERG HEK cells (n=12 over 3 experiments) and 0.61 ± 0.16 in HEK-m3 cells (n=12 over 4 experiments). These results indicate BAPTA was lowering cytoplasmic calcium concentration as well as diminishing the rise of calcium in response to ionomycin and methacholine.

The effects of buffering calcium on HERG currents were then investigated. To more precisely define the concentration of BAPTA and free calcium in the cell I took advantage of being able to dialyse cells with intracellular solution contained within the patch pipette. Intracellular solution contained 5 mM BAPTA and the free calcium concentration was estimated to be less than 1 nM (using Maxcheator software). Once whole cell configuration had been achieved, cells were held at a membrane potential of –80 mV, and left for 10 minutes to allow dialysis of BAPTA into the cell. Voltage dependent activation was not altered during this time period. Rundown of current was observed (measured using the 'depolarisation to 0 mV' protocol), however this was not significantly different to rundown in control conditions. The 'depolarisation to 0 mV' protocol was then used to ensure current amplitudes were stable before ionomycin was applied. Application of ionomycin in these conditions did not cause a significant attenuation of current. After 210 seconds of ionomycin application, current remaining was 88.23 ± 1.70% of control current (n=5), compared to 59.64 ± 4.32% in cells not dialysed with BAPTA (n=5). Current attenuation with BAPTA and ionomycin was significantly less than with ionomycin alone ($p<0.05$). The mean time-course is shown in figure 5.7A. On the same experimental day the response to ionomycin was tested in the absence of BAPTA, and a response similar to that outlined previously was observed. This served as a positive control, allowing me to be confident ionomycin was working as previously described. These results indicate that as expected, the HERG current modulation by ionomycin is dependent on elevation of cytoplasmic calcium.

Figure 5.6
Incubation of cells in 5mM BAPTA-AM abolishes the calcium responses to ionomycin and methacholine. **A** Representative fura-2 ratios showing cytosolic calcium changes in a single cell in response to 5 μM ionomycin. **B** Representative fura-2 ratios showing cytosolic calcium changes in a single cells in response to 1 mM methacholine

A

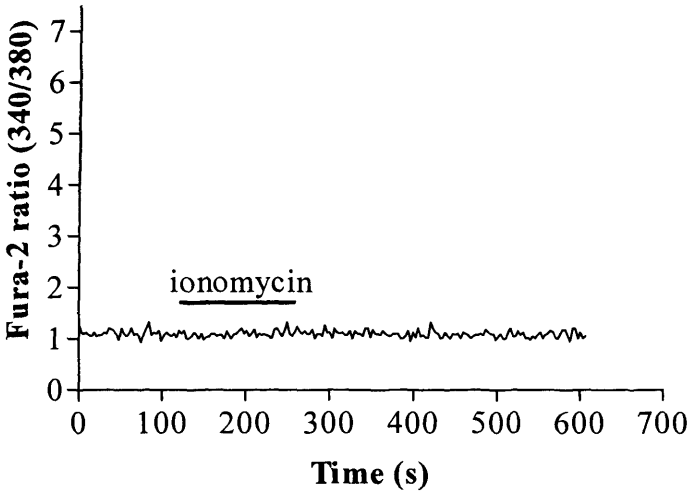

B

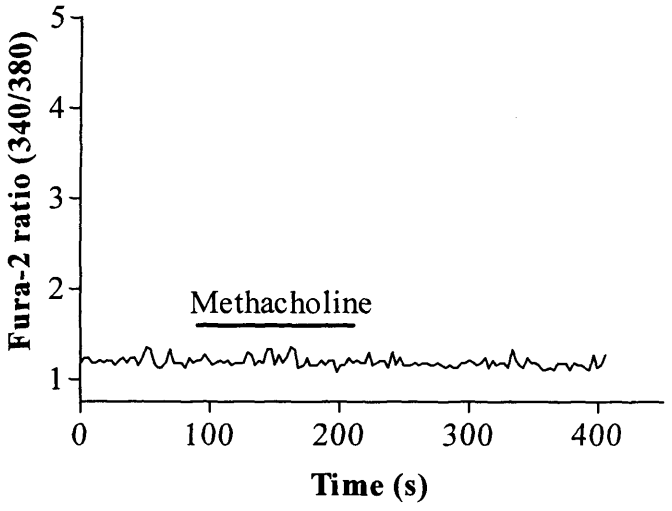

Figure 5.7

5 mM BAPTA abolishes HERG current modulation by ionomycin, but not methacholine. Time-course of 5 μM ionomycin (**A**; n=5) and 1 mM methacholine (**B**; n=5) effects on HERG currents. Peak tail currents were normalised to control amplitudes and the mean normalised currents plotted against time. **C** Voltage dependance of activation of HERG currents before and after 1 mM methacholine. Peak tail currents, normalised to control amplitudes are plotted against test potential

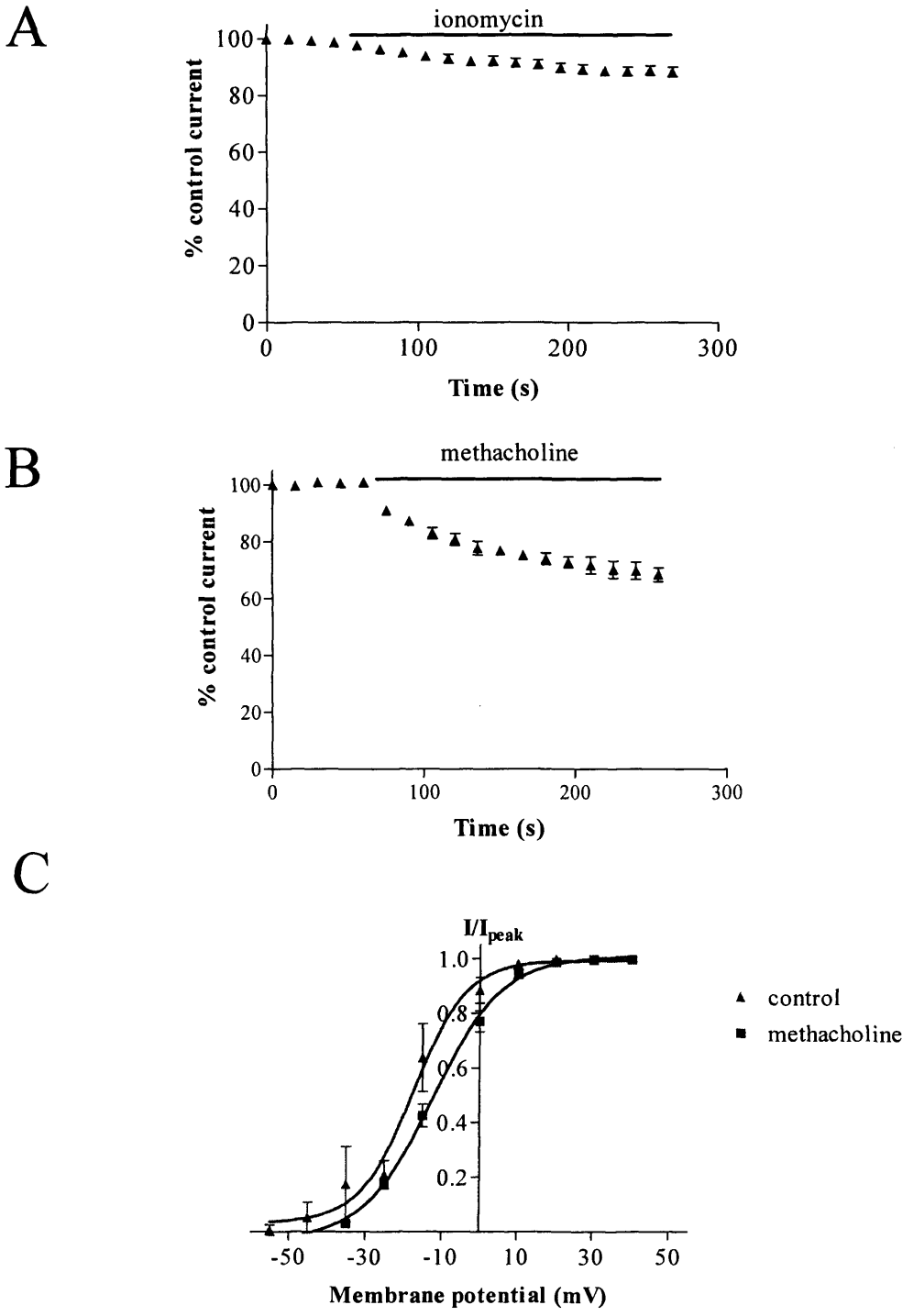

To observe the effect of methacholine on HERG currents in the presence of BAPTA I used the same recording conditions and protocols as described above. In contrast to ionomycin, methacholine continued to attenuate HERG current in cells dialysed with BAPTA. The mean time-course of the effects of methacholine on peak tail currents is shown in figure 5.7B. Maximum effects of methacholine were observed within 165 seconds after methacholine application, and currents were reduced to 68.42 ± 2.43% of control currents (n=5). This was not significantly different to the effects of methacholine without BAPTA ($p>0.05$). Methacholine caused a 4.99 ± 0.76 mV shift in voltage dependent activation of current ($p<0.05$), comparable to the shift seen in the absence of BAPTA (figure 5.7C). The time constants for deactivation at –50 mV were also significantly faster ($p<0.05$). In control conditions, the slow and fast deactivation time constants were 1375.87 ± 76.39 ms and 246.87 ± 22.94 ms, whereas in methacholine they were 1047.45 ± 45.96 ms and 179.34 ± 21.53 ms respectively (n=5).

This suggests the attenuation of current, acceleration of deactivation, and the shift in voltage dependent activation in response to methacholine application are less dependent on cytosolic calcium than the responses to ionomycin.

5.2.2 Characterising the mechanism of action of methacholine and ionomycin

5.2.2.1 Pharmacological inhibition of PKC

I wanted to determine the underlying mechanism of methacholine modulation of HERG currents. The muscarinic M_3 receptor activates PLC-β, which hydrolyses PIP_2 to produce the second messengers IP_3 and DAG. IP_3 acts on IP_3 receptors on the endoplasmic reticulum to cause a release of calcium into the cytosol. DAG activates PKC, which can translocate and phosphorylate a large number of target proteins. Since I have shown the effects of methacholine to be independent of calcium, we wanted to investigate if the effects were due to activation of PKC.

HERG was transiently expressed in HEK-m3 cells for these experiments. After the whole cell configuration was achieved, the 'depolarisation to 0 mV' protocol was used. Currents were of stable amplitude before 300 nM bisindolylmaleimide 1 (bis-1), a PKC-selective inhibitor was applied. No significant effect of bis-1 on HERG current was observed during a

Figure 5.8
PKC inhibition with bis-1 blocks modulation of HERG by methacholine. **A** Time course of effects of 300 nM bis-1 and 1 mM methacholine on HERG current (n=5). Peak tail currents were normalised against control amplitudes and mean normalised currents were plotted against time. **B** Mean activation curves in the control conditions and with 300 nM bis-1 and 1 mM methacholine (n=4). Peak tails, normalised to control amplitudes were plotted as a function of membrane potential

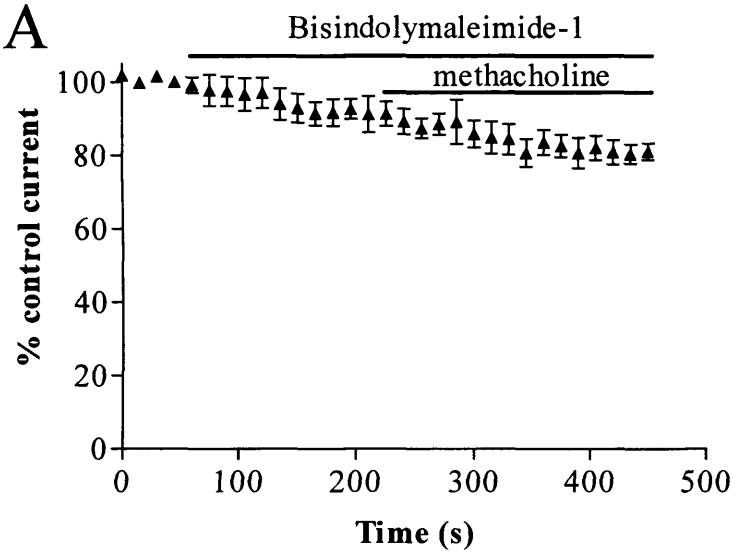

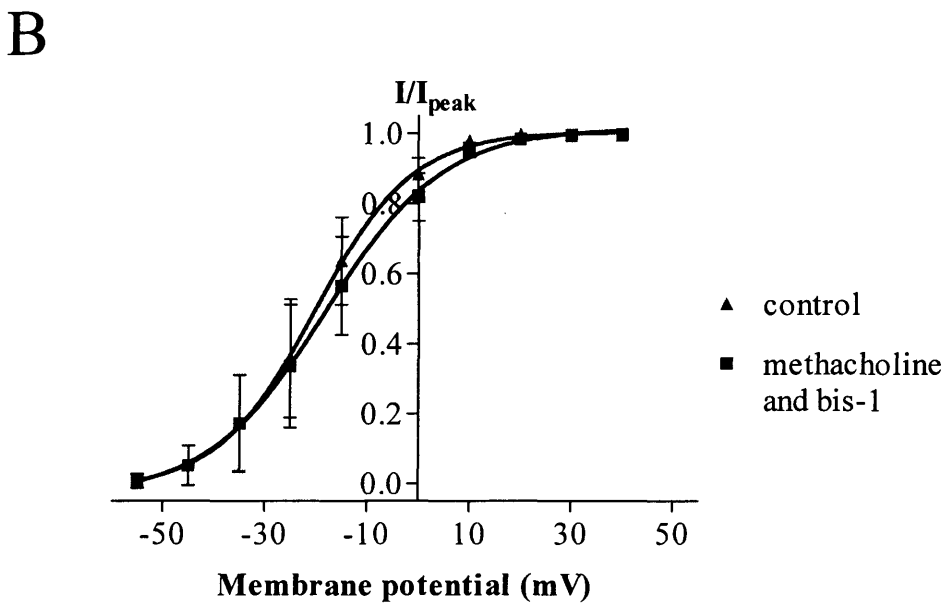

3 minute period. Currents in bis-1 were 91.31 ± 3.33% of control currents, consistent with rundown of the current. After incubation with bis-1, methacholine was applied. After 200 seconds of methacholine application, HERG currents were 89.34 ± 2.51% of control currents (n=5). The mean time-course of the effects of methacholine on peak tail current is shown in figure 5.8A. The response to methacholine was significantly reduced by bis-1, as the small reduction in current was not significantly different to rundown ($p>0.05$). Activation and deactivation kinetics of the current were also measured under these conditions. The $V_{0.5}$ of activation was shifted by 0.51 ± 0.72 mV in the presence of methacholine and bis-1 (n=4, $p>0.05$, 5.8B). The slow and fast time constants of deactivation at –50 mV in control conditions were 1348.54 ± 64.95 ms and 238.34 ± 16.87 ms, compared to 1299.54 ± 71.64 ms and 241.34 ± 19.74 ms with methacholine (n=5, $p>0.05$). Taken together, these data suggest the effects of methacholine are mediated by PKC.

Ionomycin and methacholine produced similar effects on HERG currents in control conditions. Although the effects of ionomycin were inhibited by buffering of calcium, it may be that calcium activates a downstream signalling pathway. It is well known that an increase in cytosolic calcium can activate the α, β and γ (calcium-sensitive isoforms) of PKC. Therefore, I investigated whether the HERG current response to ionomycin could also be blocked by the PKC inhibitor bis-1.

For these experiments, the HERG–HEK cell iine was used. Cells were held at a membrane potential of –80 mV before the 'depolarisation to 0 mV' protocol was applied. Bis-1 was applied for 3 minutes, and during this time, little effect on current amplitudes was observed. After the 3 minutes, currents were 96.31 ± 3.52% of control currents. After this time period, ionomycin was applied. In these conditions, the effects of ionomycin were significantly reduced. Representative current traces in control conditions and with ionomycin are shown in figure 5.9A. HERG currents were measured 200 seconds after ionomycin application, when currents were 88.22 ± 6.16% of control current (n=5), and not significantly different from rundown ($p>0.05$). The mean time-course of the effects of ionomycin in the presence of bis-1 on peak tail currents is shown in figure 5.9B.

Figure 5.9
PKC inhibition with bis-1 blocks modulation of HERG current by ionomycin. A Representative HERG currents in control conditions, with 300 nM bis-1 alone and with 300 nM bis-1 and 5 μM ionomycin. Current traces are overlaid. **B** Time course of 5 μM ionomycin effects in the presence of 300 nM bis-1 (n=5). Peak tail currents were normalised to control amplitudes and mean normalised currents plotted against time (n=4).

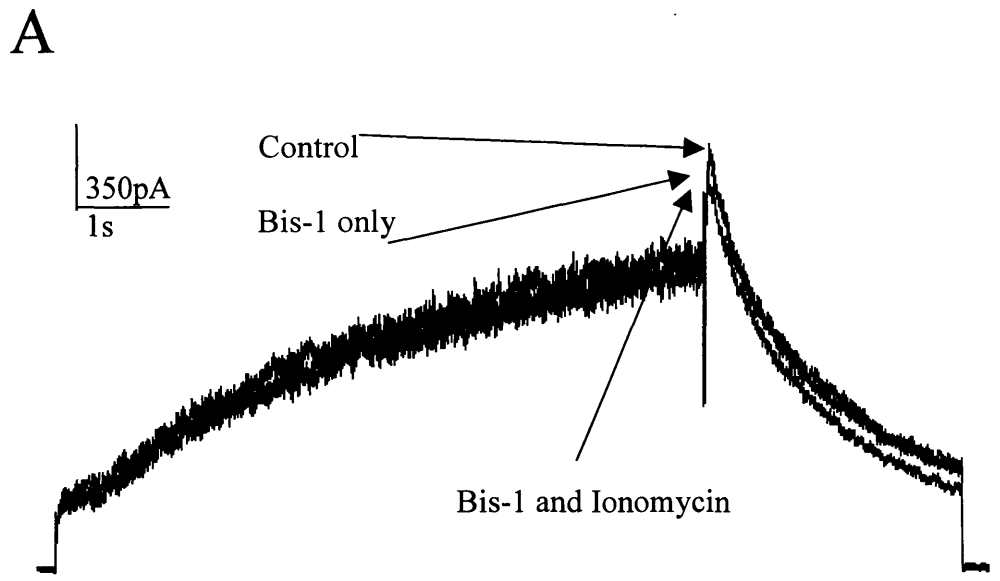

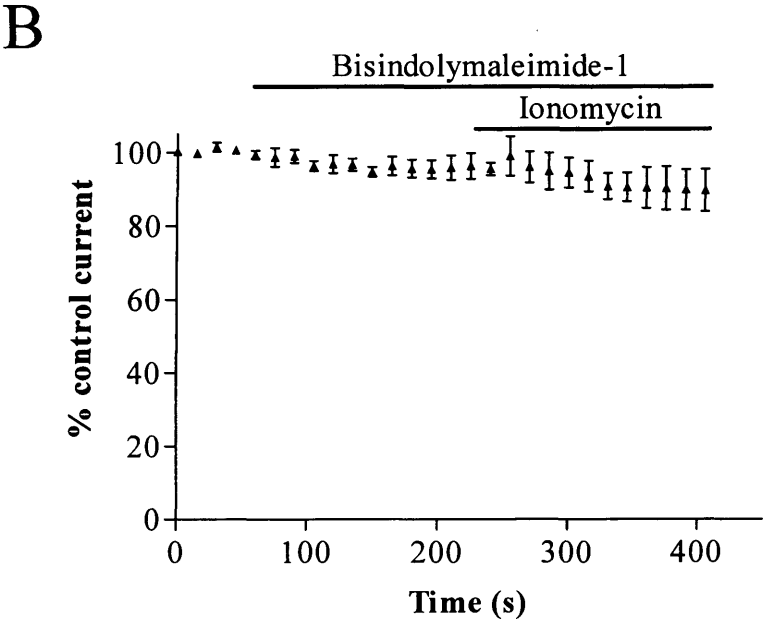

Although the effect of ionomycin was greatly reduced by 300 nM bis-1, it was not completely abolished. However, higher concentrations of bis-1 inhibited HERG currents and therefore could not be used. After a three minute incubation with 1 μM bis-1, peak tail currents were 66.43 ± 1.06% of control currents (n=5, data not shown).

5.3.2 Down-regulation of PKC isoforms by chronic PMA treatment

5.3.2.1 Acute effects of PMA on HERG currents

Several studies on modulation of HERG by protein kinases suggest there may be cross-talk between signalling pathways. For example a supposed PKC-mediated effect on the HERG channel can be (partially) inhibited using PKA inhibitors such as 2.5 μM KT-5720 (Thomas et al., 2003). However, many protein kinase inhibitors are not very specific (Davies et al., 2000). Davies et al. showed the IC_{50} of KT5720 to inhibit PKA (3.3 μM) was 10 times higher than that required to inhibit 3-phosphoinositol-dependent protein kinase 1 (PDK1) and 300 times higher that that required to inhibit phosphorylase kinase (PHK). Many protein kinase inhibitors compete with ATP at the ATP binding site, and therefore their potency is dependent on the ATP concentration. Furthermore, protein kinase inhibitors can directly block HERG channels. Thus, a number of considerations must be taken into account when using protein kinase inhibtors. Although bis-1 is though to be relatively specific for PKC (Davies et al., 2000), at the 300 nM concentration I used, this was not quite sufficient to completely block the response to ionomycin. Therefore, rather than using higher concentrations of PKC inhibitors we down-regulated PKC isoforms to reduce their activity. Chronic stimulation of kinases leads to selective down-regulation. Chronic activation of PKC by phorbol 12-myristate 13-acetate (PMA) effectively depletes several isoforms of PKC due to a net increase in proteolysis by proteases (Sano et al., 1989; Xu et al., 1996; Srivastava et al., 2002). Before investigating the effects of chronic PMA application on HERG currents, I investigated the calcium and HERG current responses to acute application.

Cytosolic calcium levels were not altered by 1 μM PMA application (figure 5.10A). The baseline fura-2 340/380 ratio was 0.83 ± 0.14, compared to 1.02 ± 0.22 during PMA application (n=7, $p>0.05$). To measure the effects of PMA application on HERG currents, the 'depolarisation to 0 mV' protocol was used and representative currents in control conditions and during application of 1 μM PMA are shown in figure 5.10B. PMA attenuated

Figure 5.10

Acute PMA attenuates HERG current. **A** Representative fura-2 ratios showing cytosolic calcium in a single cell in response to 1 μM PMA. **B** Representative HERG currents in control conditions and with PMA. **C** Time course of 1 μM PMA on HERG currents (n=10). Peak tail currents were normalised to control amplitudes and mean normalised data plotted against time. **D** Mean activation curves in control conditions and with PMA (n=10). Peak tail currents, normalised to control amplitudes, were plotted as a function of membrane potential.

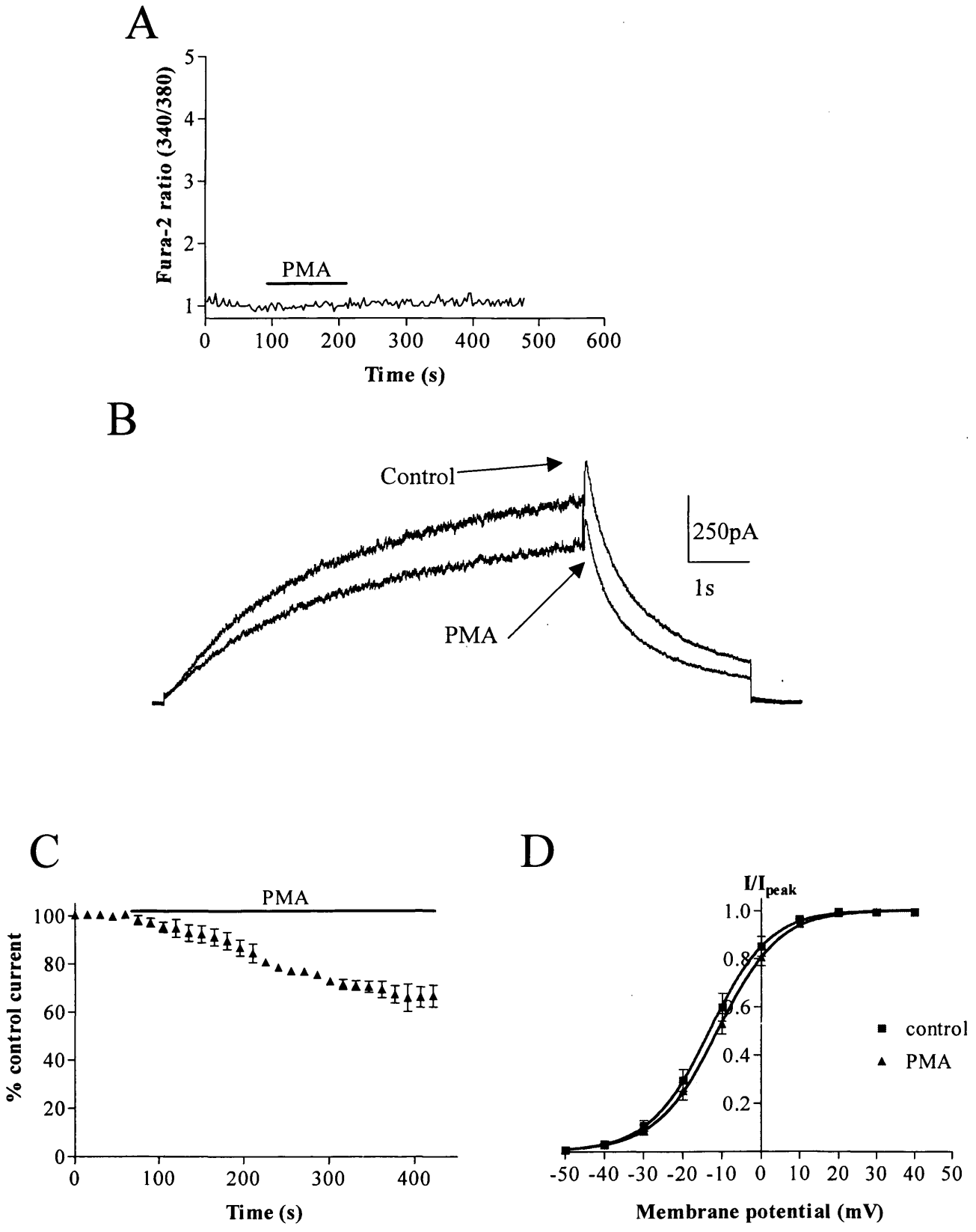

Figure 5.11

The inactive analogue of PMA, 4αPMA, does not affect HERG channel currents. A Representative HERG currents in control conditions and in the presence of 1 μM 4αPMA. **B** Time course of 1μM 4αPMA on HERG currents (n=5). Peak tail currents were normalised to control amplitudes and mean, normalised data was plotted against time.

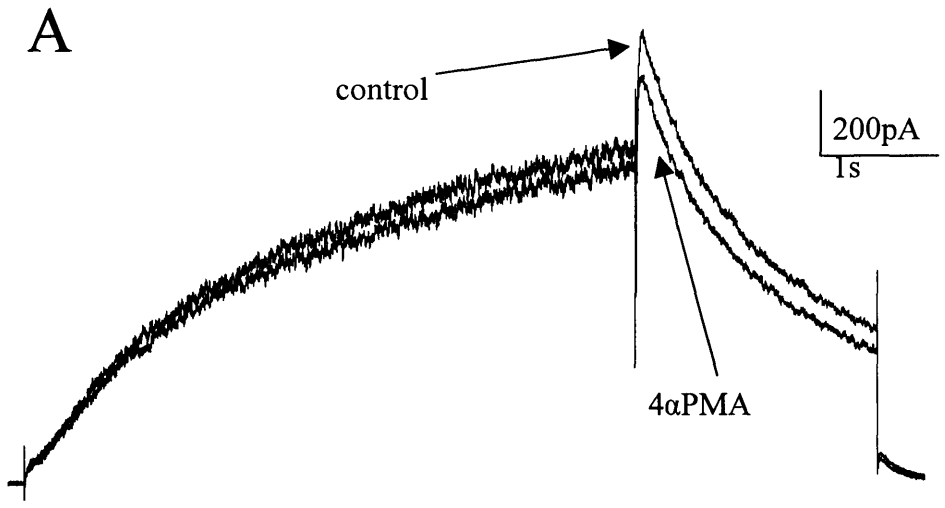

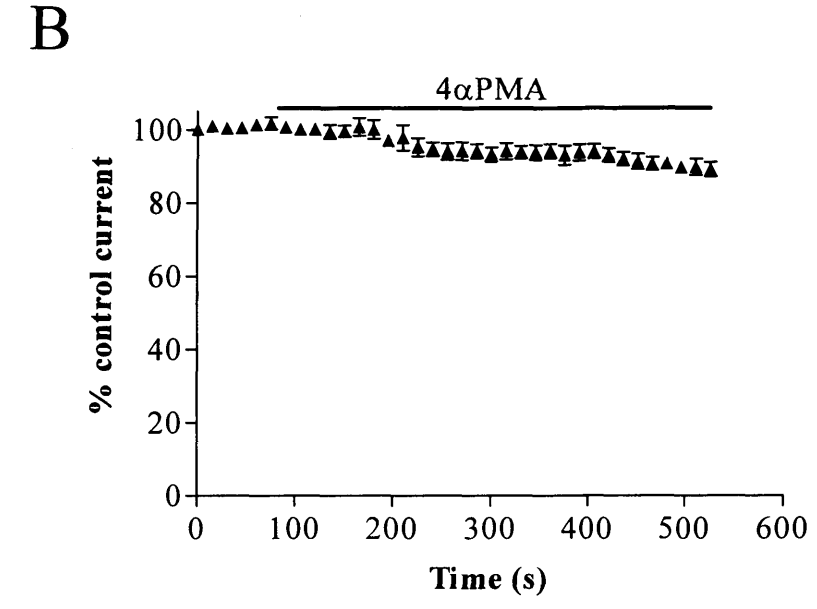

currents with a mean time constant of 670.19 ± 136.81 seconds. After 6-7 minutes current amplitudes were 69.32 ± 2.31% of control (n=10, figure 5.10C). PMA shifted the $V_{0.5}$ for activation by 3.36 ± 0.76mV (n=10, figure 5.10D). This shift, although not statistically significant ($p>0.05$) was observed in all cells. The slope factor was unaltered. Deactivation at –50 mV was significantly faster ($p<0.05$). The slow and fast time constants in control conditions were 1365.01 ± 76.93 ms and 256.94 ± 34.86 ms, compared to 1106.45 ± 83.65 ms and 190.45 ± 21.35 ms with PMA (n=10).

To confirm that the acute effects of PMA were due to PKC activation we tested the biologically inactive analogue of PMA, 4αPMA. This compound acts as a useful negative control as it lacks the ability to bind to and activate PKC. We applied 4αPMA at a concentration of 1 μM. Representative currents in control conditions and with 4αPMA are shown in figure 5.11A. After a 7-minute application of 4αPMA, HERG currents were 88.21 ± 1.32% of control (n=5) and not significantly different to the average rundown of currents over this time period ($p<0.05$). The mean time-course of the effects of 4αPMA are shown in figure 5.11B. This is consistent with activation of PKC causing a modulation of HERG channels, rather than a direct block of the channel by PMA.

5.2.3 PKC isoforms in HERG-HEK cells

Western blots were carried out to probe for individual isoforms of PKC in untreated cells and cells that had been incubated in 1 μM PMA for 24 hours. Untreated HERG-HEK cells expressed α, β, δ, ε, θ, ι and λ isoforms of PKC. Of these, it is known that the α, β, δ, ε and θ isoforms are phorbol ester sensitive. In four independent experiments, the α, β, δ and ε isoforms of PKC were consistently down-regulated with chronic PMA treatment (Figure 5.12). The α and β isoforms were down-regulated to levels that could not be detected in our blots, and the δ and ε isoforms were partially down-regulated, to expression levels lower than in untreated cells. As a further control, PKC isoform expression was also investigated in cells chronically treated with 4αPMA. In three experiments, chronic treatment with 4αPMA failed to alter the expression level of PKC isoforms (Figure 5.12C).

Figure 5.12

Chronic treatment of HERG-HEK cells with PMA, but not 4αPMA, causes down regulation of PKC isoforms. **Ai** Representative western blot for PKC isoforms from cells treated with 0.1% DMSO for 24 hours. **(ii)** The same blot stripped and re-probed for β-actin to check for equal protein loading. **Bi** Representative western blot for PKC isoforms from cells treated with 1μM PMA for 24 hours. **(ii)** The same blot stripped and re-probed for β-actin. **Ci** Represetative western blot for PKC isoforms from cells treated with 1μM 4αPMA for 24 hours. **(ii)** The same blot stripped and re-probed for β-actin.

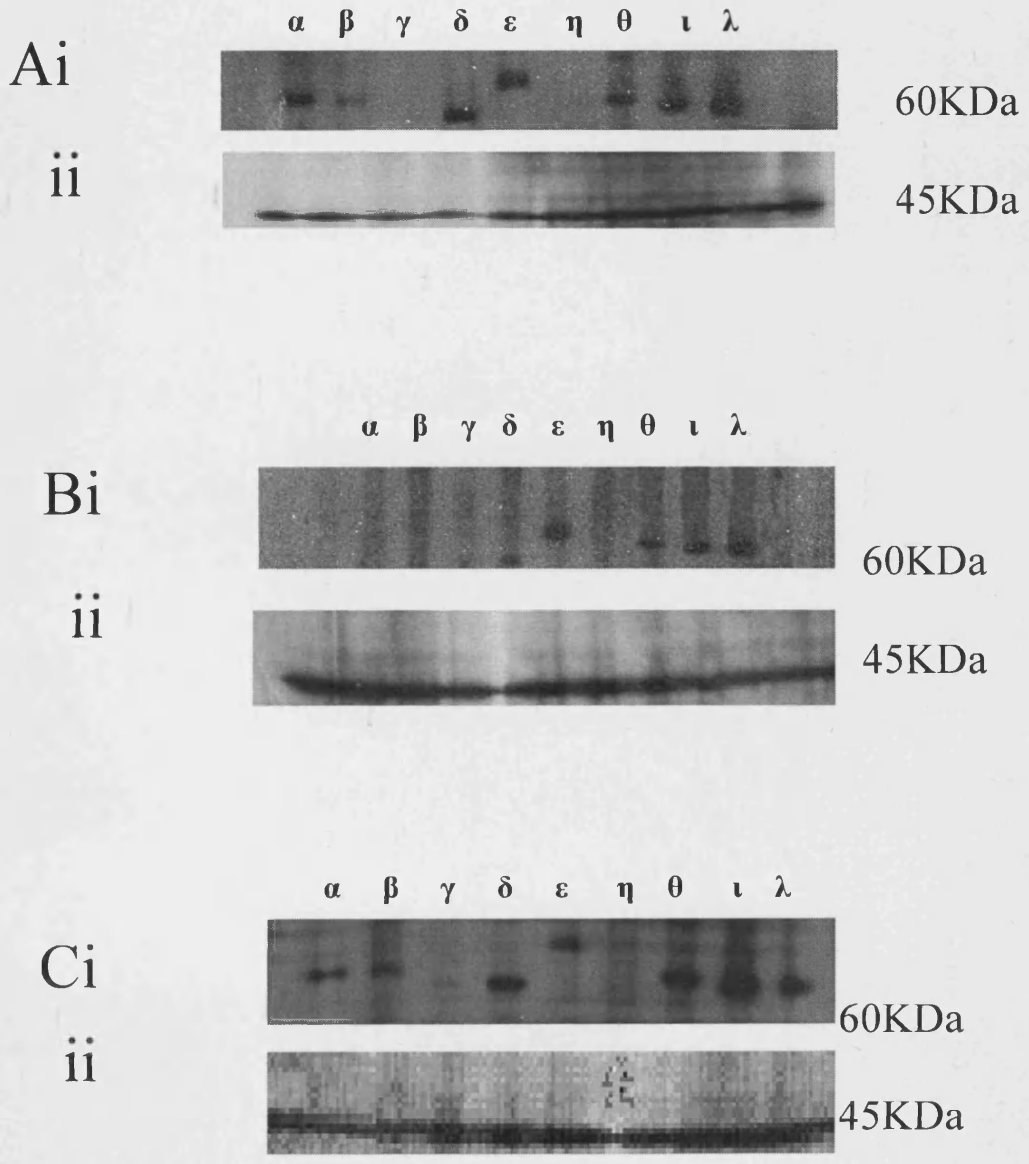

Figure 5.13

The modulatory effects of methacholine are abolished in cells chronically treated with PMA. **A** Representative HERG currents before and during methacholine application. Both currentstraces are overlaid. **B** Time course of HERG current response to methacholine in chronic PMA-treated cells. Peak tail currents were normalised to control amplitudes and mean, normalised data were plotted against time. **C** Representative fura-2 ratio showing changes to cytosolic calcium in a single cell in response to methacholine.

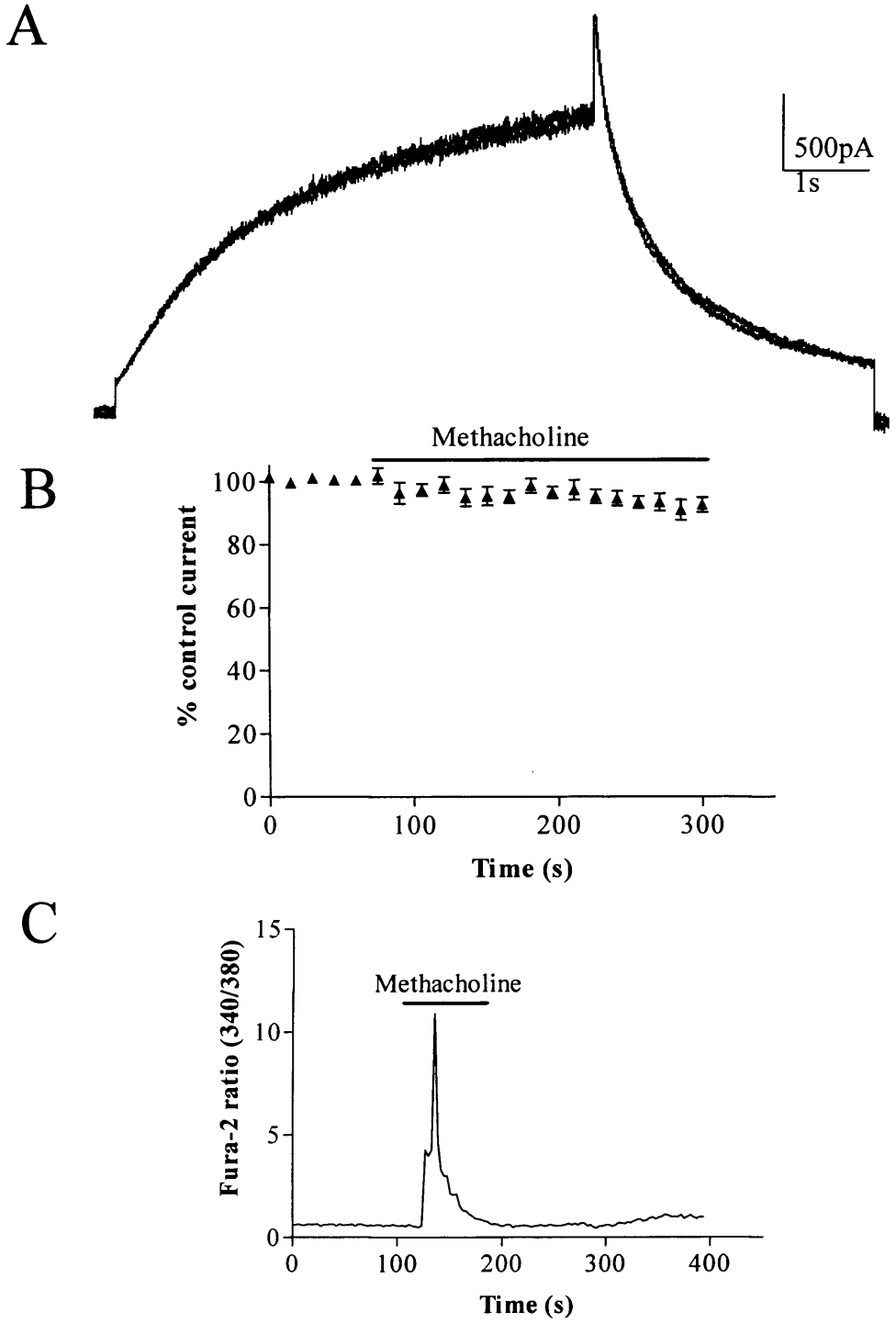

5.2.4 HERG current response to ionomycin and methacholine is abolished by chronic PMA pre-treatment

The next questions I addressed were: does down regulation of PMA sensitive PKC isoforms abolish modulation of HERG currents by ionomycin and methacholine; or have additional effects on HERG currents? A comparison of PMA-treated and untreated cells revealed no significant differences in the voltage dependence of activation and inactivation and of time constants for deactivation kinetics of HERG currents. I then tested the response to methacholine, using the 'depolarisation to 0 mV' voltage protocol. Representative current traces before and during methacholine application in PMA-treated cells are shown in figure 5.13A. Methacholine did not alter HERG channel currents. After a four-minute application of methacholine, HERG currents were 92.31 ± 2.33% of control currents (n=5, 5.13B). Furthermore, chronic PMA treatment had no effects on the calcium response to methacholine. The baseline fura-2 340/380 ratio was 0.79 ± 0.90 in these cells. The calcium profile observed in response to methacholine application was very similar to that seen in control cells (5.13C). Peak fura-2 340/380 ratio was 9.02 ± 1.64, with the ratio decaying to 0.71 ± 0.10 within 80 seconds. (n=12). These values were not significantly different to values measured from control cells (which had a peak fura-2 ratio of 10.86 ± 1.65). These results strongly suggest that the effects of methacholine are mediated by a mechanism dependent upon one or more of the α, β, δ or ε isoforms of PKC, that are down-regulated by PMA treating cells.

Ionomycin also failed to attenuate HERG current in cells chronically treated with PMA (figures 5.14). After a 225 second application of 5 μM ionomycin, currents were 91.31 ± 1.84% of control currents (n=5), which was not significantly different from reduction due to rundown ($p>0.05$). The abolition of the response to ionomycin was not due to a change of calcium response, which was not statistically different from untreated cells (figure 5.14C). As with methacholine, the abolition of the modulation of HERG current in response to ionomycin application is probably due to the down-regulation of one or more of the α, β, δ or ε isoforms of PKC rather than direct effects of calcium on HERG channels.

5.3.4 Chronic PMA treatment does not effect HERG modulation by PKA

How selective is chronic PMA treatment for PKC dependent processes? Are HERG currents still modulated by PKA? To answer these questions I compared the response of HERG

currents to forskolin in untreated and PMA-treated cells. In control conditions I found application of 40 μM forskolin reduced current amplitudes to 63.21 ± 1.32% of control with a mean time constant of 123.26 ± 29.90 seconds (n=5). In cells chronically treated with PMA, 71.32 ± 5.45% of current remained after forskolin application, and the time constant of the forskolin effect was 136.21 ± 22.37 seconds (n=5). Representative currents and mean time-courses of the effects of forskolin are shown in figure 5.15. There was no statistical difference between the attenuation of current seen in untreated and chronically PMA treated cells ($p>0.05$), suggesting down regulation of PKC by chronic PMA treatment does not alter cAMP or PKA-mediated responses in HERG-HEK cells.

Figure 5.14

The modulatory effects of ionomycin are abolished in cells chronically treated with PMA. A Representative HERG currents before and during 5 μM ionomycin application. **B** Time course of HERG current response to 5 μM ionomycin in cells chronically treated with 1 μM PMA (n=5). Peak tail currents were normalised to control amplitudes and mean, normalised data were plotted against time. **C** Representative fura-2 ratios showing changes in cytosolic calcium in a single cell in response to 5 μM ionomycin.

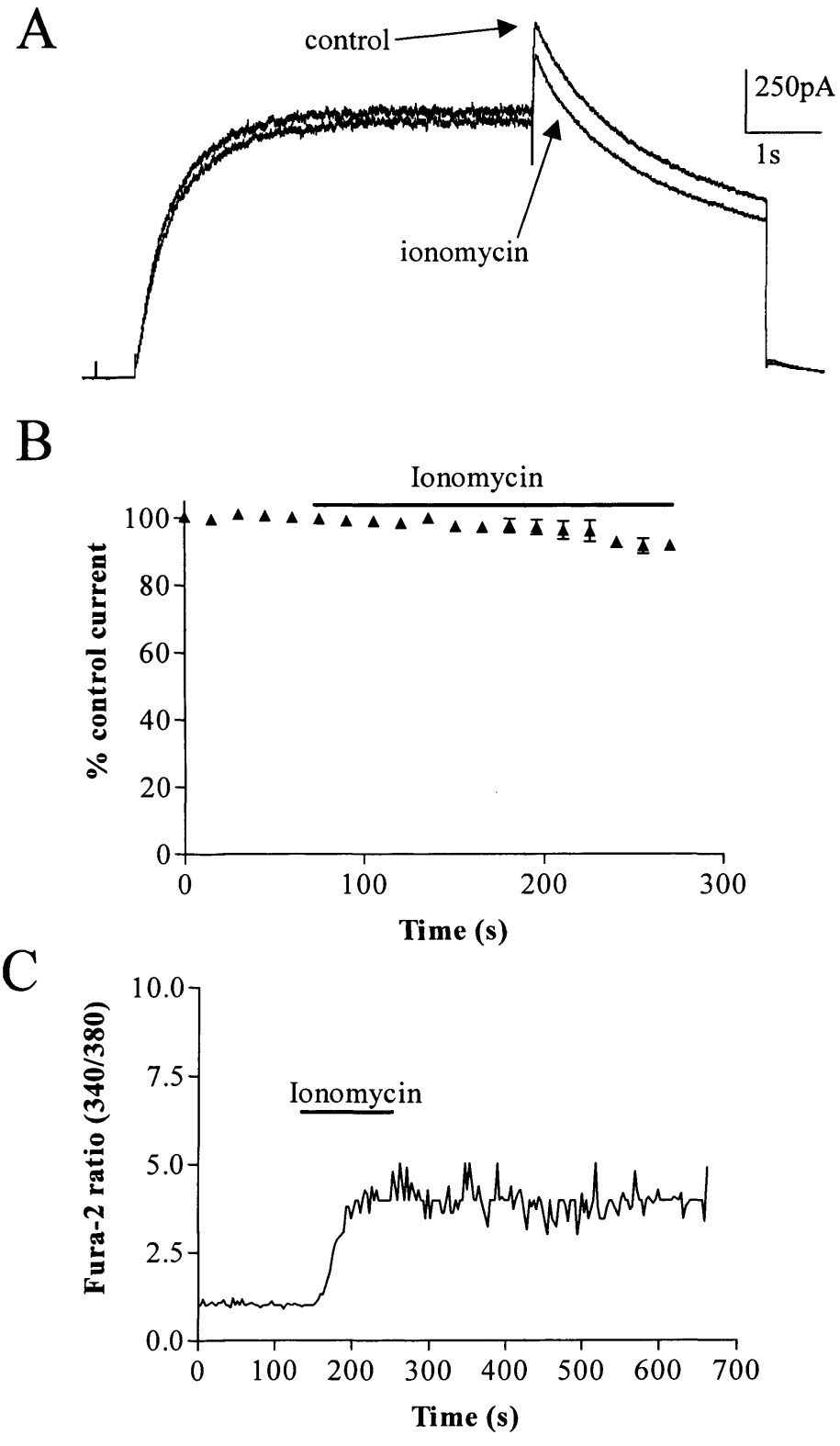

Figure 5.15
Chronic treatment of cells with PMA does not alter modulation of HERG by forskolin. Representative HERG currents before and after 40 μM forskolin application in untreated cells (A) and 1 μM PMA-pre-treated (B) HERG-HEK cells. **C** Comparison of the time course of 40 μM forskolin on mean HERG peak tail currents that were normalised to control amplitudes and plotted against time (n=5 for each data set).

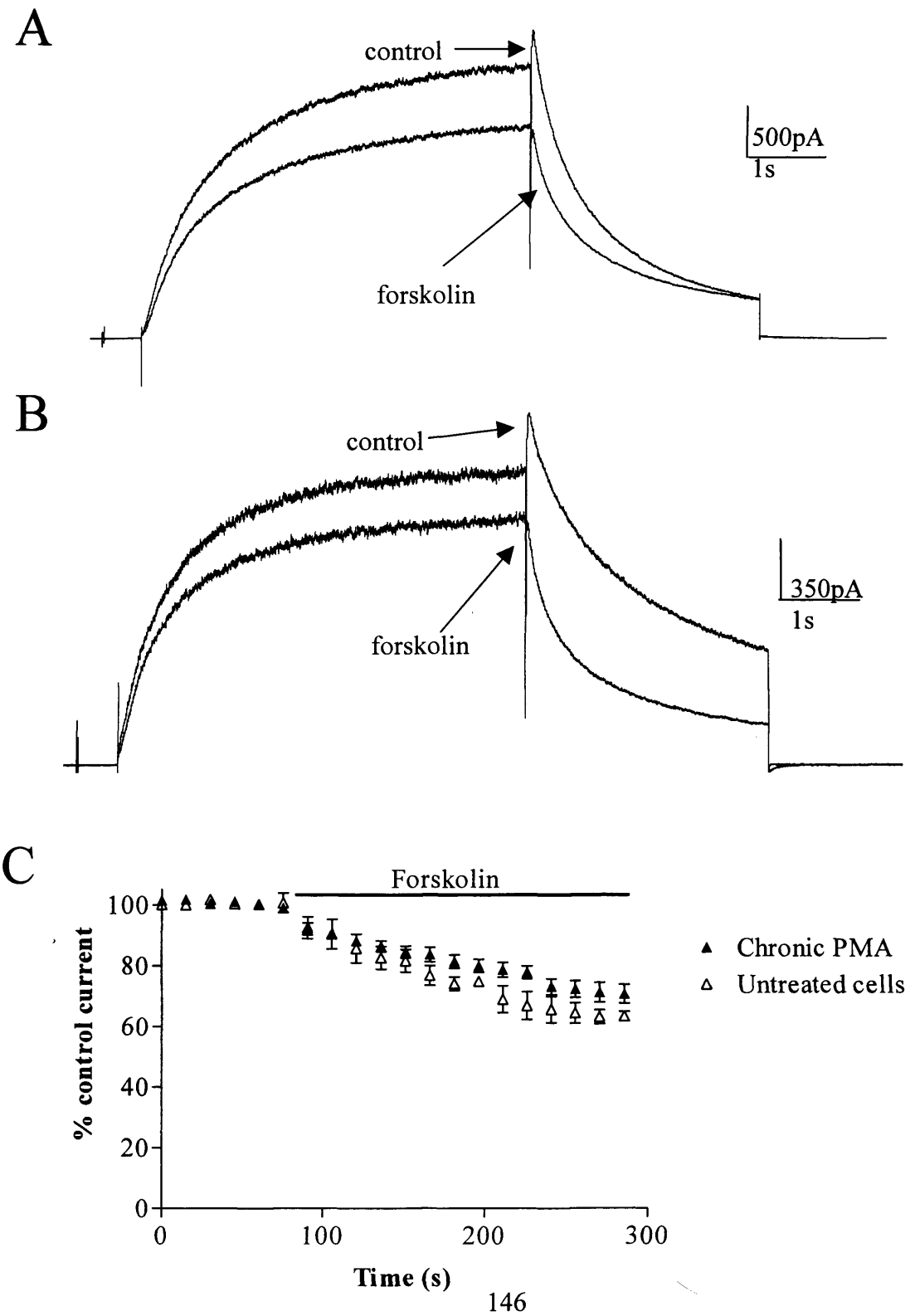

5.3 Discussion

5.3.1 Modulation of HERG by PKC and calcium

In this chapter of work I have shown the HERG channel is modulated by PKC activation by $G_{q/11}$-coupled receptors, calcium and PMA. Activation of PKC significantly attenuated HERG current, shifted voltage dependent activation to more positive potentials and accelerated deactivation. The relative proportions of deactivation fitted with each τ value was not calculated. However, it may be that the proportion of fast and slow deactivation is altered with PKC activation.

I have shown the shift of voltage dependent activation, the attenuation of current, and the acceleration of deactivation are attenuated during pharmacological inhibition of PKC using bis-1, and abolished when PKC isoforms are down-regulated with chronic PMA treatment. One or more of the α, β, δ or ε PKC isoforms must mediate this modulation, as it is these isoforms that are down-regulated. Since the effects of ionomycin are due to calcium-dependent activation of PKC, it is likely that only the calcium-sensitive, PMA down regulated isoforms, that is the α and β isoforms, modulate HERG current in response to ionomycin.

The results of this study concur with those of Thomas et al. (2003) who used PMA to activate PKC, and showed PKC activation to attenuate current, positively shift voltage dependent activation and accelerate deactivation of HERG currents. Barros et al. (1998) used a $G_{q/11}$-coupled GPCR (TRH receptor) to activate PKC, which also attenuated current, rightward-shifted activation, accelerated deactivation and slowed activation. In this study the effects of TRH were mimicked by PMA. Thomas et al. and Barros et al. both conducted studies on the HERG channel expressed in *Xenopus* oocytes. Although they show some similar responses, there are also some fundamental differences to my work. In oocytes, large positive shifts in the voltage dependence of activation (+20 mV shift in Barros et al., +37 mV shift in Thomas et al.), are observed, aswell as an ~ 50% attenuation of current in response to PMA. These effects are much larger than in my study. The time courses for effects were also much longer, with maximal effects following PMA application taking 30 minutes (Thomas et al.), and 10 minutes (Barros et al.). This may reflect important mechanistic differences in how HERG is modulated in amphibian and mammalian cells. It is therefore essential to investigate modulation of the HERG current in mammalian tissue.

In a study carried out on anterior pituitary cells, activation of the TRH $G_{q/11}$-coupled receptor attenuated rERG1, rERG2, rERG3 and HERG current, accelerated deactivation and shifted voltage dependent activation by ~10 mV (Schledermann et al., 2001). However, the group could not inhibit the effects of TRH with inhibitors of PKC, PKA, tyrosine kinase or MAP kinase, nor could they mimic the effects of TRH with PMA, concluding that none of these signalling pathways modulated HERG current. This group also showed 1 μM bis-1 directly inhibited HERG current. The muscarinic agonist oxotremorine-M (oxo-M) modulated rERG current in tsA-201 cells over expressing either M_1 or M_3 muscarinic receptors (Hirdes et al., 2004), causing a 30% inhibition of current at all potentials. Muscarinic receptor activation had only minor effects on deactivation and inactivation of the current. rERG current was entirely abolished when the constitutively active form of G_q was transfected into cells, whereas expressing the dominant negative form of G_q reduced inhibition with oxo-M, suggesting oxo-M modulated ERG current via G_q. When internal and external calcium were removed, and BAPTA was included in the solution, oxo-M did not alter ERG current. However, when calcium levels were buffered to 129 nM, the oxo-M response was seen, suggesting a minimum level of calcium was required. These results may reflect a mimimum requirement for calcium of PLCβ (Ryu et al., 1987). The group were not able to fully inhibit the effect of oxo-M using a wide variety of agents, including inhibitors of tyrosine kinase, PKB, the general kinase inhibitor staurosporine, and a PIP_2-neutralising antibody. However, the response was reduced by 40% using the PKC inhibitor calphostin C. Bis-1 did not inhibit oxo-M mediated attenuation, however, concentrations of this compound that were used in this study have previously been shown to directly inhibit the HERG channel (my data; Thomas et al., 2003; Schledermann et al., 2001), suggesting this may be the reason the oxo-M modulation of current was not reduced. The study was unable to reach a firm conclusion on the mechanism of oxo-M modulation of ERG current, but did suggest that the phospholipase C pathway was involved. Therefore, modulation of HERG by PKC in mammalian cells remains controversial.

I have shown the effects of ionomycin, but not methacholine, to be inhibited by buffering calcium to extremely low levels. This suggests that it is calcium-dependent PKC activation in response to ionomycin that modulates HERG current. In contrast, the rise in intracellular calcium is not required for the HERG current response to methacholine. Taken together,

these results suggest that calcium does not directly modulate HERG current in HEK 293 cells. However, a study carried out by Heath and Terrar (2000) showed I_{Kr} in guinea pig ventricular myocytes to be attenuated when cells were pre-incubated in BAPTA-AM. This study also showed I_{Kr} amplitude was increased (by a reduction of inactivation) by what was hypothesised to be a PKC-dependent pathway. The differences between these results, my results and those of Thomas et al. (2003) and Barros et al. (1998) may be due to several differences between the tissue types used. In myocytes, HERG may co-assemble with β subunit(s), that could confer modulation onto the I_{Kr} channel. In minK and KvLQT1 channels (I_{Ks}), the sensitivity to PKC is mediated by minK (Busch et al., 1992). Mutating a PKC phosphorylation consensus site on human minK inhibited modulation by PKC, which was suggestive of a direct phosphorylation of the channel (Lo and Numann, 1999). The modulation was species dependent. Whilst rat and mouse minK currents are attenuated with PKC activation, guinea pig minK currents are enhanced with increased PKC activity. If minK does coassemble with HERG in native cardiac channels, the final modulation of I_{Kr} may be influenced by phosphorylation of both HERG and minK subunits. So far there is no evidence that co-expression of β subunits influences modulation of HERG currents (Thomas et al., 2003)

My work has shown HERG current is only partially reduced by PKC-dependent modulation. The reason for this is not yet clear. Rapid desenitisation of the muscarinic M_3 receptor may cause a partial activation of PKC to modulate current. However, I also observe partial modulation with ionomycin and PMA, so it is unlikely this is the reason. Modulation of HERG may be state dependent. I am presently unable to determine if only a portion of the total population of channels are able to be modulated or whether the total channel population can be modulated by PKC.

I have shown activation of PKC shifts voltage dependent activation by approximately +5 mV, causing a small attenuation of current at a given potential. This shift in voltage dependent activation could be due to PKC-dependent phosphorylation of the channel close to the voltage sensor, thus changing the internal environment and altering voltage sensitivity. Alternatively, phosphorylation may alter coupling between voltage sensing and channel opening, thus the channel would open less at a given potential. Measuring single channel

events would allow me to discriminate if PKC activation is causing a reduced open probability of the channel, or altering single channel conductance to attenuate current.

5.5 Physiological relevance of HERG modulation

5.5.1 Modulation of cardiac HERG currents

The activation of PKC, and possible modulation of the HERG channel in the heart is very physiologically relevant. There are a number of GPCRs in the heart which couple to the $G_{q/11}$ family of G-proteins. These are the α_1-adrenergic receptor subtypes A, B and D, the angiotensin-II receptor and the endothelin receptor (reviewed in Rockman and Lefkowitz, 2002). A recent study has also shown, albeit small, expression of a functional M_3-muscarinic receptor in adult rat ventricular tissue (Pönicke et al., 2003), which would also cause activation of PKC through the $G_{q/11}$ pathway. So activation of PKC could occur through stimulation of a number of receptors. The PKC isoforms expressed in cardiac tissue seems to be highly species-dependent. Hudman and Standen (2004) showed rat ventricular tissue to express α, β, γ, δ, ι. λ and ξ isforms. Rabbit cardiac tissue has been shown to express the isoforms α, β, γ, ε and ξ (Rouet-Benzineb et al., 1996), and although not studied fully, guinea-pig cardiac tissue has been shown to express α, ε, and γ isoforms (Jalili et al., 1999). So it could be hypothesised that the response of I_{Kr} to receptor-mediated activation of PKC may be dependent on which species is investigated.

PKC dependent modulation of HERG may be pathophysiologically relevant. It has previously been shown that stress, either physical or emotional, can be a trigger for long QT syndrome (reviewed in Kamarck and Jennings, 1991). Activation of the sympathetic nervous system leads to release of catecholamines that would cause an activation of α-adrenergic receptors in the heart, which in turn could cause the activation of PKC. This activation could attenuate I_{Kr}. Futher studies are required to investigate the link between HERG channel modulation and cardiac disease.

5.6.2 Modulation of neuronal HERG currents

ERG channels are expressed in a number of regions of the central nervous system (Papa et al., 2003), including in celebellar Purkinje neurons (Sacco et al., 2003), where they are thought to contribute to the resting membrane potential. The M_1 muscarinic receptor, which

is coupled to the $G_{q/11}$ pathway like the muscarinic M_3 receptor, has also been found in this tissue (Tayebati et al., 2001), suggesting a possibility of coupling between this receptor and the ERG channel. It has previously been shown that activation of the muscarinic M_1 receptor can modulate ERG and HERG current in cell lines (Schledermann et al., 2001; Hirdes et al., 2003), although neither of these studies could conclude if this modulation was due to activation of PKC. If this coupling can occur *in vivo*, activation of the muscarinic receptor would attenuate ERG current, thus depolarising the resting membrane potential and increasing neuronal excitability.

5.6.3 Modulation of HERG current in cancerous tissue

The HERG channel is expressed in a number of cancer cells and tumour-derived cultured cell lines. It may influence cell invasion (Lastrailoi et al., 2004), proliferation rate and apoptosis (Wang et al., 2002a). Although it remains unclear if it is the presence of the protein itself or potassium conductance that alters cellular properties, the possible modulation of the HERG current and its effects in tumour cells must be considered. No studies have been carried out investigating PKC modulation of the channel in cancer, and how this modulation alters cell properties. However, a study showed the oncogene *v*-src, which is a constitutively active form of the protein tyrosine kinase src, phosphorylates HERG to cause augmentation of current (Cayabyab et al., 2002). It is well documented that aberrant function of proteins in the *ras-src* signalling pathway occurs in transformed (tumour) cells, suggesting src-mediated modulation may regulate HERG function *in vivo*. I have shown HERG current is decreased in response to PKC and PKA, which may decrease both cell invasion and proliferation rate of cancer cells. However, activation of PKC or PKA in cancer cells, and the possible effects on HERG current in these tissues is yet to be investigated.

Chapter 6
Direct activation of PKC

6.1 Introduction

In chapter 5 I showed HERG current in HEK cells is modulated by PKC. However, using the approaches in chapter 5, that is, both calcium- and $G_{q/11}$-induced activation of PKC, activation of a number of different signalling pathways, including calcium dependent pathways such as calcium dependent phosphatases and calcium-calmodulin dependent pathways may occur. In this chapter, the effects of PKC activation on HERG currents were investigated in isolation using the DAG analogue 1-oleoyl-2-acetylglycerol (OAG). Previous studies characterising PKC-mediated modulation of HERG have used the phorbol ester PMA or have used GPCR-coupled PKC activation, which may result in activation of signalling pathways other than PKC. In addition to this, many of these studies have been carried out on HERG expressed in *Xenopus* oocytes (Barros et al., 1999; Thomas et al., 2003; Gómez-Varela et al., 2003), which, as amphibian cells, may have different signalling pathways to mammalian cells. For this study I used HEK cells stably transfected with the HERG protein. Using OAG we found HERG current was attenuated, the voltage dependence of activation was shifted to more positive potentials and deactivation was accelerated in a similar manner to the effects of methacholine and ionomycin reported in chapter 5. This provides further evidence that calcium itself does not alter HERG channel currents. Modulation of HERG current by OAG was due to one or more of the α, β, δ and ε isoforms of PKC, shown by an abolition of the effects of OAG in cells chronically treated with PMA.

To investigate the PKC isoforms responsible HERG channel modulation, isoform specific PKC inhibitors and PKC isoform over-expression was tried. I also investigated if channel modulation in mammalian cells was abolished in HERG mutants in which phosphorylation sites had been mutated. 4M and ΔPKC HERG (kindly provided by Dr. Dierk Thomas, University of Heidelberg, Germany) lack putative PKA and 17 of 18 putative PKC phosphorylation sites respectively.

6.2 Results

6.2.1 Application of the DAG analogue OAG

Experiments were carried out in HERG-HEK cells to characterise the effects of OAG on HERG channel currents at 0 mV. A concentration-response curve was generated to find a suitable concentration for further experiments. Concentrations between 10 nM and 100 μM were applied ($n \geq 4$ for each concentration). Figure 6.1A shows OAG caused a concentration-dependent attenuation of current. The data points were fit with a Hill function and the Hill slope was measured as 1.49 ± 0.50. The IC_{50} value of OAG on peak tail currents was 1 μM, and maximal effects of OAG were seen with 10 μM. This concentration was therefore chosen for use in all further experiments. Representative HERG currents before and during 10 μM OAG application are shown in figure 6.1B. The mean time constant for the effects of OAG was 252.86 ± 47.58 seconds, and steady state currents were 54.43 ± 2.22% of control (n=9, figure 6.1C). OAG caused a significant positive shift in the $V_{0.5}$ for activation of 5.94 ± 1.77 mV (n=5, $p<0.05$), but the slope factor was unaltered (figure 6.2A). The voltage dependence of inactivation was not significantly affected, with OAG causing a 1.90 ± 1.90 mV shift (n=5, $p>0.05$, figure 6.2B). Current deactivation kinetics at –50 mV were significantly faster ($p<0.05$). The slow and fast deactivation time constants in control conditions were 1229.15 ± 150.3 ms and 246.62 ± 41.09 ms, compared to 782.01 ± 35.53 ms and 144.44 ± 15.13 ms with OAG (n=9, figure 6.2C). This suggests that OAG attenuates the HERG channel current by a positive shift in activation and an acceleration of deactivation kinetics. Cytosolic calcium concentrations were not altered by OAG application. Baseline fura-2 ratios were 0.91 ± 0.26 compared to 1.17 ± 0.16 with OAG (n=6, $p>0.05$, measured 2 minutes after OAG addition).

As expected the effects of OAG were similar to ionomycin and methacholine. They could be blocked by chronic treatment of cells with 1 μM PMA (but not 1 μM 4αPMA), indicating the response to OAG was mediated by one or more of the α, β, δ and ε isoforms of PKC. Representative currents from these experiments are shown in figure 6.3A and B. After a 300 second application of OAG to PMA treated cells, current remaining was 91.45 ± 1.35% of control (n=5), compared to 50.73 ± 6.93% of control in 4αPMA treated cells (n=5, figure 6.3C). The $V_{0.5}$ of activation was shifted by 0.53 ± 0.74 mV with OAG in PMA treated cells (n=5, $p>0.05$, figure 6.3D), and deactivation time constants at –50 mV were also unaltered

Figure 6.1
OAG modulates HERG currents in a concentration-dependent manner. **A** Concentration-response curve for OAG. Peak tail currents with OAG were normalised to control amplitudes. Percentage attenuation of current was measured and mean, normalised data was plotted against OAG concentration. $n \geq 4$ for each concentration. **B** Representative HERG currents in control conditions and with 10 μM OAG. **C** Time course of 10 μM OAG on HERG currents (n=9). Peak tail currents were normalised to control amplitudes and mean, normalised current was plotted against time.

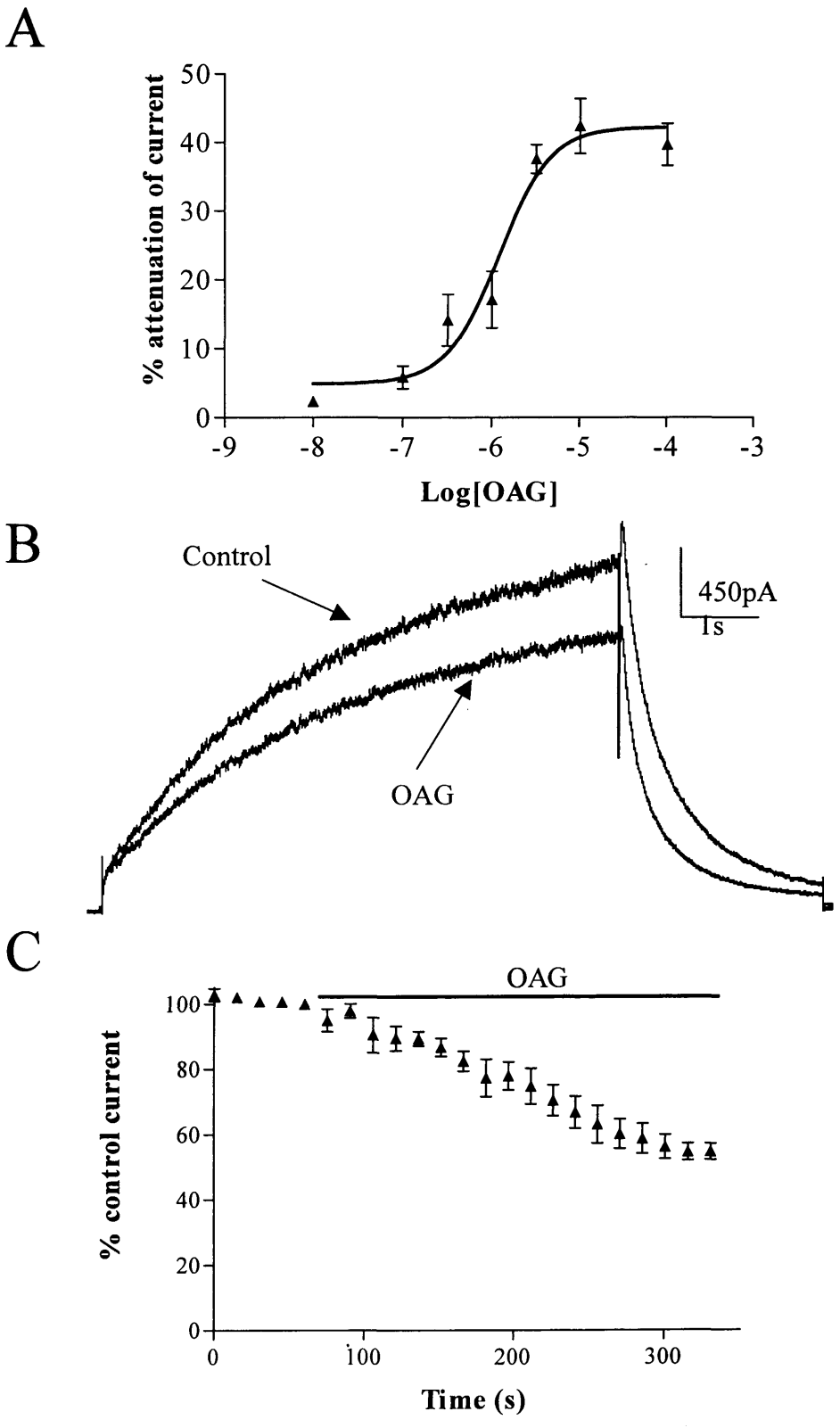

Figure 6.2
OAG alters activation and deactivation of HERG current, but not inactivation. **A** Mean activation curves in control conditions and with 10 μM OAG (n=5). Peak tail currents, normalised to control amplitudes are plotted against test potential. **B** Voltage dependence of inactivation of HERG current, measured using a triple pulse protocol (n=5). **C** The slow (i) and fast (ii) time constants of deactivation in control conditions and in the presence of OAG (n=9 for each data set). * shows significance at $p<0.05$ compared to control.

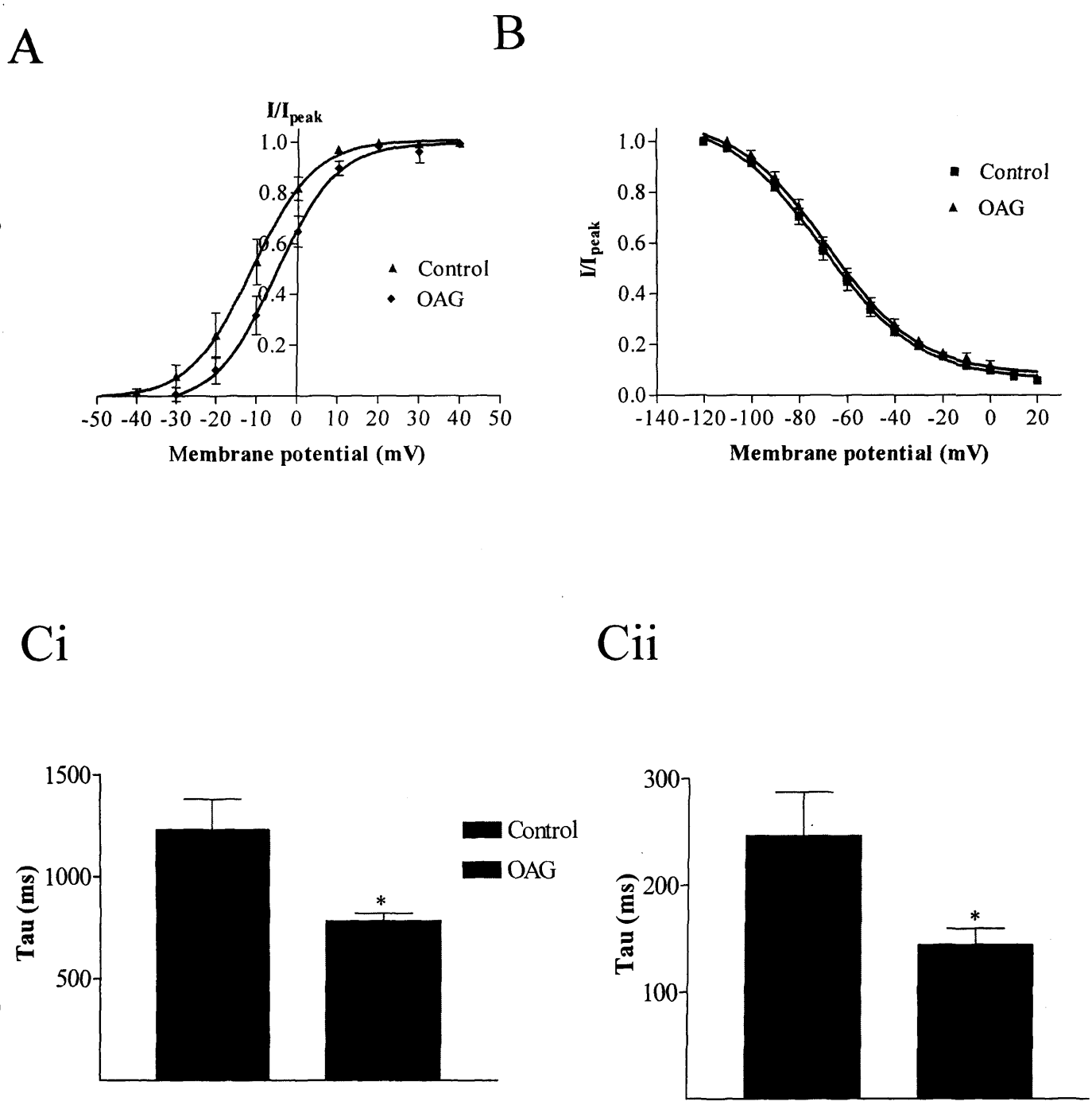

Figure 6.3

The effects of OAG are abolished in cells chronically treated with PMA, but not 4αPMA. Representative HERG currents before and during 10 μM OAG application in 1 μM PMA (A) and 1 μM 4αPMA (B) treated HERG –HEK cells. **C** Time course of 10 μM OAG effects on HERG current (n=5 for each data set). Peak tail currents were normalised to control amplitudes and mean, normalised currents were plotted against time. **D** Mean activation curves in control conditions and with OAG in PMA-treated cells (n=5).

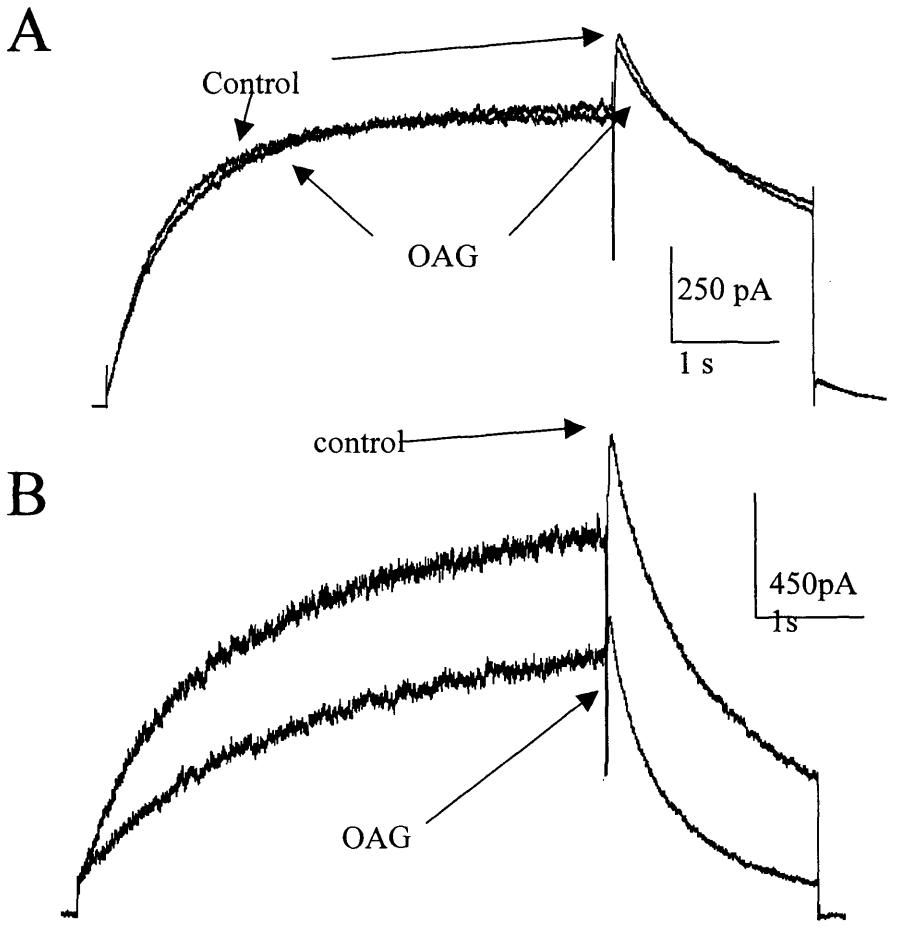

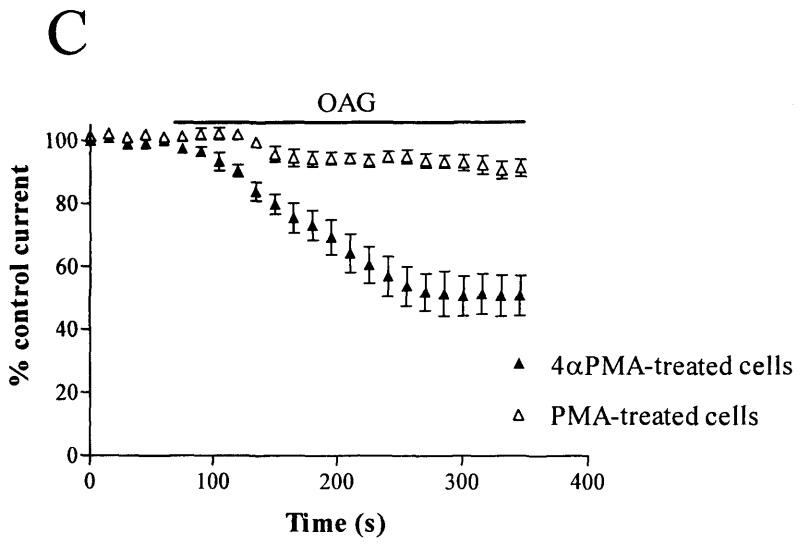

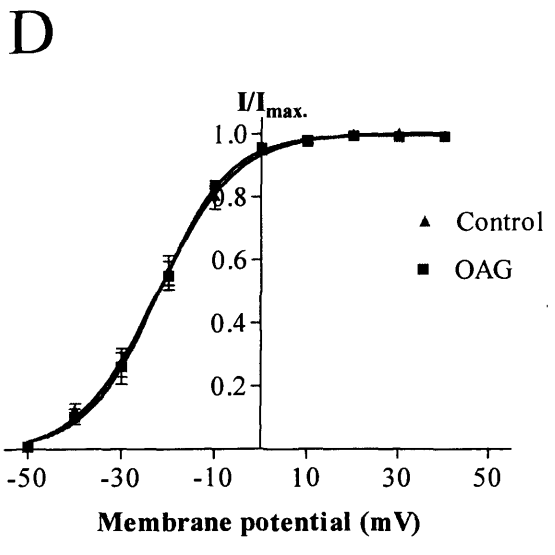

with OAG in these conditions ($p>0.05$). The slow and fast time constants were 1232.13 ± 122.96 ms and 256.04 ± 23.09 ms before OAG, compared to 1043.34 ± 91.38 ms and 209.14 ± 20.57 ms with OAG (n=5).

6.2.2 Which PKC isoform is important in the modulation of HERG?

6.2.2.1 Pharmacological inhibition of PKCα and βI

I have shown modulation of HERG channel current in response to ionomycin, methacholine and OAG to be due to one or more of the PKC isoforms α, β, δ and ε. To identify which of these PKC isoforms are important in the modulation of the channel, I tested a PKC-isoform specific inhibitor to investigate which isoform mediates modulation of HERG currents by OAG. These experiments were carried out HERG-HEK cells. The compound 12-(2-cyanoethyl)-6,7,12,13-tetrahydro-13-methyl-5-oxo-5H-indolo (2,3-a) pyrrolo (3,4-c)-carbazole (Gö6976) selectively inhibits the α and βI isoforms of PKC with IC_{50} values of 2.3 nM and 6.2 nM respectively. It is reported not to inhibit δ or ε isoforms of PKC even when used in the micro-molar range (Martiny-Baron et al., 1993). The 'depolarisation to 0 mV' protocol was used to evoke currents. Once currents had stabilised, 100 nM Gö6976 was applied for three minutes. During this time Gö6976 had no effect on HERG current amplitude. This was expected, as I have previously shown there is no PKC-dependent modulation of HERG under basal conditions. After a 300 second application of 10 μM OAG in the continued presence of Gö6976, HERG current was 83.49 ± 3.90% of control currents (n=5, figure 6.4A). This was a significant but not complete attenuation by Gö6976 of the effects of OAG ($p<0.05$). Gö6976 also reduced the shift by OAG of the $V_{0.5}$ for HERG current activation from 5.94 ± 1.77 mV to –0.23 ± 0.41 mV (n=5, $p>0.05$, figure 6.4B). The acceleration of current deactivation at –50 mV by OAG was also reduced ($p>0.05$). The slow and fast time constants of deactivation were 1502.41 ± 75.48 ms and 195.61 ± 1.72 ms before OAG, compared to 1431.03 ± 48.99 ms and 186.92 ± 7.21 ms after Gö6976 and OAG (n=5). These data suggest the attenuation of current, shift in voltage dependent activation and acceleration of deactivation seen in response to application of OAG are due, at least in part; to the α and/or βI isoforms of PKC. However, Gö6976 does not completely abolish the attenuation of HERG current by OAG.

Figure 6.4

The effects of OAG are inhibited by the PKCα and βI-specific inhibitor Gö6976. A Time course of 100 nM Gö6976 and 10 μM OAG effects on HERG current. Peak tail currents were normalised to control amplitudes and mean, normalised data plotted against time (n=5). **B** Mean activation curves in control conditions and with 100 nM Gö6976 and 10 μM OAG (n=5). Peak tail currents were normalised against control amplitudes and plotted as a function of membrane potential.

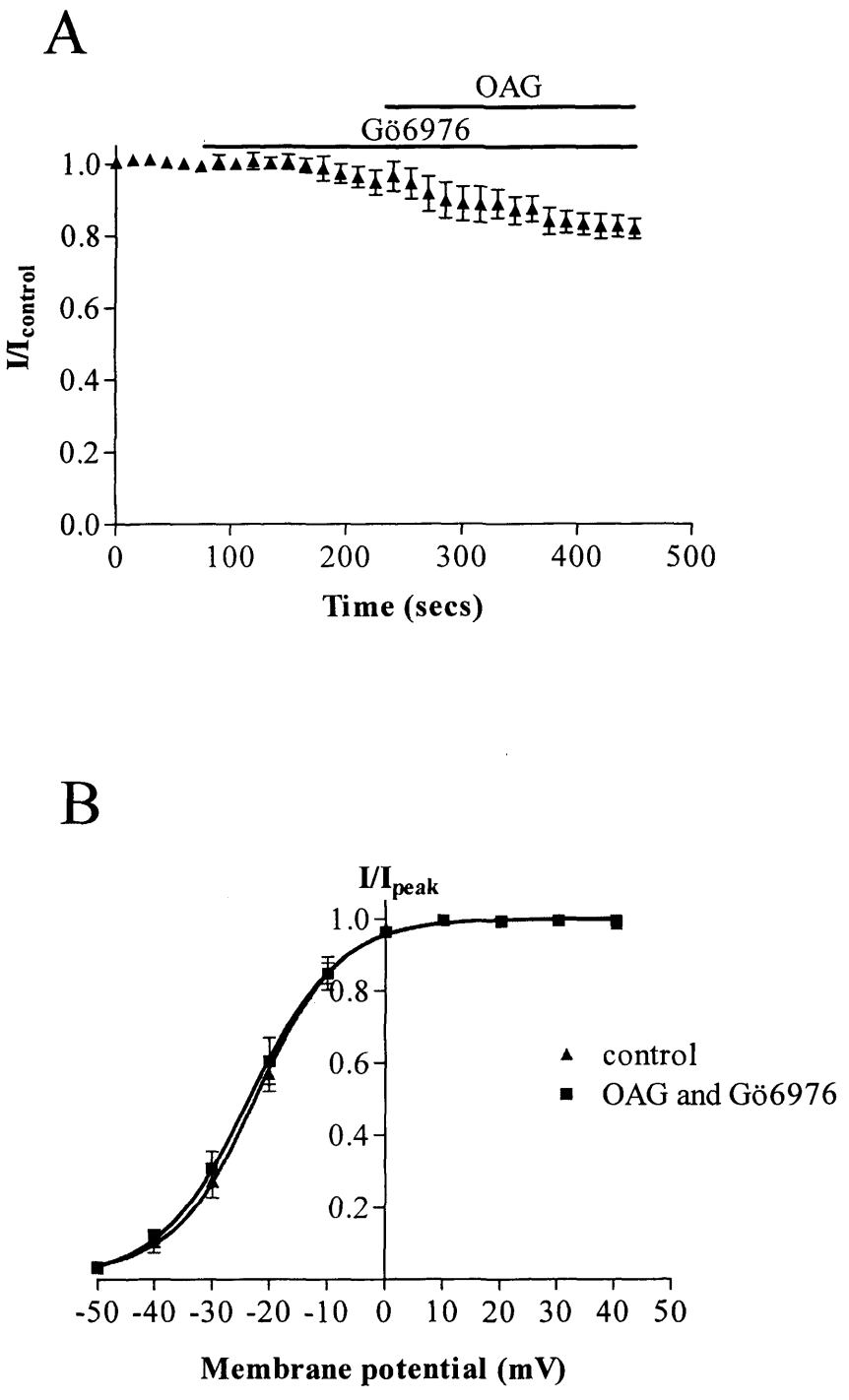

6.2.2.2 Over-expression of PKC isoforms

I was unable to identify an inhibitor specific for either the α or β isoforms of PKC, so was unable to distinguish pharmacologically which of these isoforms played a prominent role. Instead, a different approach was tried. If a specific isoform of PKC plays a prominent role in the modulation of current, over-expression of that isoform may cause an increased effect on the target protein. I over-expressed the α, β, δ and ε PKC isoforms individually in HERG-HEK cells to elucidate which of these kinase isoforms are important in the modulation of HERG current in response to OAG.

Figure 6.5 shows representative western blots from mock-transfected cells compared to cells transfected with α, β, δ or ε PKC cDNA. Transfection of cells caused a large increase in expression of the individual PKC isoform protein levels. The PKC isoforms were GFP-tagged, allowing easy identification of transfected cells when choosing individual cells for electrophysiology. The 'depolarisation to 0 mV' protocol was used to evoke currents. Application of 10 μM OAG to cells over-expressing α, β, δ or ε PKC isoforms caused an attenuation of current, to 58.73 ± 3.39%, 59.78 ± 3.51%, 67.54 ± 4.61% and 68.53 ± 1.78% of control respectively ($n \geq 5$ each data set, figure 6.6A). The OAG dependent attenuation of current in cells over-expressing PKCs α, β or δ was not significantly different to untransfected cells ($p>0.05$). OAG-mediated effects could be inhibited by a three minute pre-incubation of cells with 100 nM Gö6976 (figure 6.6A). The mean time constants for the effects of OAG were 348.02 ± 77.97 seconds, 299.31 ± 21.50 seconds, 335.14 ± 76.78 seconds and 342.42 ± 51.26 seconds respectively (data not shown). There was no significant difference between these values and that seen in untransfected cells ($p>0.05$). The $V_{0.5}$ of activation was shifted significantly by OAG by 5.41 ± 0.93 mV, 4.94 ± 1.03 mV, 4.39 ± 1.03 mV and 5.01 ± 0.29 mV respectively ($n \geq 5$ each data set, figure 6.6B). There was no significant difference between these shifts in transfected and untransfected cells ($p>0.05$). Current deactivation at –50 mV was significantly accelerated by OAG in cells over-expressing the α, β, δ and ε PKC isoforms ($p<0.05$, data not shown).

Although we have previously shown a role for the α and β isoforms of PKC, the data above suggests that over-expression of α or β PKC does not alter the response to OAG. Over-expression of PKC isoforms doesn not increase the response to a maximal concentration of OAG. However, the OAG concentration-response curve

Figure 6.5
Over-expression of PKC isoforms does not alter the response to 10μM OAG. Representative western blots probing for PKCα (Ai), β (Bi), δ(Ci) and ε (Di) in mock transfected HERG-HEK cells and HERG-HEK cells transfected with the appropriate PKC cDNA. Panel (ii) for each shows the same blot shown in panel (i), but stripped and re-probed for β-actin to ensure equal protein loading.

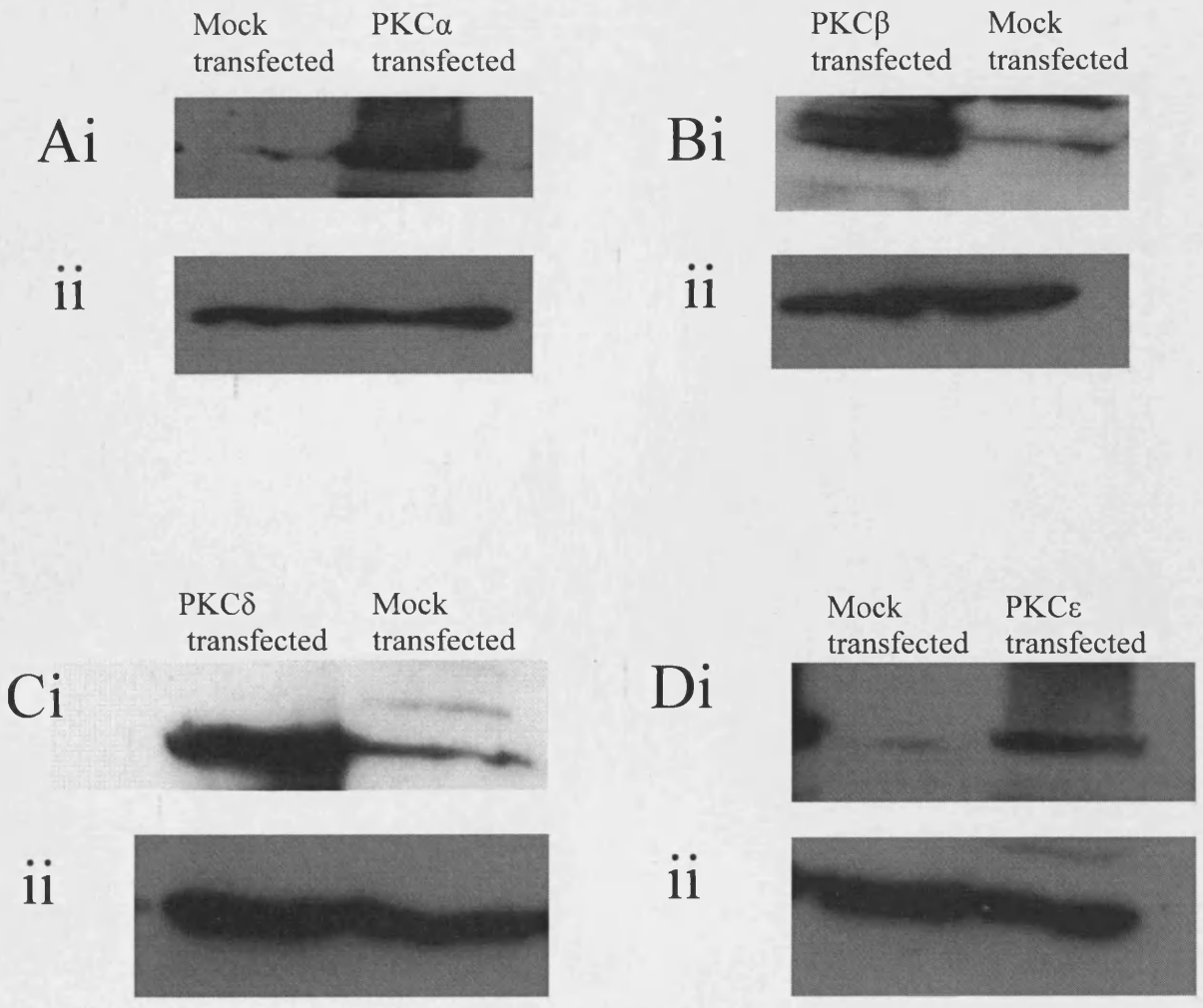

Figure 6.6
Over-expression of PKC isoforms does not alter the maximum attenuation of current by OAG, or the mean positive shift in the voltage dependence of activation in response to OAG **A** Mean, normalised tail currents remaining after 10 μM OAG application alone (solid bars) and with 100 nM Gö6976 and 10 μM OAG (shaded bars). n≥ 5 for each data set. The "mock" bar represents the mock experiments for each data set combined (n=14). **B** Mean shifts of voltage dependent activation with OAG in untransfected cells and those over expressing either PKCα β δ or ε (n≥ 5 for each data set). The bar colours correspond to those shown in panel A. The "mock" bar represents the mock experiments for each data set combined.

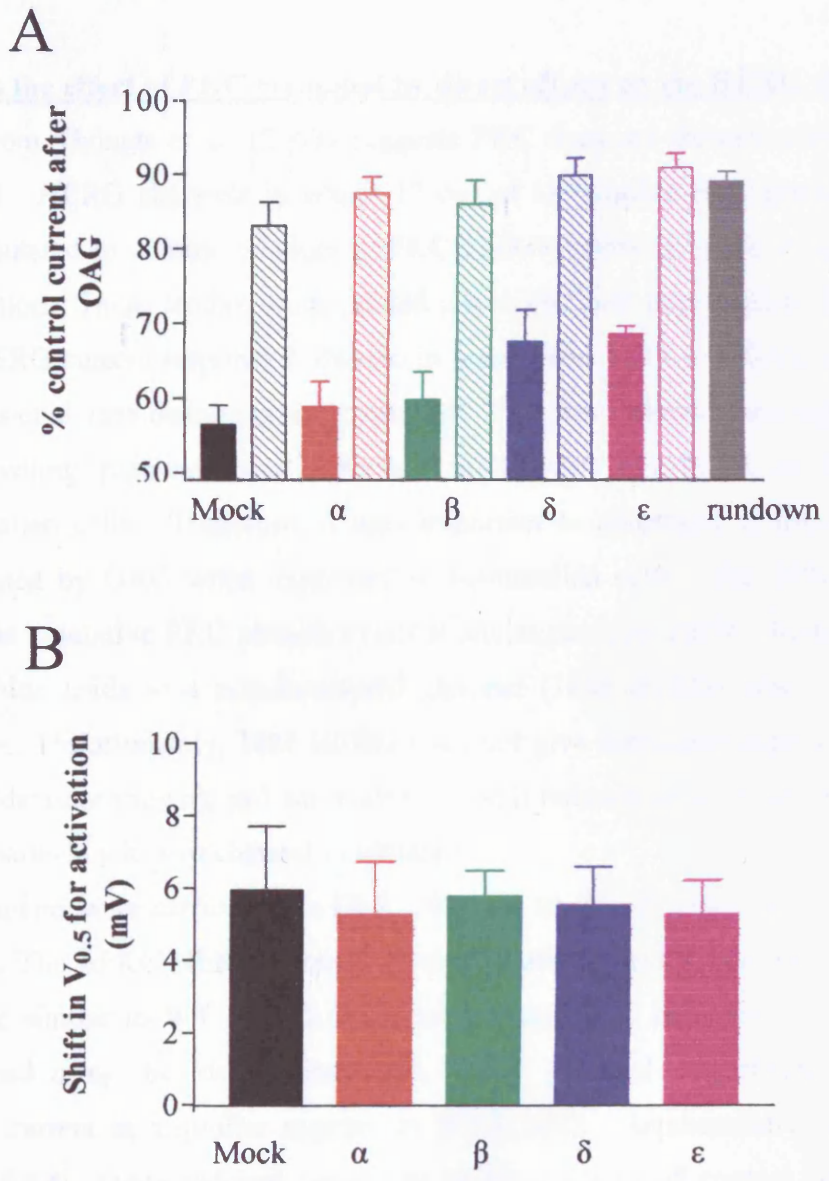

might be shifted to the left. To test for this I applied 1μM OAG, which is the IC_{50} concentration in untransfected HERG-HEK cells. In untransfected cells 1μM OAG attenuated currents to 82.16 ± 4.02% of control (n=5). In cells over-expressing PKCα, 1μM OAG caused a small attenuation of current, to 88.01 ± 1.34% of control (n=5), similar to untransfected cells ($p>0.05$). Application of 1 μM OAG to cells over-expressing PKCβ attenuated currents to 82.34 ± 3.46% of control (n=5), similar to untransfected cells ($p>0.05$). These results suggest over-expression of PKC α and β does not alter OAG-mediated modulation of the HERG (see figure 6.7).

6.2.3 Is the effect of PKC mediated by direct effects on the HERG channel?

Data from Thomas et al. (2003) suggests PKC does not directly phosphorylate the HERG channel. HERG channels in which 17 out of 18 putative PKC phosphorylation sites have been mutated to alanine residues (ΔPKC HERG) continue to be modulated by acute PMA application. These studies were carried out in channels expressed in *Xenopus* oocytes. The WT HERG current response I observe in response to PMA and OAG is rather different from Thomas et al. (see discussion in chapter 5). This may indicate there are important differences in signalling pathways and therefore modulation of HERG in *Xenopus* oocytes and mammalian cells. Therefore, it was important to determine if the ΔPKC mutant can be modulated by OAG when expressed in mammalian cells. The ΔPKC HERG mutant still contains a putative PKC phosphorylation site at position Thr74. Mutation of this residue to an alanine leads to a non-functional channel (18M HERG) when expressed in *Xenopus* oocytes. Unfortunately, 18M HERG does not give functional expression in HEK 293 cells either (data not shown), so I am unable to test if removal of all putative PKC phosphorylation sites results in a loss of channel modulation.

Experiments were carried out in HEK 293 cells transiently transfected with the ΔPKC HERG mutant. The ΔPKC HERG currents have activation, inactivation and deactivation properties that are similar to WT HERG (data not shown). The response to 10 μM OAG was first examined using the 'depolarisation to 0 mV' protocol. Application of OAG attenuated ΔPKC current in a similar manner to WT HERG. Representative currents are shown in figure 6.8A. OAG reduced current to 66.57 ± 3.91% of control with a time constant of 289.41 ± 42.63 seconds (n=7,

Figure 6.7
Over expression of PKC α or β does not alter the attenuation of current or acceleration of deactivation by 1μM OAG. **A** Mean, normalised tail current remaining after application of 1μM OAG in mock transfected cells and those transfected with either PKC α or β. The mock transfected data is mock experiments for each data set combined. **B** Percentage acceleration of slow (i) and fast (ii) deactivation time constants in response to 1μM OAG in untransfected cells and those transfected with either PKC α or β. The mock transfected data is mock experiments for each data set combined to form one data set.

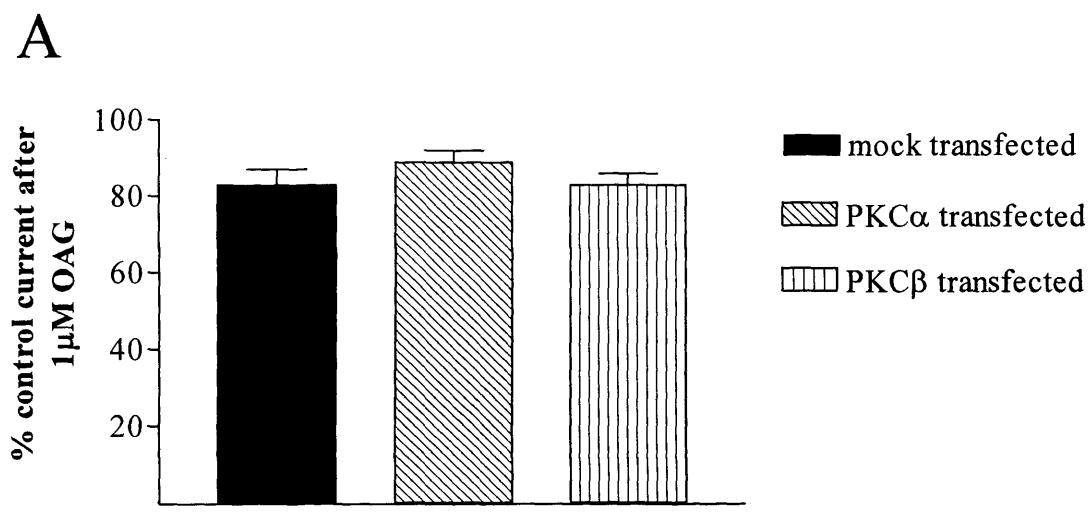

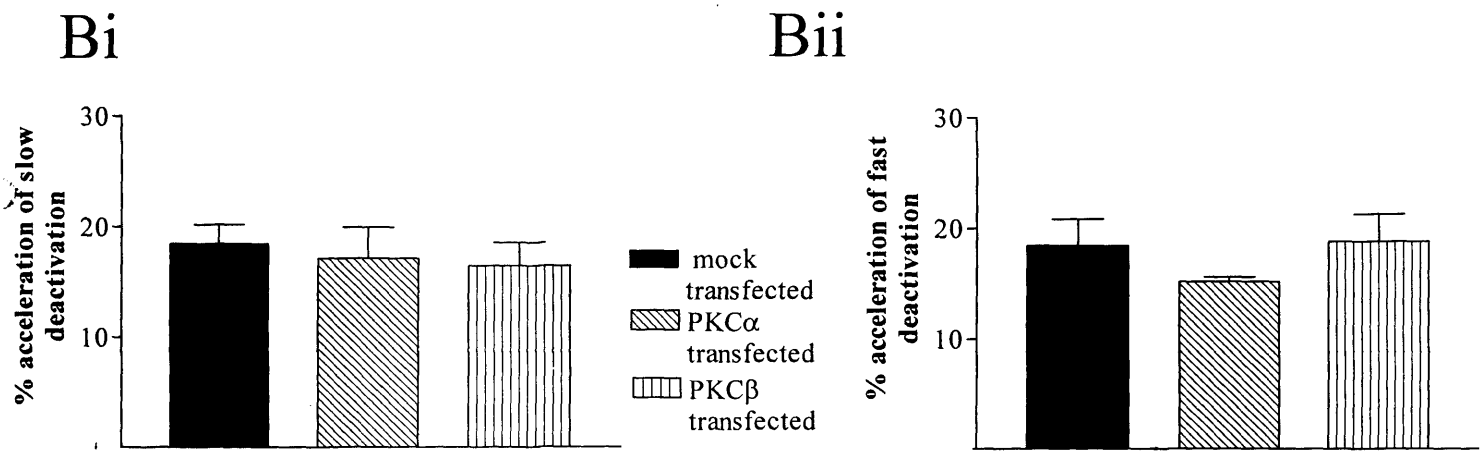

Figure 6.8
OAG modulation of current remains in the absence of putative PKC phosphorylation sites. A Representative ΔPKC HERG currents in control conditions and with 10 μM OAG. **B** Time course of the effects of 10 μM OAG on ΔPKC HERG (n=7). Peak tail currents were normalised to control amplitudes and mean, normalised currents were plotted against time. **C** Mean activation curves in control conditions and with OAG (n=5).

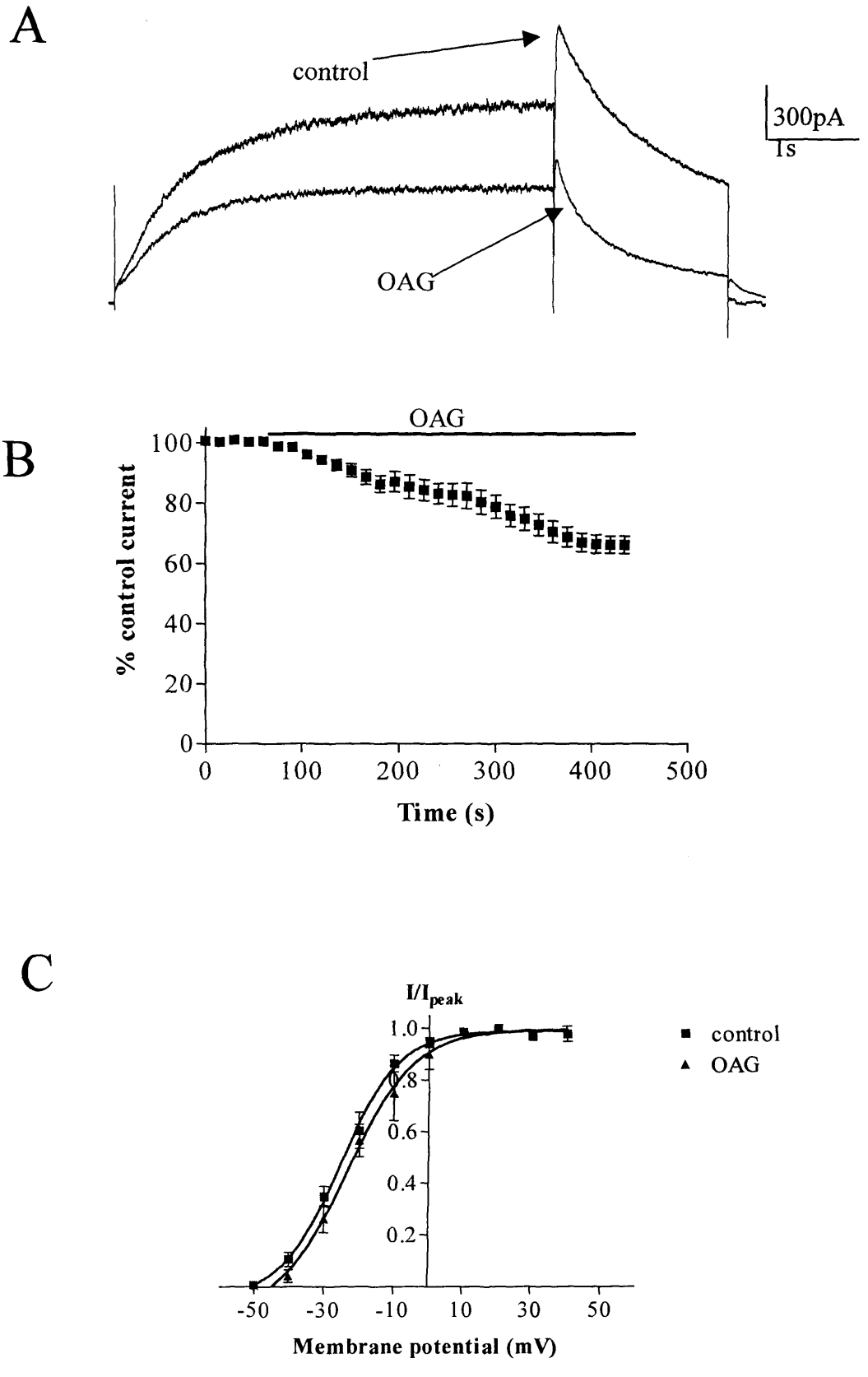

figure 6.8B). Thus, attenuation of ΔPKC HERG currents were not significantly different from WT HERG ($p<0.05$). Like WT HERG, deactivation of ΔPKC at –50 mV was significantly accelerated. The slow and fast time constants were 1646.03 ± 41.00 ms and 276.94 ± 3.62 ms in control conditions, compared to 1092.32 ± 57.87 ms and 165.02 ± 12.66 ms in the presence of OAG (n=7, data not shown). The $V_{0.5}$ of voltage-dependent activation was shifted by 2.21 ± 0.46 mV in the presence of OAG (n=5, $p>0.05$), but this was not significantly different than the shift seen in WT channels (figure 6.8C). The effects of OAG were mediated by PKC since they were blocked in cells chronically treated with 1 μM PMA. After a six-minute application of 10 μM OAG to these cells, currents were 94.25 ± 1.91% of control (n=5, figure 6.9A and B).

6.2.4 Are OAG effects mediated by PKA phosphorylation sites?

To further examine if the effect of OAG was PKC-specific, I used a mutant of the HERG channel that contains point mutations to alanine at the four putative PKA phosphorylation sites on the HERG channel, thus removing PKA modulation of the current. Applying 40 μM forskolin to WT HERG channels caused an attenuation of current as previously described (chapter 5), to 63.21 ± 1.32% of control. However, this modulation was significantly reduced in 4M HERG channels transiently expressed in HEK cells. After a four-minute application of forskolin, 4M HERG current was 89.91 ± 3.91% of control (n=5, figure 6.10A). The mean time course of the effects of forskolin on peak tail current of WT channels and 4M channels is shown in figure 6.10B. This data shows the 4M HERG mutant is not sensitive to PKA, and I could therefore use the 4M HERG channel as a tool to test if the effects of OAG are mediated through the PKA phosphorylation sites on HERG.

The 'depolarisation to 0 mV' protocol was used to assess the effects of OAG. Application of 10 μM OAG to 4M HERG currents attenuated current, and once steady state was reached, currents were 61.45 ± 2.91% of control (n=5, figures 6.11A and B), similar to OAG effects on WT channels ($p>0.05$). From these data, I can conclude that OAG is not modulating HERG channel current by phosphorylation at the four putative PKA phosphorylation sites on HERG.

These data suggests the modulation of the HERG channel currents that are observed in response to application of OAG are independent of the putative PKC phosphorylation sites

Figure 6.9
The effects of OAG on ΔPKC HERG channel currents can be abolished with chronic treatment of cells with PMA. **A** Representative ΔPKC HERG currents in control conditions and with 10 μM OAG. **B** Time course of 10 μM OAG effects on HERG currents (n=5). Peak tail currents were normalised to control amplitudes and mean, normalised currents were plotted against time.

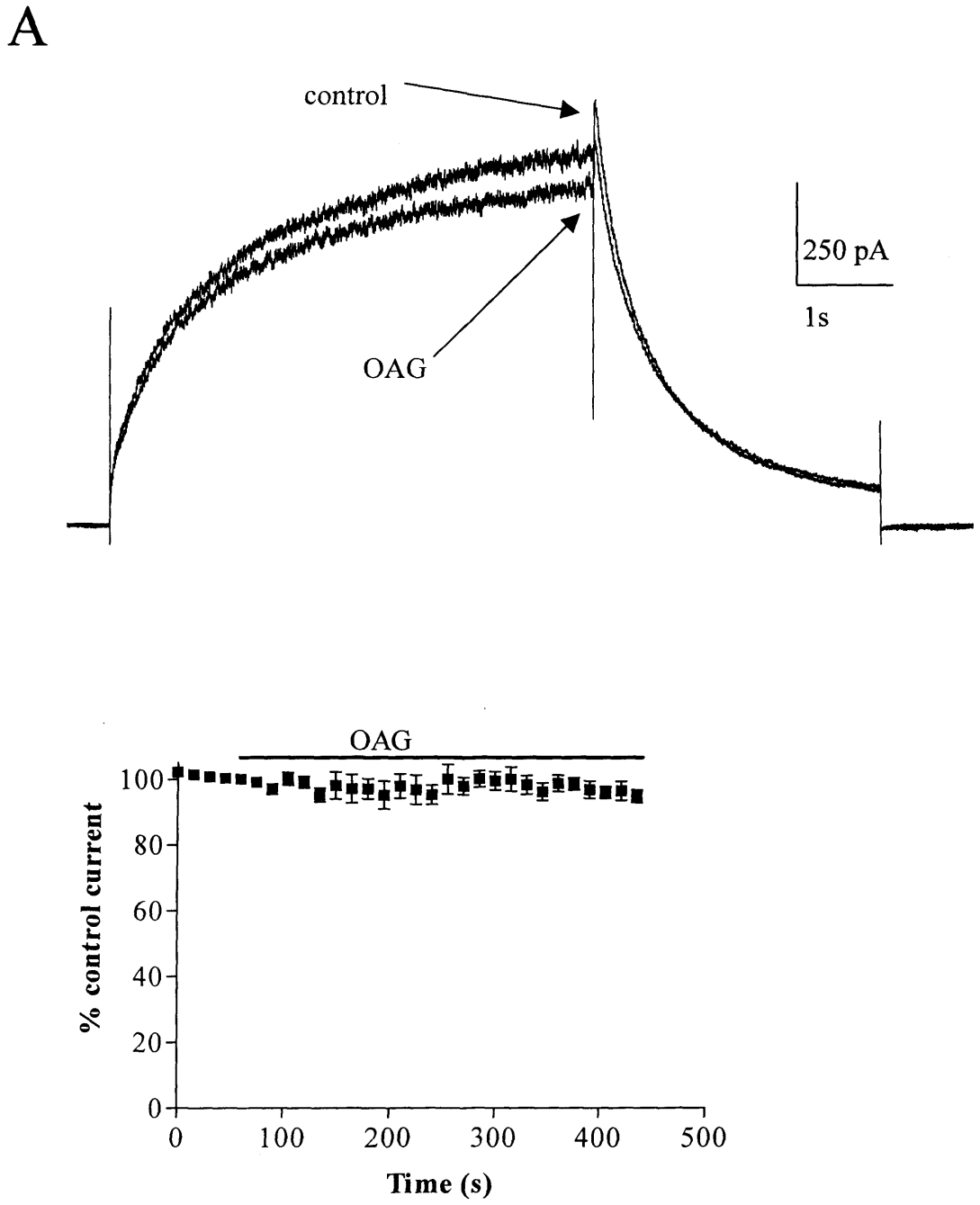

Figure 6.10
Forskolin attenuation of current is abolished in the 4M HERG mutant. **A** Representative 4M HERG currents in control conditions and with 40 μM forskolin. **B** Time-course of 40 μM forskolin effects on WT HERG and 4M HERG currents. Peak tail currents were normalised to control amplitudes and mean, normalised currents were plotted against time. n=5 for each data set.

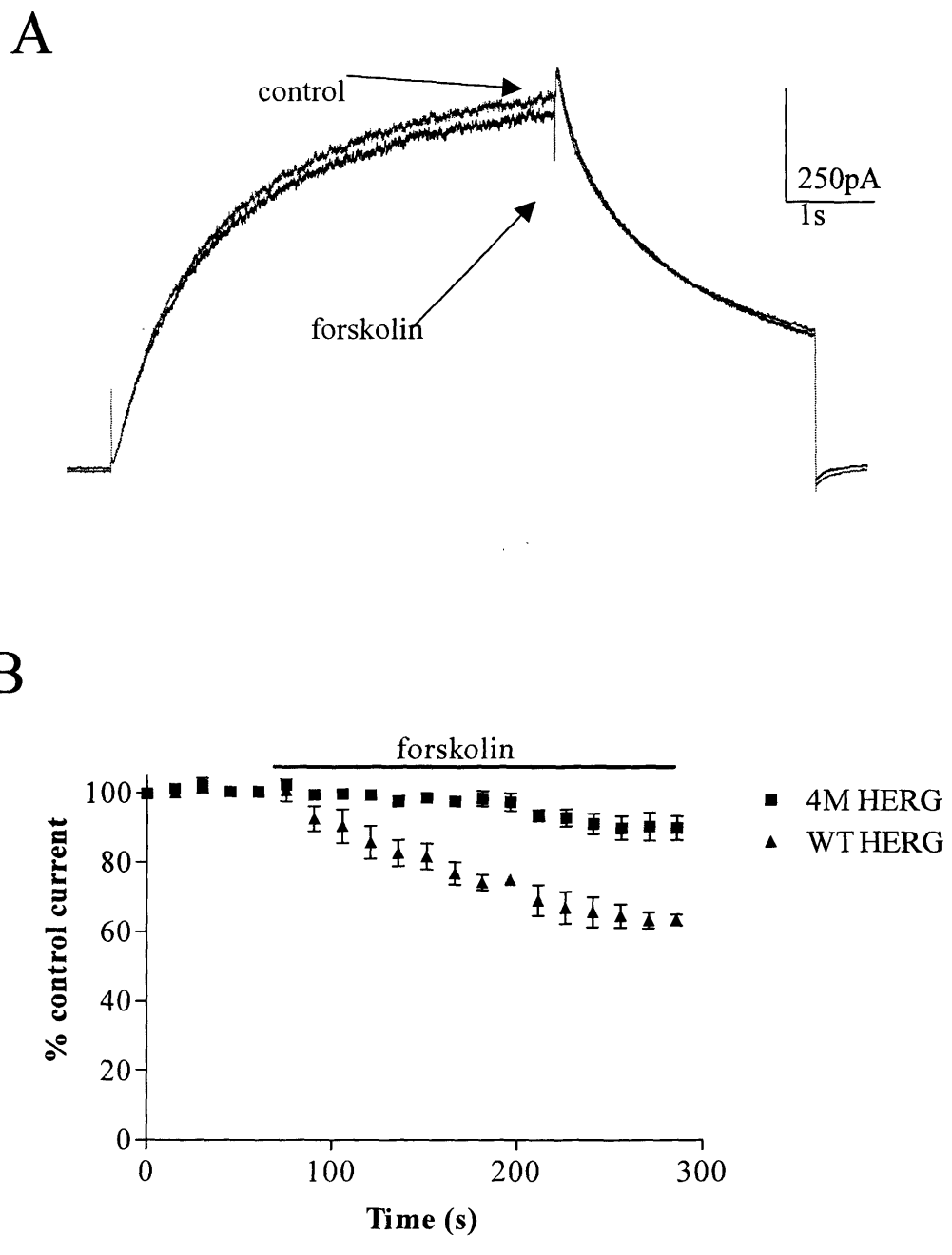

Figure 6.11
The effects of OAG are not mediated by the PKA phosphorylation sites on the HERG channel. **A** Representative 4M HERG currents in control conditions and with 10 μM OAG. **B** Time course of 10 μM OAG effects on 4M HERG (n=5). Peak tail currents were normalised to control amplitudes and mean, normalised current was plotted against time.

A

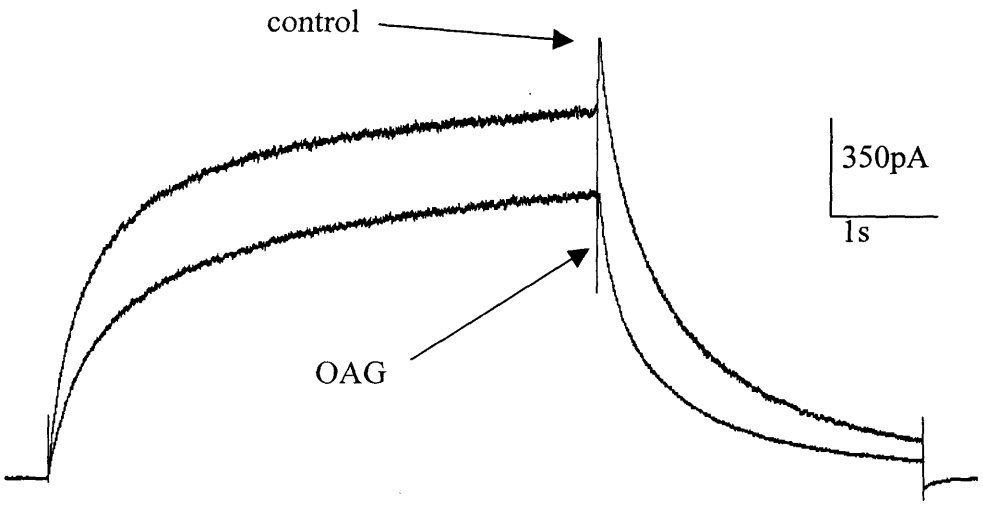

B

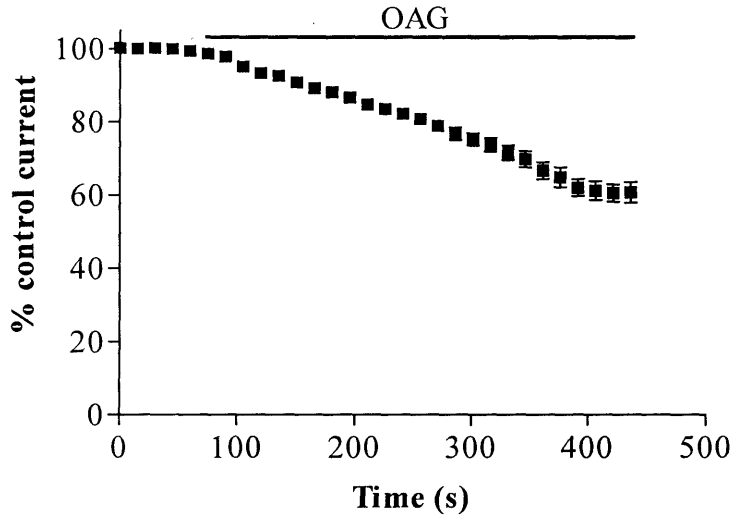

found at positions Ser26, Thr162, Thr174, Thr179, Ser250, Ser278, Ser354, Thr371, Thr526, Ser606, Ser636, Thr670, Ser890, Thr895, Ser918, S960 and Thr1133. The potential alternative mechanisms for modulation of the channel by PKC will be outlined in the discussion.

6.3 Discussion

In this chapter I have shown HERG current is modulated by the DAG analogue OAG. HERG current is significantly attenuated, the voltage dependence of activation is significantly shifted to more positive potentials and deactivation is significantly accelerated. The relative proportions of fast and slow deactivation were not measured in this study, and it is entirely plausible that PKC activation may alter the proportion of fast and slow deactivation in addition to accelerating the rate of both τ values. Inactivation of current is not affected with PKC stimulation. Barros et al. (1998), Gómez-Varela et al. (2003) and Thomas et al. (2003) showed the HERG current expressed in *Xenopus* oocytes to be modulated by PKC, causing an attenuation of current, positive shift of voltage dependent activation and acceleration of deactivation. However, in anterior pituitary GH_3 cells (Schledermann et al., 2001) and the tsA-201 cell line (Hirdes et al., 2004), HERG current was attenuated by activation of the $G_{q/11}$-pathway apparently independently of PKC. In guinea pig ventricular myocytes I_{Kr} was augmuented by a PKC-dependent mechanism by an attenuation of inactivation (Heath and Terrar, 2001). Differences between these studies may reflect differences in signal transduction between these expression systems, and possibly differences in expression of HERG β subunits (discussed in chapters 4 and 5). In this study, I investigated modulation of the HERG channel expressed HEK cells, to overcome the problems of recording I_{Kr} in guinea pig myocytes, yet still measure HERG current in a mammalian environment.

Since OAG does not alter cytosolic calcium concentrations, and OAG-mediated modulation of current produced similar effects to methacholine and ionomycin-mediated modulation (as shown in chapter 5), this suggests the calcium increases caused by both methacholine and ionomycin do not in themselves alter HERG current. Modulation by OAG in my study was abolished when the α, β, δ and ε isoforms of PKC were down regulated using chronic PMA treatment. Using the PKCα and βI-specific inhibitor Gö6976, I showed HERG current to be modulated, at least in part by the α and βI isoforms of PKC. I was unable to assess if the βII isoform contributes to the modulation due to a lack of isoform-specific inhibitors. This data concurs both with data from Thomas et al. (2003), who showed the conventional PKC isoform activator thymeleatoxin to mimic the effect of PMA, and my data shown in chapter

5, showing the modulatory effect of ionomycin is likely to be due to calcium-sensitive isoforms of PKC (α and/or β).

The modulatory effects of OAG were independent of 17 putative PKC phosphorylation sites on the HERG channel. This is in agreement with work carried out in *Xenopus* oocytes by Thomas et al. (2003), who showed activation of PKC using PMA continued to modulate ΔPKC HERG currents in a similar manner to WT currents. There may be several mechanisms causing the continued modulation of current in this mutant channel. 1) The ΔPKC HERG channel has one remaining putative PKC site, Thr74. It was found that mutation of this site led to a non-functional mutant, suggesting this site on the N-terminus is functionally important. This remaining site may mediate all the PKC-dependent modulation of the channel. Future studies are aimed at testing this hypothesis. 2) The modulation of the HERG channel may continue due to the presence of atypical PKC phosphorylation sites on the channel that have not been identified. 3) Another potential explanation is cross-talk between signalling pathways. Thomas et al. (2003) showed the effect of PMA could be partially attenuated by a PKA inhibitor, and Heath and Terrar (2000) showed the effects of forskolin and isoprenaline, which both activate PKA, could be inhibited using a PKC inhibitor. However, my results with the 4M HERG channel, indicate the effects of OAG are not mediated through PKA phosphorylation sites. 4) Modulation of the HERG channel may be by direct phosphorylation of an auxillary subunit. This will be addressed in chapter 7 of this thesis. 5) Modulation of the ΔPKC HERG channel may not due to direct effects of PKC, but through a further signalling cascade, such as activation of the MAP kinase pathway (reviewed in Luttrell, 2002). Further experiments are required to dissect the mechanism of PKC-dependent modulation of the HERG channel. These experiments could include inhibition of potential signalling pathways down stream of PKC, to observe if this abolishes OAG-mediated modulation of current. The role of Thr74 could be tested by mutation to a residue other than an alanine. This would allow me to investigate the potential role of the Thr74 residue in the modulation of current.

Although I have shown the modulation of HERG is likely to be at least partially PKCα and/or βI dependent, over-expression of these isoforms did not alter modulation of HERG by OAG. This could be due to a number of possibilities. 1) The amount of PKC expressed in the cell under basal conditions may already be sufficient to produce a maximal effect on the HERG

channel. 2) Based on the hypothesis that PKC activation does not modulate the channel directly, but rather activates another signalling molecule which then goes on to directly modulate HERG channel current, the same principle can be applied. If endogenous PKC levels are adequate to maximally activate a down stream signalling pathway, increasing the protein expression of PKC will not affect modulation of the HERG channel. 3) The GFP-tagged PKC isoform constructs that were over-expressed were not biologically active. However, these constructs have previously been shown to be biologically active in HEK 293 cells, and translocate in response to stimulus when over expressed (Babwah et al., 2003). 4) Exogenous PKC isoforms are not in the same location as HERG or can not compete with endogenous kinases.

I observed less attenuation of current with OAG in cells over-expressing PKCs δ and ε compared to mock transfected cells. It is likely OAG would preferentially activate over-expressed isoforms due to an excess of protein, and therefore OAG application to cells over expressing PKC δ or ε would activate PKCα and β to a lesser extent compared to untransfected cells. If PKCα and/or β do modulate HERG, this would lead to an effect similar to using a lower concentration of OAG in untransfected cells, as I observe. Further experiments, including co-immunoprecipitation studies after OAG application, might elucidate which isoforms interact with HERG to cause its modulation.

As I have been unable to map the site of PKC phosphorylation on the HERG channel, I can only speculate to how PKC activation modulates HERG channel activity. PKC activation significantly accelerates deactivation kinetics, which may suggest the possibility that PKC-mediated phosphorylation hinders access of the N-terminal to the intracellular side of the pore, thus reducing the slowing of deactivation. Indeed, the Thr74 residue is close to the PAS domain of HERG (Morais-Cabral et al., 1998b), a motif that can mediate protein-protein interactions (Anantharaman et al., 2001). Alternatively, phosphorylation in the region where the N-terminal binds to the intracellular side of the pore may also hinder N-terminal slowing of deactivation. Allosteric effects of phosphorylation at the N- or C-termini could alter voltage sensitivity, or phosphorylation near the voltage-sensing domain of the channel could change the intracellular environment around the voltage sensor. A recent study showed PKC-mediated effects on HERG current were abolished when the proximal domain of the N-terminus (residues 138-373) was deleted (Gómez-Varela et al., 2003). This study further

narrowed this to a region between residues 325-346 that was essential for PKC-mediated positive shift of voltage dependent activation. Deletion of residues 223-373 partially removed PKC-mediated acceleration of deactivation, therefore suggesting the effects may be independent. In the region between residues 223-373 there are four putative PKC and five putative casein kinase II sites of phosphorylation. Although the PKC sites do not seem relevant, the contribution of casein kinase II sites has not been investigated.

Chapter 7 results

Phosphorylation of HERG channel subunits

7.1 Introduction

Results in this body of work, and work of others (Thomas et al., 1999; Barros et al., 1999; Thomas et al 2003) strongly suggests protein kinases modulate HERG channel activity. However, none of these studies have directly measured the phosphorylation of the HERG channel by these kinases. As a result, questions remain about the mechanism of this modulation. A study carried out by Thomas et al. (2003) showed the HERG channel expressed in *Xenopus* oocytes to be modulated by the phorbol ester and PKC activator, PMA. This modulation continued when PMA was applied to the ΔPKC HERG mutant, a channel mutant containing point mutations at 17 of the 18 putative PKC phosphorylation sites on the HERG channel. These point mutations from serine or threonine residues to alanine residues meant the channel could no longer be phosphorylated at these sites. Mutation of the 18th site (Thr74) resulted in no functional expression. This left several possibilities: 1) PKC may be phosphorylating the HERG channel at Thr74. 2) PKC may be phosphorylating the channel at atypical PKC phosphorylation sites. 3) Stimulation of PKC activates a further signalling pathway that may phosphorylate the HERG channel at different (non-PKC) sites. 4) Modulation of HERG occurs via phosphorylation of an auxillary subunit.

Zhang et al. (2002) showed that HERG expressed in *Xenopus* oocytes was phosphorylated under basal conditions, but they were unable to detect a change in phosphorylation in response to application of PMA or forskolin. However, as outlined in the previous chapter, modulation of HERG in mammalian cells shows some important differences from modulation in *Xenopus* oocytes, raising the possibility that there are important mechanistic differences in how HERG channels are modulated in mammalian compared to amphibian cell types.

In this study I sought to determine if HERG subunits are directly phosphorylated in mammalian cells by PKA and PKC. Changes in HERG phosphorylation in response to ionomycin, OAG and forskolin were investigated.

Previous studies have shown that mutation of the putative PKA phosphorylation sites in HERG attenuates the modulatory effects of forskolin and phosphodiesterase inhibitors. Thus,

an increase of phosphorylation of HERG channels in response to forskolin would be expected, but has never been shown. I initially intended to use forskolin as a positive control to test for an increase in phosphorylation of the cells. As a further positive control, I also looked at phosphorylation of muscarinic M_3 receptors in HEK-m3 cells, as it is well documented that this receptor is phosphorylated upon PKC activation (Tobin and Nahorski, 1993; Willars et al., 1999). To investigate PKC-dependent phosphorylation of the HERG channel, I applied ionomycin or OAG.

7.2 Results

7.2.1 Measuring basal phosphorylation of the HERG channel

Initially, I wanted to observe if the HERG channel expressed in HEK 293 cells is phosphorylated under basal conditions. Figure 7.1 shows an autoradiograph from a phosphorylation assay on untransfected HEK cells and HERG-expressing HEK cells. Approximately equal antibody levels were detected in each lane, measured by observing staining with Coomassie blue. In the autoradiograph no bands were present in untransfected HEK cell lanes, indicating no phospho-proteins were precipitated by the anti-HERG antibody. In the HERG-HEK cell lanes, two bands are visible in each lane. These ran at approximately 135 and 155 kDa, the molecular weights reported previously for the immature, core glycosylated, and mature, fully glycosylated forms of HERG respectively (Zhou et al.,1998). The presence of these two bands shows both the immature form (located in the endoplasmic reticulum) and the mature form (found on the cell surface) are phosphorylated under basal conditions. This suggests the HERG channel protein is phosphorylated early during processing of the protein. This phosphorylation could be due to a number of intracellular proteins. The HERG channel shows putative phosphorylation sites for PKC, PKA, tyrosine kinase and casein kinase II, (Figure 1.11), and the putative phosphorylation sites on the HERG channel total around 44 individual sites. The high basal phosphorylation of the channel suggests there are a number of sites at which phosphate turnover occurred during the one hour incubation with ^{32}P.

7.2.2 Activation of PKC

7.2.2.1 Activation of PKC increases phosphorylation of the muscarinic m3 receptor

I wanted to use a positive control to ensure we could measure a PKC-mediated change in phosphorylation. It is well documented that PKC activation causes an increase in the phosphorylation of the muscarinic M_3 receptor (Tobin and Nahorski, 1993; Willars et al., 1999). I applied 10 μM OAG to HEK-m3 cells to activate PKC. I then used an anti-M_3 antibody to immunoprecipitate the muscarinic M_3 receptor. Phosphorylation of the muscarinic M_3 receptor was significantly increased by 90.65 ± 4.83% ($n=3$, $p<0.05$) (data not shown). This control shows a change in phosphorylation of a cellular protein can be detected using this methodology.

Figure 7.1
Basal phosphorylation of HERG expressed in unstimulated HEK293 cells. Lanes A and B from untransfected HEK cells. Lanes C and D from HERG-HEK cells. Equal quantities of antobody were loaded in each lane. The autoradiograph was exposed for 16 hours.

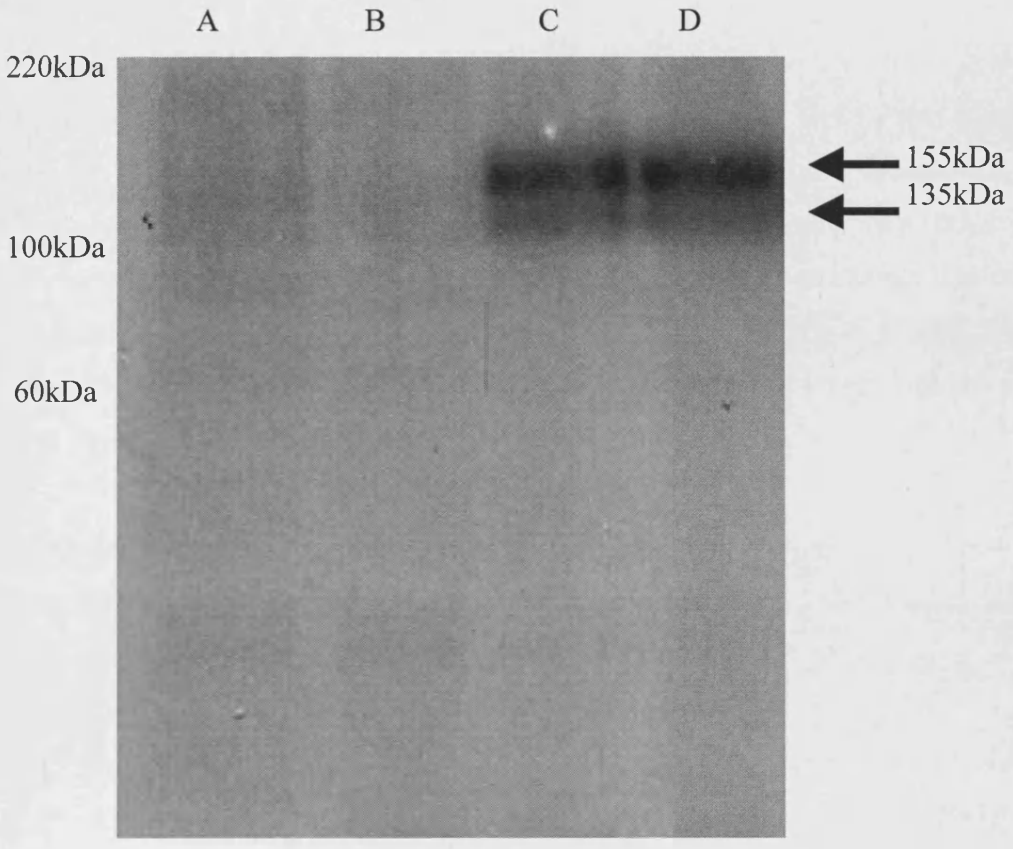

Figure 7.1
Basal phosphorylation of HERG expressed in unstimulated HEK293 cells. Lanes A and B from untransfected HEK cells. Lanes C and D from HERG-HEK cells. Equal quantities of antobody were loaded in each lane. The autoradiograph was exposed for 16 hours.

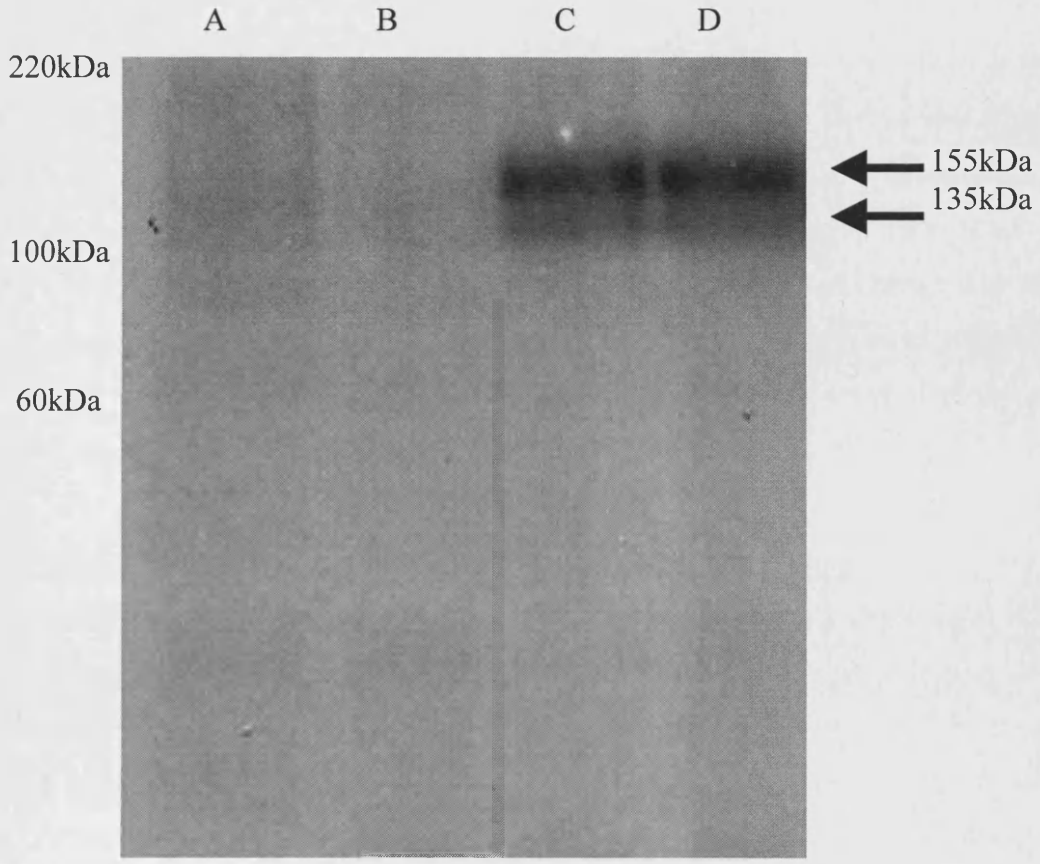

7.2.2.2 Activation of PKC increases phosphorylation of HERG subunits

Application of OAG attenuates HERG current via a PKC-dependent mechanism. I investigated if the effects that I observe in electrophysiological experiments were due to a change in the phosphorylation state of the HERG channel subunits. Following incubation in ^{32}P-labelled phosphate free Krebs for 1 hour, 10 μM OAG was added and the cells were incubated for a further 5 minutes. This time period was chosen as it represents approximately the time period that OAG showed its maximal effects during the electrophysiological experiments. Figure 7.2A shows a typical autoradiograph comparing ^{32}P labelling in control and OAG treated cells. In the presence of OAG, phosphorylation of both the immature and mature forms of the HERG channel increased to a similar extent. The density of signal of both lanes was measured and a percentage change in signal intensity calculated. In six independent experiments, the phosphorylation of HERG increased each time, with a significant mean change of 18.08 ± 1.74% ($p=0.005$). The percentage change was relatively small. I cannot tell if this is because phosphorylation is occurring in a relatively small population of channels, or whether the change of phosphorylation per subunit is small, particularly in comparison to the high level of basal phosphorylation.

7.2.2.3 Inhibition of the OAG-mediated increase in phosphorylation

To confirm that the increase in phosphorylation in response to OAG application was PKC-dependent I used the two approaches described in the last chapter; inhibition by bis-1 and PKC down-regulation with chronic PMA application.

Cells were incubated in 3 μM bis-1 for 15 minutes prior to application of 10 μM OAG. Figure 7.2B shows a typical autoradiograph from these experiments. Application of bis-1 alone did not alter phosphorylation relative to levels in untreated cells, suggesting that PKC does not contribute to HERG channel basal phosphorylation. Bis-1 abolished the effects of OAG. In three experiments bis-1 and OAG resulted in a 2.33 ± 1.27% decrease of phosphorylation, which was not significantly different from control cells ($p<0.05$).

In addition to using 3 μM bis-1, which may not be selective for PKC and blocks HERG, I down regulated PKC isoforms by incubating cells in PMA for 24 hours. I found expression of the α, β, δ and ε isoforms of PKC to be down regulated by PMA, but 4αPMA, the inactive analogue of PMA, had no effects. A typical

Figure 7.2

OAG application increases phosphorylation of the HERG protein. The OAG response can be abolished by PKC inhibitors or PKC down regulation. **A** Representative autoradiograph showing HERG phosphorylation following incubation with or without 10 μM OAG. Equal antibody loading was shown between lanes. **B** Typical autoradiograph showing the effects of 3 μM bis-1 and 10 μM OAG on the phosphorylation state of the channel. A 15 minute incubation with 3 μM bis-1 did not alter phosphorylation of untreated cells and prevented increase of phosphorylation by 10 μM OAG. **C** Representative autoradiograph showing chronic PMA (1 μM) also prevented the increase of phosphorylation by 10 μM OAG.

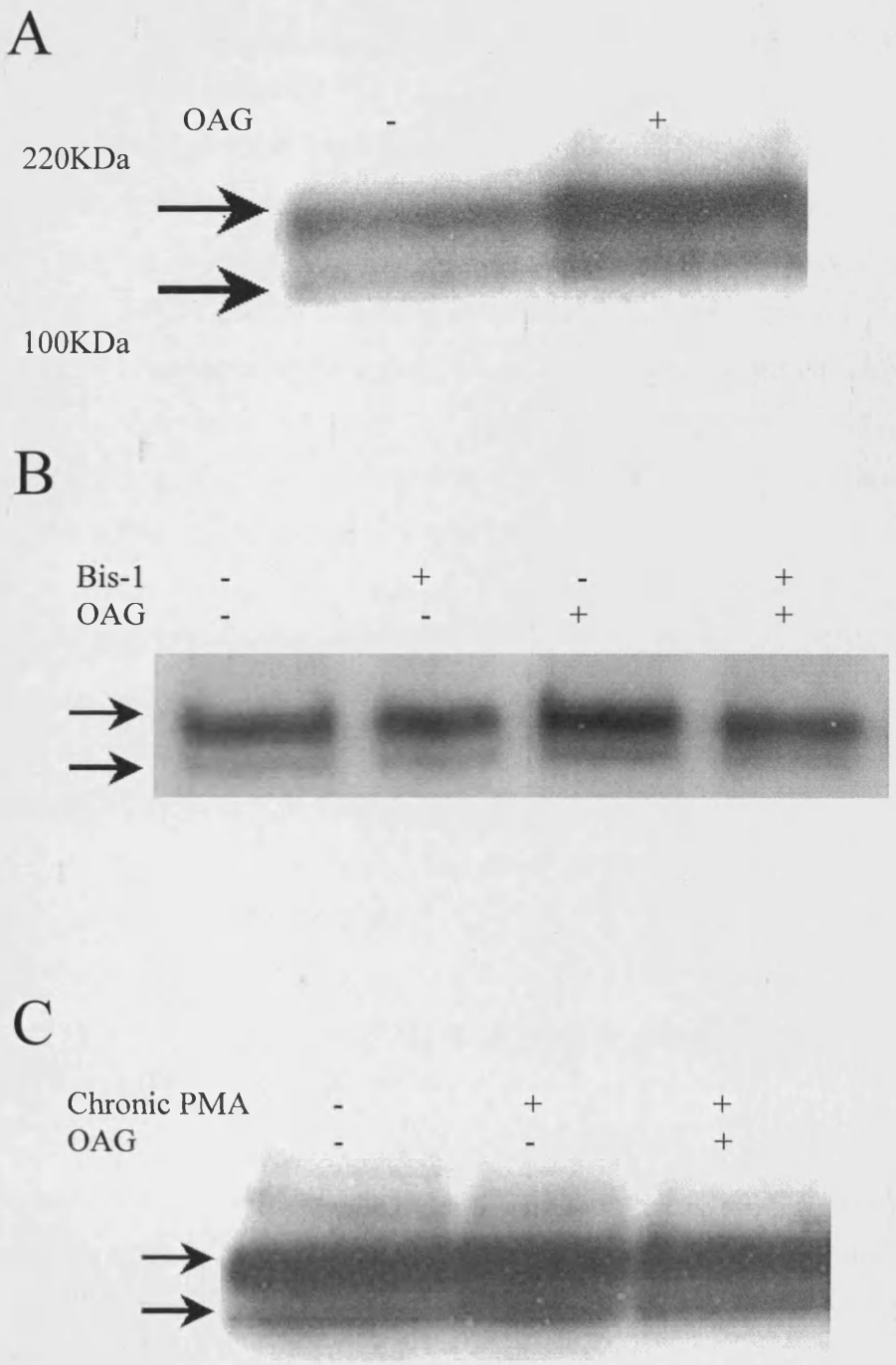

autoradiograph from these experiments is shown in figure 7.2C. Chronic PMA treatment did not effect the amount of HERG phosphorylation compared to non-PMA treated cells, suggesting the α, β, δ and ε isoforms of PKC do not contribute to the basal phosphorylation of the HERG channel or influence channel expression. Application of OAG failed to significantly increase phosphorylation. The change was +1.02 ± 2.70% (n=3, $p>0.05$).

7.2.2.4 The effects of OAG are PKA-phosphorylation site independent

Thomas et al. (2003) showed PMA-modulation of HERG current in *Xenopus* oocytes was partially inhibited by PKA inhibitors. In contrast, I have shown OAG effects on HERG current to be independent of putative PKA phosphorylation sites. To test if the OAG-mediated increase in phosphorylation was independent of PKA I used the 4M HERG mutant that lacks the four putative PKA phosphorylation sites. Application of OAG resulted in a 17.81 ± 2.26% increase in phosphorylation ($p<0.05$, n=3), which was abolished in cells chronically treated with 1 μM PMA to down regulate PKC (figure 7.3A). The results on 4M HERG were not significantly different from WT HERG, and suggest the effects of OAG are independent of PKA phosphorylation sites on HERG.

In summary, I have been able to show phosphorylation of the WT HERG channel to increase in response to OAG in a PKC-dependent manner. The increase of phosphorylation could be abolished by the PKC inhibitor bis-1, or down-regulation of PMA sensitive isoforms of PKC. This strongly suggests that HERG channels are directly phosphorylated in response to stimulation of PKC. We have shown this phosphorylation to be independent of the four PKA phosphorylation sites on the channel.

7.2.3 Does rapid dephosphorylation contribute to small changes in phosphorylation in response to OAG?

Protein phosphorylation can be enhanced by applying phosphatase inhibitors to block dephosphorylation. To test if rapid dephosphorylation was contributing to the small change of phosphorylation, I used a phosphatase inhibitor cocktail, containing cantharidin, an inhibitor of protein phosphatase 2A (PP-2A), bromotetramisole, an inhibitor of alkaline phosphatases, and microcystin LB, an

Figure 7.3
OAG stimulation of PKC continues to cause an increase in phosphorylation in the absence of putative PKA phosphorylation sites. A Representative autoradiograph showing 4M HERG phosphorylation in response to 10 μM OAG with and without chronic PMA treatment. Phosphorylation of 4M HERG increased in response to 10 μM OAG, but this was blocked by chronic PMA treatment **B** Mean results from densitomtry analyses of autoradiographs ($n \geq 3$ for each data set). * shows significance at $p<0.05$ comapred to OAG treatements alone.

A

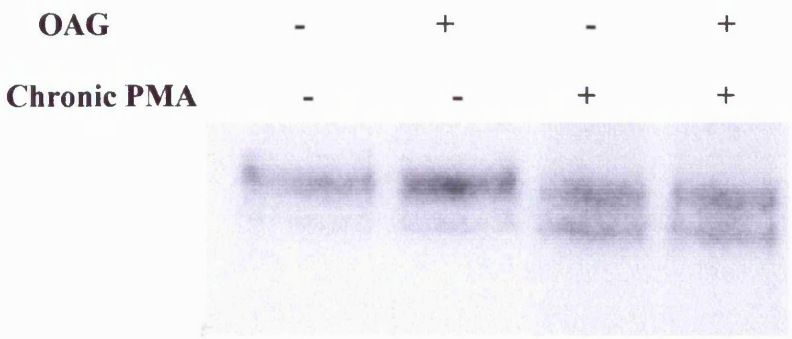

B

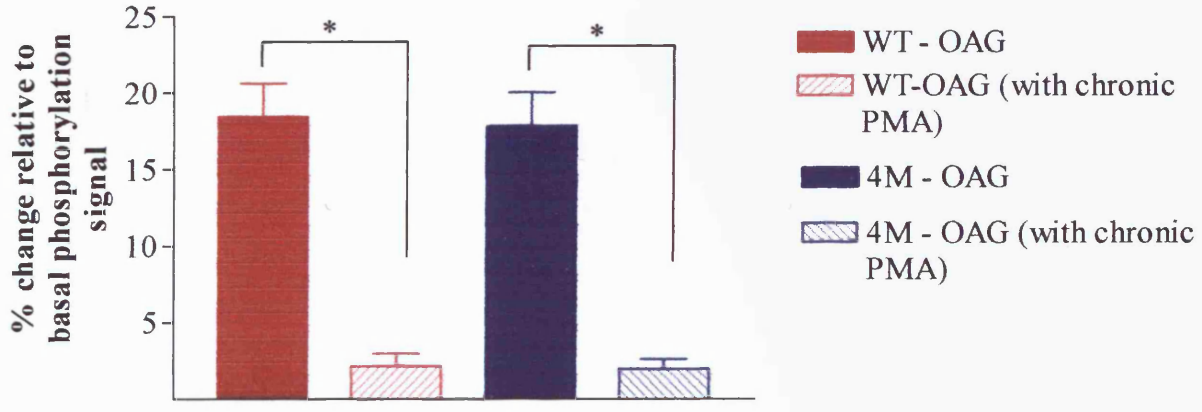

inhibitor of protein phosphatases 1 (PP-1), and 2A (PP-2A). I hypothesised that phosphatase inhibition would increase the phosphorylation response to OAG application. Cells were incubated in the inhibitor cocktail for 15 minutes prior to application of OAG. Inhibition of phosphatases increased the basal phosphorylation of the HERG channel, as expected. Basal phosphorylation of the channel was increased by 10.62 ± 3.94% compared to basal phosphorylation of the channel with appropriate DMSO controls ($p<0.05$). Phosphorylation of the HERG channel in response to OAG was increased by 20.27 ± 0.56% (n=3, data not shown). This was only slightly more than the average OAG-dependent increase in the absence of phosphatase inhibitors, suggesting a rapid dephosphorylation is not responsible for the small change in phosphorylation by PKC stimulation.

7.2.4 Is the OAG-mediated increase in phosphorylation mediated via PKC phosphorylation sites?

PKC dependent modulation of HERG currents remains in the ΔPKC HERG mutant (see chapter 6; Thomas et al., 2003). I wanted to test if the ΔPKC channel was still phosphorylated in response to OAG. Unfortunately, I was unable to detect phospho-proteins in a phosphorylation assay. My inability to detect any ^{32}P labelled HERG could result from a loss of phosphorylation or a failure of the antibody to immunoprecipitate the mutated HERG subunits. None of the mutations are within the antibody epitope, nevertheless the mutations could cause misfolding of the channel, restricting access of the antibody to the protein. I was also unable to detect any protein for the 18M HERG mutant channel. This is not unexpected, as the 18M HERG channel contains identical mutations in the C-terminus of the HERG channel as the ΔPKC HERG mutant. I also tried a second antibody to HERG that recognises a region between amino acids 571 and 585, on the P-loop of the channel. Neither the ΔPKC HERG or 18M HERG channels contain any point mutations in this region. Again, I was unable to detect any phospho-protein for either the ΔPKC HERG or 18M HERG mutants (Figure 7.4). Sequencing ΔPKC HERG and 18M HERG DNA in both antibody binding regions detected no extra mutations. I am confident that the cells are expressing the ΔPKC HERG construct, as robust currents were expressed in all transfections, of similar amplitude as the 4M HERG mutant, which is consistently detected in phosphorylation assays (shown later in this chapter).

Figure 7.4
ΔPKC HERG or 18M HERG are not detected by immunoprecipitation and autoradiography with two different antibodies. Typical autoradiograph from cells mock transfected or transiently transfected with WT, ΔPKC HERG or 18M HERG channels. Two antibodies that recognise completely different HERG channel domains were tested. Intracell Ab. recognises the C terminus between residues 983-998. Extracell. Ab. recognises the P-loop region, between residues 571-585 on the channel.

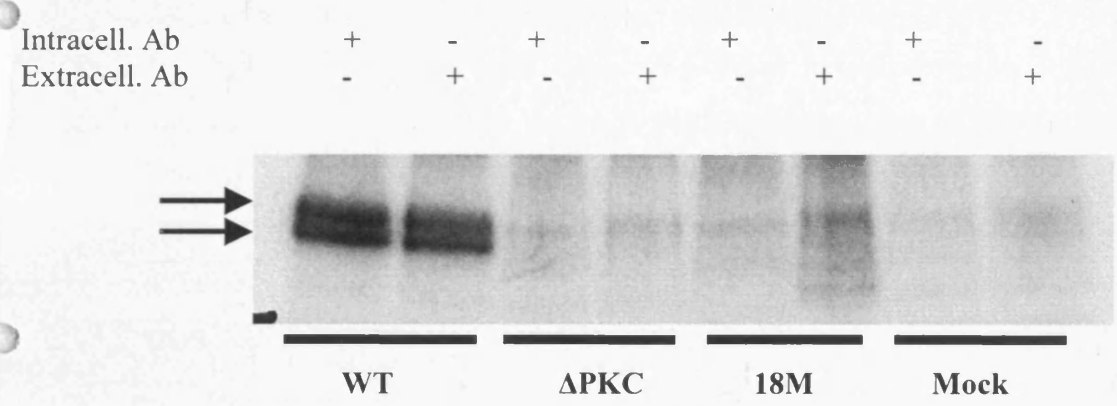

7.2.5 Activation of PKA decreases phosphorylation of HERG subunits

7.2.5.1 Application of forskolin to WT HERG channels

Application of forskolin attenuates HERG current and shifts the voltage dependence of activation (Thomas et al., 1999). This effect is lost in 4M HERG. These results suggest PKA directly phosphorylates the HERG channel, and the PKA phosphorylation sites are required for the response to forskolin. I predicted forskolin would increase HERG channel phosphorylation and planned to use it as a positive control for phosphorylation of the HERG channel expressed in HEK cells. 40 μM forskolin was applied to cells for five minutes. Forskolin significantly reduced the phosphorylation of the HERG channel by 19.49 ± 4.21% (n=4) and shifted the position of the bands relative to control (figure 7.5). These data suggest that forskolin application results in a net dephosphorylation of HERG. To determine if this was PKA mediated, cells were incubated in the PKA-selective inhibitor H-89 (5 μM) for 15 minutes. H-89 did not alter the basal phosphorylation state of HERG, but did abolish the effect of forskolin on dephosphorylation of HERG (figure 7.5B). In the presence of H-89 forskolin produced an increase of phosphorylation of 1.69 ± 1.92%. There was no significant difference in phosphorylation from untreated cells ($p>0.05$). This suggests the dephosphorylation effects of forskolin are PKA-dependent.

7.2.5.2 Application of forskolin to 4M HERG channels

Mutation of putative PKA sites (4M HERG) prevents modulation of currents by forskolin and phosphodiesterase inhibitors. Therefore, I investigated if the phosphorylation response to forskolin was also altered in 4M HERG. As described previously (Zhang et al., 2002), I found 4M HERG channels were robustly phosphorylated in untreated cells. However, unlike in WT channels, there was no significant change of phosphorylation of 4M HERG with forskolin (4.92 ± 1.52%, n=3, $p>0.05$, figure 7.6A).

The forskolin-mediated dephosphorylation was blocked by the phosphatase inhibitor cocktail (as described in section 7.2.3). This cocktail was added to cells 15 minutes prior to forskolin application and increased basal phosphorylation of the channels as described previously. The change of phosphorylation with forskolin was -0.39 ± 0.92%, which was not significantly different to untreated cells ($p>0.05$, data not shown, n=3). Since PKA seems to be a requirement for dephosphorylation to occur, the

Figure 7.5
Forskolin application decreases phosphorylation of the WT HERG channel. A Typical autoradiograph showing WT HERG phosphorylation with and without 40μM forskolin. **B** Typical autoradiograph showing that the phosphorylation induced by forskolin is blocked by 5μM H-89. Incubation of cells in H-89 did not alter HERG phosphorylation compared to untreated cells.

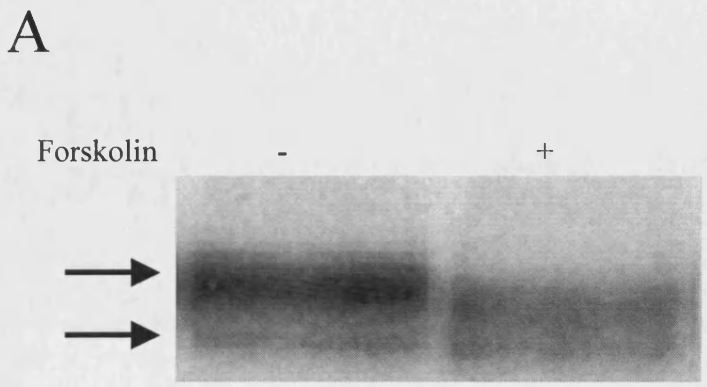

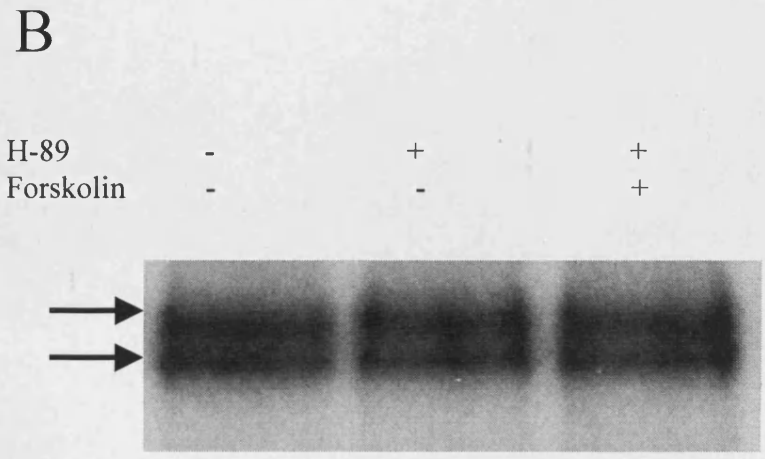

Figure 7.5
Forskolin application decreases phosphorylation of the WT HERG channel. A Typical autoradiograph showing WT HERG phosphorylation with and without 40μM forskolin. **B** Typical autoradiograph showing that the phosphorylation induced by forskolin is blocked by 5μM H-89. Incubation of cells in H-89 did not alter HERG phosphorylation compared to untreated cells.

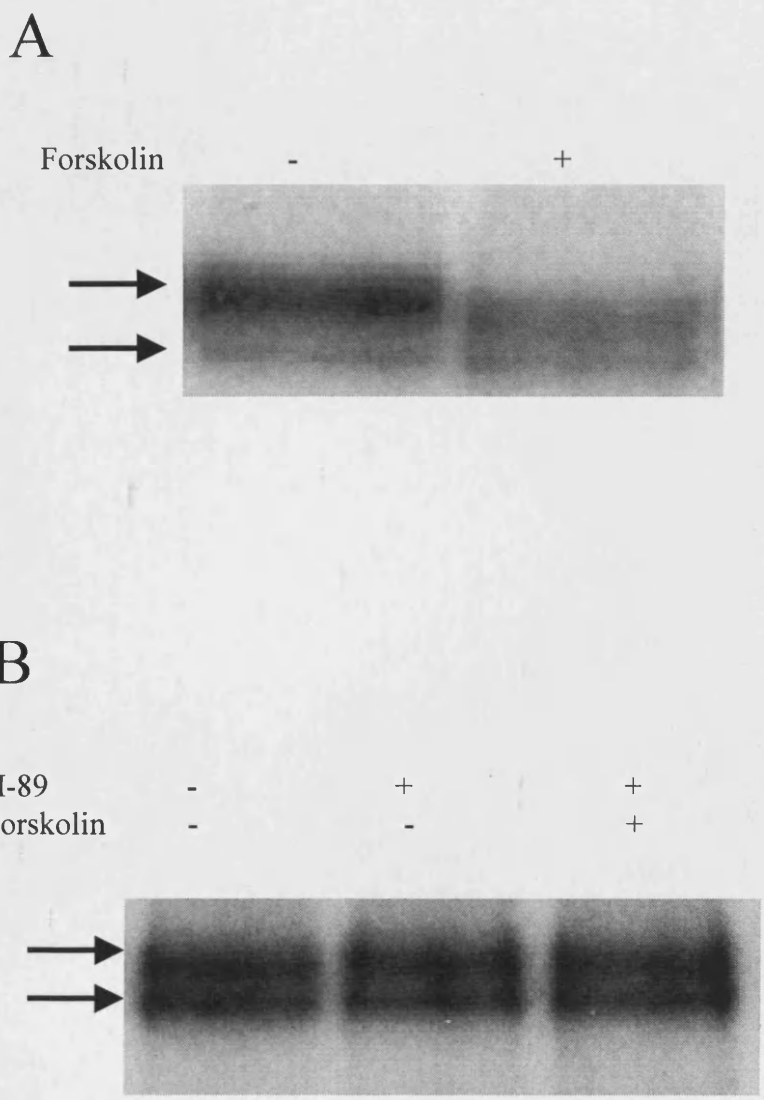

Figure 7.6

The dephosphorylation in response to forskolin is abolished in the 4M HERG mutant that lacks PKA phosphorylation sites. **A** Representative autoradiograph comparing the response of WT and 4M HERG to 40 μM forskolin . Forskolin did not cause dephosphorylation of 4M HERG. **B** Mean results from densitometry analyses of autoradiographs (n≥ 3 for each data set). * shows significance at $p<0.05$ compared to forskolin treatment alone. **C** Flow diagram suggesting the possible mechanism of action of forskolin on the WT HERG channel.

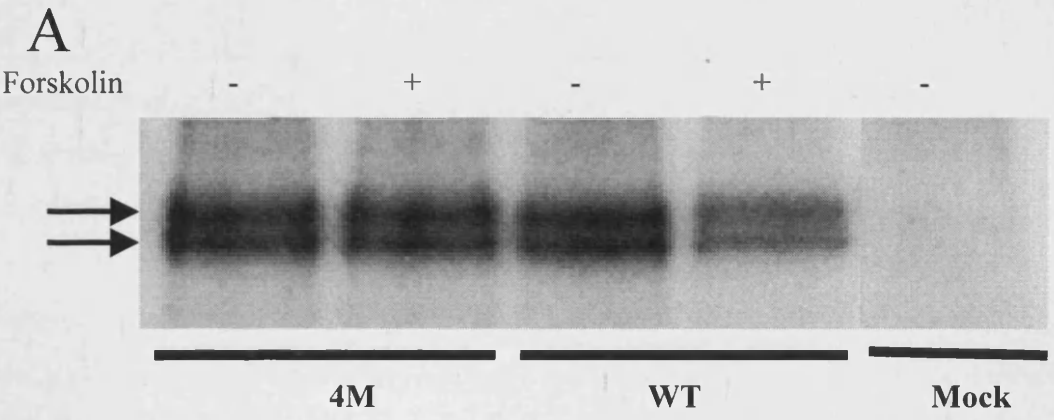

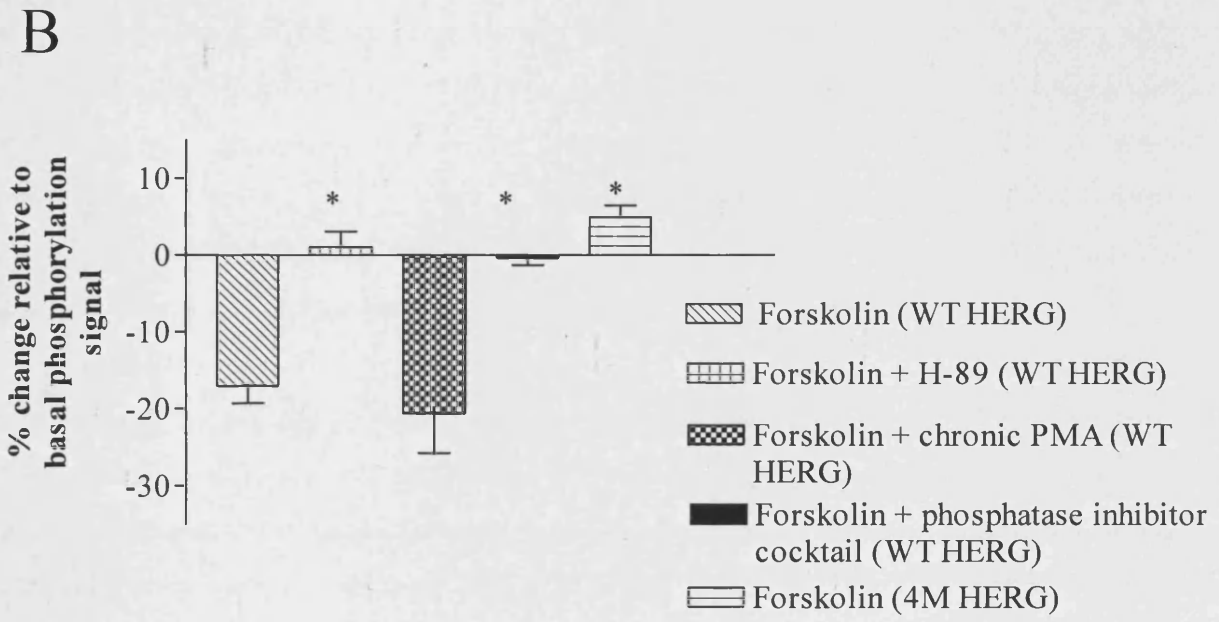

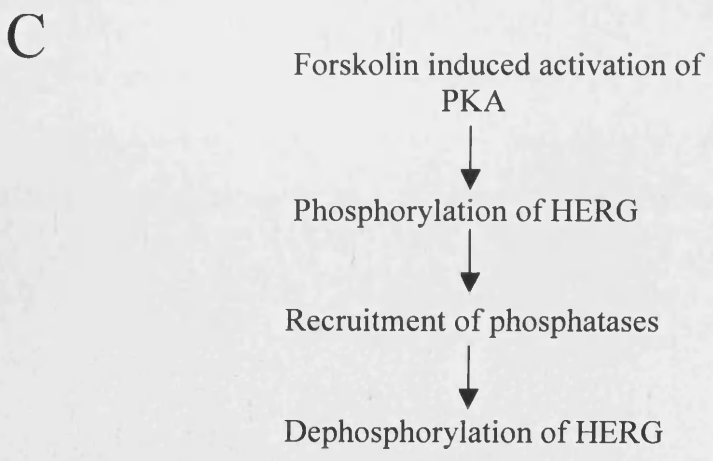

HERG channel may first need to be phosphorylated by PKA, which then leads to an activation of protein phosphatases, and a net loss of phosphorylation. Although I have no direct evidence for this, this simultaneous modulation of the channel by protein kinases and phosphatases may be indicative of the channel acting within a complex.

7.2.6 Cross talk of PKA and PKC signalling pathways

Results from previous studies suggest that cross talk between signalling pathways that can modulate HERG channel activity may occur. Heath and Terrar (2000) showed the effects of forskolin and isoprenaline, both well-known activators of the PKA signalling pathway, to modulate I_{Kr} in guinea pig ventricular myocytes by pathway blocked by PKC inhibitors. Other studies have also shown the effects of a well-known PKC activator, PMA, to modulate HERG current expressed in *Xenopus* oocytes by a partially PKA-dependent pathway (Thomas et al., 2003). I wanted to investigate if the effects I observe in response to forskolin are PKC-dependent. Cells were chronically treated with the phorbol ester PMA, at 1 μM for 24 hours to down-regulate PKC isoforms. Forskolin application to these cells significantly reduced phosphorylation of the HERG channel by 20.60 ± 5.13% (n=3, data not shown). Analysis of autoradiographs by densitometry showed there was no significant difference between forskolin effects in control conditions compared to chronic PMA conditions ($p>0.05$). This suggests that the effects of forskolin are PKC-independent.

7.2.7 Raising intracellular calcium causes a dephosphorylation of the HERG channel

Previously, I have shown that application of ionomycin to HEK cells expressing the HERG channel causes an attenuation of current in a PKC-dependent manner (chapter 5). I therefore wanted to investigate if ionomycin acts in a similar manner to OAG application, that is, to increase phosphorylation of the channel. However, in contrast to OAG, 5 μM ionomycin applied for 5 minutes caused a large and significant decrease in phosphorylation of WT HERG of 30.37 ± 5.11% (n=4, $p<0.05$, figure 7.7A). This dephosphorylation suggests the ionomycin response is not only due to stimulation of PKC, which increases phosphorylation. To investigate if the decrease in phosphorylation was PKC-dependent I treated cells

Figure 7.7

Ionomycin induces a dephosphorylation of HERG which is not PKC dependent, or mediated by PP-1, PP-2A, or alkaline phosphatases. **A** Representative autoradiograph showing HERG phosphorylation with and without ionomycin. **B** Typical autoradiograph showing the effects of ionomycin on HERG in cells chronically treated with PMA. Chronic PMA treatment did not reduce the effects of ionomycin. **C** Effects of ionomycin in the presence of phosphatase inhibitor cocktail containing inhibitors for PP-1, PP-2A and alkaline phosphatases. This cocktail did not reduce the effects of ionomycin

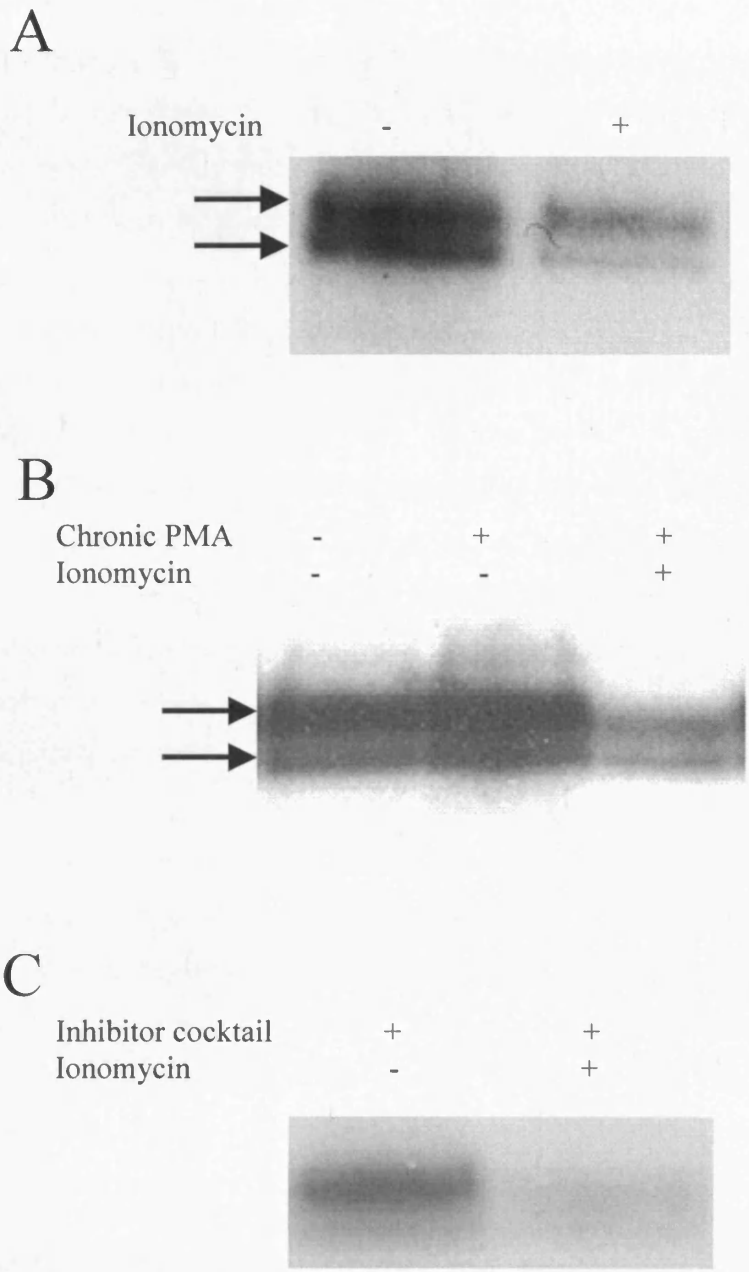

with 1 μM PMA for 24 hours, to down-regulate PKC. In these conditions, ionomycin still significantly decreased phosphorylation of the HERG channel by 26.15 ± 8.26% (n=3, $p<0.05$, figure 7.7B) which was not significantly different to effects of ionomycin in non PMA-treated cells. This suggests the effects of ionomycin are independent of PKC.

To investigate the dephosphorylation of HERG in response to ionomycin further, I tried the phosphatase inhibitor cocktail we had used previously (as described in section 7.2.3) and 5 μM cyclosporin A, a calcineurin A inhibitor. Incubation of cells in phosphatase inhibitor cocktail prior to incubation with ionomycin did not alter the response to ionomycin. Phosphorylation was significantly reduced by 32.00 ± 12.43% (n=3, $p<0.05$, figure 7.7C) which was comparable to effects of ionomycin in control conditions. This suggests the effects of ionomycin in this assay are not due to PP-1, PP-2A or alkaline phosphatases. Dephosphorylation of HERG in cells incubated in cyclosporin A for 15 minutes prior to ionomycin application was less pronounced. Phosphorylation was reduced by 19.98 ± 4.95% (n=3, figure 7.8A). Although this is still a significant change from control values, this is a reduction compared to the dephosphorylation with ionomycin alone. Thus, calcineurin, which is activated by calcium, may mediate some of the dephosphorylation induced by calcium elevation in response to ionomycin.

7.2.8 Phosphorylation of I_{Kr}

To measure phosphorylation of I_{Kr}, guinea pig ventricular myocytes were isolated and the phosphorylation assay carried out as described in section 3.5.3. Unfortunately, in 10 separate experiments, I was unable to detect basal or PKC-mediated phosphorylation of I_{Kr} even when all ventricular myocytes from a heart were used and exposure of autoradiographs was increased to 9 days. These problems could be due to several possibilities, which will be discussed in section 7.3.2.

Figure 7.8
Ionomycin effects are reduced when calcineurin is inhibted by cyclosporin A. A Typical autoradiograph showing HERG phosphorylation in response to 5μM ionomycin in the presence of 5 μM cyclosporin A. The effects of ionomycin were significantly reduced in the presence of cyclosporin A. **B** Mean results from analyses of the autoradiographs (n≥ 3 for each data set).

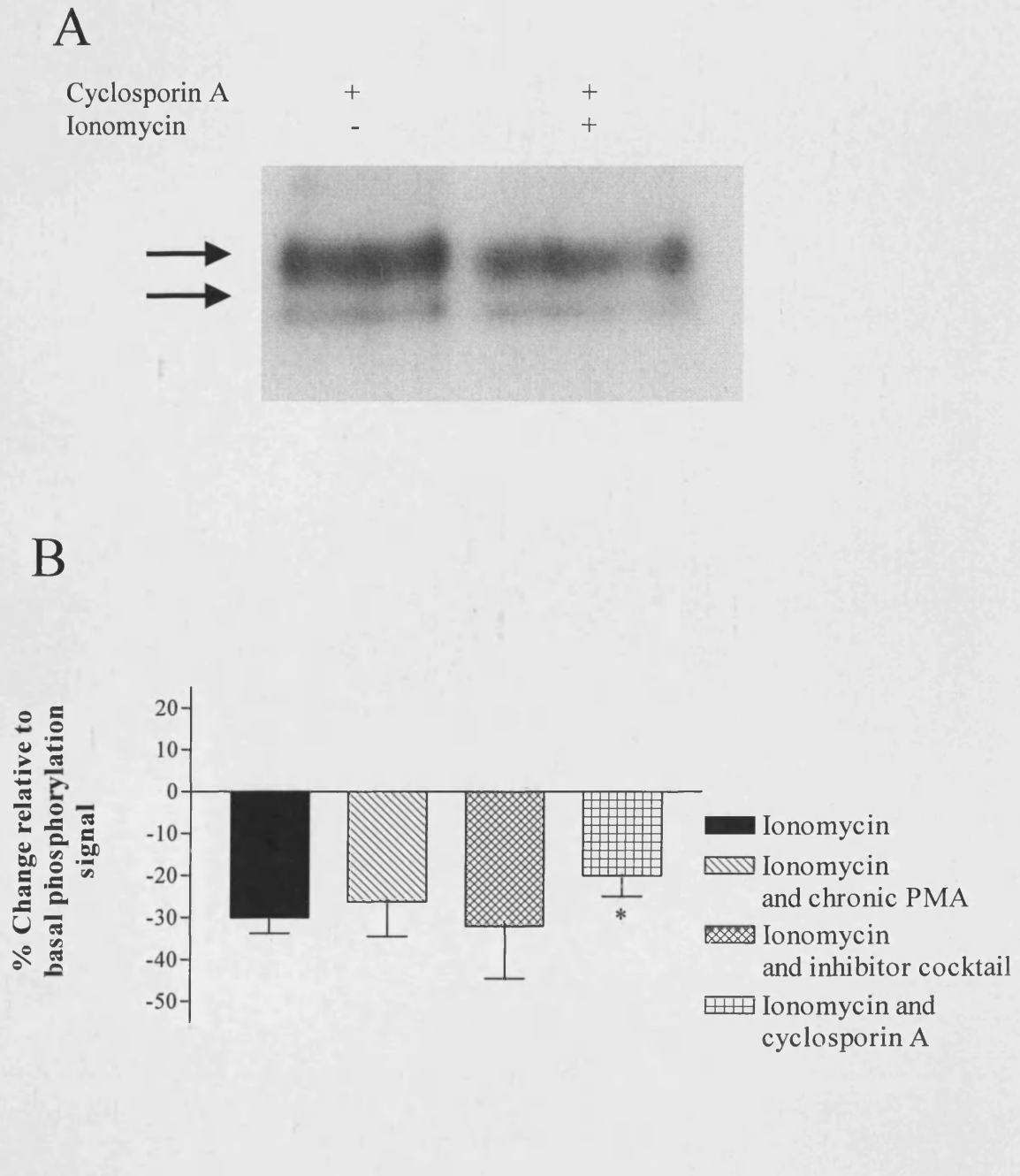

Figure 7.8
Ionomycin effects are reduced when calcineurin is inhibted by cyclosporin A. A Typical autoradiograph showing HERG phosphorylation in response to 5μM ionomycin in the presence of 5 μM cyclosporin A. The effects of ionomycin were significantly reduced in the presence of cyclosporin A. **B** Mean results from analyses of the autoradiographs (n≥ 3 for each data set).

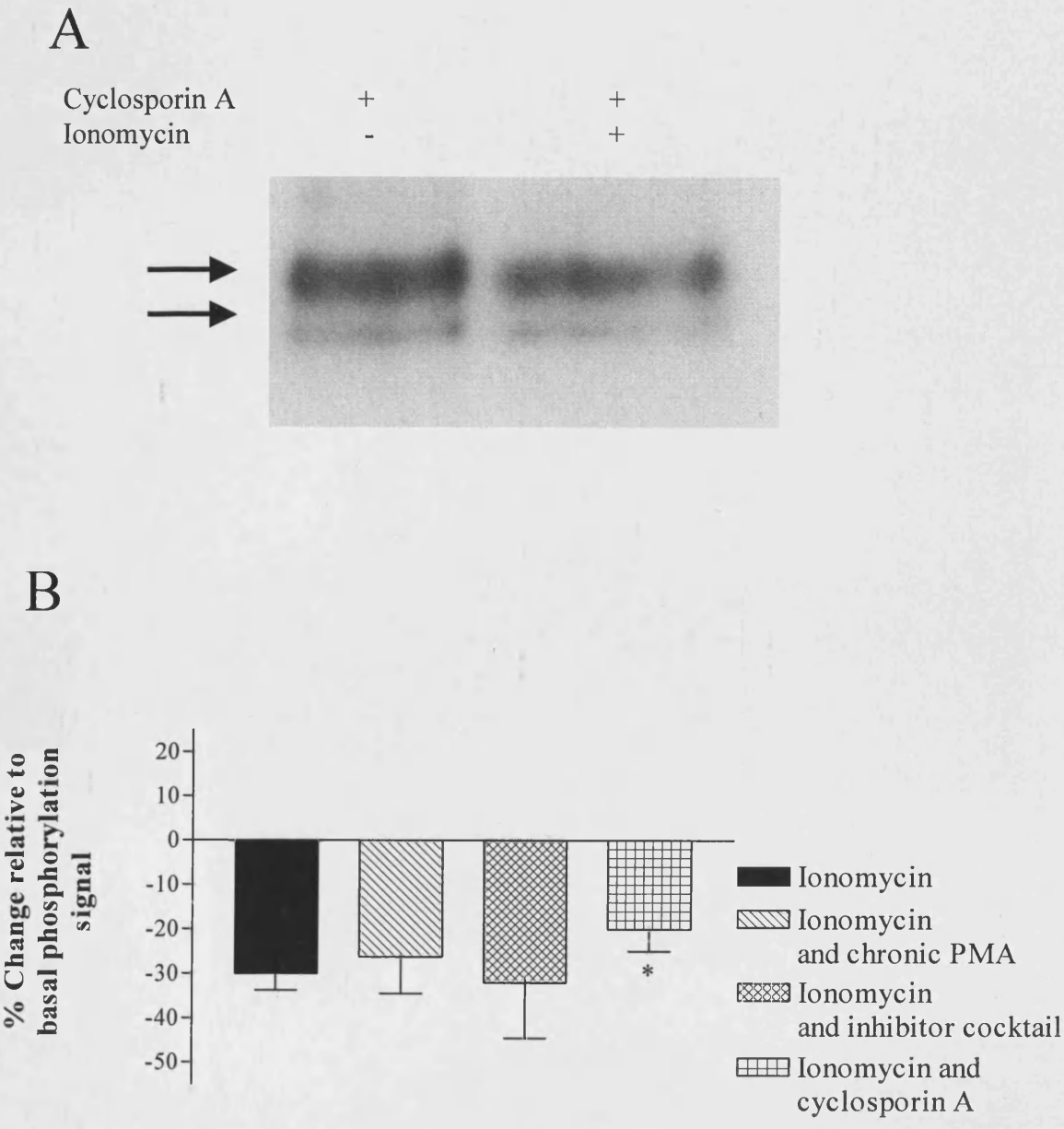

7.3 Discussion

7.3.1 Phosphorylation of HERG in HEK cells

In this chapter I demonstrate an increase of ^{32}P labelled phosphate incorporation into HERG channels in response to OAG application. This is consistent with the HERG channel being directly phosphorylated by PKC activation. This is in contrast to work carried out by Zhang et al. (2002) who were unable to detect changes in HERG phosphorylation in response to PMA, and work by Thomas et al. (2003 and 2004), who suggest PKC modulates HERG channels via indirect mechanisms. Although the increase in phosphorylation I observe is small in comparison to the PKC-mediated increase measured in the muscarinic M_3 receptor, this may be due to the robust basal phosphorylation seen with the HERG channel. Any increase in phosphorylation measured would be low when measured as a percentage of a large starting signal. Thus, basal phosphorylation of HERG may mask the number of sites phosphorylated in response to direct activation of PKC.

Several lines of evidence indicate that the increase in phosphorylation in response to OAG was mediated by PKC. The increase was abolished by bis-1 and by down-regulation of PKC using chronic PMA treatment. Since I have previously shown chronic PMA treatment to down-regulate the α, β, δ and ε isoform of PKC, it is likely that one or more of these isoforms are responsible for the increased phosphorylation of the HERG channel.

The basal phosphorylation of the HERG channel was not altered by short-term or long-term attenuation of PKC activity. This suggests that PKC is not responsible for the basal phosphorylation of the channel. This observation correlates with our previous observations (chapters 5 and 6), from HERG current recordings.

There have been several reports suggesting HERG modulation through cross talk between the PKC and PKA signalling pathways (Heath and Terrar, 2000; Thomas et al., 2003). However, I can find little evidence of this. OAG increases phosphorylation even in the absence of the four putative PKA phosphorylation sites on the channel. The increase is also abolished when cells were chronically treated with PMA. This suggests that the increase in phosphorylation I observe is not due to phosphorylation at the PKA sites of the HERG channel, and is PKC-specific. Likewise, PKA stimulation alters HERG phosphorylation in a manner that is not dependent on PKC.

It has previously been reported that PKC modulation of the HERG channel in *Xenopus* oocytes continues in the absence of 17 putative PKC phosphorylation sites on the HERG channel (ΔPKC HERG mutant: Thomas et al., 2003). My results on ΔPKC HERG currents in mammalian cells agree with Thomas et al. This suggests a number of possibilities, including the conclusion reached by Thomas et al., that PKC stimulation did not directly modulate HERG current and that an auxillary subunit was involved. I wanted to test if there was an increase in phosphorylation of the channel, but were unable to detect either the ΔPKC HERG or 18M HERG phospho-proteins using an antibody directed to either intracellular or extracellular regions of the HERG channel. This was presumably due to the high number of point mutations contained within the channel that prevented the antibodies from recognising their epitopes. Therefore, I was unable to measure phosphorylation of the channel. Future studies could address this by tagging ΔPKC and 18M HERG with an antibody epitope on the C-terminus. I would then be able to immunoprecipitate HERG proteins and repeat the phosphorylation assays. A possibility to why we are not detecting the ΔPKC HERG or 18M HERG channels in phosphorylation assays is a loss of phosphorylation due to removal of the putative PKC phosphorylation sites. However, I have previously shown that PKC does not contribute to the basal phosphorylation of HERG. I am also unable to detect either ΔPKC HERG or 18M HERG proteins in western blots, suggesting the protein is not detected by the antibody, rather than no phosphorylation is present.

Ionomycin caused a large decrease in phosphorylation of the HERG channel. The effects of ionomycin on the HERG channel currents are PKC-dependent. Therefore, I predicted that the effects of ionomycin and OAG on HERG phosphorylation would be similar. However, the differences between the results with OAG and ionomycin can be explained by a number of mechanisms. Firstly, OAG specifically activates PKC only, acting as a DAG analogue, whereas ionomycin acts to increase cytosolic calcium in the cell. This could activate a number of pathways, including activation of calcium-dependent PKC isoforms, calcium dependent phosphatases, calcium-calmodulin dependent pathways and other intracellular signalling molecules. The effects of ionomycin on HERG currents were abolished with chronic PMA treatment, suggesting a role for one or more of the α, β, δ or ε isoforms of PKC in the modulation of the current. This suggests that the effects of ionomycin are mediated by

PKC but does not necessarily indicate direct PKC phosphorylation. The results of the phosphorylation assays did not clarify matters. When carrying out a phosphorylation assay it is net phosphorylation of the channel that is measured. Therefore, it may be that PKC phosphorylates the HERG channel, but this increase is obscured by the decrease in phosphorylation at other sites. The phosphopeptide mapping technique, which would allow the phosphorylation status of individual regions of the channel to be monitored, may help address this problem.

In cells chronically treated with PMA, ionomycin caused a similar decrease in phosphorylation as in control cells. This could suggest that ionomycin does not influence HERG channel phosphorylation in a PKC-dependent manner since no decrease in total phosphorylation was observed. However, in control cells, because of the number of mechanisms possibly activated during ionomycin application, including activation of calcium-dependent phosphatases, it may be that any increase in phosphorylation in response to PKC activation is rapidly removed by activated phosphatases. Therefore, a PKC-dependent change in phosphorylation would not be observed.

Forskolin also decreased phosphorylation of HERG channels. I found this surprising, as previously it has been reported that the PKA phosphorylation sites are required for the effect of forskolin and phosphodiesterase inhibitors (Thomas et al., 1999). I would therefore hypothesise that the effects of forskolin are due to a PKA-mediated phosphorylation of the HERG channel, which would be detected as an increase in channel phosphorylation. The decrease in phosphorylation is likely to be mediated by one or more of protein phosphatases PP-1, PP-2A or alkaline phosphatases. I found that active PKA, and the presence of the PKA phosphorylation sites on the HERG channel were necessary for the de-phosphorylation, but it is not yet clear whether dephosphorylation is functionally important. It is possible that forskolin first causes an increase in phosphorylation at the four PKA sites on the channel. This may have been observed if cells were harvested after a shorter application of forskolin. If both phosphorylation and dephosphorylation of the channel were to have an effect on the channel currents, I might expect to be able to distinguish two separate processes during forskolin application. In fact, I observe a steady, monophasic decrease of current, which is suggestive of only one process occurring. PKA phosphorylation of the HERG channel may not have an effect directly on channel currents, but may permit further regulatory processes

such as a recruitment of phosphatases or the binding of regulatory proteins. Indeed, evidence showing phosphorylation-dependent interactions between HERG and 14-3-3 binding proteins has been shown (Kagan et al., 2002). These data suggested binding of 14-3-3ε was dependent on PKA phosphorylation of HERG, and acted to shield the channel from dephosphorylation.

Perhaps it is dephosphorylation of the channel that causes the attenuation of current in response to forskolin. The effect of phosphatase inhibitors on the HERG currents response to forskolin was not examined. Thomas et al., (1999) showed the removal of single PKA phosphorylation sites from the HERG channel to reduce the effect of forskolin. Each of the four sites contributed approximately equally to the effects seen in the presence of forskolin. This suggests each individual PKA site to be important in the modulation of the channel.

Dynamic modulation by kinases and phosphatases has been reported for the ERG channel. Cayabyab and Schlichter (2002) reported that src tyrosine kinase regulates the ERG channel expressed in MLS-9 cells. They found the ERG protein to be constitutively phosphorylated by src tyrosine kinase. This phosphorylation could be reduced using tyrosine kinase inhibitors, and in corresponding experiments, ERG current was reduced upon application of these inhibitors. Conversely, the current was increased upon application of a src-activating peptide. The same group later published the ERG current could also be modulated by the tyrosine phosphatase src-homology 2-containin protein (SHP-1) (Cayabyab et al., 2002). Using co-immunoprecipitation assays, they were able to show this protein physically associated with ERG. Transfection of cells with SHP-1 decreased current, which corresponds with the decrease in current seen with tyrosine kinase inhibitors in their previous study. This decrease was accompanied by a positive shift in activation of the channel. These effects were reduced using phosphatase inhibitors. Taking into account data from both studies, the group hypothesised that the ERG channel exists in a multimolecular complexes that allows this dynamic regulation to occur.

Our data also implies the HERG channel may be part of a complex. This may involve AKAP proteins. These have previously been shown to form macromolecular complexes with many ion channels, protein kinases and protein phosphatases to allow dynamic regulation of target proteins by PKA, including the K_{ATP} channel (Hayabuchi et al., 2001), I_{Ks} (Marx et al., 2002) and ROMK1 channels (Ali et al., 1998). Mason et al. (2002) showed modulation of Kv1.5 by

PKA, tyrosine kinase and tyrosine phosphatase required an intact cytoskeleton. Evidence of PKC interaction with AKAP proteins has also been shown (Klauck et al., 1996; Coghlan et al., 1995; Faux et al., 1999). The latter study showed PKCβII to physically associate with AKAP79 independent of kinase activation.

A number of further experiments could be carried out to investigate PKC-mediated HERG channel modulation in more detail. This includes phosphopeptide mapping, a technique that allows sites of phosphorylation to be mapped to channel fragments. This would allow me to investigate which sites of phosphorylation were being modulated with each process. Previous studies using this technique have mapped the PKA phosphorylation sites on the Kv4.2 channel (Anderson et al., 2000), and L-type calcium channel (Gerhardstein et al., 1999).

Of course, although I have been able to exclude PKA and PKC making any contribution to the basal phosphorylation of the channel, I have not investigated the sites that do make a contribution. Phosphopeptide mapping would also allow me to investigate this. Knowing the phosphorylation sites on the HERG channel that contribute to the basal phosphorylation of the channel would allow me to assess their role in normal functioning of the channel. Phosphorylation, in addition to altering channel open probability has also been shown to have an important regulatory role on K_{ATP} channel trafficking (Hu et al., 2003), where PKC was shown to down-regulate K_{ATP} channels. It is possible this may apply to other channels, including HERG.

7.3.2 Phosphorylation of I_{Kr} in guinea pig ventricular myocytes

I was unable to detect any phosphoproteins at the expected weight for HERG when carrying out phosphorylation assays in guinea pig ventricular myocytes. The antibody also detected other phosphoproteins in myocytes (but not HEK cells), and so I was confident that the ^{32}P labelled phosphate incorporation into myocytes was occurring. It is unknown why I was not able to detect HERG, however, there are a number of possible explanations. 1) In phosphorylation assays, the antibody is added to proteins that have not been denatured. Hence, binding of any secondary subunits or changes in folding of the native channel may cause the antibody not to be able to detect the protein. 2) Expression of I_{Kr} in ventricular

tissue is known to be small, so although we were using the full yield of ventricular myocytes for each assay, the amount of HERG may not have been large enough to detect. I was unable to detect HERG protein in western blots or phosphorylation assays. 3) HERG expressed in guinea pig ventricular myocytes may not be basally phosphorylated, or be phosphorylated upon PKC activation. Refining the experiments further may allow this to be investigated.

Chapter 8

Modulation of the HERG channel by caffeine

8.1 Introduction

Elevation of cytosolic calcium ($[Ca^{2+}]_i$) has a critical role in regulating contraction in cardiac tissue (Berridge et al., 2000). Depolarisation of the membrane potential by a propagating action potential opens L-type calcium channels that results in an influx of calcium to trigger a much greater release of calcium from intracellular stores through ryanodine receptors. This process is known as calcium induced calcium release (CICR). Caffeine has been widely used to study the role of ryanodine receptors in cardiac and other cell types. Its effects are rapid and reversible. Caffeine is a member of the class of organic compounds known as alkaloids. The core of the molecule is a purine, and caffeine is very similar in structure to adenosine. Caffeine releases calcium from cytosolic stores by opening the ryanodine receptor at physiological calcium concentrations, transiently raising cytosolic calcium and depleting the ryanodine releasable component. Caffeine also inhibits phosphodiesterase activity (Butcher and Sutherland, 1962; Lindaman et al., 2002), increasing cAMP concentrations in the cell, and activating PKA. Caffeine was initially used in my study as a tool to increase cytosolic calcium. Subsequently, I found caffeine to alter HERG currents in a manner quite different from ionomycin and methacholine. In particular, I found it attenuated HERG currents with a very rapid time course and its effects were rapidly reversible. Since caffeine is such a widely used and important pharmacological tool I wanted to investigate its mode of action on HERG current, and used a number of different approaches. 1) To investigate the role of caffeine induced calcium release, two approaches were used. A) Intracellular calcium was buffered to low levels using the calcium chelator BAPTA. B) Conversely, the effect of caffeine was tested when intracellular calcium had been raised to high levels with ionomycin. 2) Previously I have shown that increasing cytosolic calcium activates PKC and this modulates HERG channel currents. I therefore investigated if the effects of caffeine were PKC-dependent with the PKC-selective inhibitor bis-1. 3) Finally, since caffeine may act as a phosphodiesterase inhibitor, I investigated if the modulatory effects its has on the HERG channel were due to this mechanism. The effect of caffeine was tested in the presence of forskolin, an adenylyl cyclase agonist, which increases the cAMP concentration in the cell. I

hypothesised that if caffeine was only working as a phosphodiesterase inhibitor, no additional effects of caffeine would be seen in the presence of forskolin.

8.2 Results

8.2.1 Effects of caffeine on HERG currents in HEK cells

HERG-HEK cells were held at a membrane potential of –80 mV, and the 'depolarisation to 0 mV' protocol was used to evoke currents. I started with a 5 mM caffeine concentration as this concentration is within the range of concentrations most frequently used in experiments on cardiac myocytes (McDowell et al., 2004; Plank et al., 2003; Sjaastad et al., 2002). Extracellular application of 5 mM caffeine to HERG-HEK cells attenuated HERG current in a rapid and fully reversible fashion. Figure 8.1A shows currents in control conditions and with maximal effects of caffeine. The action of caffeine was seen within the first voltage pulse after application, with maximal effects seen within 30 seconds (figure 8.1B). Current amplitudes remained attenuated throughout the duration of caffeine application. Current remaining during caffeine application was 61.24 ± 2.22% of control currents (n=7, $p<0.05$). The effect of washout of caffeine from the recording chamber was rapid. HERG currents recovered to 99.04 ± 1.56% of control currents with the first subsequent voltage pulse.

The effects of caffeine were concentration-dependent (Figure 8.1C), but there was not a well defined sigmoidal concentration-response relationship. The onset and recovery of current attenuation was rapid at all concentrations. Small effects of caffeine were seen at concentrations of 100 μM, with currents in these conditions being 88.1 ± 1.42% of control (n=5). Current amplitude declined dramatically between 5 and 20 mM. Currents were 12.7 ± 1.11% of control current with 20 mM caffeine (n=5).

To determine if there was any voltage dependence to the reduction of current by caffeine, currents were measured at a range of potentials using the I-V protocol. Currents measured using this protocol in control conditions and in the presence of caffeine can be seen in figure 8.2A. Currents were reduced at all potentials by caffeine. The voltage dependence of activation of HERG was not shifted significantly with caffeine application (figure 8.2B). $V_{0.5}$ values in control conditions were –22.27 ± 1.90 mV, compared to –23.09 ± 2.33 mV with caffeine (n=6, $p>0.05$). The slope factor was also not significantly altered in the presence of caffeine (7.79 ± 0.34, compared to 7.80 ± 0.36 with caffeine ($p>0.05$)). The isochronal I/V relationship was also unaffected (figure 8.2C). These data suggest

Figure 8.1

Application of caffeine to HERG-HEK cells causes a rapid and reversible inhibition of HERG current. **A** Representative HERG current traces showing in control conditions and during 5 mM caffeine application. **B** Time course of caffeine effects (n=7). Peak tail currents were normalised to control amplitudes and mean, normalised data were plotted against time. **C** Concentration-response relationship for caffeine effects on HERG peak tail current amplitude (n ≥ 5 for each data set).

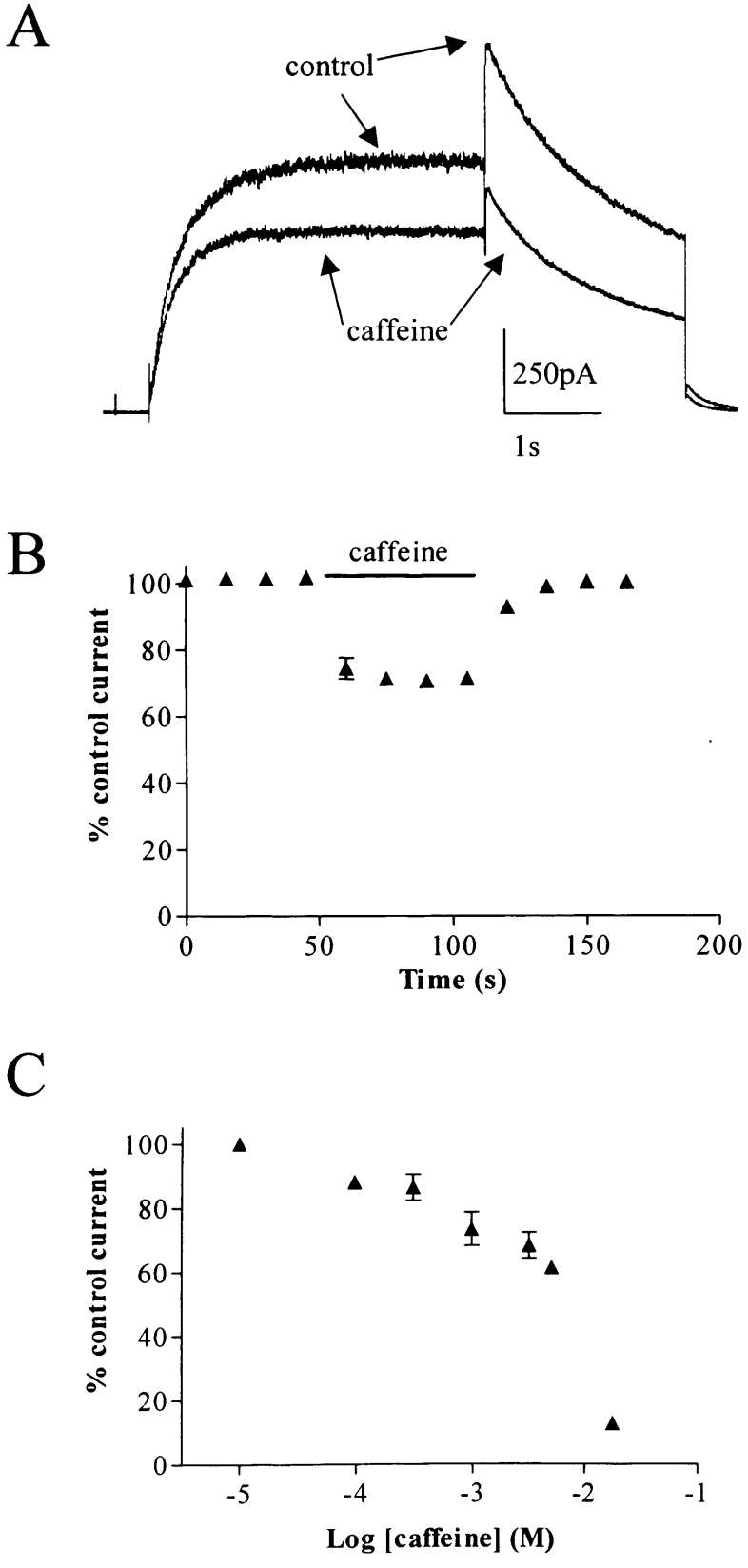

Figure 8.2
Caffeine attenuation of HERG current does not exhibit any voltage dependence **A** Representative current traces from the I-V protocol in control conditions (left) and with 5 mM caffeine (right). Only current traces with test pulses to –40, -20 and +20 mV are shown. **B** Voltage dependence of activation before and during 5 mM caffeine application (n=6). Peak tail currents were normalised to peak amplitudes, plotted against test pulse potential and fitted with a Boltzmann function (solid lines). Also shows voltage dependent block by caffeine (purple), normalised to peak tail current in control conditions. **C** Mean isochronal end pulse currents in control conditions and with 5 mM caffeine, normalised to maximal amplitudes (n=6). **D** Current availability due to channel inactivation in control conditions and with caffeine. Currents were normalised to maximal currents in each recording solution.

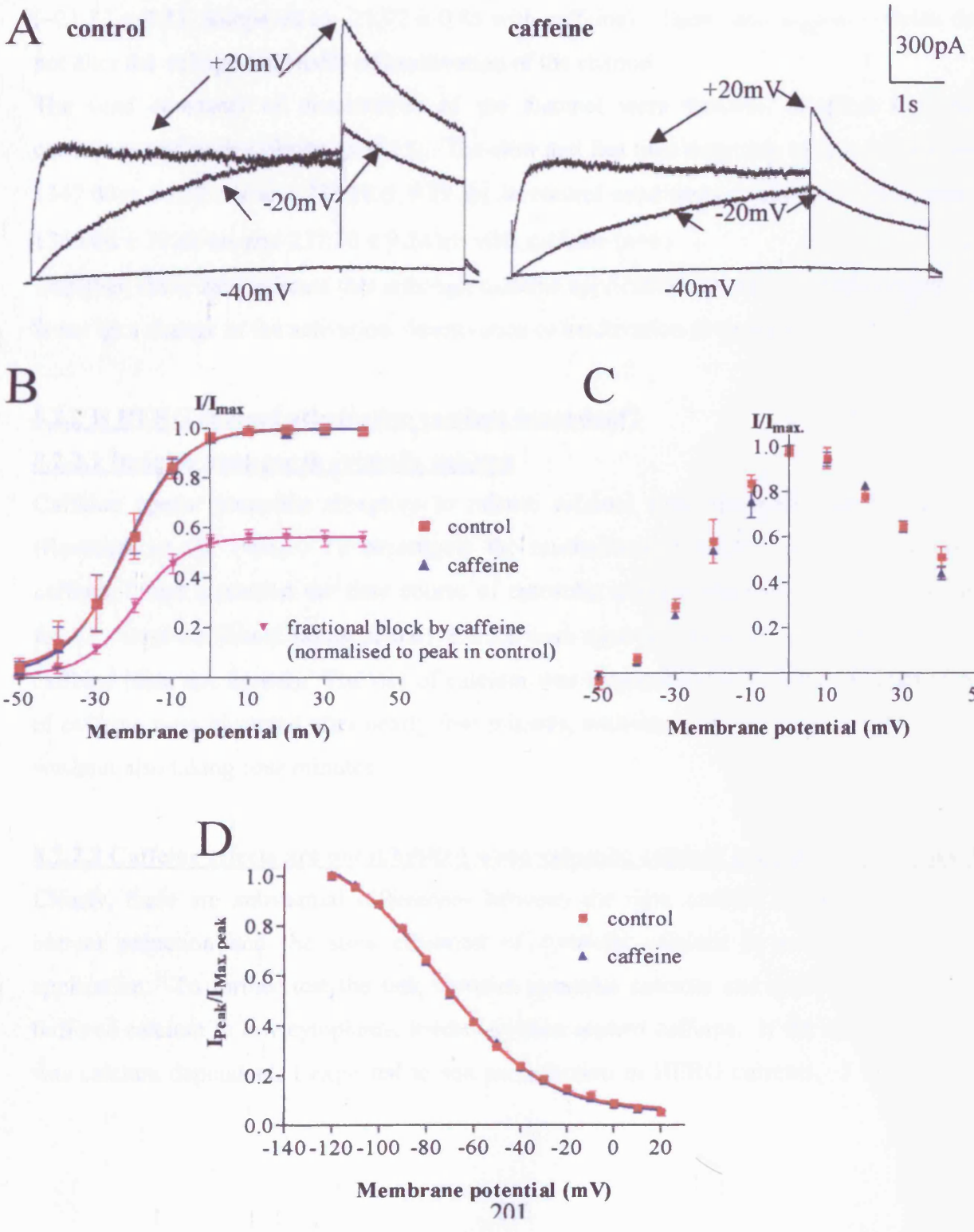

that caffeine did not attenuate current by altering the voltage sensitivity of activation of the channel.

Steady state inactivation was measured as previously described using a triple pulse protocol (chapter 4). Inactivation of the current was unaffected by caffeine (figure 8.2D). $V_{0.5}$ values for inactivation in control conditions were –73.70 ± 0.84 mV, compared to –73.83 ± 0.99 mV with caffeine (n=6, p>0.05). Slope factors were also unchanged in the presence of caffeine (–21.12 ± 0.73, compared to –21.77 ± 0.85 with caffeine). These data suggest caffeine does not alter the voltage sensitivity of inactivation of the channel.

The time constants of deactivation of the channel were virtually identical in control conditions and with caffeine (p>0.05). The slow and fast time constants of deactivation were 1347.00 ± 55.92 ms and 238.10 ± 9.83 ms in control conditions respectively, compared to 1360.00 ± 70.48 ms and 237.70 ± 9.24 ms with caffeine (n=6)

Together, these data indicate that although caffeine application attenuates HERG current, this is not by a change in the activation, deactivation or inactivation properties.

8.2.2 Is HERG current attenuation calcium dependent?

8.2.2.1 Imaging changes in cytosolic calcium

Caffeine opens ryanodine receptors to release calcium from the endoplasmic reticulum (Rousseau et al., 1988). To investigate the mechanism of HERG current reduction by caffeine I first measured the time course of cytosolic calcium changes in HEK cells using fura-2. Baseline fura-2 ratios of 0.61 ± 0.22 were increased to ratios of 1.98 ± 0.21 with caffeine (data not shown). The rise of calcium was surprisingly slow and maximum effects of caffeine were observed after nearly four minutes, with recovery of cytosolic calcium after washout also taking four minutes.

8.2.2.2 Caffeine effects are not inhibited when cytosolic calcium is buffered to low levels

Clearly, there are substantial differences between the time courses of effects on HERG current reduction and the slow elevation of cytosolic calcium in response to caffeine application. To further test the link between cytosolic calcium and reduction of HERG I buffered calcium to low cytoplamic levels and then applied caffeine. If the effect of caffeine was calcium dependent, I expected to see no reduction in HERG currents. 5 mM BAPTA

was applied to cells via the patch pipette for 10 minutes after the whole cell configuration was achieved, to allow complete dialysis of BAPTA into the cell, and the 'depolarisation to 0 mV' protocol was used to evoke currents. Once currents had stabilised 5 mM caffeine was applied. Application of caffeine continued to rapidly attenuate current. Currents can be seen in Figure 8.3A. Currents during caffeine application were attenuated to 53.91 ± 5.52% of control current (n=5), suggesting caffeine does not exert its effects by an increase in calcium. I am confident that using BAPTA at this concentration and allowing dialysis for 10 minutes is sufficient for maximal calcium buffering, as we have previously shown this to inhibit the effects of ionomycin (chapter 5). Washout of caffeine in these conditions was rapid, with currents reaching 98.31 ± 1.63% of control currents (figure 8.3B).

It is likely that cell dialysis with BAPTA depletes calcium stores since calcium slowly leaks out and stores cannot be replenished. However, to check no calcium is released by caffeine I applied it twice. The first application would deplete endoplasmic reticulum calcium stores so that with the second application little or no calcium could be released. If the effect of caffeine was calcium dependent, I would expect a greatly reduced response with the second caffeine application. HERG current was reduced to 62.83 ± 2.05% of control (n=5) with the second caffeine application (figure 8.4A), and this was not significantly different to 60.75 ± 1.99% of control seen with the first application (Figure 8.4B). These results provide further evidence that caffeine does not act via a calcium-dependent mechanism.

8.2.2.3 Caffeine effects are not inhibited when cytosolic calcium is raised

To further investigate the response of HERG to caffeine, I used ionomycin. I have previously shown external application of the calcium ionophore to cause a slower, non-reversible attenuation of current, which can be inhibited in BAPTA-dialysed cells (chapter 5). Since ionomycin shows such a different time-course to caffeine, it is likely that caffeine does not act through calcium. To fully clarify if caffeine was exerting its effects via calcium, cells were pre-treated with ionomycin to raise cytosolic calcium. I hypothesised if caffeine does exert its effects through an increase in cytosolic calcium, the effect of caffeine should be inhibited when calcium is already at high levels. Ionomycin was applied until steady state effects were achieved, attenuating current to 65.98 ± 0.62% of control current (n=6).

Figure 8.3

Chelating intracellular calcium with BAPTA does not alter the response to caffeine. A Representative current traces in control conditions just before 5 mM caffeine application, and in the presence of 5 mM caffeine. **B** Representative time course of 5 mM caffeine effects in the presence of 5 mM BAPTA (representative of 5 experiments). Cells were left for 10 minutes once the whole cell configuration was achieved before recording started.

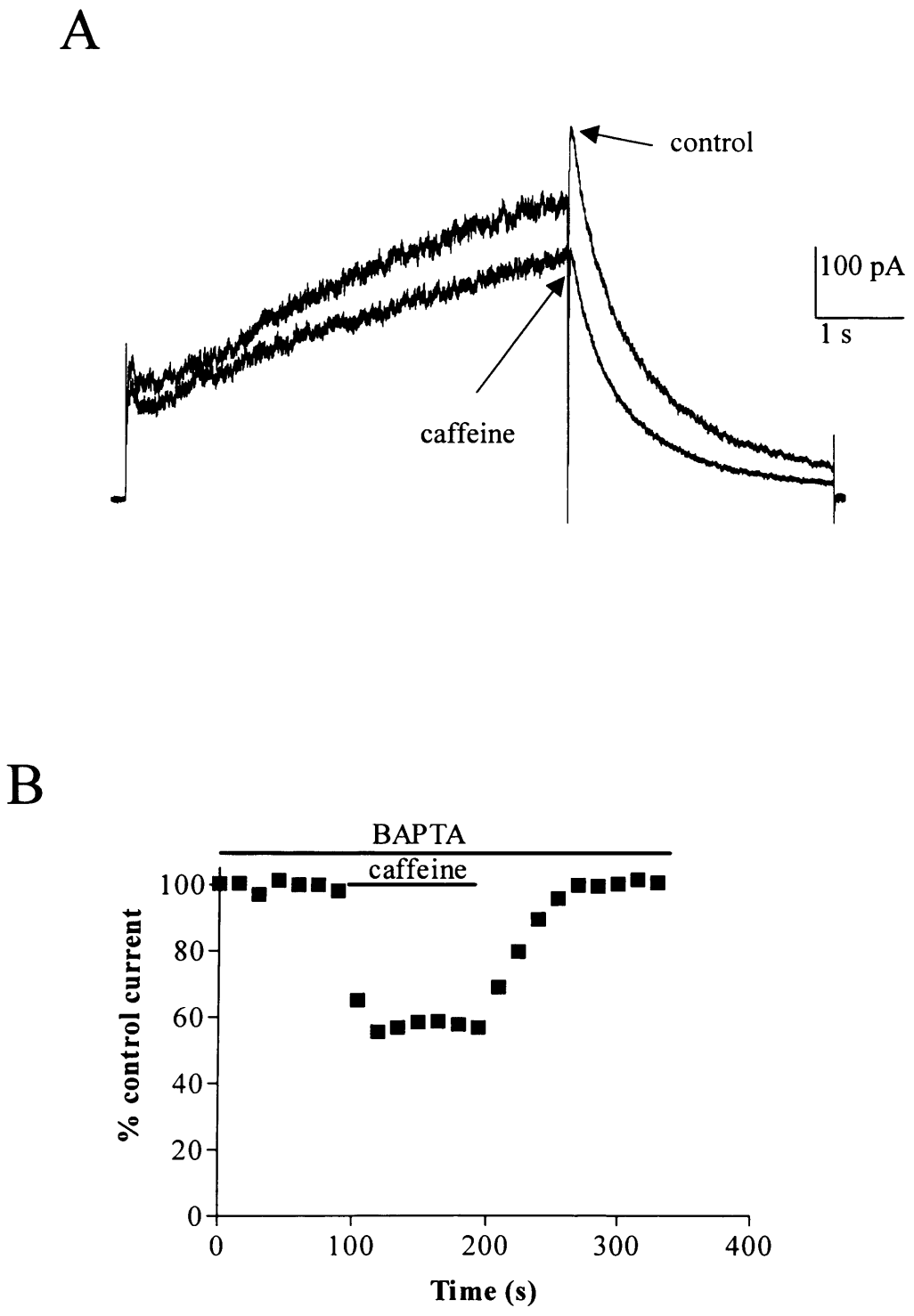

Figure 8.4

A second application of caffeine results in the same inhibition. **A** Representative current traces in control conditions, with the first and second applications of 5 mM caffeine, and with washout. **B** Representative time course of caffeine effects with multiple applications (representative of 5 experiments). All of these experiments were carried out with 5mM BAPTA in the pipette solution.

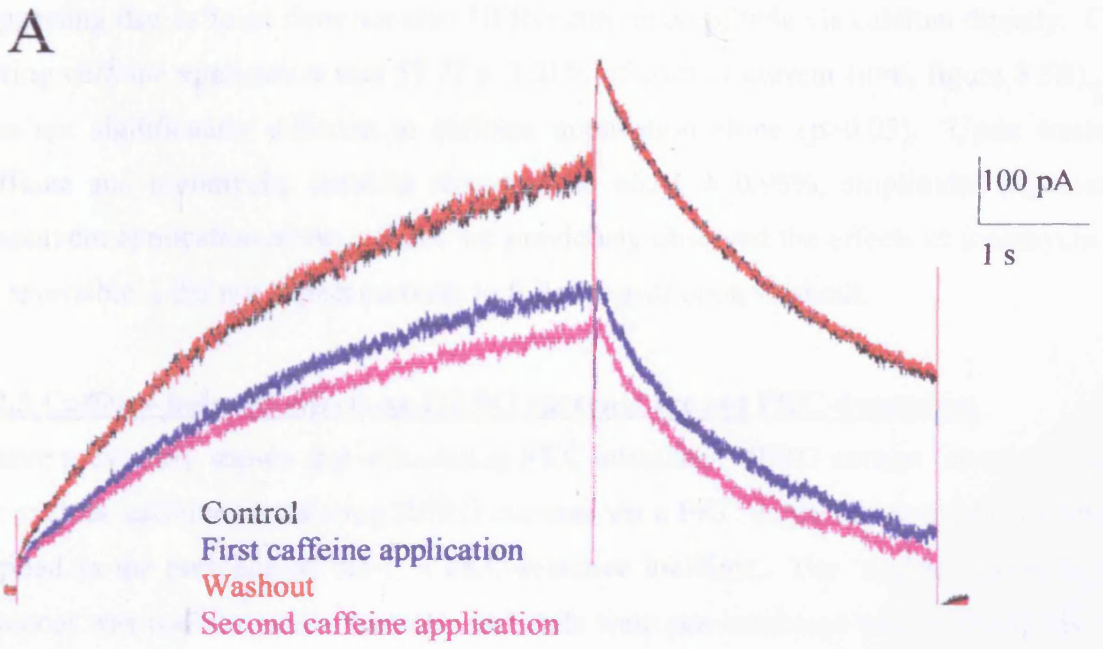

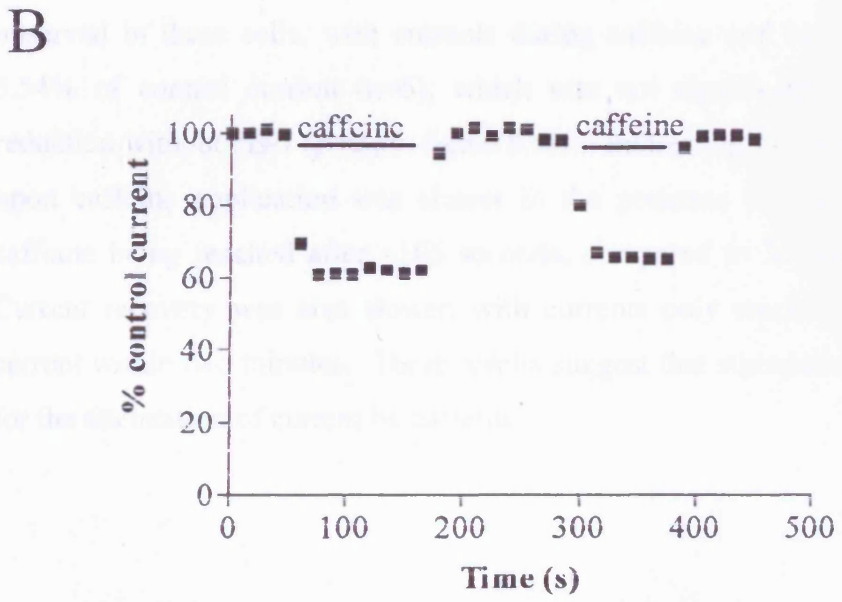

Caffeine was then co-applied with ionomycin. Representative currents are shown in figure 8.5A . Caffeine application continued to attenuate current in a rapid, fully reversible manner, suggesting that caffeine does not alter HERG current amplitude via calcium directly. Current during caffeine application was 57.72 ± 3.21% of control current (n=6, figure 8.5B), which was not significantly different to caffeine application alone ($p>0.05$). Upon washout of caffeine and ionomycin, currents recovered to 66.01 ± 0.96%, amplitudes expected with ionomycin application alone. Since we previously observed the effects of ionomycin not to be reversible, I did not expect currents to fully recover upon washout.

8.2.3 Caffeine induced effects on HERG currents are not PKC-dependent

I have previously shown that stimulating PKC attenuates HERG current (chapters 5 and 6). To exclude caffeine modulating HERG currents via a PKC dependent pathway, caffeine was applied in the presence of bis-1, a PKC-selective inhibitor. The 'depolarisation to 0 mV' protocol was used to evoke currents, and cells were pre-incubated with 300 nM bis-1 for 3 minutes, which I have previously shown to be sufficient to inhibit the action of PKC upon the HERG channel. After bis-1 application, caffeine was applied in the continued presence of bis-1. Representative currents are shown in figure 8.6A. Effects of caffeine were still observed in these cells, with currents during caffeine and bis-1 application being 51.34 ± 5.54% of control current (n=6), which was not significantly different from the current reduction without bis-1 ($p>0.05$, figure 8.6B). Interestingly, attenuation of the HERG current upon caffeine application was slower in the presence of bis-1, with maximal effects of caffeine being reached after ~105 seconds, compared to 30 seconds in control conditions. Current recovery was also slower, with currents only reaching 90.99 ± 1.94% of control current within two minutes. These results suggest that stimulation of PKC is not responsible for the attenuation of current by caffeine.

Figure 8.5
Raising intracellular calcium levels does not alter the response to caffeine. **A** Representative HERG current traces recorded in control conditions, with 5 μM ionomycin, and with 5 μM ionomycin and 5 mM caffeine. **B** Representative time course of 5 mM caffeine effects (representative of 6 experiments). Peak tail current was normalised to control amplitudes and plotted against time.

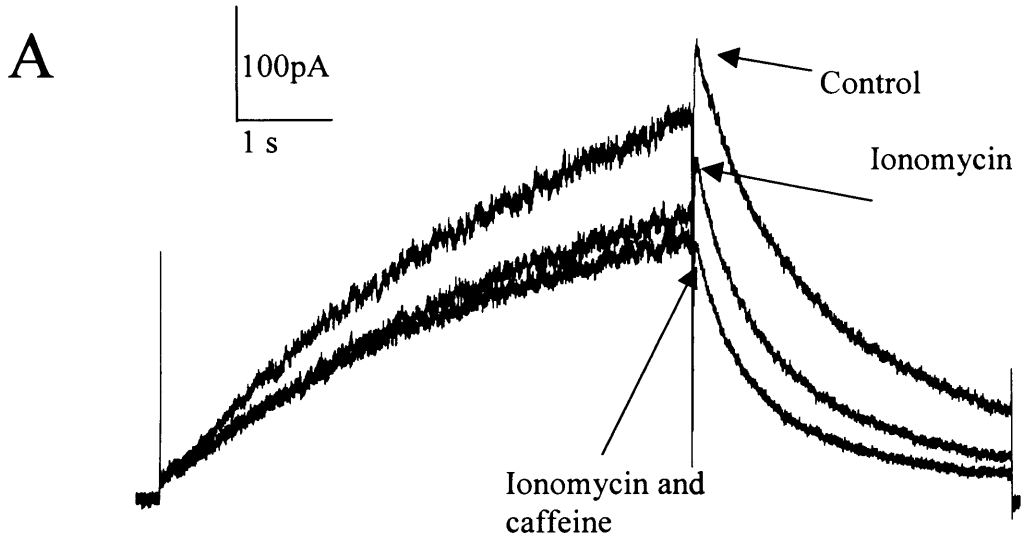

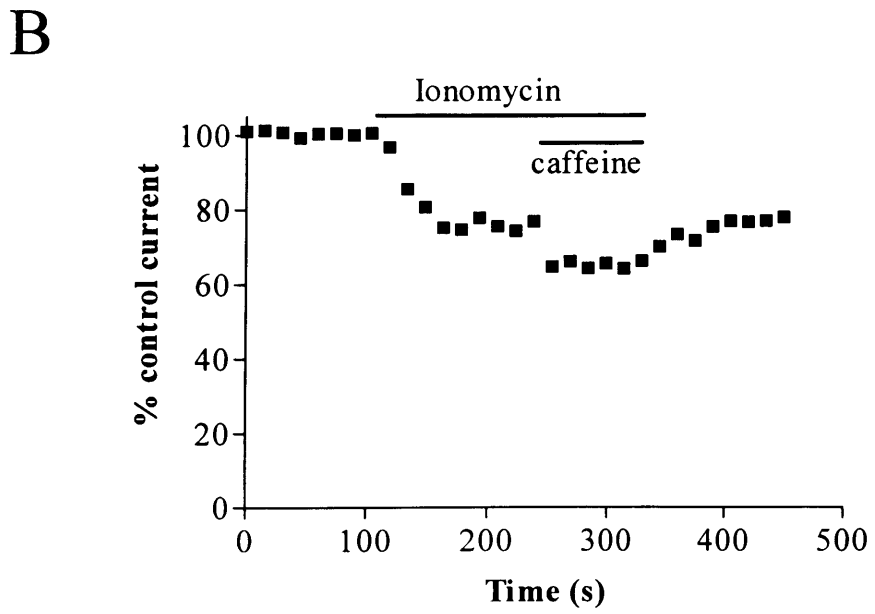

Figure 8.6
The response to caffeine is not reduced by inhibition of PKC by bis-1. **A** Representative HERG currents recorded in control conditions, with 300 nM bis-1 only, and with 300 nM bis-1 and 5 mM caffeine. **B** Representative time course of caffeine effects with bis-1 (representative of 6 experiments).

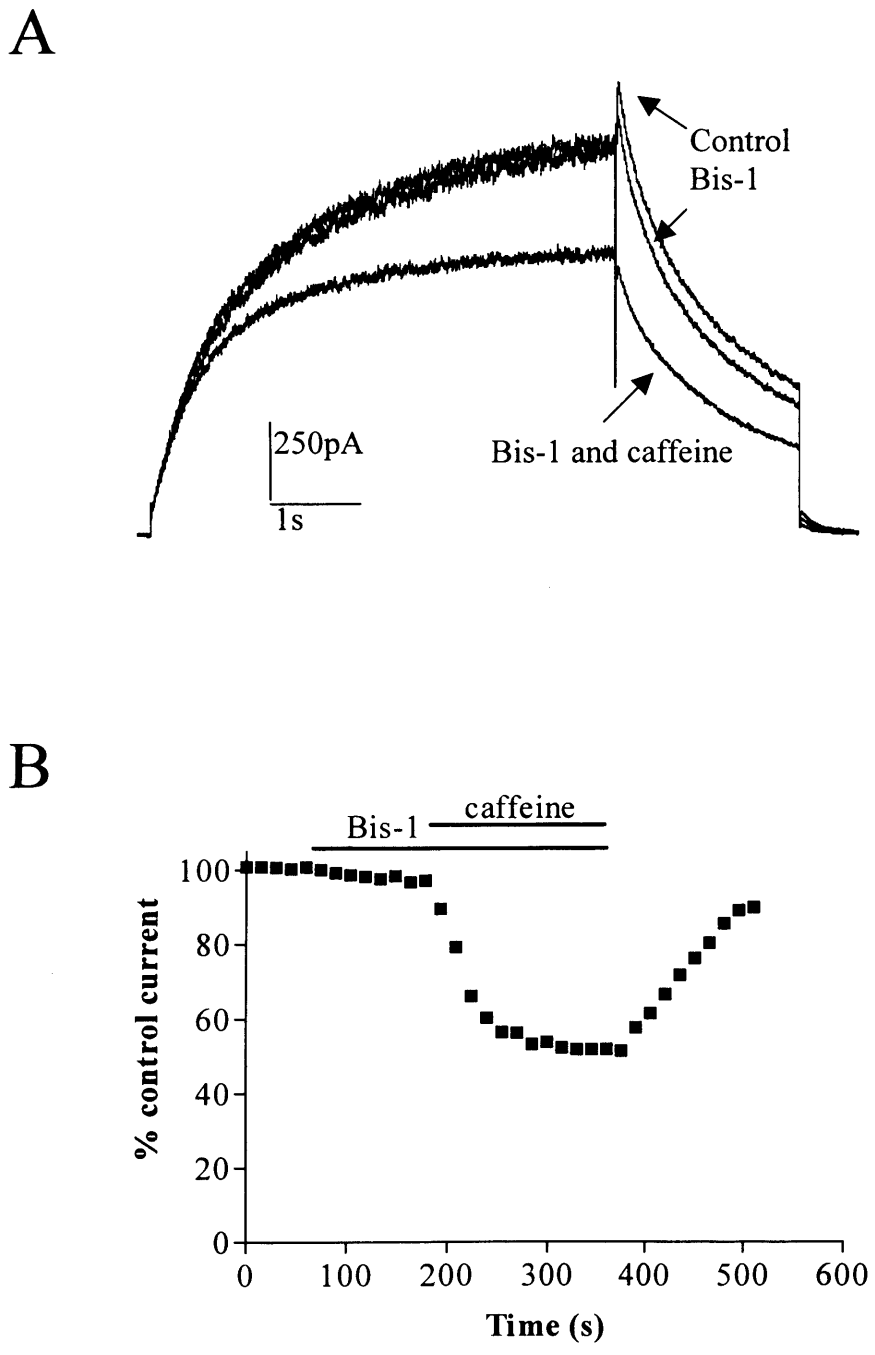

8.2.4 Caffeine-induced effects on HERG currents are not due to its phosphodiesterase inhibitor action

Caffeine also acts as a phosphodiesterase inhibitor, to increase cAMP levels (Butcher and Sutherland, 1962; Lindaman et al., 2002). Effects of both cAMP and PKA on the HERG channel have been previously documented (Cui et al. 2000), and so I wanted to determine if caffeine exerts its effects through either of these mechanisms. Forskolin, an adenylyl cyclase agonist, also raises cAMP and has been shown to cause a slow, non-reversible attenuation of HERG current under our experimental conditions (see chapter 5). The effect of forskolin is also mimicked by the phosphodiesterase inhibitor Ro-20-1724 (data not shown), consistent with a mechanism that raises cytosolic cAMP. As the time courses between forskolin and Ro-20-1724 effects are so different from the time course of caffeine, I predicted caffeine did not modulate HERG current via a cAMP dependent pathway. To test for this, 40 μM forskolin was applied to cells to raise cAMP levels, and caffeine was subsequently applied. Currents were evoked using the 'depolarisation to 0 mV' protocol, and forskolin was applied until maximal attenuation of current was reached. Currents after forskolin application were 75.92 ± 0.72% of control currents. If cAMP levels are already high, it is unlikely that caffeine-induced phosphodiesterase inhibition would further modulate current. However, 5 mM caffeine continued to result in a rapid and reversible attenuation of current. Representative currents are shown in figure 8.7A. Currents during caffeine application were 65.14 ± 4.75% of control currents (n=5), (Figure 8.7B). Washout of caffeine was rapid in these conditions, with currents returning to 88.88 ± 0.45% within one minute.

Together, my results suggest that caffeine does not exert its effects on HERG channel current amplitude by a calcium-, PKC-, PKA- or cAMP-dependent pathway. The rapid changes in current amplitude upon caffeine application and washout suggest caffeine may directly inhibit HERG currents. This possibility was explored using HERG channel mutants that reduced binding of drugs within the main drug binding site in the inner cavity.

Figure 8.7

The response to caffeine is unaltered in the presence of forskolin. **A** Representative HERG currents recorded in control conditions, with 40 μM forskolin only, and with forskolin and 5 mM caffeine. **B** Representative time course of the 5 mM caffeine effects on currents in the presence of 40 μM forskolin (representative of 5 experiments).

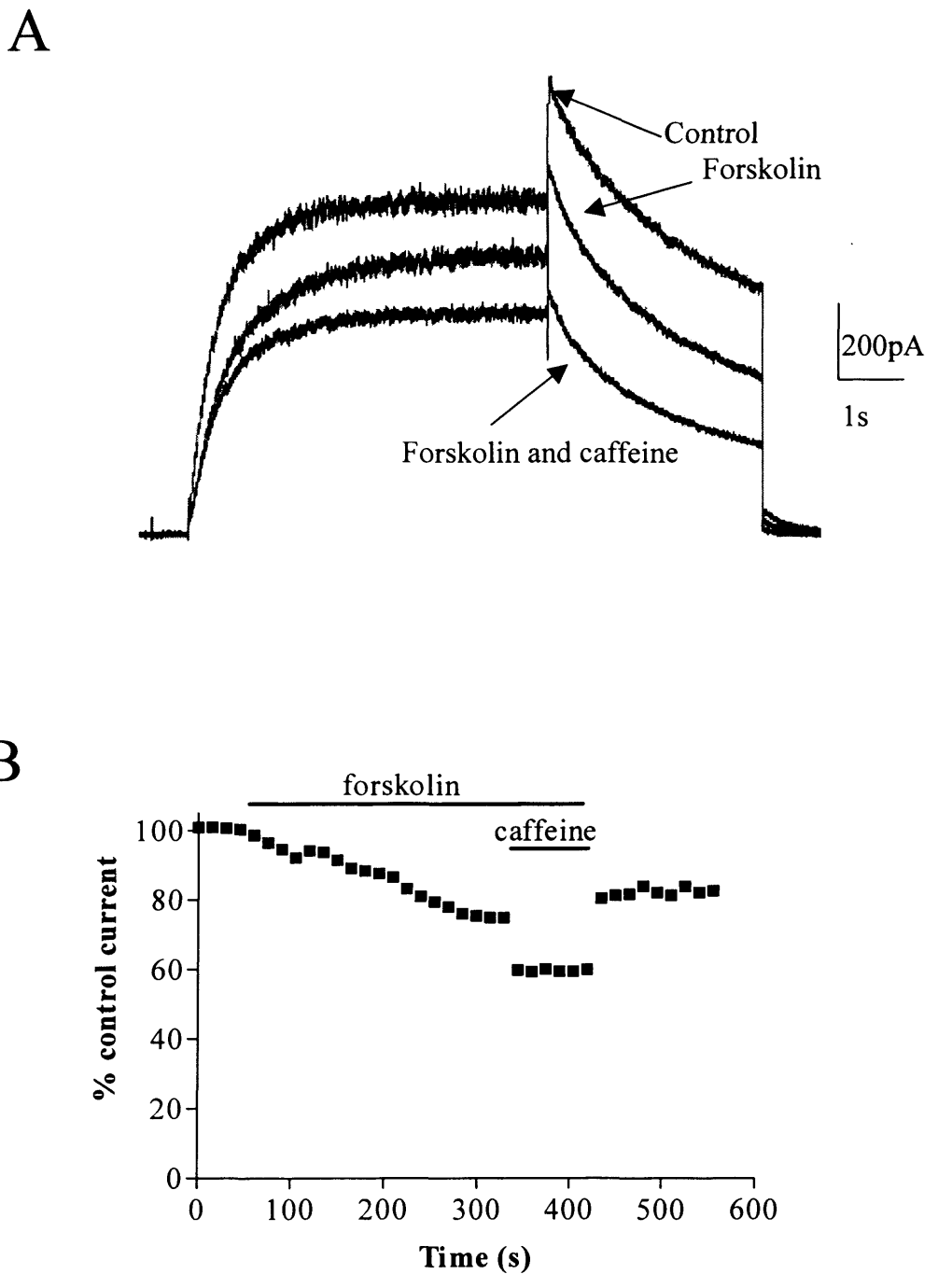

8.2.5 Open channel block and trapping of caffeine within the inner cavity of HERG

Most blockers of HERG exhibit open-state dependence of block, and are thought to bind within the inner cavity of the channel (Perry et al., 2004; Witchel et al., 2004; Mitcheson et al., 2000). To investigate open channel block by caffeine, cells were held at –100 mV, so that the open probability of the HERG channel was very low, then briefly pulsed to +40 mV for 150 ms to rapidly open channels. A 60 ms pulse to –50 mV was then applied to evoke tail currents. The interval between each pulse was 1 second. Once the current had stabilised and control recordings had been made, the cell was held at –100 mV and 5 mM caffeine was applied for two minutes. The voltage protocol described above was then applied in the continued presence of caffeine. Current with the first depolarisation was 64.31 ± 9.36% of control (n=5, figure 8.8A). Continued pulsing in the presence of caffeine did not significantly alter current attenuation. After a two minute washout period, during which cells were again held at –100 mV, currents were 69.41 ± 9.89% of control currents (n=5), thus recovery was not complete. If the attenuation of current is due to direct block of channels by caffeine, block and recovery from block may show use dependence. Thus, longer depolarisations may increase current inhibition and also recovery from inhibition. Cells were held at a membrane potential of –100 mV, and pulsed to +40 mV for a longer duration of 250 ms. Once current had stabilised, membrane potential was again held at -100mV for two minutes as caffeine was applied, before depolarisations were continued. The mean tail current was 56.72 ± 1.96% of control currents with the first pulse, which was a slightly greater block than with the 150 ms pulse. After a two minute washout period, during which cells were held at –100 mV, currents recovered to 82.72 ± 3.69% of control current on the first pulse, rising to 86.41 ± 3.41% with subsequent depolarisations (n=5). The mean time course for these effects is shown in figure 8.8A. However, the finding that inhibition is maximal with the first pulse could indicate either very rapid open state block or closed state block. To distinguish between these possibilities I used the envelope of tails protocol (described in chapter 3). This allows the amount of block to be measured as the pulse duration is lengthened. If caffeine is a closed state blocker then the block will be independent of pulse duration. If, however, caffeine is an open state blocker then inhibition will increase with progressively longer depolarisations as more channels are activated. This protocol was applied whilst

Figure 8.8

Caffeine acts as an open channel blocker. **A** Each data point represents mean, normalised to control peak tail current amplitudes plotted against time. 5 mM caffeine application and washout were carried out while the cells were held at –100 mV, to keep channels in the closed state. Pulse duration was either 150 or 250 ms at a frequency of 1Hz (n=5 for each data point). **B** Onset of block assessed with an envelope of tails protocol. Peak tail currents before and during 5 mM caffeine application were normalised to maximum control amplitudes and plotted against time (n=5). **C** Percentage inhibition of HERG current by 5 mM caffeine with progressively longer depolarisations (n=5).

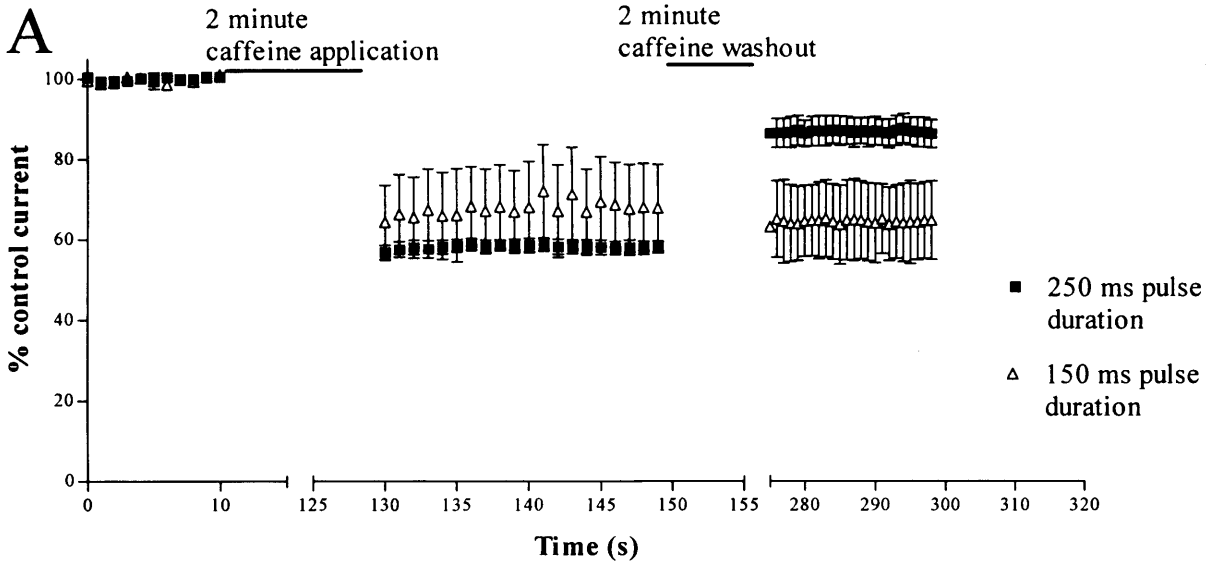

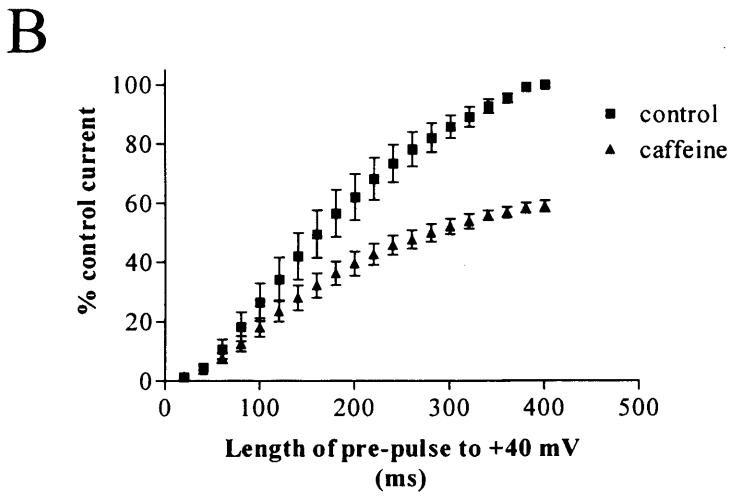

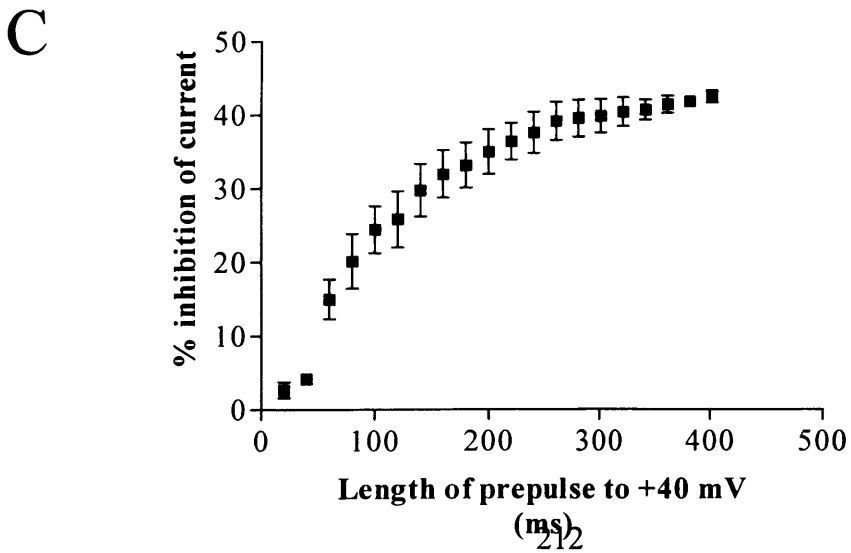

cells were superfused with control Tyrode. Cells were then held at a membrane potential of –100 mV for two minutes, whilst caffeine was applied. After this time, the envelope of tails protocol was run again, in the continued presence of caffeine. Peak tail currents, normalised to maximal current with a 400 ms pulse in control conditions, were calculated for each cell and mean results can be seen in figure 8.8B. The difference in current amplitudes before and during caffeine application was measured and a mean percentage inhibition was calculated and plotted against time (Figure 8.8C). Caffeine caused only a 2.69 ± 1.08% inhibition after 20 ms but this block increased progressively as pulse duration was lengthened, with a mean time constant for inhibition of 95.82 ± 20.95 ms. These results suggest caffeine block of HERG is gating-dependent, and that the site of interaction between caffeine and the channel is in the inner cavity, behind the activation gate.

8.2.6 Phe656 and Tyr652 residues mediate caffeine binding

The drug binding site within the inner cavity is formed by amino acid residues from the inner helices and part of the potassium channel selectivity filter. Two aromatic residues on the inner helices (S6), Phe656 and Tyr652 are required for high affinity block by many well known HERG channel blockers, including clofilium and ibutilide (Perry et al., 2004), propafenone (Witchel et al., 2004), MK-499 (Mitcheson et al., 2000) and quinidine (Sănchez-Chapula et al., 2003). Mutating these residues to alanine can reduce the IC_{50} more than 100-fold. To investigate if caffeine binds within the inner cavity by interacting with Phe656 or Tyr652, the effect of the alanine mutants on caffeine inhibition was determined. The gene for expression of these two mutants (F656A and Y562A) was in a plasmid for expression in *Xenopus* oocytes, and therefore subsequent experiments were done in this expression system. WT HERG channels were also expressed in *Xenopus* oocytes to compare the block of caffeine in mammalian tissue and oocytes. WT HERG currents were recorded by pulsing to 0 mV for 5 seconds from a potential of –90 mV and tail currents were elicited with a 400 ms pulse to –70 mV. This protocol was repeated every six seconds, so that channels were in the open state and activated for most of the time. Representative currents are shown in figure 8.9A. 5 mM caffeine caused less attenuation of current in oocytes over HEK cells in wild type channels, with currents during caffeine application being 77.76 ± 2.14% of control currents (n=7,

Figure 8.9
WT HERG currents in *Xenopus* oocytes are blocked by caffeine to a lesser extent than HERG currents in HEK cells. **A** Representative WT HERG currents recorded in *Xenopus* oocytes before and during 5 mM caffeine application. **B** Mean time course of 5 mM caffeine effects on WT HERG currents (n=7). Peak tail currents were normalised to control amplitudes and mean, normalised current plotted against time.

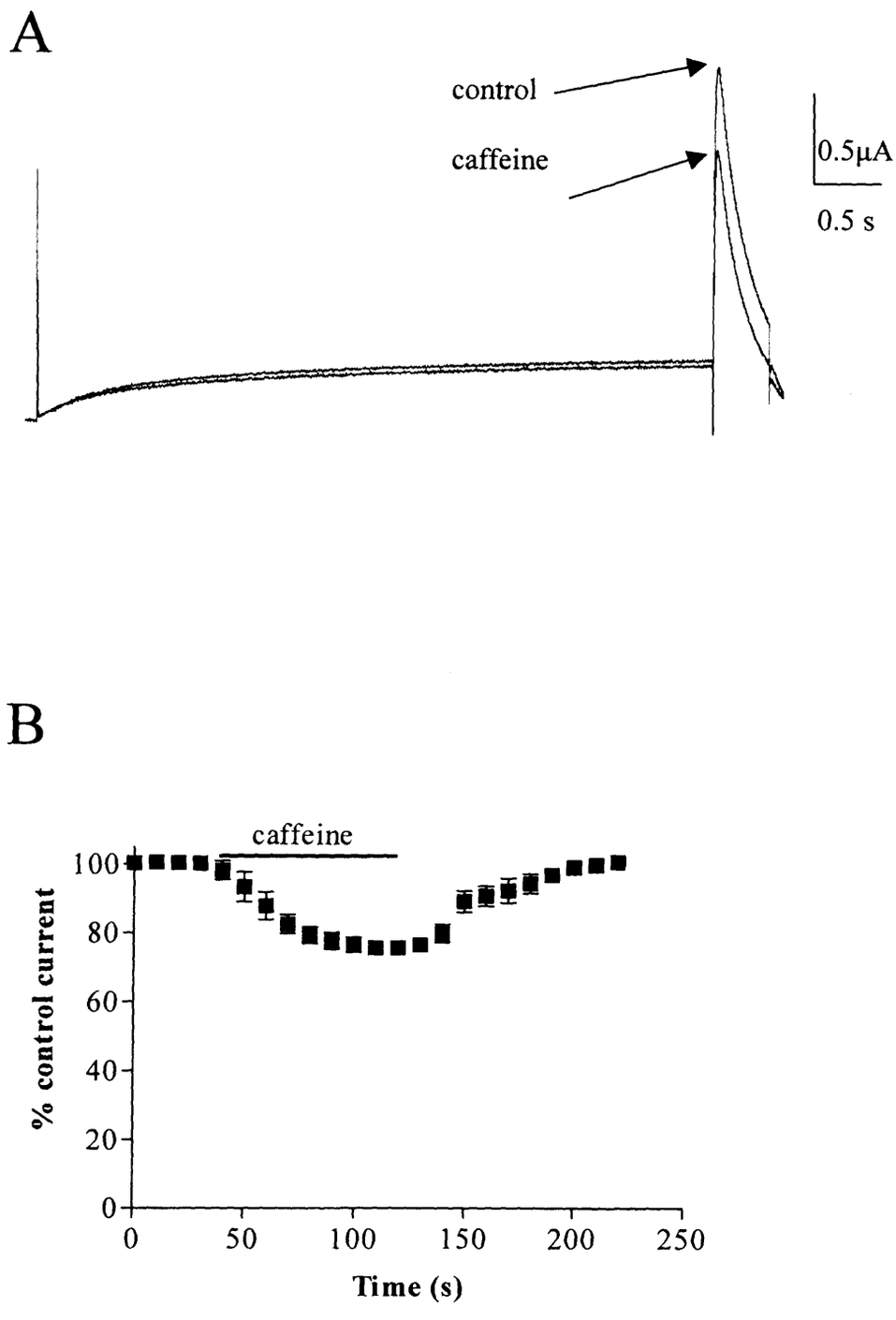

figure 8.9B and 8.10C). This is expected, as many drugs are less potent in oocytes than mammalian cells. Attenuation of current with caffeine was still rapid and fully reversible. Full effects of caffeine were observed within 24 seconds. Washout was rapid, with currents recovering to 98.79 ± 0.81% of control currents within 24 seconds.

Y652A currents were recorded using the same voltage protocol as for WT channels. These channels showed a reduced sensitivity to caffeine, as current during caffeine application was 92.64 ± 1.49% of control current (n=9, figure 8.10A and C). This was significantly different to inhibition of WT currents ($p<0.05$), and suggests that this mutant decreases the ability of caffeine to bind to and block the channels.

To record currents from F656A HERG channels, similar protocols were used but tail currents were elicited with steps to –140 mV. F565A mutant channels also showed a lowered sensitivity to application of caffeine. Current during caffeine application was 93.59 ± 1.42% of control current (n=9, figure 8.10B and C) and was significantly different to the effects of caffeine on WT channels ($p<0.05$). To investigate if this loss of sensitivity to caffeine for the F656A mutant channel is due to a decreased ability of caffeine to bind to these channels, or just simply due to measuring tail currents at –140 mV, therefore reversing ion flux, I recorded WT currents using the F656A voltage protocol. In these conditions, caffeine inhibition was not significantly different to current block by caffeine in WT channels when tails were measured at –70 mV (n=7, $p>0.05$). This suggests the decreased sensitivity of the F656A mutant to caffeine is due to a decreased ability of caffeine to bind to the channel, rather than reduction of inhibition due to inward potassium flux at the tail potential. Thus, both Phe656 and Tyr652 are required for WT-like inhibition of HERG currents by caffeine. Since these residues are located in the inner cavity it provides further evidence that caffeine exerts its effects on HERG via an open channel block rather than by a second messenger mediated mechanism.

Figure 8.10

F656A and Y652A HERG mutants shown reduced sensitivity to block by caffeine. A Representative Y652A HERG tail currents in control conditions (black) and with 5 mM caffeine (red). Inset shows portion of the voltage protocol from which the current trace is taken. **B** Representative F656A HERG tail currents in control conditions (black) and with 5 mM caffeine (red). Inset shows the portion of the voltage protocol from which the current trace is taken. **C** Mean data showing percentage tail current remaining in WT, Y656A and F656A HERG measured at 70 mV (WT and Y652A) or 140 mV (WT and F656A). Peak tail currents was normalised to control amplitudes ($n \geq 7$ for each data set). * shows significance at $p<0.05$ compaed to the appropriate WT control.

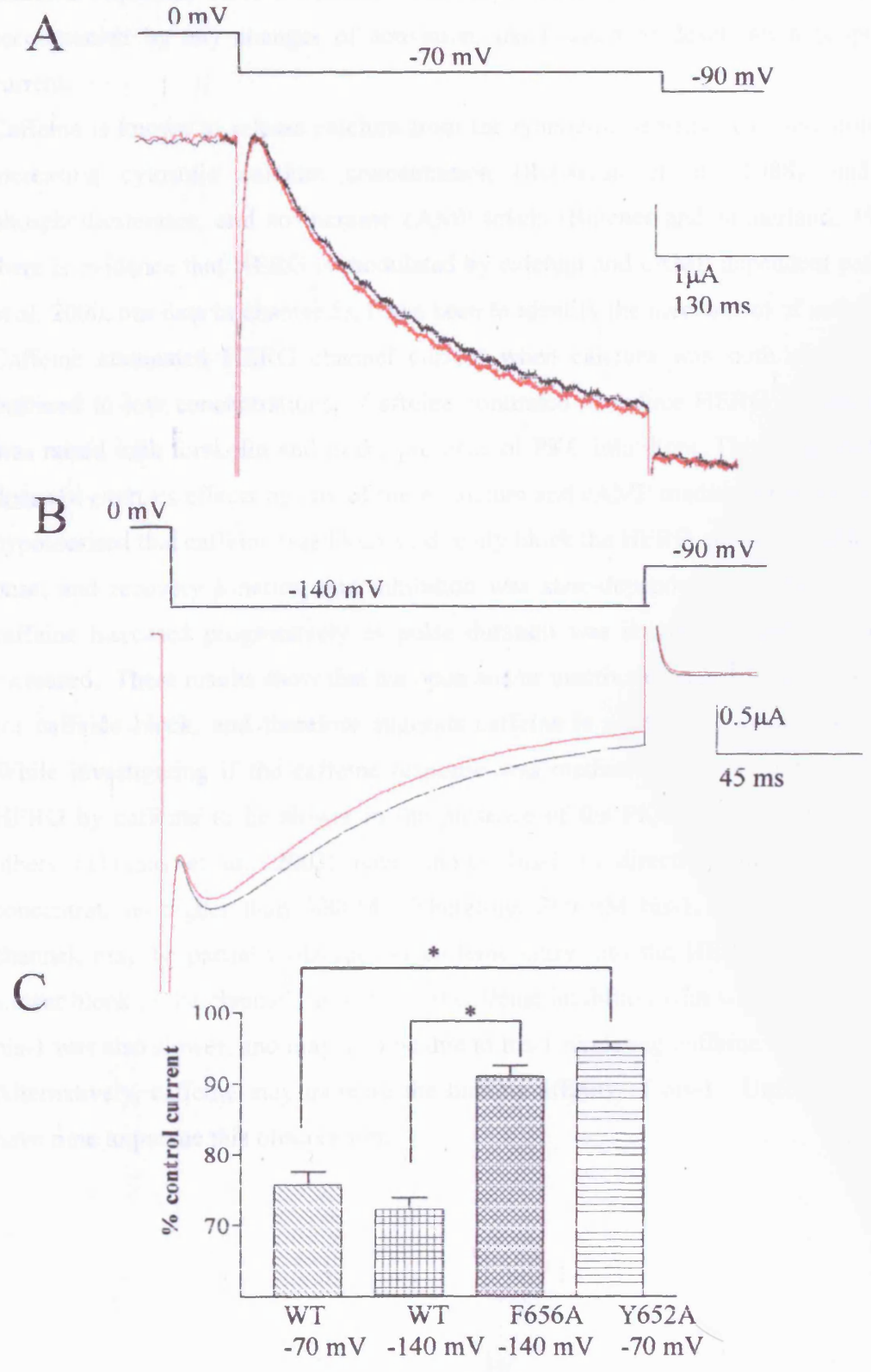

8.3 Discussion

8.3.1 Effects of caffeine

In this series of experiments I have shown caffeine to rapidly and reversibly attenuate HERG channels expressed in both HEK 293 cells and *Xenopus* oocytes. This attenuation was not accompanied by any changes of activation, inactivation or deactivation properties of the current.

Caffeine is known to release calcium from the ryanodine-sensitive calcium stores, therefore increasing cytosolic calcium concentration (Rousseau et al., 1988), and to inhibit phosphodiesterases, and so increase cAMP levels (Butcher and Sutherland, 1962). Since there is evidence that HERG is modulated by calcium and cAMP dependent pathways, (Cui et al. 2000, our data in chapter 5), I was keen to identify the mechanism of action of caffeine. Caffeine attenuated HERG channel current when calcium was both elevated and when buffered to low concentrations. Caffeine continued to reduce HERG current when cAMP was raised with forskolin and in the presence of PKC inhibitors. This suggests that caffeine does not exert its effects by any of these calcium and cAMP mediated pathways. I therefore hypothesised that caffeine was likely to directly block the HERG channel. Caffeine had rapid onset and recovery kinetics, and inhibition was state-dependent. Inhibition of HERG by caffeine increased progressively as pulse duration was lengthened and channel activation increased. These results show that the open and/or inactivated state of the channel is required for caffeine block, and therefore suggests caffeine is an open-channel blocker of HERG. While investigating if the caffeine response was mediated by PKC, I found inhibition of HERG by caffeine to be slower in the presence of the PKC inhibitor bis-1. Myself, and others (Thomas et al., 2003) have shown bis-1 to directly inhibit HERG current at concentrations higher than 300nM. Therefore, 300 nM bis-1, although not blocking the channel, may be partially obstructing caffeine entry into the HERG channel, leading to a slower block of the channel. Recovery of caffeine inhibition with washout in the presence of bis-1 was also slower, and may also be due to bis-1 hindering caffeine exit from the channel. Alternatively, caffeine may increase the binding affinity of bis-1. Unfortunately, I did not have time to pursue this observation.

8.3.2 Locating the HERG binding site of caffeine

To locate the binding site of caffeine, I used two mutants of the HERG channel, F656A and Y652A, that are known to reduce the sensitivity of HERG to a large number of long QT-inducing drugs that are open channel blockers. The mutated residues are located on the inner vestibule of the HERG channel, shown as a cartoon in Figure 8.11A and face into the cavity of the channel. Both are aromatic residues, which can mediate hydrophobic and electrostatic interactions, the latter of which can be of two types. The π electron faces of the aromatic groups can mediate π-stacking interactions with other aromatic groups, and cation-π interactions with charged amines. I found that replacing either the Phe656 or Tyr652 residues with the small amino acid alanine, reduced the sensitivity of the channel to caffeine. This suggests caffeine interacts with these residues in the WT channel, and therefore binds within the inner cavity of the channel.

Figure 8.11B shows the structure of caffeine. Caffeine is a member of the alkaloid family. The core of the molecule is a purine, containing five carbon atoms and four nitrogen atoms linked together. A number of studies have shown that caffeine is able to interact with aromatic residues on other proteins. In 2000, Tsitsanou et al. showed caffeine to bind at the purine inhibitor site on glycogen phosphorylase A. This binding occurred by caffeine intercalating between the two aromatic rings of Phe285 and Tyr613 to form π-stacking interactions. Kapuscinski et al., 2002 found that caffeine binds to aromatic mutagens, for example quinacrine mustard, and reduces the pharmacological activity of these mutagens. Thus, caffeine may act as a protective agent in some cancer types. The interaction between caffeine and the aromatic agents was again due to π stacking interactions. Caffeine has also been shown to decrease the effective concentrations of carcinogenic polycyclic aromatic agents such as quinacrine mustard, but not aliphatic agents (Piosik et al., 2003). These three studies, although not carried out on ion channels, indicate caffeine has the ability to interact with aromatic residues. My results are consistent with π-stacking interactions between caffeine and the Phe656 and Tyr652 residues on HERG, although I cannot rule out additional interactions that may take place.

Figure 8.11
The HERG channel inner cavity and caffeine structure. **A** Cartoon of the inner vestibule of the HERG channel. Cartoon only shows 2 subunits for clarity. Tyr652 and Phe656 residues are shown in green, potassium ions shown as purple circles. **B** The chemical structure of caffeine.

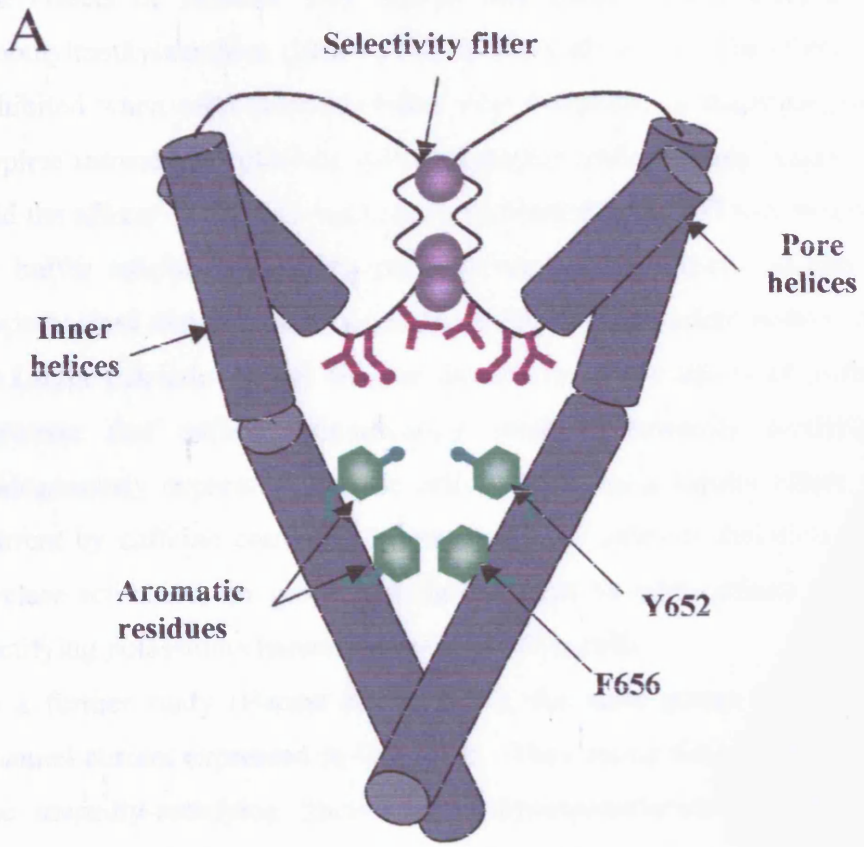

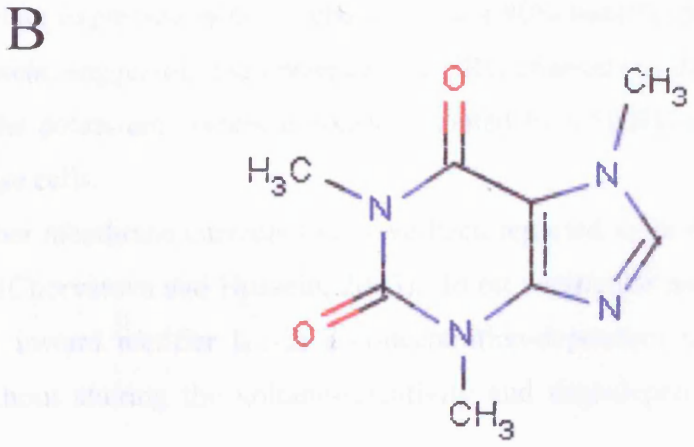

8.3.3 Effects of caffeine on other ion channels

Several studies have shown that caffeine can inhibit other ion channels. The rapid, reversible effects of caffeine shown in my study concur with results of Barros et al (1996), who showed caffeine to cause a reversible increase of electrical activity along with a depolarisation of membrane potential in GH_3 cells, a rat anterior pituitary cell line. They were unable to mimic the effects of caffeine with agents that cause similar effects, such as forskolin and isobutylmethylxanthine (IBMX) that raise cAMP levels. The effects of caffeine could not be inhibited when cells were incubated with ryanodine or thapsigargain, both of which would deplete intracellular calcium stores, therefore inhibiting any release of calcium by caffeine, and the effects of caffeine could not be inhibited used EGTA-containing intracellular solution to buffer calcium. Caffeine partially blocks the L-type calcium channel, so the group hypothesised that this may be reducing the Ca^{2+}-dependent potassium currents. Nisoldipine, an L-type calcium channel blocker, did not mimic the effects of caffeine. The group did find however that caffeine significantly inhibited inwardly rectifying potassium currents endogenously expressed in these cells, to produce a similar effect. Since the reduction of current by caffeine could not be attenuated by calcium chelation or mimicked by adenylyl cyclase activators, the group hypothesised that 10 mM caffeine directly blocks the inwardly rectifying potassium channel expressed in GH_3 cells.

In a further study (Barros et al., 1997), the same group further identified the potassium channel current expressed in GH_3 cells. They found the effects of caffeine to be specific to the inwardly-rectifying fraction of a hyperpolarisation-evoked potassium current. The current was also inhibited by astemizole, a histamine receptor agonist known to block the HERG channel. The group was also able to show a partial sequence of 300 base pairs from protein expressed in GH_3 cells to show a 90% homology to channels encoded by the HERG protein, suggesting the presence of HERG channels in this tissue. The group concluded that it the potassium current is likely mediated by a HERG-like potassium channel expressed in these cells.

Other membrane currents that have been reported to be inhibited by caffeine include I_{K1} and I_{to} (Chorvatova and Hussein, 2003). In rat ventricular mycocytes, caffeine partially inhibited the inward rectifier I_{K1} in a concentration-dependent manner. Caffeine also inhibited I_{to} without altering the voltage-sensitivity and time-dependence of activation or inactivation.

The effects of caffeine were fully reversible. The same study also showed 10 mM caffeine to partially inhibit the delayed rectifier I_K.

$GABA_A$ current in hippocampal slices is also significantly inhibited by caffeine (Taketo et al., 2004), in a manner not dependent on cytoplasmic calcium, and which could not be mimicked by ryanodine or forskolin, indicating the inhibtion may be due to direct block of channels. Taking the results from this study, along with results from other studies, implies that caffeine may act as a general inhibitor of ion channels. My study has shown that application of caffeine inhibits the HERG channel.

8.3.4 Relevance of caffeine inhibition of HERG currents

8.3.4.1 Caffeine use as a calcium-release tool

Several studies now suggest it caffeine not specific for the ryanodine receptor, and that this needs to be taken into account when using caffeine as a calcium-release tool. At present, caffeine is widely used to investigate mechanisms of E-C coupling in cardiac myocyte preparations. Many studies use caffeine at concentrations higher than 5 mM, which I have found to profoundly inhibit HERG currents. Caffeine may not only elicit calcium release, but it may also inhibit I_{Kr}. This could therefore prolong action potential duration or contaminate measurements of calcium dependent currents such as the Na/Ca exchange current. Caffeine also blocks a number of other channels expressed in cardiac myocytes (as already discussed), which again could lead to a misinterpretation of data when using caffeine. Of course, what must be taken into account is that mostly, caffeine is applied in 'puffs' – short applications to myocyte preparations to induce calcium release. Under these conditions it is unclear what effect caffeine would have on ion channels, although inhibition of HERG is also rapid. HERG is expressed in a variety of tissues in addition to cardiac myocytes. These include some cancer cells and neuronal tissues. Again, application of caffeine for the purpose of calcium release in these tissues could result in a misinterpretation of results.

8.3.4.2 Caffeine as a long QT-inducing drug?

Caffeine is a substance that is commonly part of the diet and lifestyle in today's culture. However, we believe caffeine is unlikely to be a long QT syndrome-inducing drug, since it only produces a significant inhibition of HERG channel current when used in the milli-molar

concentration range. A study carried out in 1982 showed the average bloodstream concentration of caffeine in non-smoking males to be 10.9 μM (Smith et al., 1982). This is not at a concentration that would significantly block HERG. Added to this is the fact that caffeine does not accumulate in the body. Caffeine is almost fully metabolised by the liver, with the half-life of caffeine in the blood stream being between 2.5 - 4.5 hours. This means the concentration of caffeine in the blood stream is extremely unlikely to reach the concentrations used in this study, and therefore caffeine is unlikely to cause any significant change to the ECG as a result of blocking the HERG channel.

Chapter 9
General Discussion and Summary

9.1 Modulation of the HERG channel by second messengers

9.1.1 Modulation of HERG by PKC

My studies have shown PKC activation to modulate HERG channel currents, and HERG subunits. Activation of PKC caused a significant attenuation of HERG current, which was accompanied by a positive shift in voltage-dependent activation, and an acceleration of deactivation of currents. My evidence suggests these effects are due to an increase in phosphorylation of HERG channel subunits in response to PKC activation. Phosphorylation of HERG subunits has not previously been investigated in mammalian cells. Zhang et al. (2002) showed the HERG channel expressed in *Xenopus* oocytes to be phosphorylated under basal conditions, but were unable to detect a change in phosphorylation in response to application of PMA or forskolin. However, modulation of HERG in mammalian cells shows differences from modulation in *Xenopus* oocytes, raising the possibility that there are important differences in how HERG channels in mammalian and amphibian cell types are modulated.

The effects of PKC activation on HERG current are independent of conventional PKC and PKA phosphorylation sites on the channel, and although I have shown OAG-mediated increases in phosphorylation to be PKA-independent, I have been unable to investigate if it is independent of conventional PKC phosphorylation sites. I can therefore draw several hypotheses about how activation of PKC modulates HERG current. 1) PKC may phosphorylate the HERG subunits at atypical phosphorylation sites, 2) Signalling pathways down-stream of PKC may phosphorylate HERG subunits, 3) PKC may phosphorylate the HERG channel at Thr74, the remaining conventional PKC phosphorylation site in the ΔPKC HERG mutant. Obviously, further experiments must be carried out to fully dissect the modulation of HERG by PKC. These experiments could include tagging of the 18M and ΔPKC HERG mutants with an antibody epitope to allow phosphorylation to be monitored with PKC activation. Inhibition of signalling pathways down-stream of PKC, such as MAP kinase and the src-family of kinases could also reveal the PKC-mediated mechanism. Indeed, it has been previously shown that src kinase interacts with ERG subunits and modulates

current expressed in MLS-9 cells (Cayabyab and Schlichter, 2002a), although this study showed the channel was constitutively phosphorylated by the kinase.

Phosphopeptide mapping could be a useful tool in mapping the sites of PKC phosphorylation on the HERG channel. This technique allows the phosphorylation state of individual regions of the channel to be monitored in response to a stimulus, such as PKC activation. This technique has previously been used to map the sites of PKA phosphorylation on the Kv4.2 channel (Anderson et al., 2000), and the L-type calcium channel (Gerhardstein et al., 1999). Results from this technique would allow us to observe changes in phosphorylation in response to PKC and other stimuli. The technique could be applied to investigate many aspects of HERG phosphorylation.

PKC-mediated phosphorylation of HERG channel subunits shifts the voltage dependence of activation to more positive potentials, and accelerates deactivation kinetics of HERG current. Deactivation of the HERG channel is thought to be due, in part, to interactions of the N-terminus with the voltage sensing domain. Studies have shown that if the first portion of the HERG channel is deleted (up to amino acid 370), deactivation of the channel is significantly faster (Schronherr and Heinemann, 1996). Morais-Calbris et al. (1998a) showed deactivation of N-truncated channels could be rescued by intracellular application of a peptide encoding the first 135 amino acids of the channel. Mutating Gly546 produced a mutant that was identical to N-truncated mutants, suggesting this residue was important for N-terminal binding to the pore of the channel (Wang et al., 1998). I have shown PKC activation to significantly accelerate deactivation kinetics, which may suggest the possibility that PKC-mediated phosphorylation hinders access of the N-terminal to the intracellular side of the pore. This may be due to several mechanisms. PKC phosphorylation on the N-terminus (which may be possible at Thr74, atypical phosphorylation sites or non-PKC phosphorylation sites) may hinder access to the pore either alone, or by recruitment of accessory subunits, modifying N-terminus interactions. Indeed, the Thr74 residue is close to the PAS domain of HERG (Morais-Cabral et al., 1998b), a motif that can mediate protein-protein interactions (Anantharaman et al., 2001). Alternatively, phosphorylation at the site of N-terminal binding domain may also hinder N-terminal slowing of deactivation. Phosphopeptide mapping could allow me to map the site of PKC-mediated phosphorylation to test these hypotheses. Although PKC-mediated phosphorylation of HERG positively shifts

the voltage dependence of activation in my study, it does not alter inactivation of the channel. Although these two processes are seemingly controlled by a single voltage sensor, the processes appear paradoxically seperate. Mutations in the S4-S5 linker also alter activation, but not inactivation (Sanguinetti and Xu, 1999), whereas several mutants that shift or remove inactivation activate normally. The effect PKC activation has on voltage dependent activation of the channel may be due to several mechanisms. Allosteric effects of phosphorylation at the N- or C-termini as well as the voltage sensor could alter voltage sensitivity. How phosphorylation modifies channel activity remains largely unknown.

9.1.2 Modulation of HERG by PKA

I have also shown that HERG current amplitude is attenuated by activation of PKA. Previous evidence suggested all four phosphorylation sites on HERG contribute to forskolin- and phosphodiesterase-mediated responses (Thomas et al., 1999, Zhang et al., 2002), and it is the belief that phosphorylation of the channel causes attenuation of current and a positive shift of voltage-dependent activation. However, I have shown in this study that HERG subunits are dephosphorylated by forskolin. Dephosphorylation depends on both PKA activity and the presence of PKA phosphorylation sites on HERG, and can be blocked by phosphatase inhibition. This evidence suggests PKA phosphorylation permits recruitment of phosphatases, and a net dephosphorylation of the channel. There are many examples of dynamic regulation of target proteins. A family of proteins known to co-ordinate signalling pathways and bind to target proteins are the AKAPs. It would therefore be of interest to determine if AKAP proteins form complexes with the HERG channel. The HERG channel sequence contains a modified leucine zipper (personal communication, Caroline Dart, Department of Cell Physiology and Pharmacology, University of Leicester). The leucine/isoleucine zipper motif on proteins has previously been shown to mediate AKAP interactions with BK channels (Tian et al., 2003), Ryanodine receptors (Marx et al., 2000; Marks et al. 2002), L-type calcium channels (Hulme et al., 2002) and I_{Ks} channels (Marx et al., 2002). Potential future experiments to investigate a role for AKAPs in the modulation of HERG could include generation of a HERG channel mutant, containing point mutations at the leucine zipper of HERG to break interactions with AKAPs, then investigate if modulation of the channel is modified or lost.

It is likely that HERG subunits form part of a macromolecular complex. It has previously been shown HERG can interact with 14-3-3 proteins (Kagan et al., 2002) and β-integrins (Cherubini et al., 2002). Although neither of these studies investigated HERG in primary tissues, it is likely that I_{Kr}, the current for which HERG encodes the pore-forming subunit, is also due to formation of a macromolecular complex. The contribution of AKAPs to cardiac ion channel currents was shown with I_{Ks}, which associates with yotiao, a 210kDa protein, which is also capable of binding the NMDA receptor and protein phosphatase I in the brain (Westphal et al., 1999). The binding of yotiao to I_{Ks} mediated PKA modulation of the current, and binding was blocked by a single point mutation of the channel, G589D (Marx et al., 2002). This mutation has been observed in some patients with long QT syndrome, and lies within the leucine zipper motif of I_{Ks}, found at the C-terminal of the channel. A loss of AKAP binding causes attenuation of I_{Ks}, therefore reducing its impact on the cardiac action potential, and inducing long QT syndrome. Further studies would allow assessment of the contribution of AKAPs in modulation of HERG and I_{Kr}.

9.1.3 Physiological relevance of modulation of HERG

I have shown HERG current is attenuated upon stimulation of both PKC and PKA due to changes in overall phosphorylation of the channel subunits. The physiological relevance of this must be taken into account, as HERG current attenuation can cause long QT syndrome and sudden death due to cardiac arrhythmias. Activation of PKC and PKA are linked to a large variety of receptors in cardiac and other HERG-expressing tissues, so potentially a large variety of extracellular signals could cause attenuation of HERG current. However, the specificity of these signalling pathways must be considered. Specificity of signalling pathways is conveyed in a number of ways, including scaffolding proteins such as AKAPs and RACKs, which act to decrease the occurrence of inappropriate phosphorylation events, and may be expressed in cardiac myocytes but not HEK cells, in which I have characterised HERG phosphorylation. Therefore, to fully understand *in vivo* modulation of HERG further studies need to be carried out.

9.2 Drug block of HERG current

In this study I have shown caffeine to act as an open channel blocker of the HERG channel. Block of the channel by caffeine seems to be mediated by Phe656 and Tyr652 residues in the WT channel, which are located within the inner cavity. HERG is unique in that it has an unusually large inner cavity, and two aromatic amino acid residues (Phe656 and Tyr652) that face into this cavity, which may allow HERG to form hydrophobic, polar and cationic interactions with drugs and make HERG more susceptible to drug block. Many studies have shown that one or both of these binding sites co-ordinate binding of drugs to HERG, including clofilium and ibutilide (Perry et al., 2004), propafenone (Witchel et al., 2004), MK-499 (Mitcheson et al., 2000) and quinidine (Sănchez-Chapula et al., 2003). A number of studies have shown caffeine to bind to aromatic groups of proteins (Tsitsanou et al., 2000; Kapuscinski et al., 2002; Piosik et al., 2003), by π-stacking interactions, suggesting this may be the mechanism by which caffeine binds to HERG. However, it seems that caffeine-block is not limited to HERG channels. Studies have suggested caffeine-block of potassium channels (Barros et al., 1996; Chorvatova and Hussein, 2003) and voltage-gated calcium channels (Zhao et al., 2002), suggesting caffeine acts as a rather non-specific blocker. However, none of these studies have mapped the site of interaction of caffeine. The blocking effects of caffeine must be taken into account when using caffeine as a tool to raise cytosolic calcium on HERG-expressing preparations such as cardiac, neuronal and some cancerous tissue.

Chapter 10
Bibliography

Abbott G and Goldstein S. Physiology and pathophysiology of the *Min*K-Related Peptides (MiRPs). Molecular Interventions 1: 95-107, 2001.

Abbott G, Sesti F, Splawski I, Buck M, Lehmenn M, Timothy K, Keating M and Goldstein S. MiRP1 forms I_{Kr} potassium channels with HERG and is associated with cardiac arrhythmia. Cell 97: 175-187, 1999.

Ali S, Chen X, Lu M, Xu J, Lerea K and Hebert S. The A kinase anchoring protein is required for mediating the effect of protein kinase A on ROMK1 channels. Proceedings - National Academy of Science - USA 95: 10274-10278, 1998.

Alkondon M, Reinhardt S, Lobron C, Hermsen B, Maelicke A, Albuquerque E. Diversity of nicotinic acetylcholine receptors in rat hippocampal neurons. II. The rundown and inward rectification of agonist-elicited whole-cell currents and identification of receptor subunits by in situ hybridization. Journal of Pharmacology and Experimental Theraputics 271(1):494-506, 1994.

Anantharam A, Lewis A, Panaghie G, Gordon E, McCrossen Z, Lerner D and Abbott G. RNAi interference reveals that endogenous xenopus *Min*K-related peptides govern mammalian K^+ channel function in oocytes expression studies. The Journal of Biological Chemistry 278: 11739-11745, 2003.

Anantharaman V, Koonin E, Aravind L. Regulatory potential, phyletic distribution and evolution of ancient, intracellular small-molecule-binding domains. Journal of molecular biology 307(5):1271-92, 2001.

Anderson A, Adams J, Qian Y, Cook R, Pfaffinger P and Sweatt J. Kv4.2 phosphorylation by cyclic AMP-dependent protein kinase. The Journal of Biological Chemistry 275: 5337-5346, 2000.

Arcangeli A, Becchetti A, Cherubini A, Crociani O, Defilipp P, Guasti, G, Pillozzi, S, Olivotto M, Wanke E. Physical and functional interaction between integrins and hERG potassium channels. Biochemical Society Transactions 32 (5): 826-827, 2004.

Arcangeli A, Bianchi L, Becchetti A, Faravelli L, Coronnello M, Mini E, Olicotta M and Wanke E. A novel inward-rectifying K^+ current with a cell cycle dependence governs the resting potential of mammalian neuroblastoma cells. Journal of Physiology 489.2: 455-471, 1995.

Arcangeli A, Faravelli L, Bianchi L, Rosati B, Gritti A, Vescovi A, Wanke E, Olivotto M. Soluble or bound laminin elicit in human neuroblastoma cells short- or long-term potentiation of a K+ inwardly rectifying current: relevance to neuritogenesis. Cell Adhesion Communications 4(4-5): 369-85, 1996.

Arcangeli A. HERG potassium channels are more frequently expressed in human endometrial cancer as compared to non-cancerous endometrium. British Journal of Cancer 83: 1722-1729, 2000.

Aydar, E., and C. Palmer. Functional characterisation of the C-terminus of the human ether-a-go-go-related gene K channel (HERG): Journal of Physiology, 534.1: 1-14, 2001.

Babwah, A, Dale L, and Ferguson S. Protein Kinase C isoform-specific differences in the spatial-temporal regulation and decoding of the metabotrophic glutamate recptor 1a-stimulated second messenger responses. The Journal of Biological chemistry, 278: 5419-5426, 2003.

Barros F, Del Camino D, Pardo L and De la Pena P. Caffeine enhancement of electrical activity through direct blockade of inward rectifying K^+ currents in GH3 rat anterior pituitary cells. Pflugers Arch-European Journal of Physiology 431: 443-451, 1996.

Barros F, Del Camino D, Pardo L, Palomero T, Giraldez T and De la Pena P. Demonstration of an inwardly rectifying K^+ current component modulated by thyrotropin-releasing hormone in GH3 rat anterior pituitary cells. Pflugers Arch-European journal of Physiology 435: 119-129, 1997.

Barros F, Gomez-Varela D, Viloria C, Palomero T, Giraldez T and Pena P. Modulation of human erg K^+ channel gating by activation of a G-protein coupled receptor and protein kinase C. Journal of Physiology 511.2: 333-346, 1998.

Bauer C, Wulfsen I, Schafer R, Glassmeier G, Wimmers S, Flitsch J, Ludecke D and Schwartz J. HERG K^+ currents in human prolactin-secreting adenoma cell. Pflugers Arch-European journal of Physiology 445: 589-600, 2003.

Belevych A, Juranek I, Harvey R. Protein kinase C regulates functional coupling of beta1-adrenergic receptors to $G_{i/o}$-mediated responses in cardiac myocytes. FASEB Journal 18(2): 367-9, 2004.

Bell D, Yao H, Saenger R, Riley J and Siegelbaum S. Changes in local S4 environment provide a voltage-sensing mechanism for mammalian hyperpolarisation-activated HCN channels. Journal of General Physiology 123: 5-19, 2004.

Bennett J, Cockcroft S, Gomperts B. Ionomycin stimulates mast cell histamine secretion by forming a lipid-soluble calcium complex. Nature 282(5741):851-3, 1979.

Bers, D.M. 'Excitation-contraction coupling and cardiac contractile force' (2001). ISBN 0-7923-7158-5.

Berridge M and Irvine R. Inositol trisphosphate, a novel second messenger in cellular signal transduction. Nature 312(5992): 315-21, 1984.

Berridge M, Lipp P and Bootman M. The versatility and universality of calcium signalling. Nature Reviews - Molecular Cell Biology 1: 11-21, 2000.

Berube J, Chahine M and Daleau P. Modulation of HERG potassium channel properties by external pH. Pflugers Arch-European journal of Physiology 438: 419-422, 1999.

Bhattacharyya ML, Sarker S, Mull KP, Debnam Q Clofilium-induced block of delayed rectifier type K+ current in atrial tumor cells (AT-1 cells). Journal of Molecular and Cellular Cardiology 29(1): 301-7, 1997.

Bian J-S, Cui J and McDonald T. HERG K^+ channel activity is regulated by changes in phosphatidyl inositol 4,5-bisphosphate. Circulation Research 89: 1168-1176, 2001.

Bian J-S, Kagan A and McDonald T. Molecular analysis of phosphatidyl Inositol 4,5-Bisphosphate regulation of HERG/I_{Kr}. American Journal of Physiology, 2004.

Bianchi L, Wible B, Arcangeli A, Taglialatela M, Morra F, Castaldo P, Crociani O, Rosati B, Faravelli L, Olivotto M, Wanke E. herg encodes a K+ current highly conserved in tumors of different histogenesis: a selective advantage for cancer cells? Cancer Research 58(4): 815-22, 1998.

Bright GR, Fisher GW, Rogowska J, Taylor DL. Fluorescence ratio imaging microscopy. Methods in cell biology 30: 157-192, 1989.

Brown A and Rampe D. Drug-induced long QT syndrome: Is HERG the root of all evil? Pharmaceutical News 7, 2000.

Bolger G, Triggle C, Triggle D. The action of the ionophore ionomycin in guinea-pig intestinal smooth muscle. Canadian Journal of Physiology and Pharmacology 61(5):535-8, 1983.

Brown D, Caulfield M, Kirby P. Relation between catecholamine-induced cyclic AMP changes and hyperpolarization in isolated rat sympathetic ganglia. Journal of Physiology 290(2): 441-51, 1979.

Budd D, Challiss R, Young K and Tobin A. Cross talk between m3-muscarinic and β2-adrenergic receptors at the level of receptor phosphorylationand desensitization. Molecular Pharmacology 56: 813-823, 1999.

Busch A, Eigenberger B, Jurkiewicz NK, Salata JJ, Pica A, Suessbrich H, Lang F. Blockade of HERG channels by the class III antiarrhythmic azimilide: mode of action. British Journal of Pharmacology 123 (1): 23-30, 1998

Busch A, Kavanaugh M, Varnum M, Adelman J and North R. Regulation by second messengers of the slowly activating, voltage-dependent potassium current expresed in xenopus oocytes. Journal of Physiology 450: 491-502, 1992.

Butcher R and Sutherland E. Adenosine 3',5'-phosphate in biological materials. I. Purification and properties of cyclic 3',5'-nucleotide phosphodiesterase and use of this enzyme to characterize adenosine 3',5'-phosphate in human urine. Journal of Biological Chemistry 237:1244-50, 1962.

Callaghan B, Koh S, Keef K. Muscarinic M2 receptor stimulation of Cav1.2b requires phosphatidylinositol 3-kinase, protein kinase C, and c-Src. Circulation Research 94(5): 626-33, 2004.

Carlisle Michel J and Scott J. AKAP mediated signal transduction. Annual Review of Pharmacology and Toxicology 42: 235-257, 2002.

Carmeliet E. Voltage- and time-dependent block of the delayed K+ current in cardiac myocytes by dofetilide. Journal of Pharmacology and Experimental Theraputics 262(2):809-17, 1992.

Cayabyab F and Schlichter L. Regulation of an ERG K^+ current by Src Tyrosine Kinase. The Journal of Biological chemistry 277: 13673-13681, 2002.

Cayabyab F, Tsui F and Schlichter L. Modulation of the ERG K^+ current by the tyrosine phosphatase SHP-1. The Journal of Biological chemistry 277: 48130-48138, 2002.

Cherubini A, Pillozzi S, Hofmann G, Crociani O, Guasti L, Lastraioli E, Polvani S, Masi A, Becchetti A, Wanke E, Olivotto M and Arcangeli A. HERG K^+ channels and β1 intergrins interact through the assembly of a macromolecular complex. Annals of the New York Academy of Sciences 973: 559-561, 2002.

Cherubini, A., G. Taddel, O. Crociani, M. Paglierani, A. Buccoliero, L. Fontana, I. Noci, P. Borri, E. Borrani, M. Giachi, A. Becchetti, B. Rosati, E. Wanke, M. Olivotto, and A. Arcangeli. HERG potassium channels are more frequently expressed in human endometrial cancer as compared to non-cancerous endometrium: British Journal of Cancer, 83: 1722-1729, 2000.

Chorvatova A and Hussein M. Effects of caffeine in potassium currents in isolated rat ventricular mocytes. Pflugers Arch-European journal of Physiology 446: 422-428, 2003.

Chouabe C, Drici M, Romey G, Barhanin J, Lazunski M. HERG and KvLQT1/IsK, the cardiac K^+ channels involved in long QT syndromes, are targets for calcium channel blockers. Molecular Pharmacology 54 (4): 695-703, 1998.

Clay J, Ogbaghebriel A, Paquette T, Sasyniuk B, Shrier A. A quantitative description of the E-4031-sensitive repolarization current in rabbit ventricular myocytes. Biophysical Journal 69(5):1830-7, 1995.

Coghlan V, Hausken Z, Scott J. Subcellular targeting of kinases and phosphatases by association with bifunctional anchoring proteins. Biochemical Society Transactions 23(3): 592-6, 1995.

Colledge M and Scott J. AKAPs: from structure to function. Trends in Cell Biology 9: 216-221, 1999.

Cordeiro J, Spitzer K, Giles W. Repolarizing K+ currents in rabbit heart Purkinje cells. Journal of Physiology 508 (Pt 3): 811-23, 1998.

Crociani O, Guasti L, Balzi M, Becchetti A, Wanke E, Olivotto M, Wymore R and Arcangeli A. Cell-cycle-dependent expression of HERG1 and HERG1B isoforms in tumour cells. The Journal of Biological chemistry 278: 2947-2955, 2003.

Cui J, Kagan A, Qin D, Mathew J, Melman Y and McDonald T. Analysis of the cyclic nucleotide binding domain of the HERG potassium channel and interactions with KCNE2. Journal of Biological Chemistry 276: 17244-17251, 2001.

Cui J, Menman Y, Palma E, Fishman G and McDonald T. Cyclic AMP regulates the HERG K channel by dual pathways. Current Biology 10: 671-674, 2000.

Curran M, Splawski I, Timothy K, Vincent G, Green E, Keating M. A molecular basis for cardiac arrhythmia: HERG mutations cause long QT syndrome. Cell 80 (5): 795-803, 1995

Daleau P and Turgeon J. Angiotensin II modulates the delayed rectifier potassium current of guinea-pig ventricular myocytes. Pflugers Archiv - European Journal of Physiology 427: 553-555, 1994.

Dart C and Leyland M. Targeting of an A kinase-anchoring protein, AKAP79, to an inwardly rectifying potassium channel, Kir 2.1. The Journal of Biological chemistry 276: 20499-20505, 2001.

Davies S, Reddy H, Caivano M and Cohen P. Specificity and mechanism of action of some commonly used protein kinase inhibitors. Biochemical Journal: 95-105, 2000.

Davies M, An R, Doevendans P, Kubalak S, Chien K, Kass R. Developmental changes in ionic channel activity in the embryonic murine heart. Circulation Research 78 (1): 15-25, 1996.

DiFrancesco D and Tortora P. Direct activation of cardiac pacemaker channels by intracellular cyclic AMP. Nature 351 (6322): 145-7, 1991.

DiFrancesco D. Pacemaker mechanisms in cardiac tissue. Annual Reviews in Physiology 55:455-72, 1993.

Doyle D, Morais Cabral J, Pfuetzner R, Kuo A, Gulbis J, Cohen S, Chait B, MacKinnon R. The structure of the potassium channel: molecular basis of K+ conduction and selectivity. Science 280:69-77, 1998.

Elhamdani A, Bossu J, Feltz A. ADP exerts a protective effect against rundown of the Ca2+ current in bovine chromaffin cells. Pflugers Arch-European journal of Physiology 430(3):401-9, 1995.

Emmi A, Wenzel H, Schwartzkroin PA Taglialatela M, Castaldo P, Bianchi L, Nerbonne J, Robertson G, Janigro D. Do glia have heart? Expression and functional role for ether-a-go-go currents in hippocampal astrocytes. Journal of Neuroscience 20(10): 3915-25, 2000.

Fan Z and Makielski J. Anionic phospholipids activate ATP-sensitive potassium channels. Journal of Biological Chemistry 272(9): 5388-95, 1997.

Faux M, Rollins E, Edwards A, Langeberg L, Newton A and Scott J. Mechanism of A-kinase achoring proteins 79 (AKAP79) and protein kinase C interaction. Biochemical Journal 343: 443-452, 1999.

Fermini B and Fossa A. The impact of drug-induced QT interval prolongation on drug discovery and development. Nature Reviews - Drug Discovery 2: 439-447, 2003.

Ficker E, Jarolimek W, Kiehn J, Baumann A, Brown A. Molecular determinants of dofetilide block of HERG K+ channels. Circulation Research 82 (3): 386-395, 1998.

Follmer C and Colatsky T. Block of delayed rectifier potassium current, IK, by flecainide and E-4031 in cat ventricular myocytes. Circulation 82(1):289-93, 1990.

Gamper N and Shapiro M. Calmodulin mediated Ca^{2+}-dependent modulation of M-type K^+ channels. Journal of General Physiology 122: 17-31, 2003.

Gandhi C, Clark E, Loots E, Pralle A and Isacoff E. The orientation and molecular movement of a K^+ channel voltage-sensing domain. Neuron 40: 515-525, 2003.

Gerhardstein B, Puri T, Chien A and Hosey M. Identification of the sites phosphorylated by cyclic AMP-dependent protein kinase on the β2 subunit of the L-type voltage-dependent calcium channel. Biochemistry 38: 10361-10370, 1999.

Ghandi C and Isacoff E. Molecular models of voltage sensing. Journal of General Physiology 120: 455-463, 2002.

Glauner K, Mannuzzu L, Gandhi C and Isacoff E. Spectroscopic mapping of voltage sensor movement in the shaker potassium channel. Nature 402 (6763): 813-817, 1999.

Gomez-Varela D, Barros F, Viloria C, Giraldez T, Manso D, Dupuy S, Miranda P and De la Pena P. Relevance of the proximal domain in the amino terminus of HERG channels for regulation by a phospolipase C-coupled hormone receptor. FEBS Letters 535: 125-130, 2003.

Gomperts B, Kramer I, Tatham, P. Signal transduction. Third edition. 2003. ISBN: 0-12-289632-7.

Guillard C, Chretien S, Pelus A, Porteu F, Muller O, Mayeux P, Duprez V. Activation of the mitogen-activated protein kinases Erk1/2 by erythropoietin receptor via a G_i protein beta gamma-subunit-initiated pathway. Journal of Biological Chemistry 278(13): 11050-6, 2003.

Hamill O, Neher M, Sakmann B and Sigworth F. Improved Patch-clamp techniques for high-resolution current recordings from cells and cell-free membrane patches. Pflugers Arch-European journal of Physiology 391: 85-100, 1981.

Han H, Wang J, Zhang Y, Long H, Wang H, Xu J and Wang Z. HERG K^+ channel conductance promotes H_2O_2 -induced apoptosis in HEK293 cells: cellular mechanisms. Cellular Physiology and Biochemistry 14: 121-134, 2004.

Hanahan D and Weinberg R. The hallmarks of cancer. Cell. 100 (1): 57-70, 2000.

Hancox J, Levi A and Witchel H. Time Course and voltage dependence of expressed HERG current compared with native 'rapid' delayed rectifier K current during the cardiac ventricular action potential. Pflugers Arch-European journal of Physiology 436: 843-853, 1998.

Hayabuchi Y, Dart C and Standen N. Evidence for involvement of A-kinase anchoring protein in activation of rat arterial K_{ATP} channels by protein kinase A. Journal of Physiology 536.2: 421-427, 2001.

Heath, B., and D. Terrar. Separation of the components of the delayed rectifier potassium current using selective blockers of I_{Kr} and I_{Ks} in guine-pig isolated ventricular myocytes: Experimental Physiology, 81: 587-603, 1996.

Heath B and Terrar D. Protein Kinase C enhances the rapidly activating delayed rectifier potassium current, I_{Kr}, through a reduction in C-type inactivation in guinea-pig ventricular myocytes. Jounal of Physiology 522.3: 391-402, 2000.

Hille B. Ion channels of excitable membranes, 2001. ISBN: 0-87893-321-2

Hirdes W, Horowitz L and Hille B. Muscarinic modulation of erg potassium current. Journal of Physiology 559.1: 67-84, 2004.

Hoffman G, Bernabei P, Crociani O, Cherubini A, Guasti L, Pillozzi S, Lastraioli E, Polvani S, Bartalozzi B, Solazzo V, Gragnani L, Deflippi P, Rosati B, Wanke E, Olivotto M and Arcangeli A. HERG K^+ channels activation during β1-integrin-mediated adhesion to fibronectin induces an up-regulaton of avβ1 integrin in the prosteoclastic leukemia cell line FLG 29.1. The Journal of Biological chemistry 276: 4923-4931, 2001.

Hoshi N, Zhang J-S, Omaki M, Takeuchi T, Yokoyama S, Wanaverbecq N, Langeberg L, Yoneda Y, Scott J, Brown D and Higashida H. AKAP150 signalling complex promotes suppression of the M-current by muscarinic agonists. Nature Neuroscience 6: 564-571, 2003.

Hu K, Huang C, Jan Y and Jan L. ATP-sensitive potassium channel traffic regulation by adenosine and protein kinase C. Neuron 38: 417-432, 2003.

Hudman D and Standen N. Protection from the effects of metabolic inhibition and reperfusion in contracting isolated ventricular myocytes via protein kinase C activation. Journal of molecular and cellular cardiology. 37 (2): 579-591, 2004.

Hulme J, Lin TW-C, Westenbrook R, Scheuer T and Catterall W. β-adrenergic regulation requires direct anchoring of PKA to cardiac Cav1.2 channels via a leucine zipper interaction with A Kinase-anchoring protein 15. Proceedings - National Academy of Science - USA 100: 13093-13098, 2003.

Ishii M and Kurachi Y. The 14-3-3 protein as a novel regulator of ion channel localisation. Journal of Physiology 545: 2, 2002.

Jalili T, Takeishi Y, Song G, Ball N, Howles G, Walsh R. PKC translocation without changes in G alpha q and PLC-beta protein abundance in cardiac hypertrophy and failure. American Journal of Physiology 277 (6 Pt2): H2298-2304, 1999.

Jiang Y, Lee A, Chen J, Cadene M, Chalt B and MacKinnon R. Crystal structure and mechanism of a calcium-gated potassium channel. Nature 417: 515-522, 2002.

Jiang Y, Lee A, Chen J, Ruta V, Cadene M, Chalt B and MacKinnon R. X-ray structure of a voltage-dependent K^+ channel. Nature 423: 33-41, 2003a.

Jiang Y, Ruta V, Chen J, Lee A and MacKinnon R. The principle of gating charge movement in a voltage-dependent K^+ channel. Nature 423: 42-48, 2003b.

Johnson Jr J, Balser J and Bennett P. A novel Extracellular Calcium sensing mechanism in voltage-gated potassium ion channels. The Journal of Neuroscience 21: 4143-4153, 2001.

Johnson Jr J, Mullins F and Bennett P. Human ether-a-go-go related gene K^+ channel gating probed with extracellular calcium. Journal of General Physiology 113: 565-580, 1999.

Jones E, Roti Roti E, Wang J, Delfosse S and Robertson G. Cardiac I_{Kr} channels minimally comprise hERG 1a and 1b subunits. The Journal of Biological chemistry 279(43): 44690-4, 2004.

Juliano R. Signal transduction by cell adhesion receptors and the cytoskeleton: functions of integrins, cadherins, selectins, and immunoglobulin-superfamily members. Annual Reviews in Pharmacology and Toxicology 42: 283-323, 2002.

Kabir SM, Bhattacharyya ML, Robinson TR. Indapamide blocks the rapid component of the delayed rectifier current in atrial tumor cells (AT-1 cells). International Journal of Cardiology 73(1): 27-32, 2000.

Kagan A, Melman Y, Krumerman A and McDonald T. 14-3-3 amplifies and prolongs adrenergic stimulation of HERG K^+ channel activity. The EMBO Journal 21: 1889-1898, 2002.

Kamarck T and Jennings R. Behavioural factors in sudden cardiac death. Psychological Bulletin 109 (1): 42-75, 1991.

Kapiloff M. Contributions of protein kinase A anchoring proteins to compartmentalisation of cAMP signalling in the heart. Molecular Pharmacology 62: 193-199, 2002.

Kapuscinski J, Ardelt B, Piosik J, Zdunek M and Darzynkiewicz Z. The modualtion of the DNA-damaging effect of polycyclic aromatic agents by xanthines Part I. Reduction of cytostatic effects of quinacrine mustard by caffeine. Biochemical Pharmacology 63: 625-634, 2002.

Kara C, Liou H, Ivashkiv L, Glimcher L. A cDNA for a human cyclic AMP response element-binding protein which is distinct from CREB and expressed preferentially in brain. Molecular and Cell Biology 10(4): 1347-57, 1990.

Karle C, Zitron E, Zhang W, Kathofer S, Schoels W and Kiehn J. Rapid component Ikr of the guinea pig cardiac delayed rectifier K^+ current is inhibited by beta-1 adrenoceptor activation, via cAMP/protein kinase A dependent pathways. Cardiovascular Research 53: 355-362, 2002.

Kass R, Kurokawa J, Marx S and Marks A. Leucine/iosloeucine zipper coordination of ion channel macromoleculr signalling complexes in the heart: roles in inheritied arrythmias. Trends in Cardiovascular Medicine 13: 52-56, 2003.

Kathöfer S, Zhang W, Karle C, Thomas D, Schoels W and Kiehn J. Functional coupling of human beta3-adrenoreceptors to the KvLQT1/*Min*K potassium channel. The Journal of Biological chemistry 275: 26743-26747, 2000.

Klauck T, Faux M, Labudda K, Langeberg L, Jaken S, Scott J. Coordination of three signaling enzymes by AKAP79, a mammalian scaffold protein. Science 271(5255):1589-92, 1996.

Keen J, Khawaled R, Farrens D, Neelands T, Rivard A, Bond C, Janowsky A, Fakler B, Adelman J, Maylie J. Domains responsible for constitutive and Ca^{2+}-dependent interactions between calmodulin and small conductance Ca^{2+}-activated potassium channels. Journal of Neuroscience 19(20): 8830-8, 1999.

Kiehn J, Karle C, Thomas D, Yao X, Brachmann J and Kubler W. HERG potassium channel activation is shifted by phorbol esters via protein-kinase A dependent pathways. Journal of Biological Chemistry 273: 25285-25291, 1998.

Kofuji P, Davidson N, Lester H. Evidence that neuronal G-protein-gated inwardly rectifying K+ channels are activated by G beta gamma subunits and function as heteromultimers. Proceedings of the National Academy of Sciences U S A 92(14): 6542-6, 1995.

Kupershmidt S, Snyders D, Raes A and Roden D. A K^+ channel splice variant common in human heart lacks a C-terminal domain required for expression of rapidly activating delayed rectifier current. The Journal of Biological chemistry 273: 27231-27235, 1998.

Kupershmidt S, Yang T, Anderson M, Wessels A, Niswender K, Magnuson M, Roden D. Replacement by homologous recombination of the *mink* gene with *lacZ* reveals restriction of mink expression to the mouse cardiac conduction system. Circulation Research 84: 146-152, 1999

Lastraioli E, Guasti L, Crociani O, Polvani S, Hofmann G, Witchel H, Bencini L, Calistri M, Messerini L, Scatizzi M, Moretti R, Wanke E, Olivotto M, Mugnai G and Arcangeli A. herg1 gene and HERG1 protein are overexpressed in colorectal cancers and regulate cell invasion of tumour cells. Cancer Research 64: 606-611, 2004.

Lawrence C and Rodrigo G. A Na^+-activated K^+ channel ($I_{K, Na}$) is present in guinea pig but not rat vetricular myocytes. Pflugers Arch-European journal of Physiology 437: 831-838, 1999.

Lees-Miller J, Kondo C, Wang L, Duff H. Electrophysiological characterization of an alternatively processed ERG K+ channel in mouse and human hearts. Circulation Research 81(5): 719-26, 1997.

Lei Q, Jones M, Talley E, Schrier A, McIntire W, Garrison J, Bayliss D. Activation and inhibition of G protein-coupled inwardly rectifying potassium (Kir3) channels by G protein beta gamma subunits. Proceedings of the National Academy of Sciences U S A. 97(17): 9771-6, 2000.

Lewis A, McCrossen Z and Abbott G. MinK, MiRP1, and MiRP2 diversify Kv3.1 and Kv3.2 potassium channel gating. The Journal of Biological chemistry 279: 7884-7892, 2004.

Liman E and Hess P. Voltage-sensing residues in the S4 region of a mammalian K^+ channel. Nature 353: 752-756, 1991.

Lindaman B, Hinkhouse M, Conklin J, Cullen J. The effect of phosphodiesterase inhibition on gallbladder motility in vitro. Journal of Surgical Research 105(2):102-8, 2002.

Liu E, Goldhaber J, Weiss J. Effects of lysophosphatidylcholine on electrophysiological properties and excitation-contraction coupling in isolated guinea pig ventricular myocytes. Journal of Clinical Investigation 88(6): 1819-32, 1991.

Liu J, Zhang M and Tseng G. Structural and functional role of the extrcellular S5-P linker in the HERG potassium channel. Journal of General Physiology 120: 723-737, 2002.

Liu J, Zhang M, Jiang M and Tseng G-N. Negative charges in the transmembrane domains of the HERG K channel are involved in the activation and deactivation gating processes. Journal of General Physiology 121: 599-614, 2003.

Liu S-Q, Yin J and Bhatnagar A. Protein Kinase C-dependent phosphorylation of the β-subunit of the voltage sensitive potasium channels (Kvβ2). Chemico-Biological Interactions 143-144: 597-604, 2003.

Lo CF and Numann R. Independent and Exclusive modulation of cardiac delayed rectifying K^+ current by protein kinase C and protein kinase A. Circulation Research 83: 995-1002, 1998.

Locati E, Zareba W, Moss A, Schwartz P, Vincent M, Lehmenn M, Towbin J, Proior S, Napolitano C, Robinson J, Andrews M, Timothy K and Hall J. Age- and sex- related differences in clincal manifestations in patients with congenital long QT syndrome. Circulation 97: 2237-2244, 1998.

London B, Trudeau M, Newton K, Beyer A, Copeland N, Gilbert D, Jenkins N, Satler C and Robertson G. Two isoforms of the mouse ether-a-go-go-related gene coassemble to form channel with properties similar to the rapidly activating component of the cardiac delayed rectifier K^+ current. Circulation Research 81: 870-878, 1997.

Loots E and Isacoff E. Protein rearrangements underlying slow inactivation of the shaker K^+ channel. Journal of general physiology 112 (4): 377-389, 1998.
Lopez G, Jan Y and Jan L. Evidence that the S6 segment of the shaker voltage-gated K^+ channel comprises part of the pore. Nature 367: 179-182, 1994.

Loussouarn G, Park K-H, Bellocq C, Baro I, Charpentier F and Escande D. Phosphatidylinositol-4, 5-bisphosphate, PIP_2, controls KCNQ1/KCNE1 voltage-gated potassium channels: a functional homology between voltage-gated and inward rectifier K^+ channels. The EMBO Journal 22: 5412-5421, 2003.

Lowry O, Rosebrough N, Farr L and Randall R. Protein measurement with the folin phenol reagent. The Journal of Biological chemistry, 1951.

Magyar J, Iost N, Kortvely A, Banayasz T, Virag L, Szigligeti P, Varro A, Opincarui M, Szecsi J, Papp J and Nanasi P. Effects of endothelin-1 on calcium and potassium currents in undiseased human ventricular myocytes. Pflugers Arch-European journal of Physiology 441: 144-149, 2000.

Mannuzzu L, Moronne M and Isacoff E. Direct physical measure of conformational rearrangement underlying potassium channel gating. Science. 271 (5246): 213-217, 1996.

Marks A, Marx S, Reiken S. Regulation of ryanodine receptors via macromolecular complexes: a novel role for leucine/isoleucine zippers. Trends in Cardiovascular medicine 12(4):166-70, 2002.

Martiny-Baron G, Kazanietz M, Mischak H, Blumberg P, Kochs G, Hug H, Marme D and Schachtele C. Selective inhibition of protein kinase C isozymes by the indolocarbazole Gö6976. The Journal of Biological chemistry 268: 9194-9197, 1993.

Marx S, Kurokawa J, Reiken S, Motoike H, D'Armiento J, Marks A and Kass R. Requirement of a macromolecular signalling complex for beta adrenergic receptor modulation of the KCNQ1-KCNE1 potassium channel. Science 295: 496-499, 2002.

Marx S, Reiken S, Hisamatsu Y, Jayaraman T, Burkhoff D, Rosemblit N, Marks A. PKA phosphorylation dissociates FKBP12.6 from the calcium release channel (ryanodine receptor): defective regulation in failing hearts. Cell 101(4):365-76, 2000.

Mason H, Latten M, Godoy L, Horowitz B and Kenyon J. Modulation of Kv1.5 currents by protein kinase A, Tyrosine kinase and protein tyrosine phosphatase requires an intact cytoskeleton. Molecular Pharmacology 61: 285-293, 2002.

Matsumoto Y, Ogura T, Uemura H, Saito T, Masuda Y and Makaya H. Histamine H1-receptor-mediated modaultion of the delayed rectifier current in guinea-pig atrial cells:opposite effects on I_{Kr} and I_{Ks}. British Journal of Pharmacology 128: 1545-1553, 1999.

McDonald T, Yu z, Ming Z, Palma E, Meyers M, Wang K, Goldstein S and Fishman G. A minK-HERG complex regulates the cardiac potassium current I_{Kr}. Nature 388: 289-292, 1997.

Meves H, Schwarz JR, Wulfsen I. Separation of M-like current and ERG current in NG108-15 cells. British Journal of Pharmacology 127(5):1213-23, 1999.

Meyer R and Heinemann S. Characterization of an eag-like potassium channel in human neuroblastoma cells. Journal of Physiology 508.1: 49-56, 1998

Miake J, Marban E, Nuss H. Functional role of inward rectifier current in heart probed by Kir2.1 overexpression and dominant-negative suppression. Journal of clinical investigation 111(10): 1529-36, 2003.

Mitcheson J and Hancox J. An investigation of the role played by the E-4031 sensitive (rapid delayed rectifier) potassium current in isolated rabbit atrioventricular nodal and ventricular myocytes. Pflugers Arch-European journal of Physiology 438: 843-850, 1999.

Mitcheson J, Chen J and Sanguinetti M. Trapping of a methanesulfonamide by closure of the HERG potassium channel activation. Journal of General Physiology 115: 229-240, 2000.

Mochly-Rosen, D., and A. Gordon. Anchoring proteins for protein kinase C: a means for isozyme selectivity: FASEB Journal, 12: 35-42, 1998.

Morais-Cabral J, Lee A, Cohen S, Chait B, Li M and MacKinnon R. Crystal structure and function analysis of the HERG potassium channel N-terminus: a eukaryotic PAS domain. Cell 95: 649-655, 1998b.

Nerbonne J and Guo W. Heterologous expression of voltage gated potassium channels in the heart: roles in normal excitation and arrythmias. Journal of cardiovascular electrophysiology. 13 (4): 406-409, 2002.

Neri, L, Borgatti P, Capitani S, and Martelli A. The nuclear phosphoinositide 3-kinase.AKT pathway: a new second messenger system: Biochimica et Biophysica Acta 1584: 73-80, 2002.

Nicholson, K, and Anderson N. The protein kinase B/Akt signalling pathway in human malignancy: Cellular signalling 14: 381-395, 2002.

Papa M, Boscia F, Canitano A, Castaldo P, Sellitti S, Annunziato L and Taglialetela M. Expression pattern of the ether-a-gogo-related (ERG) K^+ channel-encoding genes ERG1, ERG2 and ERG3 in the adult rat central nervous system. The Journal of Comparative Neurology 466: 119-135, 2003.

Papazian DM, Shao XM, Seoh SA, Mock AF, Huang Y, Wainstock DH. Electrostatic interactions of S4 voltage sensor in Shaker K+ channel. Neuron 14(6):1293-301, 1995.

Pape H. Queer current and pacemaker: the hyperpolarization-activated cation current in neurons. Annual Reviews in Physiology 58: 299-327, 1996.

Perry M, de Groot M, Helliwell R, Leishman D, Tristani-Firouzi M, Sanguinetti M and Mitcheson J. Structural determinants of HERG channel block of clofilium and ibutilide. Molecular Pharmacology 66: 240-248, 2004.

Peterson B, DeMaria C and Yue D. Calmodulin is the Ca^{2+} sensor for Ca^{2+} dependent inactivation of L-type calcium channels. Neuron 22: 549-558, 1999.

Piosik J, Ulanowska K, Gwizdek-Wisniewska A, Czy A, Kapuscinski J and Wegrzyn G. Alleviation of mutagenic effects of polycyclic aromatic agents (quinacrine mustard, ICR-191 and ICR-170 by caffeine and pentoxifylline. Mutation Research 530: 47-57, 2003.

Piper D, Varghese A, Sanguinetti M and Tristani-Firouzi M. Gating currents associated with intramembrane charge displacement in HERG potassium channels. Proceedings - National Academy of Science - USA 100: 10534-10539, 2003.

Poggioli J, Leslie B, McKinney J, Weiss S, Putney J Jr. Actions of ionomycin in rat parotid gland. Journal of Pharmacology and Experimental Theraputics 221(1):247-53, 1982.

Pond A and Nerbonne J. ERG proteins and functional cardiac I_{Kr} channels in rat, mouse, and human heart. Trends in Cardiovascular Medicine 11: 286-294, 2001.

Ponicke K, Heinroth-Hoffman I and Brodde O-E. Demonstration of functional m3-muscarinic receptors in ventricular cardiomyocytes of adult rats. British Journal of Pharmacology 138: 156-160, 2003.

Priori S, Mortara D, Napolitano C, Diehl L, Paganini V, Cantu F, Cantu G, Schwartz P. Evaluation of the spatial aspects of T-wave complexity in the long-QT syndrome. Circulation 96(9): 3006-12, 1997.

Rang, Dale and Ritter. Pharmacology: Churchill Livingstone, 1995. ISBN: 0-443-050864.

Ribalet B, John S, Weiss J. Regulation of cloned ATP-sensitive K channels by phosphorylation, MgADP, and phosphatidylinositol bisphosphate (PIP(2)): a study of channel rundown and reactivation. Journal of General Physiology 116(3):391-410, 2000.

Robinson R and Siegelbaum S. Hyperpolarization-activated cation currents: from molecules to physiological function. Annual Reviews in Physiology 65:453-80, 2003.

Rockman H and Lefkowitz R. Seven transmembrane-spanning receptors and heart function. Nature 415: 206-212, 2002.

Roden D and George Jr A. The cardiac ion channels: relevance to management of arrhythmias. Annual Review of Medicine 47: 135-148, 1996.

Roden DM, Balser JR, George AL Jr, Anderson ME. Cardiac ion channels. Annual Reviews in Physiology 64: 431-475, 2002.

Rosenmund C, Carr D, Bergeson S, Nilaver G, Scott J and Westbrook G. Anchoring of Protein kinase A is required for modulation of AMPA/kainate receptors on hippocampal neurons. Nature 368: 853-855, 1994.

Rouet-Benzineb P, Mohammadi K, Perennec J, Poyard M, Bouanani N-H, Crozatier, B. Protein kinase C isoform expression in normal and failing rabbit hearts. Circulation research 79 (2): 153-161, 1996.

Rousseau E, Ladine J, Liu Q, Meissner G. Activation of the Ca2+ release channel of skeletal muscle sarcoplasmic reticulum by caffeine and related compounds. Archives in Biochemistry and Biophysics 267(1): 75-86, 1988.

Roux M, Olcese R, Toro L, Bezanilla F, Stefani E. Fast inactivation in Shaker K+ channels. Properties of ionic and gating currents. Journal of General Physiology 111(5): 625-38, 1998.

Ruehr M, Russell M, Ferguson D, Bhatt M, Ma J, Damron D, Scott J and Bond M. Targetting of protein kinase A by muscle A Kinase anchoring protein (mAKAP) regulates phosphorylation and function of the skeletal muscle ryanodine receptor. The Journal of Biological chemistry 278: 24831-24836, 2003.

Ryu, S., K. Cho, K.-Y. Lee, P.-G. Suh, and S. Rhee. Purification and characterisation of two immunologically distinct phosphoinositide-specific phospholipase C from bovine brain: The Journal of Biological chemistry, 262: 12511-12516, 1987.

Sacco T, Bruno A, Wanke E and Tempia F. Functional roles of an ERG current isolated in celebellar purkinje neurons. Journal of Neurophysiology 90: 1817-1828, 2003.

Saganich M, Machado E, Rudy B. Differential expression of genes encoding subthreshold-operating voltage-gated K+ channels in brain. Journal of Neuroscience 21(13): 4609-24, 2001.

Sanchez-Chapula J, Ferrer T, Navarro-Polanco R and Sanguinetti M. Voltage-dependent profile of Human ether-a-go-go Related Gene channel block is influenced by a single residue in the S6 transmembrane domain. Molecular Pharmacology 63: 1051-1057, 2003.

Sanguinetti M and Jurkiewicz N. Two components of cardiac delayed rectifier K+ current. Differential sensitivity to block by class III antiarrhythmic agents. Journal of General Physiology 96(1):195-215, 1990.

Sanguinetti M and Xu Q. Mutations of the S4-S5 linker alter activation properties of HERG potassium channels expressed in xenopus oocytes. Journal of Physiology 514.3: 667-675, 1999.

Sanguinetti M, Jiang C, Curran M and Keating M. A mechanistic link between an inherited and an aquried cardiac arrhythmia:HERG encodes the I_{Kr} potassium channel. Cell 81: 299-307, 1995.

Sano S, Kiyotaki C, Tatsumi Y, Fujiwara H, Hamaoka T. Cytotoxic T lymphocyte unresponsiveness induced by prolonged treatment with immobilized anti-CD3 antibody. Association of impairment of cytolytic activity with temporary depletion of intracellular protein kinase C. Journal of Immunology 143(9):2797-805, 1989.

Sato Y, Sakaguchi M, Goshima S, Nakamura T, Uozumi N. Molecular dissection of the contribution of negatively and positively charged residues in S2, S3, and S4 to the final membrane topology of the voltage sensor in the K+ channel, KAT1. Journal of Biological Chemistry 278(15):13227-34, 2003.

Schledermann W, Wulfsen I, Schwarz J and Bauer C. Modulation of rat erg1, erg2, erg3 and HERG K^+ currents by thyrotropin-releasing hormone in anterior pituitary cells via the native signal cascade. Journal of Physiology 532: 143-163, 2001.

Schonherr R and Heinemann S. Molecular determinants for activation and inactivation of HERG, a human inward rectifier potassium channel. Journal of Physiology 493: 635-642, 1996.

Schonherr R, Mannuzzu L, Isacoff E and Heinemann S. Conformational switch between slow and fast gating modes: allosteric regulation of voltage sensor mobility in the EAG K^+ channel. Neuron 35: 935-949, 2002.

Schonherr, Lober and Heinemann S. Inhibition of human ether-a-go-go potassium channels by calcium/calmodulin. The EMBO Journal 19: 3263-3271, 2000.

Schrader L, Anderson A, Mayne A, Pfaffinger P and Sweatt J. PKA modulation of Kv4.2 encoded A-type potassium channels requires formation of a supramolecular complex. The Journal of Neuroscience 22: 10123-10133, 2002.

Schreiber M, Salkoff L. A novel calcium-sensing domain in the BK channel. Biophysical Journal 73(3): 1355-63, 1997.

Schroeder BC, Waldegger S, Fehr S, Bleich M, Warth R, Greger R, Jentsch TJ. A constitutively open potassium channel formed by KCNQ1 and KCNE3. Nature 403 (6766): 196-199, 2000.

Schulze-Bahr E, Wang Q, Wedekind H, Haverkamp W, Chen Q, Sun Y, Rubie C, Hordt M, Towbin J, Borggrefe M, Assmann G, Qu X, Somberg JC, Breithardt G, Oberti C, Funke H. KCNE1 mutations cause jervell and Lange-Nielsen syndrome. Nature Genetics 17(3):267-8, 1997.

Selyanko A, Delmas P, Hadley J, Tatulian L, Wood I, Mistry M, London B, Brown D. Dominant-negative subunits reveal potassium channel families that contribute to M-like potassium currents. Journal of Neuroscience 22(5): RC212, 2002.

Sesti F, Goldstein S. Single-channel characteristics of wild-type IKs channels and channels formed with two minK mutants that cause long QT syndrome. Journal of General Physiology 112(6):651-63, 1998.

Shabb J. Physiological substrates of cAMP-dependent protein kinase. Chemical Reviews 101: 2381-2411, 2001.

Simonds W. G protein regualtion of adenylyl cyclase. Trends in Pharmacological Sciences 20: 66-73, 1999.

Smith G, Tsui H, Newell E, Jiang X, Zhu X-P, Tsui F and Schlichter L. Functional up-regulation of HERG K^+ channels in neoplastic hematopoietic cells. The Journal of Biological chemistry 277: 18528-18534, 2002.

Smith P and Yellen G. Fast and slow voltage sensor movements in HERG potassium channels. Journal of General Physiology 119: 275-293, 2002.

Smith P, Baukrowitz T and Yellen G. The inward rectification mechanism of the HERG cardiac potassium channel. Nature 379: 833-836, 1996.

Smith J, Pearson S, Marks V. Plasma caffeine concentration in outpatients. Lancet 2(8305):985-6, 1982.

Spector P, Curran M, Zou A, Keating M and Sanguinetti M. Fast inactivation causes rectification of the I_{Kr} channel. Journal of General Physiology 107: 611-619, 1996.

Srivastava J, Procyk K, Iturrioz X, Parker P. Phosphorylation is required for PMA- and cell-cycle-induced degradation of protein kinase Cdelta. Biochemical Journal 368(Pt 1):349-55, 2002.

Stansfeld C, Roper J, Ludwig J, Weseloh R, Marsh S, Brown D and Pongs O. Elevation of intracellular calcium by muscarinic receptor activation induces a block of voltage-activated rat ether-a-go-go channels in a stably transfected cell line. Proceedings of the National Academy of Sciences, USA 93: 9910-9914, 1996.

Storey N, O'Bryan J and Armstrong D. Rac and Rho mediate opposing hormonal regulation of the Ether-a-go-go-related potassium channel. Current Biology 12: 27-33, 2002.

Sutherland E, Oye I, Butcher R. The action of epinephrine and the role of the adenylyl cyclase system in hormone action. Recent progesss in hormone research 21: 623-646, 1965.

Sun Z, Milos PM, Thompson JF, Lloyd DB, Mank-Seymour A, Richmond J, Cordes JS, Zhou J. Role of a KCNH2 polymorphism (R1047L) in dofetilide-induced Torsades de Pointes. Journal of molecular and cellular cardiology 37 (5): 1031-1039, 2004.

Swartz, K. Towards a structural view of gating in potassium channels. Nature Reviews – Neuroscience 5: 905-916, 2004.

Taglialetela M, Castaldo P, Iossa S, Pannaccione A, Fresi A, Ficker E and Annunziato L. Regulation of the human ether-a-go-go related gene (HERG) K^+ channels by reactive oxygen species. Proceedings of the National Academy of Sciences - USA 94: 11698-11703, 1997.

Taglialetela M, Pannaccione A, Iossa S, Castaldo P and Annunziato L. Modulation of the K^+ channels encoded by the Human Ether-a-go-go Related Gene-1 (HERG-1) by nitric oxide. Molecular Pharmacology 56: 1298-1308, 1999.

Taketo M, Matsuda H, Yoshioka T. Calcium-independent inhibition of GABA(A) current by caffeine in hippocampal slices. Brain Research 1016(2):229-39, 2004.

Tayebati S, Vitali D, Scordella S, Amenta F. Muscarinic cholinergic receptor subtypes in rat cerebellar cortex: light microscope autoradiography of age-related changes. Brain Research 889 (1-2): 269-259, 2001.

Thomas D, Kiehn J, Katus H and Karle C. Adrenergic regulation of the rapid component of the cardiac delayed rectifier potassium current, I_{Kr}, and the underlying hERG ion channel. Basic Research in Cardiology 99: 279-287, 2004.

Thomas D, Wu, K, Wimmer A-B, Zitron E, Hammerling B, Kathöfer S, Lueck S, Bloehs V, Kreye V, Kiehn J, Katus H, Schoels W, Karle C. Activation of cardiac human ether-a-go-go-

related gene (hERG/I_{Kr}) potassium currents is regulated by α_{1A}-adrenoceptors. Journal of molecular medicine. 2004. In press.

Thomas D, Zhang W, Karle C, Kathofer S, Schols W, Kuber W and Keihn J. Deletion of Protein kinase A phosphorylation sites in the HERG potassium channel inhibits activation shift by protein kinase A. Journal of Biological Chemistry 274: 27457-27462, 1999.

Thomas D, Zhang W, Wu K, Wimmer A-B, Gut B, Wendt-Nordahl G, Kathofer S, Kreye V, Katus H, Schoels W, Kiehn J and Karle C. Regulation of HERG potassium channel activation by protein kinase C independent of direct phosphorylation of the channel protein. Cardiovascular Research 59: 14-26, 2003.

Tian L, Coghill L, MacDonald S, Armstrong D and Shipston M. Leucine zipper domain targets cAMP-dependent protein kinase to mammalian BK channels. The Journal of Biological chemistry 278: 8669-8677, 2003.

Tobin A and Nahorski S. Rapid agonist mediated phosphorylation of m3 muscarinic receptors revealed by imunoprecipitation. The Journal of Biological chemistry 286: 9817-9823, 1993.

Tohse N, Kameyama M and Irisawa H. Intracellular Ca^{2+} and protein kinase C modulate K^+ current in guinea pig heart cells. American Journal of Physiology 253: H1321-H1324, 1987.

Tohse N. Calcium-sensitive delayed rectifier potassium current in guinea pig ventricular myocytes. American Journal of Physiology 258: H1200-H1207, 1990.

Touyz R and Berry C. Recent advances in angiotensin II signaling. Brazillian Journal of Medical and Biological Research 35: 1001-1015, 2002.

Tovey S and Willars G. Single cell imaging of Ca^{2+} and phospholipase C reveals that RGS 2, 3 and 4 differentially regulate signaling via the Gaplha 11-linked musacrinic M3 receptor. Molecular Pharmacology. 66 (6): 1452-1464, 2004.

Tristani-Firouzi M and Sanguinetti M. Structural determiniants and biphysical properties of HERG and KCNQ1 channel gating. Journal of Molecular and Cellular Cardiology 35: 27-35, 2003.

Tristani-Firouzi M, Chen J and Sanguinetti M. Interactions between S4-S5 linker and S6 transmembrane domain modulate gating of HERG K^+ channels. The Journal of Biological chemistry 277: 18994-19000, 2002.

Tsitsanou K, Skarnaki V and Oikonomakos N. Structural basis of the synergistic inhibition of glycogen phsphorylase A by caffeine and a potential antidiabetic drug. Archives of Biochemistry and Biophysics 384: 245-254, 2000.

Vandenberg JI, Walker BD, Campbell TJ. HERG K+ channels: friend and foe. Trends in Pharmacological sciences 22 (5): 240-246, 2001.

Vandenberg J, Torres A, Campbell T and Kuchel P. The HERG K^+ channel: progress in understanding the molecular basis of its unusual gating kineteics. European Biophysics Journal 33: 89-97, 2003.

Viard P, Macrez N, Mironneau C, Mironneau J. Involvement of both G protein alphas and beta gamma subunits in beta-adrenergic stimulation of vascular L-type Ca^{2+} channels. Br J Pharmacology 132(3): 669-76, 2001.

Viscomi C, Altomare C, Bucchi A, Camatini E, Baruscotti M, Moroni A and DiFrancesco D. C terminus-mediated control of voltage and cAMP gating of hyperpolarization-activated cyclic nucleotide-gated channels. Journal of Biological Chemistry 276: 29930-29934, 2001.

Viskin S. Long QT syndromes and torsades de pointes. Lancet 354: 1625-1633, 1999.

Wainger B, DeGennaro M, Santoro B, Siegelbaum S and Tibbs G. Molecular mechanism of cAMP modulation of HCN packmaker channels. Nature 411: 805-810, 2001.

Wang H, Zhang Y, Cao L, Han H, Wang J, Yang B, Nattel S and Wang Z. HERG K^+ channel, a regulator of tumour cell apoptosis and proliferation. Cancer Research 62: 4843-4848, 2002a.

Wang J, Chen S, Siegelbaum S. Regulation of Hyperpolarisation-activated HCN channel gating and cAMP modulation due to interactions of COOH terminus and core transmembrane regions. Journal of General Physiology 118: 237-250, 2001a.

Wang J, Myers C and Robertson G. Dynamic control of deactivation gating by a soluble amino terminal domain in HERG K^+ channels. Journal of General Physiology 115: 749-758, 2000.

Wang J, Trudeau M, Zappia A and Robertson G. Regulation of deactivation by an amino terminal domain in Human Ether-a-go-go-related gene potassium channels. Journal of General Physiology 112: 637-647, 1998.

Wang J, Wang H, Han H, Zhang Y, Yang B, Nattel S and Wang Z. Phospholipid Metabolite 1-Palmitoyl-Lysophosphatidylcholine enhances human-ether-a-go-go-realted gene (HERG) K^+ channel function. Circulation 104: 2645-2648, 2001b.

Wang J, Zhang Y, Wang H, Han H, Nattel S, Yang B and Wang Z. Potential mechanisms for the enhancement of HERG K^+ channel function by phospholipid metabolites. British Journal of Pharmacology 141: 586-599, 2004.

Wang S, Liu S, Morales M, Strauss H and Rasmusson R. A quantitative analysis of the activation and inactivation kinetics of HERG expressed in xenopus oocytes. Journal of Physiology 502.1: 45-60, 1997.

Wang Z, Wilson G and Griffith L. Calcium/calmodulin-dedendent protein kinase II phosphorylated and regulates the drosophila EAG potassium channel. The Journal of Biological chemistry 277: 24022-24029, 2002b.

Wang Z, Fermini B, Nattel S. Rapid and slow components of delayed rectifier current in human atrial myocytes. Cardiovascular Research 28(10):1540-6, 1994.

Wanke E, Bianchi L, Mantegazza M, Guatteo E, Mancinelli E, Ferroni A. Muscarinic regulation of Ca2+ currents in rat sensory neurons: channel and receptor types, dose-response relationships and cross-talk pathways. European Journal of Neuroscience 6(3): 381-91, 1994.

Warth J and Hume J. Re-examination of Na+-dependent regulation of cAMP-dependent Cl- currents in the heart. Pflugers Arch-European journal of Physiology 433(5):597-607, 1997.

Weerapura M, Nattel S, Chartier D, Caballero R and Hebert T. A comparison of currents carried by HERG, with and without coexpression of MiRP1, and the native rapid delayed rectifier current. Is MiRP1 the missing link? Journal of Physiology 540: 15-27, 2002.

Weiger T, Hermann A and Levitan I. Modulation of calcium-activated potassium channels. Journal of Comparative Physiology. A, Sensory, Neural, and Behavioral Physiology 188: 79-87, 2002.

Westphal R, Tavalin S, Lin J, Alto N, Fraser I, Langeberg L, Sheng M and Scott J. Regulation of NMDA receptors by an associated phosphatase-kinase signaling complex. Science 285: 93-95, 1999.

Willars G and Nahorski S. Heterologous desensitization of both phosphoinositide and Ca^{2+} signaling in SH-SY5Y neuroblastoma cells: a role for intracellular Ca^{2+} store depletion? Molecular Pharmacology 47 (3): 509-516, 1995b.

Willars G and Nahorski S. Acute regulation of muscarinic receptor mediated stimulation of phosphoinositide hydrolysis. In: Molecular mechanisms of muscarinic acetylcholine receptor function, edited by Wess J: R.G. Landes company, p. 71-89, 1995a.

Willars G, Muller-Esterl W, Nahorski S. Receptor phosphorylation does not mediate cross talk between muscarinic M_3 and bradykinin B_2 receptors. American Journal of Physiology (Cell Physiology) 46: C859-C869, 1999.

Williams C, Hu N, Shen W, Mashburn A and Murray K. Modulation of the human Kv1.5 channel by protein kinase C activation: role of the Kvb1.2 subunit. The Journal of Pharmacology and experimental theraputics 302: 545-550, 2002.

Witchel H and Hancox J. Familial and aquired long QT syndrome and the cardiac rapid delayed rectifier potassium current. Clincal and Experimental Pharmacology and Physiology 27: 753-766, 2000.

Witchel H, Dempsey C, Sessions R, Perry M, Milnes J, Hancox J, Mitcheson J. The low-potency, voltage-dependent HERG blocker propafenone--molecular determinants and drug trapping. Molecular Pharmacology 66(5):1201-12, 2004.

Wolf M, Cuatrecasas P, Sahyoun N. Interaction of protein kinase C with membranes is regulated by Ca2+, phorbol esters, and ATP. Journal of Biological Chemistry 60(29): 15718-22, 1985.

Wu LM, Orikabe M, Hirano Y, Kawano S, Haraoka M. Effects of Na^+ channel blocker, Pilsicainide, on HERG current expressed in HEK-293 cells. Journal of cardiovascular Pharmacology 42 (3): 410-418, 2003.

Xu J, Zutter M, Santoro S, Clark R. PDGF induction of alpha 2 integrin gene expression is mediated by protein kinase C-zeta. Journal of cellular biology 134(5):1301-11, 1996.

Yang T, Kupershmidt S, Roden D. Anti-minK antisense decreases the amplitude of the rapidly activating cardiac delayed rectifier K^+ current. Circulation Research 77: 1246-1253, 1995

Zagotta W, Olivier N, Black K, Young E, Olson R and Gouaux E. Strucural basis for modulation and agonist specificity of HCN pacemaker channels. Nature 425: 200-205, 2003.

Zahradnik I and Palade P. Multiple effects of caffeine on calcium current in rat ventricular myocytes. Pflugers Arch-European journal of Physiology 424: 129-136, 1993.

Zeng W-Z, Li X-J, Hilgemann D and Huang C-L. Protein Kinase C inhibits ROMK1 channel activity via a phosphatidylinositol 4,5-bisphosphate dependent mechanism. The Journal of Biological chemistry 278: 16852-16856, 2003.

Zhang W, Thomas D, Karle C, Kathofer S, Schenkel J, Kreye V, Ficker E, Wible B and Keihn J. Protein kinase A mediated phosphorylation of HERG potassium channels in a human cell line. Chinese Medical Journal 115: 668-676, 2002.

Zhang Y, Wang H, Wang J, Han H, Nattel S and Wang Z. Normal function of HERG K^+ channels expressed in HEK293 cells requires basal protein kinase B activity. FEBS Letters 534: 125-132, 2003.

Zhao F-L, Lu S-G and Herness S. Dual actions of caffeine on voltage-dependent currents and intracellular calciumin taste receptor cells. American Journal of Physiology 283: R115-R129, 2002.

Zhou Z, Gong Q, Ye B, Fan Z, Makielski J, Robertson G and January C. Properties of HERG channels stably expressed in HEK 293 cells studied at physiological temperature. Biophysical Journal 74: 230-241, 1998.

Zitron E, Kiesecker C, Luck S, Kathofer S, Thomas D, Kreye V, Kiehn, J, Katus H, Schoels W, Karle C. Human cardiac inwardly rectifying current $I_{Kir2.2}$ is upregulated by activation of protein kinase A. Cardiovascular Research 63: 520-527, 2004.

Zou A, Curran M, Keating M and Sanguinetti M. Single HERG delayed rectifier K^+ channels expressed in xenopus oocytes. The American Physiological Society: H1309-H1314, 1997.